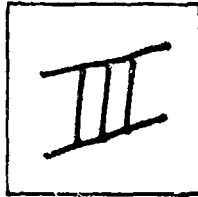


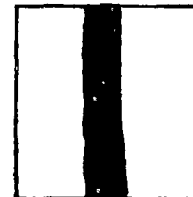
PHOTOGRAPH THIS SHEET

AD A094295

DTIC ACCESSION NUMBER



LEVEL



INVENTORY

~~GENERAL ELECTRIC CO. (GEC) ENGINE CO. AIRCRAFT
ENGINE CO. (GEC) ENGINE CO. AIRCRAFT~~
HIGH VELOCITY JET NOISE SOURCE LOCATION AND

REDUCTION: TASK 3. EXPERIMENTAL INVESTIGATION OF SUPPRESSION
PRINCIPLES. VOLUME III - SUPPRESSOR CONCEPTS OPTIMIZATION
FINAL REPT., DEC. '78, REPT. NO: R78AEG627
CONTRACT DOT-OS-30034 FAA-RD-76-79-3-3.

DISTRIBUTION STATEMENT A

Approved for public release;
Distribution Unlimited

DISTRIBUTION STATEMENT

ACCESSION FOR	
NTIS	GRA&I <input checked="" type="checkbox"/>
DTIC	TAB <input type="checkbox"/>
UNANNOUNCED	<input type="checkbox"/>
JUSTIFICATION	<input type="checkbox"/>
BY	
DISTRIBUTION /	
AVAILABILITY CODES	
DIST	AVAIL. AND/OR SPECIAL
A	

DISTRIBUTION STAMP

DTIC ELECTED
S JAN 29 1981 D
D

DATE ACCESSIONED

81 1 27 006

DATE RECEIVED IN DTIC

PHOTOGRAPH THIS SHEET AND RETURN TO DTIC-DDA-2

**HIGH VELOCITY JET NOISE
SOURCE LOCATION AND REDUCTION
TASK 3 - EXPERIMENTAL INVESTIGATION
OF SUPPRESSION PRINCIPLES
Volume III - Suppressor Concepts Optimization**

AD A094295

TECHNICAL CONTRIBUTORS:

R.H. Brown	E.J. Stringas
W.S. Clapper	P.G. Vogt
W. Joy	R.W. Whittaker
M.A. Smith	J.P. Wolf

**GENERAL ELECTRIC COMPANY
AIRCRAFT ENGINE GROUP
CINCINNATI, OHIO 45215**



DECEMBER 1978

FINAL REPORT

Document is available to the U.S. public through
the National Technical Information Service,
Springfield, Virginia 22161.

Prepared for

**U.S. DEPARTMENT OF TRANSPORTATION
FEDERAL AVIATION ADMINISTRATION
Systems Research & Development Service
Washington, D.C. 20590**

NOTICE

The contents of this report reflect the views of the General Electric Company which is responsible for the facts and the accuracy of the data presented herein. The contents do not necessarily reflect the official views or policy of the Department of Transportation. This report does not constitute a standard, specification, or regulation.

1. Report No. FAA-RD-76-79, III - III		2. Government Accession No.		3. Recipient's Catalog No.	
4. Title and Subtitle High Velocity Jet Noise Source Location and Reduction Task 3 - Experimental Investigation of Suppression Principles Volume III - Suppressor Concepts Optimization				5. Report Date December 1978	
				6. Performing Organization Code	
7. Author(s) W.S. Clapper (Task 3 Technical Director and Editor) et al. E.J. Stringas (Technical Project Manager)				8. Performing Organization Report No. R78AEG627	
				10. Work Unit No.	
9. Performing Organization Name and Address General Electric Company Advanced Engine Engineering Division Aircraft Engine Group Cincinnati, Ohio 45215				11. Contract or Grant No. DOT-OS-30034	
				13. Type of Report and Period Covered Technical Report October 1974 - October 1977	
12. Sponsoring Agency Name and Address U.S. Department of Transportation, Federal Aviation Administration Systems Research and Development Service Washington, D.C. 20590				14. Sponsoring Agency Code ARD-550	
15. Supplementary Notes This report is in partial fulfillment of the subject program. Related documents to be issued in the course of the program include final reports of the following Tasks: Task 1 - Activation of Facilities and Validation of Source Location Techniques; Task 1 Supplement - Certification of the General Electric Jet Noise Anechoic Test Facility; Task 2 - Theoretical Developments and Basic Experiments; Task 4 - Development/Evaluation of Techniques for "In-flight" Investigation; Task 5 - Investigation of "In-flight" Aero-Acoustic Effects; Task 6 - Noise Abatement Nozzle Design Guide. FAA Program Monitor R.S. Zuckerman.					
16. Abstract Experimental investigations were conducted of suppression principles, including developing an experimental data base, developing a better understanding of jet noise suppression principles, and formulating empirical methods for the acoustic design of jet noise suppressors. Acoustic scaling has been experimentally demonstrated, and five "optimum" nozzles have been selected for subsequent anechoic free-jet testing. Several studies were conducted to attempt an optimization of suppressor concepts. Trade studies of performance versus suppression, aircraft integration studies, and development of a figure-of-merit method of analysis all make up the activities in this "optimization" process. The end product of this effort was to design five nozzles for static and free-jet testing. Demonstration of acoustic scaling for several suppressor configurations was conducted to ensure the adequacy of using scale-model results to project full-scale suppression levels. Full-scale data were obtained on several suppressor configurations using J79 and J85 engines. Scale-model data were obtained for these same configurations to allow comparison of scale-model and full-scale results. This volume is part of the four volume set that constitutes the Task 3 final report. The other volumes are: Volume I - Verification of Suppression Principles and Development of Suppression Prediction Methods Volume II - Parametric Testing and Source Measurements Volume IV - Laser Velocimeter Time Dependent Cross Correlation Measurements.					
17. Key Words (Suggested by Author(s)) Jet Noise, Suppression, Performance, Weight, Mission Studies, Acoustic Scaling				18. Distribution Statement Document is available to the U.S. public through the National Technical Information Service, Springfield, Virginia 22161.	
19. Security Classif. (of this report) Unclassified		20. Security Classif. (of this page) Unclassified		21. No. of Pages 159	22. Price*

* For sale by the National Technical Information Service, Springfield, Virginia 22161

METRIC CONVERSION FACTORS

Approximate Conversions to Metric Measures		Approximate Conversions from Metric Measures		
Symbol	When You Know	Multiply by	To Find	Symbol
LENGTH				
in	inches	2.5	centimeters	cm
ft	feet	30	centimeters	cm
yd	yards	0.9	meters	m
mi	miles	1.6	kilometers	km
AREA				
sq in	square inches	6.5	square centimeters	cm ²
sq ft	square feet	0.09	square meters	m ²
sq yd	square yards	0.8	square meters	m ²
sq mi	square miles	2.6	square kilometers	km ²
acres	acres	0.4	hectares	ha
MASS (weight)				
oz	ounces	29	grams	g
lb	pounds	0.45	kilograms	kg
short tons	short tons	0.9	tonnes	t
VOLUME				
cup	cups	0.24	deciliters	dl
fl oz	fluid ounces	30	milliliters	ml
c	cups	0.24	liters	l
pt	pints	0.47	liters	l
qt	quarts	0.95	liters	l
gal	gallons	3.8	liters	l
cu ft	cubic feet	0.03	cubic meters	m ³
cu yd	cubic yards	1.35	cubic meters	m ³
TEMPERATURE (temp)				
°F	Fahrenheit temperature	5/9	Celsius temperature	°C
		subtract 32		

Approximate Conversions from Metric Measures		Approximate Conversions to Metric Measures		
Symbol	When You Know	Multiply by	To Find	Symbol
LENGTH				
mm	millimeters	0.04	inches	in
cm	centimeters	0.4	inches	in
m	meters	3.3	feet	ft
km	kilometers	1.1	yards	yd
m	meters	0.6	miles	mi
AREA				
cm ²	square centimeters	0.16	square inches	in ²
m ²	square meters	1.2	square yards	yd ²
km ²	square kilometers	0.4	square miles	mi ²
ha	hectares (10,000 m ²)	2.5	acres	acres
MASS (weight)				
g	grams	0.035	ounces	oz
kg	kilograms	2.2	pounds	lb
t	tonnes (1000 kg)	1.1	short tons	short tons
VOLUME				
ml	milliliters	0.03	fluid ounces	fl oz
l	liters	2.1	pints	pt
m ³	cubic meters	1.06	quarts	qt
m ³	cubic meters	0.26	gallons	gal
m ³	cubic meters	35	cubic feet	ft ³
m ³	cubic meters	1.3	cubic yards	yd ³
TEMPERATURE (temp)				
°C	Celsius temperature	9/5 (then add 32)	Fahrenheit temperature	°F



* 1 in = 2.54 exactly. For other metric measurements and more details, consult the Metric Conversion Tables, 1974 Edition, NIST Special Publication 446-1.

PREFACE

This report describes the work performed under Task 3 of the DOT/FAA High Velocity Jet Noise Source Location and Reduction Program (Contract DOT-OS-30034). The objectives of the contract were:

- Investigation, including scaling effects, of the aerodynamic and acoustic mechanisms of various jet noise suppressors.
- Analytical and experimental studies of the acoustic source distribution in such suppressors, including identification of source location, nature, and strength and noise reduction potential.
- Investigation of in-flight effects on the aerodynamic and acoustic performance of these suppressors.

The results of these investigations are expected to lead to the preparation of a design guide report for predicting the overall characteristics of suppressor concepts, from models to full scale, static to in-flight conditions, as well as a quantitative and qualitative prediction of the phenomena involved.

The work effort in this program was organized under the following major Tasks, each of which is reported in a separate Final Report:

Task 1 - Activation of Facilities and Validation of Source Location Techniques.

Task 2 - Theoretical Developments and Basic Experiments.

Task 3 - Experimental Investigation of Suppression Principles.

Task 4 - Development and Evaluation of Techniques for "In-flight" Investigation.

Task 5 - Investigation of "In-flight" Aero-Acoustic Effects on Suppressed Exhausts.

Task 6 - Preparation of Noise Abatement Nozzle Design Guide Report.

Task 1 was an investigative and survey effort designed to identify acoustic facilities and test methods best suited to jet noise studies. Task 2 was a theoretical effort complemented by theory verification experiments which extended across the entire contract period of performance.

The subject of the present, Task 3 report series (FAA-RD-76-79, III - 1, II, III, and IV) was formulated as a substantial part of the contract effort to gather various test data on a wide range of high velocity jet nozzle

suppressors. These data, together with supporting theoretical advances from Task 2, have led to a better understanding of jet noise and jet noise suppression mechanisms, as well as to a validation of scaling methods. Task 3 helped to identify several "optimum" nozzles for simulated in-flight testing under Task 5, and to provide an extensive, high quality data bank leading to formulation of methods and techniques useful for designing jet noise suppressors for application in the Task 6 design guide as well as in future studies.

Task 4 was similar to Task 1, except that it dealt with the specific test facility requirements, measurement techniques, and analytical methods necessary to evaluate the "in-flight" noise characteristics of simple and complex suppressor nozzles. This effort provided the capability to conduct the "flight" effects test program of Task 5.

TABLE OF CONTENTS

<u>Section</u>	<u>Page</u>
1.0 SUMMARY	1
2.0 INTRODUCTION	11
3.0 TRADE STUDIES OF PERFORMANCE VERSUS SUPPRESSION	13
4.0 AIRCRAFT INTEGRATION STUDY	20
4.1 Aircraft and Mission	24
4.2 Cycle Selection	24
4.3 Suppressor Selection	31
4.4 Mechanical Design Studies	35
4.5 Noise Prediction Methods	39
4.6 Procedure for Economic Evaluation	47
4.7 Impact of Suppressor Performance, Noise Reduction, and Weight	53
4.8 Conclusions	65
5.0 FIGURE OF MERIT	66
6.0 OPTIMUM SUPPRESSOR NOZZLES	72
7.0 CONCLUSIONS	82
APPENDIX A ACOUSTIC SCALING DEMONSTRATION	83
1.0 INTRODUCTION	84
2.0 METHOD OF APPROACH	85
3.0 TEST FACILITIES AND HARDWARE DESCRIPTION	86
4.0 TEST MATRIX	99
5.0 DATA ACQUISITION AND REDUCTION	112
6.0 DATA ANALYSIS PROCEDURES	113
7.0 SCALING RESULTS	114
8.0 CONCLUSIONS AND RECOMMENDATIONS	150
APPENDIX B TABULATION OF ACOUSTIC AND AERODYNAMIC PERFORMANCE DATA	151
LIST OF SYMBOLS	156
REFERENCES	158

LIST OF ILLUSTRATIONS

<u>Figure</u>		<u>Page</u>
1-1.	Evaluation of Noise Mechanisms for a Conical Nozzle.	2
1-2.	Correlation Between Measured and Predicted Effective Perceived Noise Level, EPNL, for all Types of Suppressor Nozzles.	4
1-3.	Typical Peak Static Noise Suppression Characteristics.	6
1-4.	Summary of Range and Noise Characteristics for Several Baseline and Suppressor Nozzles.	9
3-1.	Comparison of Static Performance and Suppression Levels.	15
3-2.	Comparison of Flight Performance and Static Suppression Characteristics.	16
3-3.	Summary of Projected Flight Performance and Suppression Characteristics.	18
4-1.	NASA Reference Aircraft Configuration.	25
4-2.	Definition of Supersonic Mission Profile.	29
4-3.	Inlet/Engine Airflow Match.	32
4-4.	Typical Turbojet Exhaust System Schematic.	37
4-5.	Typical VCE Exhaust System Schematic.	38
4-6.	Relationship Between Nozzle Exit Radius, Throat Area, and Area Ratio.	40
4-7.	Weight Increase as a Function of Radius Ratio.	41
4-8.	Definition of Jet Density Exponent (per Reference 15).	44
4-9.	Definition of Normalized PNL.	45
4-10.	Summary of Single-Flow Nozzle Suppression Characteristics.	48
4-11.	Summary of Dual-Flow Nozzle Static Suppression Characteristics.	49
4-12.	Definition of Duration Correction for Suppressor Nozzles.	50

LIST OF ILLUSTRATIONS (Continued)

<u>Figure</u>		<u>Page</u>
4-13.	Determination of Sideline Effective Perceived Noise Levels for a Typical Suppressor.	51
4-14.	Summary of Typical Sideline and Community Jet Noise Levels - AR = 1.75 40-Shallow Chute Nozzle.	52
4-15.	Baseline Nozzle Noise Characteristics.	54
4-16.	Aircraft Integration Study, Mission Characteristics.	55
4-17.	Summary of Range and Noise Characteristics for Several Baseline and Suppressor Nozzles.	58
4-18(a).	Impact of Suppression on Aircraft Range.	59
4-18(b).	Impact of Aero Performance on Aircraft Range.	60
4-13(c).	Typical Suppressor Weight Decrements.	61
4-19.	Influence of Balanced Field Length on Noise Characteristics of a Single-Flow Baseline and Suppressor Nozzle.	63
5-1.	Rating of Mechanical Suppressors Utilizing the Composite Score (C.S.) and Overall Ranking Number (O.R.N.) Techniques.	69
5-2.	Impact of Mechanical Suppressor Δ PNL, Δ C _{fg} , and Δ Wt on Overall Ranking Number.	70
6-1.	Impact of Auxiliary Injection Geometry on Peak PNL, $W_{core} = 30\% W_{duct}$.	76
6-2.	Typical Suppressor PNL Directivity Characteristics at Constant Pressure Ratio.	78
6-3.	Typical Suppressor Characteristics at Constant Pressure Ratio.	79
6-4.	Impact of Acoustically Treated Ejector on Peak PNL of Dual Flow, 36-Chute, Area Ratio = 2.0, With and Without Ejector.	80
A-1.	Ellipsoidal Mirror Setup at JENOTS.	87
A-2.	Laser Velocimeter Setup at JENOTS.	88
A-3.	J79 Engine Stackup.	90

LIST OF ILLUSTRATIONS (Continued)

<u>Figure</u>		<u>Page</u>
A-4.	Unshielded View of J79 Engine Installation at GE/EFTC.	91
A-5.	Laser Velocimeter Measurements on the J79 Engine with 32-Chute Nozzle.	98
A-6.	Comparison of Conical Nozzle Data from Engine and Model Static Tests.	115
A-7.	Directivity Comparison of Conical Nozzle Data from Engine and Model Static Tests.	116
A-8.	Directivity Comparison of Conical Nozzle Data from Engine and Model Static Tests.	117
A-9.	Comparison of Scale Model and J79 Maximum OASPL Characteristics.	118
A-10.	Comparison of Scale Model and J79 Maximum PNL Characteristics.	119
A-11.	Comparison of Scale Model and J85 Maximum OASPL Characteristics.	120
A-12.	Comparison of Scale Model and J85 Maximum PNL Characteristics.	121
A-13.	Comparison of Scale Model and J79 90° and 50° OASPL Trends.	123
A-14.	Comparison of Scale Model and J85 90° and 50° OASPL Trends.	124
A-15.	Comparison of Model and J79 PNL Directivity Patterns.	125
A-16.	Comparison of Model and J79 OASPL Directivity Patterns.	126
A-17.	Comparison of Model and J85 PNL Directivity Patterns.	128
A-18.	Comparison of Model and J85 OASPL Directivity Patterns.	129
A-19.	Model and J79 Power Spectra Comparisons.	130
A-20.	Model and J85 Power Spectra Comparisons.	131
A-21.	Model and J79 Conical Nozzle Spectra Comparisons.	132
A-22.	Model and J85 Conical Nozzle Spectra Comparisons.	133

LIST OF ILLUSTRATIONS (Concluded)

<u>Figure</u>		<u>Page</u>
A-23.	Model and J79 32-Chute Nozzle Spectra Comparisons.	134
A-24.	Model and J79 32-Chute + Ejector Spectra Comparisons.	135
A-25.	Model and J85 8-Lobe Nozzle Spectra Comparisons.	137
A-26.	Model and J85 104-Tube Nozzle Spectra Comparisons.	138
A-27.	Comparison of Conical Nozzle Axial Mean Velocity Distribution, Laser Velocimeter Data.	139
A-28.	Comparison of Conical Nozzle Radial Mean Velocity Distribution, Laser Velocimeter Data, $V_0 = 2100$ ft/sec.	141
A-29.	Comparison of 32-Chute Nozzle Axial Mean Velocity Distribution, Laser Velocimeter Data, $V_0 = 2100$ ft/sec.	142
A-30.	Comparison of 32-Chute Nozzle Radial Mean Velocity Distribution, Laser Velocimeter Data, $V_0 = 2100$ ft/sec.	143
A-31.	Comparison of Radial Distribution of Axial Turbulence, Laser Velocimeter Data.	144
A-32.	Comparison of Conical Nozzle Turbulence Characteristics, Laser Velocimeter Data, $V_0 = 2100$ ft/sec.	145
A-33.	Comparison of 32-Chute Nozzle for Axial Distribution of Axial Turbulence, Laser Velocimeter Data, $V_0 = 2100$ ft/sec.	146
A-34.	Comparison of Model and Full-Scale Apparent Noise Source Location.	148
A-35.	Comparison of Conical Nozzle 90° Ellipsoidal Mirror Spectra from Engine and Model Static Tests.	149

LIST OF TABLES

<u>Table</u>		<u>Page</u>
1-1.	Typical Summary of Nozzle Static and Projected Flight Peak PNL Suppression Characteristics.	7
4-1.	Reference Configuration Geometric Characteristics.	27
4-2.	Reference Configuration Weight Summary.	28
4-3.	Definition of Suppressors Used for the Aircraft Integration Study.	33
4-4.	Summary of Suppressor Weight Estimates.	42
4-5.	Dual-Flow System, 40 Shallow Chutes.	56
4-6.	Summary of Suppressor Noise Footprint Characteristics.	64
5-1.	Comparison of the "Composite Score" and "Overall Ranking Number" Techniques in Rating Suppressor/Engine Systems.	68
6-1.	Optimum Suppressor Nozzle Designs.	73
6-2.	Single-Flow System Configurations.	75
A-1.	Description of Test Configurations.	92
A-2.	Range of Test Conditions.	99
A-3.	Test Matrix, 5.7-inch Model.	100
A-4.	Test Matrix, 4.0-inch Model.	101
A-5.	Test Matrix, 3.56-inch Model.	102
A-6.	Test Matrix, 2.0-inch Model.	103
A-7.	Test Matrix, 32-Chute Model.	104
A-8.	Test Matrix, 32-Chute + Ejector Nozzle.	105
A-9.	Test Matrix, 8-Lobe Model.	106
A-10.	Test Matrix, 104-Tube Model.	107
A-11.	Test Matrix, J79 Conical Model.	108
A-12.	Test Matrix, J79 32-Chute Model.	109

LIST OF TABLES (Concluded)

<u>Table</u>		<u>Page</u>
A-13.	Test Matrix, J79 32-Chute + Ejector Model.	110
A-14.	Test Matrix, J85 Models.	111
B-1.	Summary of Suppression and Performance Characteristics.	153

1.0 SUMMARY

The High Velocity Jet Noise Source Location and Reduction Program (Contract DOT-OS-30034) was conceived to bring analytical and experimental knowledge to bear on understanding the fundamentals of jet noise for simple and complex suppressors.

Task 3, the subject of this report, involved the experimental investigation of suppression principles, including developing an experimental data base, developing a better understanding of jet noise suppression principles, and formulating empirical methods for the acoustic design of jet noise suppressors. Acoustic scaling has been experimentally demonstrated, and five "optimum" nozzles were selected for anechoic free-jet testing in Task 5.

Volume I - Verification of Suppression Principles and Development of Suppression Prediction Methods - Some of the experimental studies (reported in Volume II) involved acquisition of detailed, far-field acoustic data and of aerodynamic jet flow-field data on several baseline and noise-abatement nozzles. These data were analyzed and used to validate the theoretical jet noise prediction method of Task 2 (referred to as M*G*B, designating the authors' initials) and to develop and validate the empirical noise-prediction method presented herein (referred to as M*S, designating the last-name initials of the authors).*

The Task 2 theoretical studies conclude that four primary mechanisms influence jet noise suppression: fluid shielding, convective amplification, turbulent mixing, and shock noise. A series of seven suppressor configurations (ranging from geometrically simple to complex) were evaluated in Task 3 to establish the relative importance of each of the four mechanisms. Typical results of this evaluation of noise mechanisms are summarized in Figure 1-1 in terms of perceived noise level (PNL) directivity for a conical nozzle. In general, mechanical suppressors exhibit a significant reduction in shock noise relative to a baseline conical nozzle, reduce the effectiveness of fluid shielding (increase rather than suppress noise), reduce the effectiveness of convective amplification (reduce noise), and produce a modest reduction in turbulent mixing noise. The largest amount of shock noise reduction correlates with the suppressor which has the smallest characteristic dimension. Fluid shielding decreases because suppressors cause the mean velocity and temperature of the jet plume to decay faster than the conical baseline. A reduction in convection Mach number (and hence in convective amplification) occurs because a suppressor plume decays very rapidly. Turbulent mixing noise is reduced through alteration of the mixing process that results from segmenting the exhaust jet.

*The Task 3 empirical (M*S) method was initially intended for nozzle geometries which could not be modeled in the purely analytical Task 2 (M*G*B) method (a multielement nozzle with a treated ejector, for example).

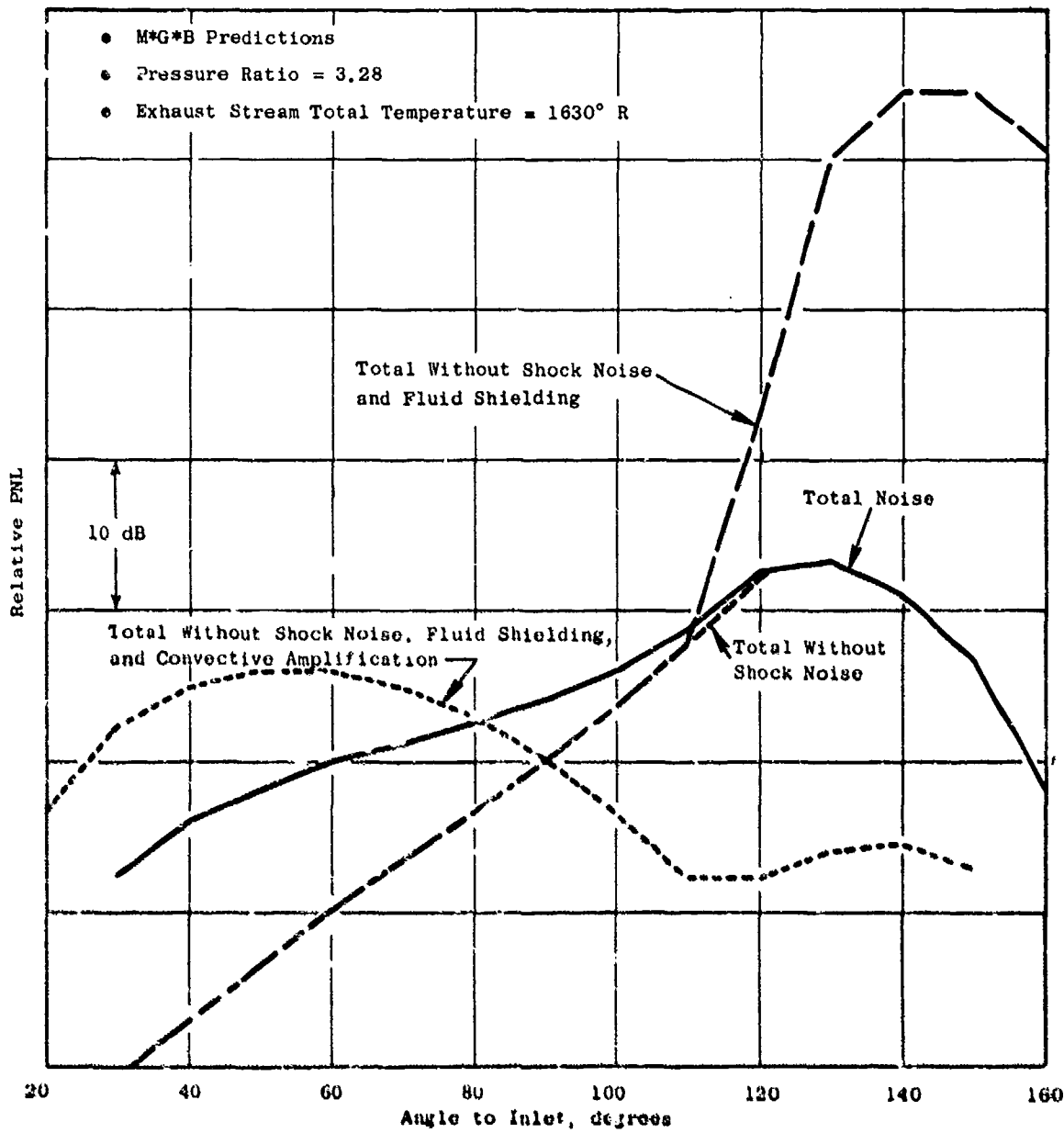


Figure 1-1. Evaluation of Noise Mechanisms for a Conical Nozzle.

Aerodynamic flow-field measurements (mean-velocity profiles) were demonstrated to be useful in verifying the flow-field predictions which were calculated by the M*G*B (theoretical) noise-prediction program. Noise source location devices such as the Ellipsoidal Mirror (EM) were demonstrated to be less useful than the Laser Velocimeter (LV) for the M*G*B theory verification studies because the LV provides data which may be directly compared with predictions made using the M*G*B program. Axial and radial mean-velocity profiles are typical examples of such comparisons.

The empirical M*S jet noise prediction method has been developed to predict the static acoustic characteristics of multielement suppressors applicable to both advanced turbojets and variable cycle engines (which are representative of power plants for future supersonic cruise aircraft). The effect of external flow on the M*S jet noise prediction is discussed in the Task 6 Design Guide Report. Inputs required to use the M*S computational procedure include: element type, element number, suppressor area ratio and radius ratio, chute-spoke planform, and cant angle plug diameter. The prediction accuracy is estimated to be ± 3.3 Effective Perceived Noise Decibels (EPNdB) at a 95 percent confidence level. Figure 1-2 illustrates the correlation between measured and predicted EPNL's for all types of suppressors.

The merits of both the M*S and M*G*B computational techniques can be stated as follows. The empirical (M*S) jet noise prediction method, based on correlations of scale-model jet data, serves as a useful preliminary design and prediction tool for selecting the basic nozzle type (chute, spoke, multi-tube, etc.) and primary geometric parameters (element number, area ratio, etc.) for a given application. It is also useful in evaluating the acoustic performance of a given suppressor nozzle, provided the nozzle is one of the types from which the correlation was derived. Further, the method is useful for doing parametric studies since the computation procedure is relatively simple and economical for both computer time and cost. The theoretical (M*G*B) prediction method, on the other hand, is more suited to detailed design and analysis of a suppressor nozzle. It can supply detailed information on the jet plume flow development as well as the far-field acoustic characteristics. It is also capable of evaluating changes in nozzle planform shape, element placement and spacing, etc. In addition, the theoretical prediction model is a useful diagnostic tool, capable of assessing the relative roles the various mechanisms play in the noise suppression process, and serving as a source location analysis tool.

Volume II - Parametric Testing and Source Measurements - A parametric experimental series was conducted to provide far-field acoustic data on 47 baseline and suppressor nozzle configurations and to provide aerodynamic nozzle performance on 18 of the configurations. The data presented in this volume were taken for use in the current program as well as to provide an extensive, high-quality data base for future studies. The impact of varying the area ratio and velocity ratio of dual-flow, baseline nozzle configurations was investigated, and the importance of shock noise was assessed. The impact of varying area ratio and element number was parametrically studied for both single- and dual-flow suppressors; core plug geometry, velocity ratio, and

- Flyover calculation using static data corrected to free-field conditions.
- The "Reference" level is the predicted value of noise for each nozzle, at a specified set of thermodynamic conditions, plus an arbitrary value of 100 dB.

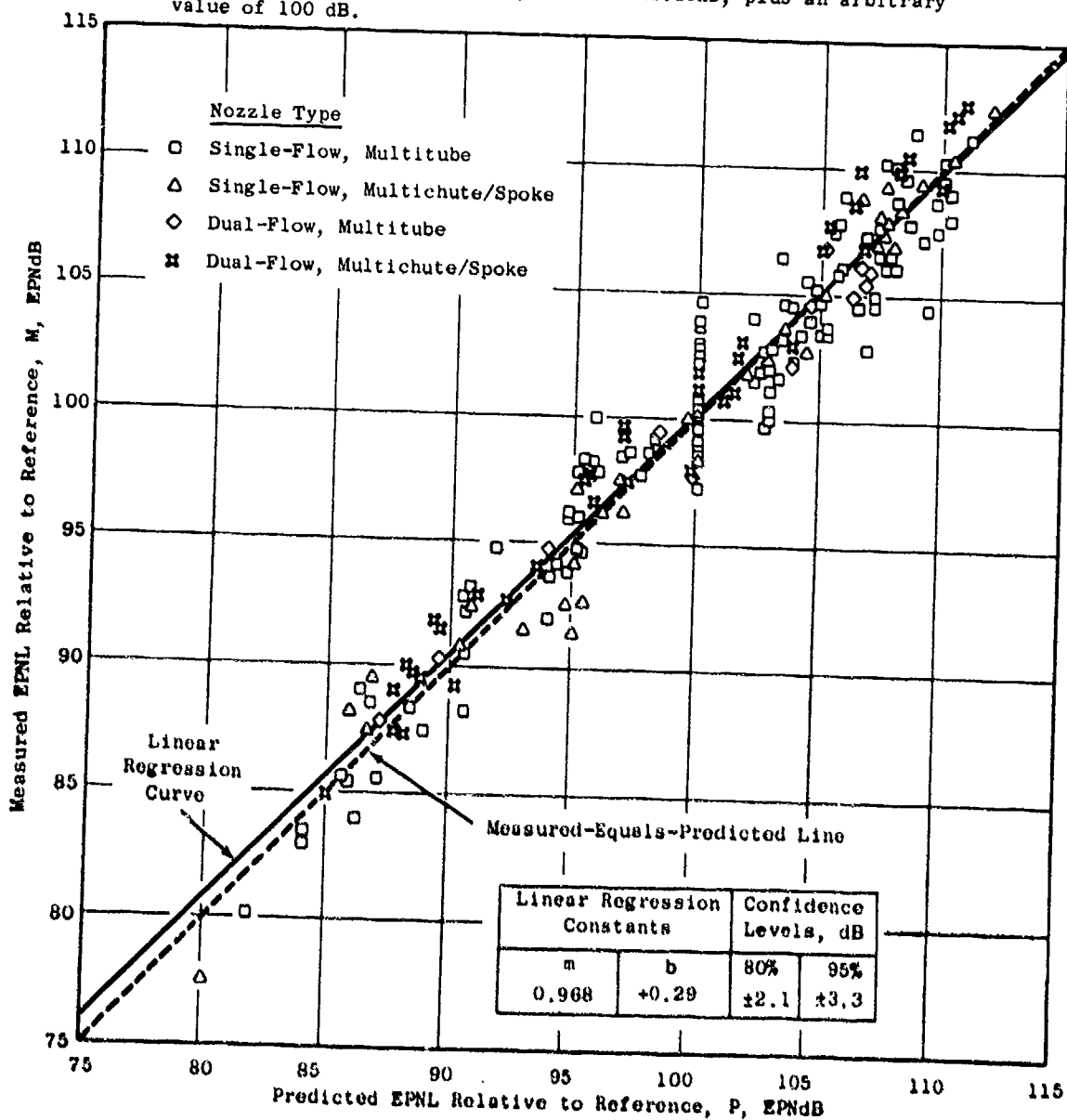


Figure 1-2. Correlation Between Measured and Predicted Effective Perceived Noise Level, EPNL, for all Types of Suppressor Nozzles.

weight flow ratio were evaluated for dual-flow suppressors. These studies establish absolute static suppression levels on the basis of normalized maximum PNL, for several families of suppressor nozzles, as illustrated in Figure 1-3.

Parametric testing identified the following primary trends for single-flow and dual-flow suppressors during static operation:

Single Flow

- Suppression increases with increasing area ratio at high jet velocity.
- Suppression decreases with increasing area ratio at low jet velocity.
- Suppression level is affected by element type (spoke systems suppress slightly better than chutes).

Dual Flow

- Suppression increases with increasing area ratio.
- Suppression increases with increasing element number at high jet velocity.
- Suppression level is affected by core plug geometry [by 2 to 3 decibels (dB)].
- Suppression increases 3 to 4 dB when a treated ejector is added to a suppressor configuration.

Selective, free-jet tests conducted on eight configurations indicate that suppression generally decreases in flight. Typical static versus free-jet results are shown in Table 1-1.

The aerodynamic performance test data recorded on 18 of the configurations at both static and wind-on conditions are also included in this volume. Base pressure measurements were taken on several of the models in order to determine base drag (which is thought to be responsible for the poor aerodynamic performance of most mechanical suppressors in flight). These wind tunnel tests identified the following primary trends in aerodynamic performance:

- Performance decreases with increasing element number.
- Performance increases with increasing chute depth.
- Performance increases with increasing ratio of inner flow area to outer flow area.

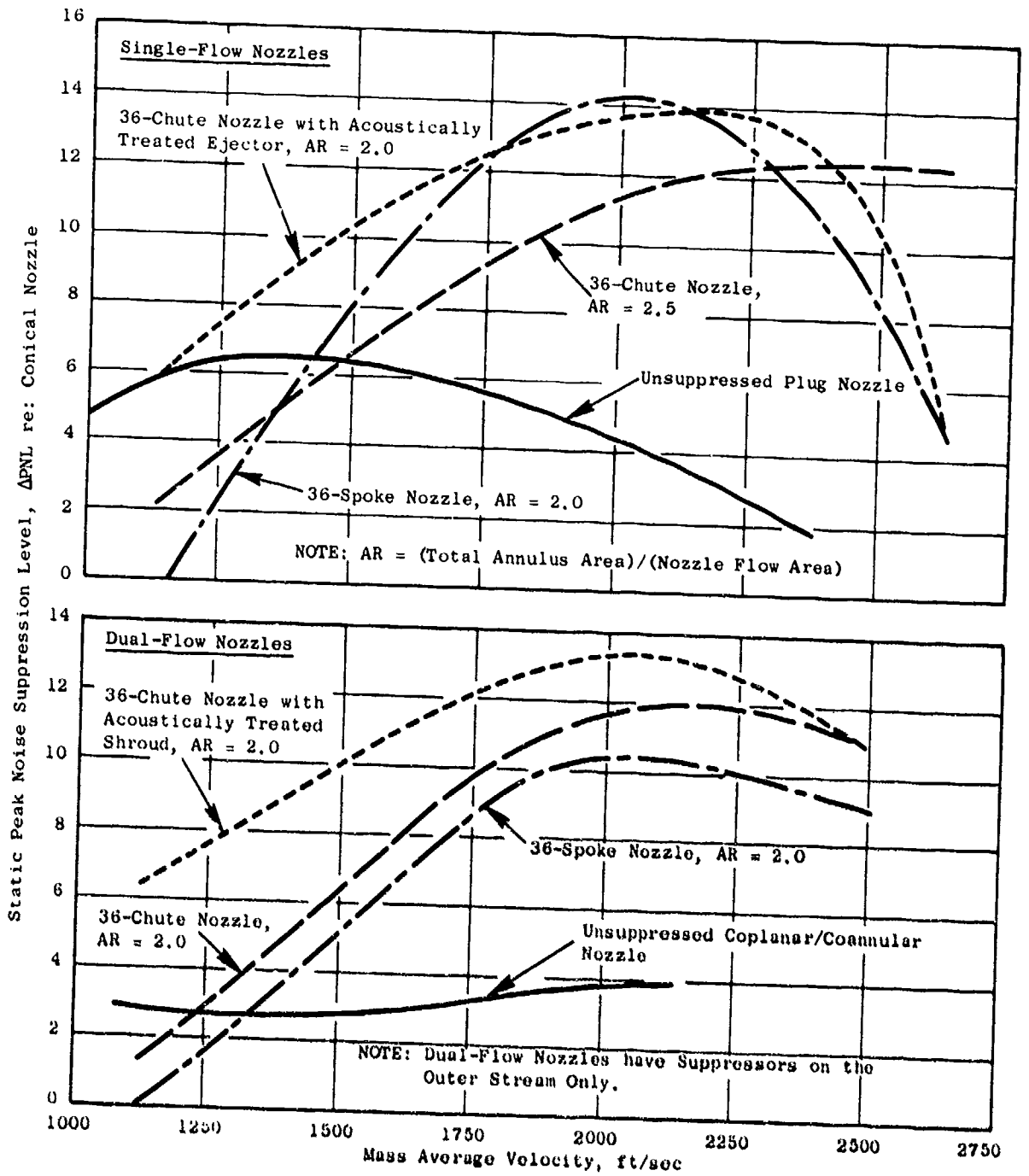


Figure 1-3. Typical Peak Static Noise Suppression Characteristics.

Table 1-1. Typical Summary of Nozzle Static and Projected Flight Peak PNL Suppression Characteristics.

- Suppression Levels are Relative to a Conical Nozzle at Equivalent Flight Conditions
- $V_j = 2500$ ft/sec

<u>Configuration</u>	<u>Suppression Level, dB</u>	
	<u>Static</u>	<u>Flight</u>
Plug Nozzle - 0.789 Radius Ratio	1.3	3.0
Plug Nozzle - 0.85 Radius Ratio	2.3	3.7
8-Lobe Nozzle	5.6	5.6
AR = 2.5 36-Chute Nozzle	13.5	10.9
AR = 2.5 36-Chute Nozzle with Auxiliary Flow	12.5	9.4
104-Tube Nozzle	12.0	12.0

- Performance is affected by element type (chutes perform better than spokes because spokes have higher base drag).

The base pressure correlations provide a procedure for predicting suppressor nozzle aerodynamic performance.

Volume III - Suppressor Concepts Optimization - Several studies were conducted to attempt an optimization of suppressor concepts. The end product of this overall effort was to design five nozzles for static and free-jet testing in Task 5. Trade studies of performance versus suppression, aircraft integration studies, and development of a figure-of-merit method of analysis all make up the activities in this "optimization" process.

Trade studies of suppression versus aerodynamic performance indicate that a properly selected and designed mechanical suppressor can attain a delta suppression to delta thrust coefficient ratio ($\Delta PNL/\Delta C_{fg}$) of almost 3.0 (based on static suppression and wind-on aerodynamic performance).

The aircraft integration study consisted of ranking nine baseline and suppressor nozzles with respect to performance level, suppression level, weight, impact on aircraft mission range, and noise footprint. In general, suppression level was found to be the most important design variable, with performance and weight ranking second and third, respectively.

The appropriate figure of merit, considering all the design variables, was found to be aircraft range. However, use of range as the figure of merit requires that the aircraft mission be specified, and several techniques for cursorily ranking the suppressors based solely on suppression level, performance, and weight may also be identified. A summary of the range versus noise characteristics of typical nozzle configurations is presented in Figure 1-4. Once a noise goal is specified, adding a suppressor provides a significant range improvement over an unsuppressed system because adding a suppressor is less costly than reducing noise by enlarging the engine to reduce jet velocity.

The design of the five optimum nozzles was based on data from previous studies, performed by Government and industry, on the M*G*B and M*S models discussed above and on the parametric data obtained in the acoustic and aerodynamic performance test series reported in Volume II. The configurations were designed and fabricated for open-throat, anechoic, free-jet testing in Task 5. The configurations chosen for evaluation were: (1) a 32-chute, single-flow nozzle, (2) a 40-shallow-chute, dual-flow nozzle, (3 and 4) a 36-chute, dual-flow nozzle, with and without a treated ejector, and (5) a 54-element, coplanar-mixer, plug nozzle.

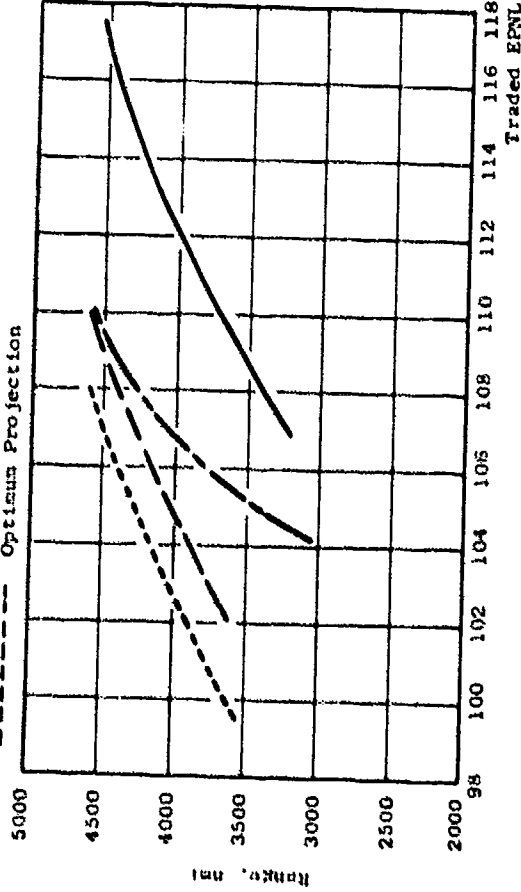
Demonstration of acoustic scaling for several suppressor configurations was conducted to assure the adequacy of using scale-model results to project full-scale suppression levels. Full-scale data were obtained on several suppressor configurations using J79 and J85 engines. The suppressors evaluated were: (1) a baseline conical nozzle, (2) a 32-chute nozzle with and without

- Four Engines
- 12,500-ft Balance Field Length; 53,500-lbf Thrust Engine
- NASA Aircraft

VARIABLE CYCLE ENGINE

Nozzle Type

- Fully Mixed, Conical
- - - 36-Chute, AR = 2.5
- - - 40-Shallow-Chute
- - - Optimum Projection



TURBOJET ENGINE

Nozzle Type

- Baseline, Conical
- - - 32-Chute
- - - 57-Tube + Ejector

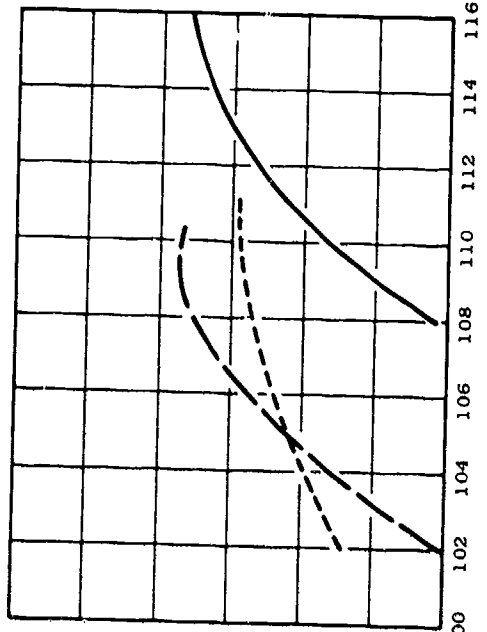


Figure 1-4. Summary of Range and Noise Characteristics for Several Baseline and Suppression Levels.

a treated ejector, (3) an 8-lobe nozzle, and (4) a 104-tube nozzle. Scale-model data were obtained for these same configurations to allow comparison of scale-model and full-scale results. In general, peak full-scale suppression levels projected from scale-model data were verified by the full-scale engine results. Directivity patterns were duplicated within ± 2 PNdB (the largest differences occurring with the conical nozzle configuration). Some spectral anomalies were observed for select cases; however, they were not of sufficient magnitude to invalidate the scale-model results. The conclusion resulting from this study is that full-scale noise levels can be predicted from scale-model test results using Strouhal scaling laws.

Volume IV - Laser Velocimeter Time Dependent Cross Correlation Measurements - The in-jet/in-jet and in-jet/far-field exhaust noise diagnostic measurements conducted using a Laser Velocimeter (LV) are reported in this volume. Measurements were performed on a conical nozzle and a coannular plug nozzle. Two-point, space/time measurements using a two-LV system were completed for the conical nozzle. Measurements of mean velocity, turbulent velocity, eddy convection speed, and turbulent length scale were made for a subsonic ambient jet and for a sonic heated jet. For the coannular plug nozzle, a similar series of two-point, laser-correlation measurements was performed. In addition, cross correlations between the laser axial component of turbulence and a far-field acoustic microphone were performed.

Volumes I, II, III, and IV contain the results of a comprehensive effort to identify and integrate the theoretical studies, parametric test data, acoustic and performance diagnostic measurements, and system studies. A logical procedure has evolved for conducting suppressor design trade-offs.

2.0 INTRODUCTION

The first 20 years of commercial aircraft operation with jet propulsion have clearly demonstrated the need for effective high velocity jet noise suppression technology in order to meet community acceptance. Aircraft system studies show that an efficient jet noise suppression device is required if a commercial supersonic aircraft is to be economically viable as well as environmentally acceptable. The current state of the art of high velocity jet noise suppression would make a supersonic transport (SST), with advanced technology engines, meet 1969 noise rules (at best). This state of the art is represented by the material in References 1 through 6.

Reference 1 describes analytical and experimental investigations which were conducted in the early 1960's. This study established a basis for development of mathematical and empirical methods for the predictions of jet flow-field, aerodynamic characteristics and for determining the directional characteristics of jet noise suppressors. This work was limited in the sense that the suppressors evaluated had only modest suppression potential, and the measurement techniques available did not allow the acquisition of high-frequency, spectral data necessary to establish full-scale, PNL suppression levels.

The development of commercial SST vehicles by the U.S. and by the British-French multinational corporation in the 1960's placed extreme emphasis on the need for effective and efficient noise suppression devices. Phase I of work conducted by the Boeing and General Electric companies is summarized in References 2 and 3. Primary emphasis was on jet noise suppressor development through model and engine testing applicable to an afterburning turbojet engine. Suppressor designs were based primarily on empirical methods. Phase II of this effort, References 4 and 5, contained the suppressor development with a stronger emphasis placed on the integration of analytical studies and experimental test data. Specifically, the Boeing Company concentrated on optimization of tube-type-suppressor systems and related semiempirical prediction methods. General Electric focused on the development both of chute and of tube-type-suppressor systems with primary emphasis placed on optimization of chute-type-suppressor nozzles.

Similar studies were conducted by the British and French in development of the Concorde, and typical results are summarized in Reference 6.

The design technology represented in References 1 through 6 is primarily semiempirical. The absence of general design rules based on engineering principles led to the Government's formulation of the High Velocity Jet Noise Program, Contract DOT-OS-30034, in 1973. The purpose has been to achieve fundamental understanding, on a quantitative basis, of the mechanisms of jet noise generation and suppression and to develop design methods.

This report presents the results of Task 3 of the contract. It provides the experimental data base which was used in conjunction with the supporting theories from Task 2 to develop a better understanding of jet noise and jet noise suppression.

The report is organized into four volumes (FAA-RD-76-79, III - I, II, III, and IV) and is presented in a format consistent with the Task 3 work plan division of subtasks. Volume I is entitled "Verification of Suppression Principles and Development of Suppression Prediction Methods." Volume II is a data report entitled "Parametric Testing and Source Measurements," and Volume III is an analysis report entitled "Suppressor Concepts Optimization." Volume IV is an analysis report entitled "Laser Velocimeter Time Dependent Cross Correlation Measurement."

Volume I uses the data base (Volume II) and the Task 2 theoretical model (Reference 7) to postulate the suppression mechanisms. Volume I also presents an independent, empirical, static jet-noise-prediction method which was developed from engineering correlations of the test data. Volume II presents the data and results of the parametric acoustic tests, the aerodynamic performance tests, and the Laser Velocimeter tests. Volume III presents the results of a trade study of performance versus suppression, an aircraft integration study, a "figure-of-merit" methodology, and a summary of the five "optimum" nozzles selected for testing in Task 5. An acoustic-scaling investigation was conducted to support the suppressor concepts optimization activities and is presented as an Appendix to Volume III. Volume IV presents the results of the in-jet/in-jet and in-jet/far-field cross correlation investigations.

The work reported in the present volume represents the results of a trade study of performance versus suppression (Section 3.0), an aircraft integration study (Section 4.0), a "figure-of-merit" methodology (Section 5.0), and a summary of the five "optimum" nozzles selected for testing in Task 5 (Section 6.0).

3.0 TRADE STUDIES OF PERFORMANCE VERSUS SUPPRESSION

The aerodynamic performance and acoustic test programs described in Volume II provide data to establish the aerodynamic performance and suppression levels of several mechanical suppressor configurations. These results, augmented by previously reported work by industry, provided the basis for establishing performance loss versus amount of suppression. This was accomplished for plug nozzles, coannular plug nozzles, multielement suppressors (tubes, chutes, and spokes), and high-radius-ratio annular nozzles with and without multielement suppressors. This information in conjunction with weight estimates was used as a basis for the aircraft integration studies.

A summary of the configurations evaluated is presented in Appendix B. Appendix B is comprised of published information taken from References 2, 3, 4, 5, 8, 9, 10, and 11 and test data obtained during the current program. Several parameters are defined to illustrate the relationship between static suppression and performance, and flight suppression and performance. The static and flight peak PNL suppression levels, and the static and flight thrust coefficients are tabulated in terms of deltas relative to a conical nozzle. The flight performance delta was determined in terms of gross thrust coefficient loss relative to a conical nozzle using wind tunnel measurements at a Mach number of 0.36. These $\Delta PNL/\Delta C_{fg}$ ratios (termed suppressor effectiveness ratio) are also defined in Appendix B:

- a. The ratio of Static suppression level to Static performance level, designated

$$\left(\frac{\Delta PNL}{\Delta C_{fg}} \right)_{\text{Static}}$$

- b. The ratio of Static suppression level to Flight performance level, designated

$$\frac{\Delta PNL_{\text{Static}}}{\Delta C_{fg \text{ Flight}}}$$

- c. The ratio of Flight suppression level to Flight performance level, designated

$$\left(\frac{\Delta PNL}{\Delta C_{fg}} \right)_{\text{Flight}}$$

These ratios are chosen to illustrate the historical evolution of suppressor evaluation in terms of exactly what type of data are necessary to establish the relationship between performance and suppression for a specific

design. The maximum suppression level which may be obtained for each of the suppression families is important and will be discussed below.

Figure 3-1 presents static suppression level plotted versus static thrust coefficient loss in terms of percent. The data presented show typical configurations from the following families: plug nozzles, slot nozzles, coannular plug nozzles, single- and dual-flow chute nozzles, spoke nozzles, tube nozzles, and ejector nozzles.

The static suppression levels presented are those measured at a jet velocity of approximately 2400 ft/sec for single-flow nozzle configurations and a mass averaged velocity of 2200 ft/sec for dual-flow configurations. The ejector configurations, based on this type of comparison, yield the highest static suppression level for a minimum performance loss. In fact, several of the ejector configurations exhibit a performance increase (i.e., thrust augmentation) due to flow entrainment. Static peak PNL suppression levels upwards of 20 PNdB have been demonstrated with ejector configurations. Tube-type suppressors without ejectors were found to place second, with Δ PNL's in excess of 14 dB for select configurations. However, the average $(\Delta$ PNL/ Δ C_{fg})_{static} ratio for this family of suppressors would range from 3 to 4. The coannular nozzles have a similar suppressor effectiveness ratio. However, the maximum suppression level which may be achieved with this type of configuration is 6 PNdB. The chute nozzle family is ranked fourth with absolute suppression levels reaching a maximum of 14 PNdB. The $(\Delta$ PNL/ Δ C_{fg})_{static} ratio was found to range from 1 to 5 depending on the configuration being evaluated. The spoke nozzles were found to yield the poorest ratio of suppression to performance, 1 to 2, with a maximum suppression level of 14 dB being measured. In summary, based on static suppression and performance measurements, the ranking of the suppressor families would be ejector nozzles, tube nozzles, coannular plug nozzles, chute nozzles, and spoke nozzles.

Ejector configurations would seem, based on the data presented thus far, to be the most effective type of suppression device if static performance and suppression are considered the appropriate yardstick for ranking suppressors. However, the suppressor must function in a flight environment and, therefore, the flight suppression level and flight performance level must be established.

In-flight information required to establish this relationship is not as abundant as static data. An intermediate step is therefore taken because of limited data availability. The suppressor families are compared where data are available for static suppression levels and flight performance levels. This comparison is valid only if the static suppression level and flight suppression level are assumed to be equivalent.

The static suppression levels as a function of flight thrust coefficient are summarized on Figure 3-2. There is a significant reduction in the data base compared to static/static information. The large data base available for tube nozzle configurations on a static basis is not available, for example, due primarily to the elimination of tube systems, because they are not considered practical to adapt to a real exhaust nozzle system, or due to the lack of wind tunnel test data to establish the flight thrust coefficient.

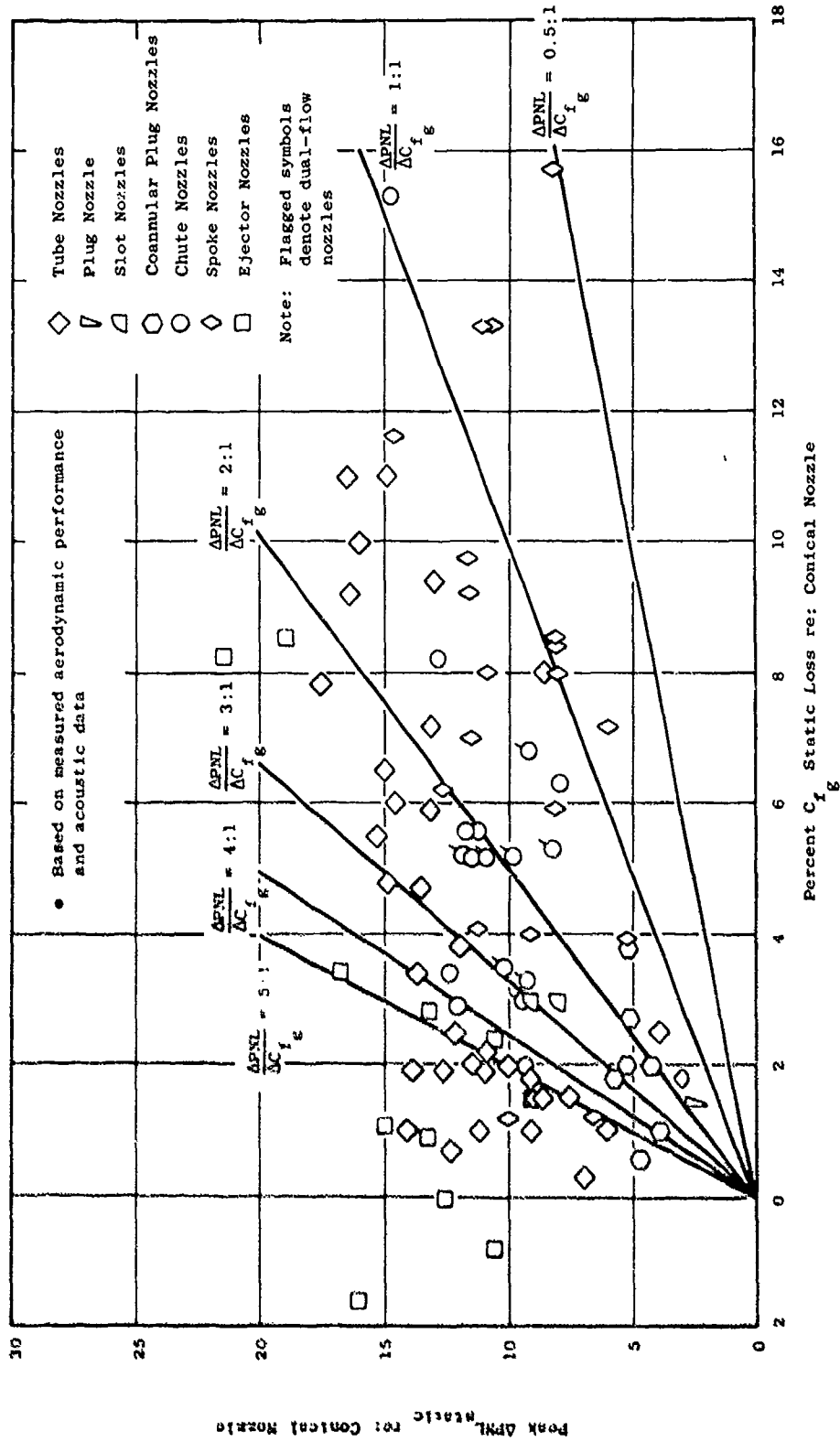


Figure 3-1. Comparison of Static Performance and Suppression Levels.

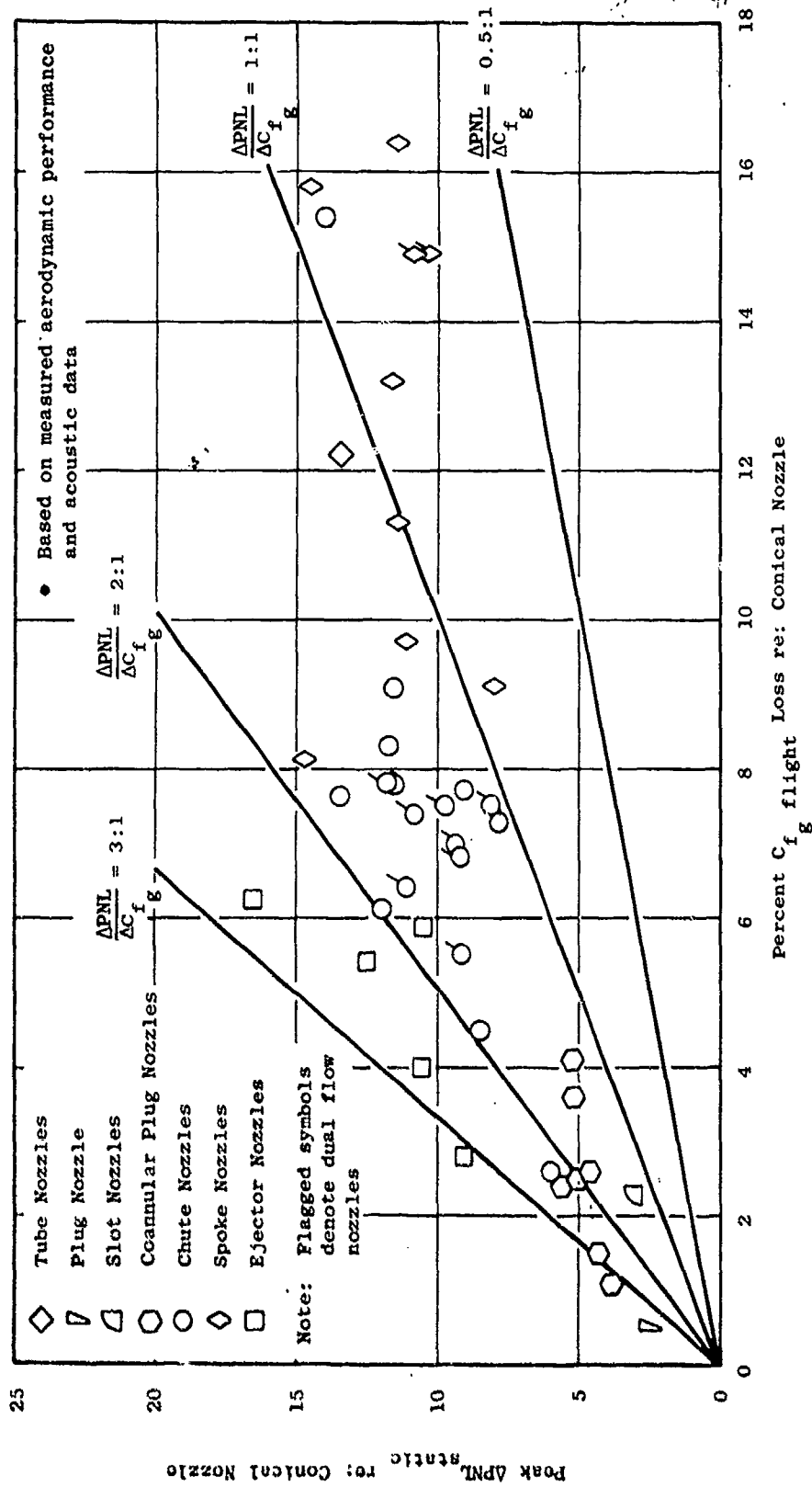


Figure 3-2. Comparison of Flight Performance and Static Suppression Levels.

The results presented in Figure 3-2 again show ejectors to be the most effective suppressor nozzle. However, the suppressor effectiveness ratio has changed significantly from Figure 3-1. In flight, ejectors do not exhibit an increase in performance relative to a conical nozzle. The maximum $(\Delta PNL)_{static}/(\Delta C_{fg})_{flight}$ ratio achieved was approximately 3. The coannular plug nozzles do not have a significant performance loss in flight relative to a conical nozzle and have a suppressor effectiveness ratio of approximately 2 to 3 with a maximum suppression level of 6 PNdB. The chute nozzles have a $(\Delta PNL)_{static}/(\Delta C_{fg})_{flight}$ ratio between 1 and 2 with a maximum suppression level of 13.5 PNdB. The dual-flow nozzles tested did not realize a significant advantage over the single-flow configurations. The spoke nozzles were found in general to yield peak suppression levels equivalent to chute nozzles. However, an additional 2 to 9 percent in performance loss was incurred due to increases in base drag as discussed in Section 4.0 of Volume II.

Comparisons of projected flight suppression levels and flight performance are summarized in Figure 3-3. The data base to establish this relationship is limited to 12 configurations. The projections were made based on free-jet data from Section 3.4.3 of Volume II, NASA-Ames 40 by 80 Wind Tunnel Test Series from Reference 12, Aerotrainer Test Series from Reference 10, and the F106 Flyover Test Series from Reference 11. The results are summarized in Figure 3-3. The plug nozzle is the most effective suppressor in terms of $(\Delta PNL/\Delta C_{fg})_{flight}$ ratio. However, the absolute suppression level achieved with this type of configuration is a very modest 2.5 PNdB. The 57-tube nozzle with a treated ejector has a suppression level of approximately 11 to 12 PNdB. The flight suppression level of this configuration was established based on degrading the static suppression level by the loss in suppression measured during the scale-model test series described in Reference 12. The 32-chute nozzle suppression level was based on degrading the static suppression by an amount equivalent to that measured on a similar configuration evaluated in the free jet, described in Volume II, Section 3.4.3. A similar procedure was used for the 36-chute, AR = 2.0 and 36-chute, AR = 2.5 configurations. The 104-tube nozzle was evaluated on the Aerotrainer and the F106 aircraft. The Aerotrainer point was established using the scale-model performance measurements described in Section 4.0 of Volume II in conjunction with the suppression levels established using the data presented in Reference 10. The F106 measurement indicates the suppression levels agree within 0.5 PNdB. However, an additional 2.8 percent performance loss was measured on the F106. The 104-tube nozzle was also evaluated on the F106 with an acoustically treated shroud. A 2 dB increase in suppression was found with no change in performance. The remaining configurations evaluated on the F106 (12-chute nozzle, 48-tube nozzle, and 32-spoke nozzle), had a suppressor effectiveness ratio ranging from 0.5 to 1.

In summary, evaluation of suppressors using static performance and static acoustic data shows trends which are significantly different than observed in a flight environment. Ejector nozzle configurations are typical examples of this observation. The maximum suppression achieved in flight, 14.5 PNdB, was with the 104-tube nozzle with an acoustically treated shroud.

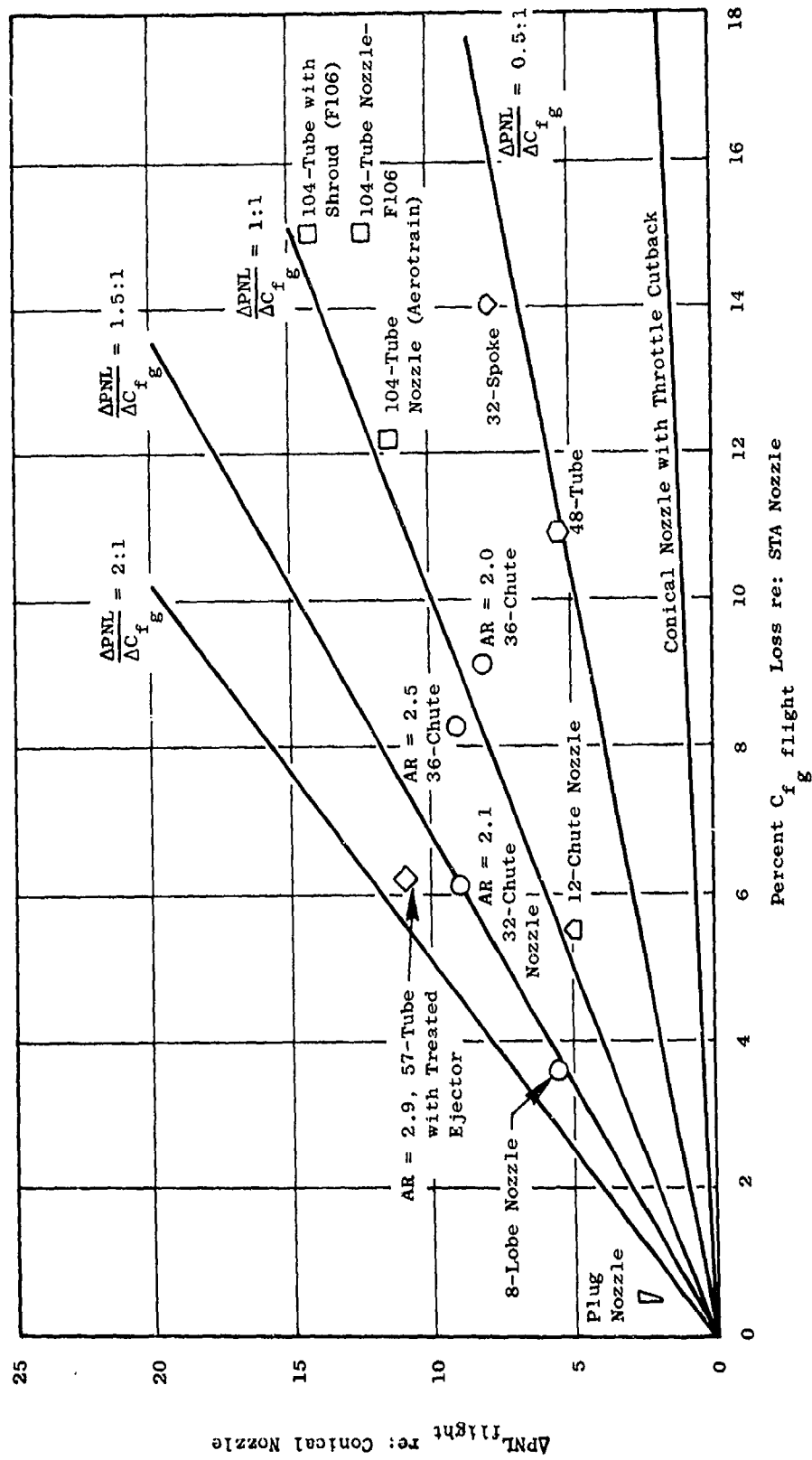


Figure 3-3. Summary of Projected Flight Performance and Suppression Characteristics.

However, there was a significant performance penalty of approximately 15 percent. Several chute configurations are projected to yield 8 to 9 dB suppression in flight with measured performance losses ranging from 6 to 9 percent. The 57-tube nozzle with treated ejector also is projected to yield 11 to 12 dB suppression with a performance loss of 6.2 percent. The plug nozzle configuration exhibited the highest suppressor effectiveness ratio, 5.0. Although the suppression levels achieved with these suppressor configurations are modest, they do represent a significant improvement over using throttle cutback to provide for lower noise levels. This throttle cutback line is also presented in Figure 3-3.

These results were used to perform the aircraft integration studies which are presented in Section 4.0. The aircraft integration study not only takes into account suppression level and performance loss, but also the weight and complexity of select exhaust nozzle systems.

4.0 AIRCRAFT INTEGRATION STUDY

Engine jet noise suppressor concepts cannot be fully evaluated without establishing their impact on the aircraft as a complete system. This section provides information needed to determine, at a preliminary design level, how different combinations of engine and suppressor systems impact aircraft performance in terms of noise levels, noise footprints, and mission range. This is accomplished by suppressor aeromechanical integration considerations and by utilizing aircraft jet noise prediction techniques. The results allow the comparison and ranking of suppressor configurations.

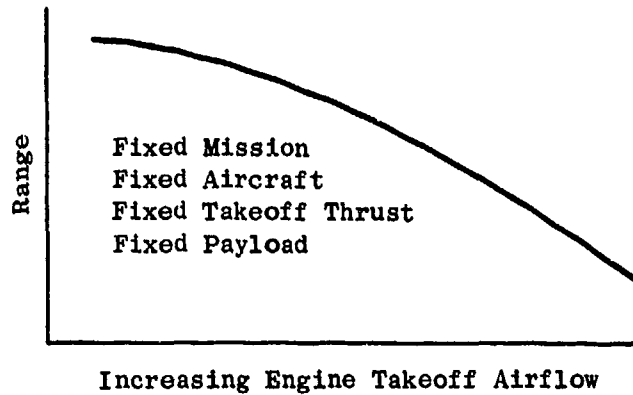
The use of a jet noise suppressor in the exhaust system of an aircraft engine has both benefits and penalties. The primary benefit is that it allows an engine with a higher specific thrust than an unsuppressed engine to be used to meet a specific noise requirement. Without noise restraints, a suppressor is not an effective device, because when a suppressor is used performance is sacrificed and weight is added. The performance degradation as measured by thrust coefficient is due primarily to the increase in suppressor nozzle base drag (Section 4.0, Volume II). The weight increase is the result of increased exhaust nozzle complexity and the need for actuators to retract and stow the suppressor during non-noise-abatement operation. The relative importance of suppression level, performance degradation, and suppressor weight are established in this section based on the results of aircraft integration studies.

Jet noise can be lowered on an unsuppressed engine by increasing engine airflow (and therefore size) at constant thrust, thereby lowering jet velocity. The increase in engine size causes a significant reduction in aircraft range, however, when takeoff gross weight, payload and balanced field length are held constant, because the larger engine weighs more and increases the drag (less fuel on board and higher fuel consumption). Mission analyses of suppressed and unsuppressed propulsion systems are necessary in order to trade these penalties on an unsuppressed system with those due to adding a mechanical suppressor.

The mission analyses conducted for this program are based on several ground rules and assumptions. The engine is sized to provide the required installed takeoff thrust. The installed takeoff thrust is determined (for a given airplane design, airport runway length, and takeoff gross weight) as a function of engine nozzle thrust coefficient. Thrust coefficients differ for each nozzle system examined. The missions were analyzed for two balance field lengths: 10,500 ft and 12,500 ft.

In the absence of a noise requirement, the engine airflow for a baseline engine is selected generally to provide high specific thrust (ratio of thrust to airflow). High specific thrust means high jet exhaust velocity (and high jet noise). When the baseline engine is increased in airflow at constant thrust, a mission characteristic can be established showing the impact on range as shown in the following sketch:

- Mission Range Variation as Increasing Engine Weight and Drag Affect Fuel Capacity and Fuel Usage



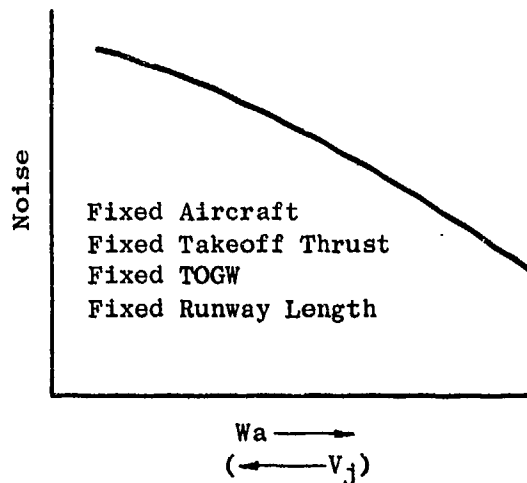
Sketch 1

This mission characteristic is common for several types of engines. This study addresses the impact of suppressors on variable cycle and turbojet engines.

The effect of increased engine size on installed cruise sfc is different for a fixed cycle turbojet and a variable cycle double bypass engine, and this change is also included in the development of the above range characteristic curves for each type of engine system.

The penalties associated with increasing engine airflow (at constant thrust) on mission range is compensated by a noise benefit due to decreasing jet velocity as illustrated in the following sketch:

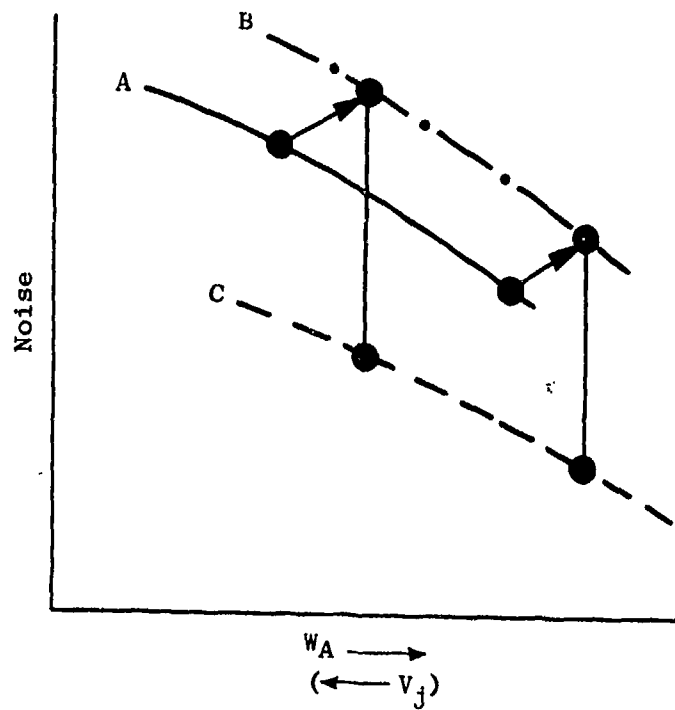
● Jet Noise Variation due to Lowering Jet Velocity



Sketch 2

The mission studies conducted herein begin with specifying a takeoff noise requirement. An appropriate curve such as is illustrated above then identifies the minimum airflow for the given engine cycle which meets the noise requirement with an unsuppressed nozzle. This airflow size is then entered in the previous mission characteristic curve to provide the corresponding range capability for the unsuppressed system.

When a suppressor system is added to a given engine cycle, the solution of proper engine size to meet a specified noise goal is more complex. Sketch 2 is modified as illustrated in Sketch 3. Curve A in Sketch 3 represents the unsuppressed curve in Sketch 2.



Sketch 3

The shift from curve A to curve B on Sketch 3 is due to the loss of thrust when a suppressor is installed. The horizontal shift in airflow is proportional to the nozzle thrust coefficient ratio, C_{f_g} unsuppressed/ C_{f_g} suppressed, because the engine must be upsized to yield the same installed thrust at takeoff. The vertical shift in noise level represents the basic noise increase due to enlarging the engine. It is proportional to $10 \log (W_A \text{ suppressed}/W_A \text{ unsuppressed})$. The shift from curve B to curve C on Sketch 3 represents the noise benefit of the suppressor including corrections for flight effects on the suppressed noise level.

In progressing from curve A to curve C, engine size and system weight have been increased. These changes decrease fuel capacity (payload and take-off gross weight are constant) and increase drag due to engine diameter beyond the levels accounted for in the mission characteristic curve of Sketch 1. Additional range adjustments are therefore required when evaluating suppressed systems. These adjustments are made in the mission analysis studies in the form of range derivatives for the extra weight and additional drag.

Mission analysis studies of various systems were conducted using the preceding method. The performance, economic, and acoustic tradeoffs of various suppressed and unsuppressed systems were established. Section 4.1 discusses the aircraft and missions which were used, and Sections 4.2 and 4.3 discuss the engine cycles and suppressor configurations, respectively.

Mechanical design studies of each combination are reviewed in Section 4.4 to show the relative feasibility of the system. Section 4.5 presents noise predictions for the systems and Section 4.6 presents a mission analysis comparing range performance and noise. Generally speaking, although the addition of a mechanical suppressor increases weight and reduces performance for a specified noise goal, the suppressor allows the use of a smaller engine which results in a range advantage.

4.1 AIRCRAFT AND MISSION

The baseline aircraft used in this study was created for NASA by LTV-Hampton and is described in Reference 13. A sketch of the aircraft configuration is presented in Figure 4-1. The aircraft is the NASA arrow-wing advanced supersonic technology design with four separate, under-wing nacelles with axisymmetric inlets. The aircraft is designed to operate from balance field lengths of 10,500 and 12,500 ft in length and to be capable of ranges up to 4000 miles.

Dimensions and weight information are summarized in Tables 4-1 and 4-2. Aerodynamic data were obtained from Reference 13.

Two mission profiles were selected to be studied. The first is an all-supersonic mission ($M = 2.4$) with a goal of 4000 miles range (Figure 4-2). The second mission is similar to the first, except that there is a 600-mile subsonic cruise leg preceding the supersonic leg. Mission studies performed herein vary the engine size and suppressor system to match a noise goal, allowing range to be the dependent variable while holding aircraft takeoff gross weight, payload, takeoff installed thrust, and balance field length constant.

Takeoff, climbout, and landing profiles for the noise evaluation are based on the aircraft flight trajectories accomplished by General Electric as part of the previous Supersonic Cruise Aircraft Research (SCAR) studies, Reference 14.

4.2 CYCLE SELECTION

The aircraft engine integration was accomplished based on previous SCAR studies including the NASA Advanced Supersonic Propulsion Study, Contract NAS3-19544, Reference 14.

The turbojet cycle used herein was defined by General Electric and studied by one of the NASA AST Study airframe contractors. It was selected because it represents a realistic advanced supersonic transport propulsion system as perceived by engine designers.

The engine incorporates the use of advanced materials and improved component efficiencies. The engine cycle characteristics of the dual-rotor turbojet engine are summarized as follows:

Geometry		Wing	Horiz	Vert	Vert Pin on Wing
Area (Gross)	S ft ²	10996.365	600.000	109.000	233.275 EA
MAC (Gross)	C in.	1343.0684	254.964	194.124	310.560
Area (Ref)	S ft ²	9969.000	————	————	————
MAC (Ref)	C in.	1154.8625	————	————	————
Area (Exposed)	S ft ²	————	441.0	————	————
Span	b ft	137.7778	32.0	7.6	10.75
Aspect Ratio (Gross)		1.72627	1.707	0.527	0.495
Aspect Ratio (Ref)		1.90417	————	————	————
Sweep Λ LE	deg	74.0, 70.84, 69.00	60.64	68.20	73.42
Root Chord	in.	2196.935	367.200	278.400	458.400
Tip Chord	in.	211.6667	62.80	66.00	62.40
Root T/C	%	See Fig V-7	3.0	2.999	2.996
Tip T/C	%	See Fig V-7	3.0	2.996	2.996
Taper Ratio		————	0.257	0.237	0.136
Incidence	deg	————	————	————	————
Dihedral	deg	————	-15.0	————	————
Vol Coeff (Gross)	V	————	0.070	0.011	0.026
Vol Coeff (Ref)	V	————	0.090	0.012	0.029

Mod. W.T. Data	* Number	Area ft ² Each
t ₁	1 and 2	146
t ₂	3 and 4	100
t ₃	5 and 6	61
t ₄	7 and 8	91
L ₁	9 and 10	198
L ₂	11 and 12	195
L ₃	13 and 14	92
	15 and 16	40
	17 and 18	26
	19 and 20	18
	21 and 22	6
	23 and 24	8

* Odd Numbers - Left Wing
Even Numbers - Right Wing

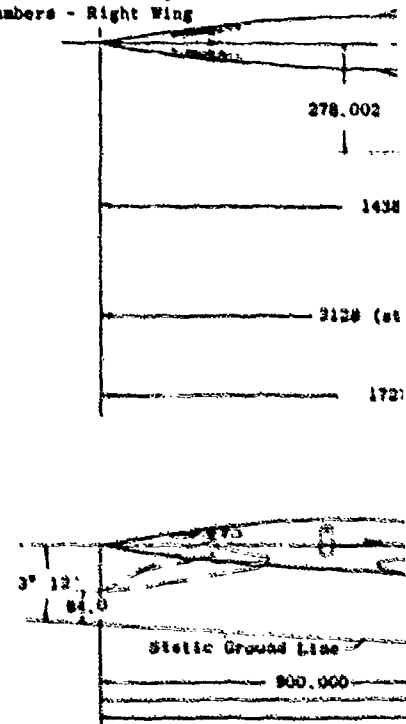
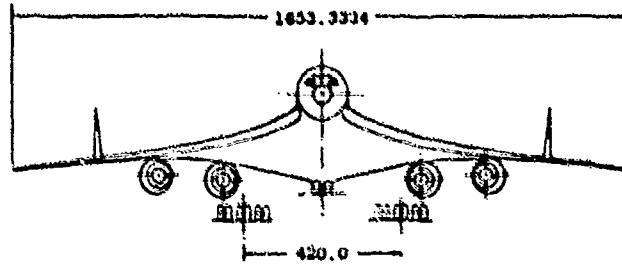


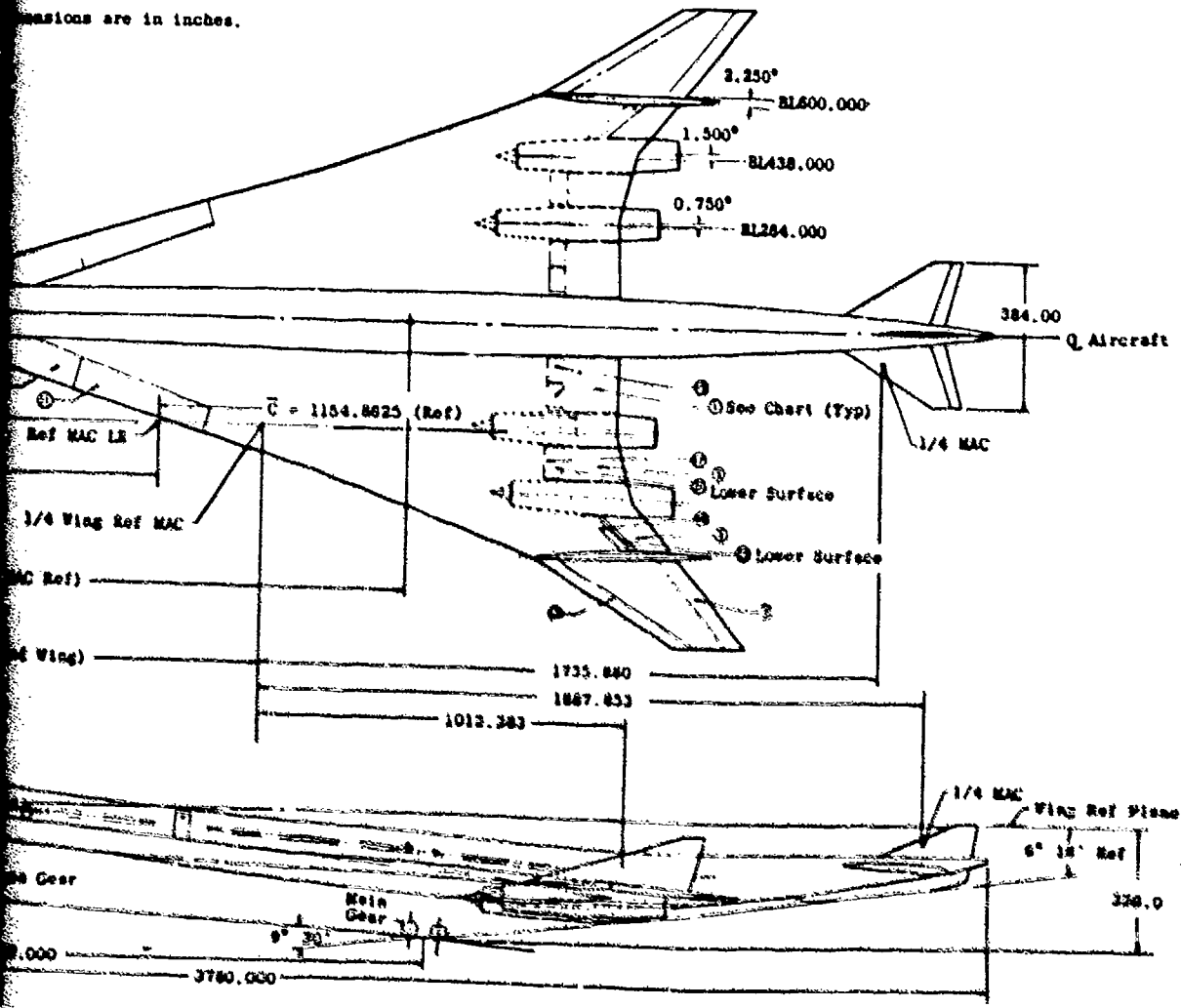
Figure 4-1. NASA Reference

Scale - meters
0 10 20

Scale - inches
0 200 400 600

Scale - feet
0 20 30 40 50

Dimensions are in inches.



Aircraft Configuration.

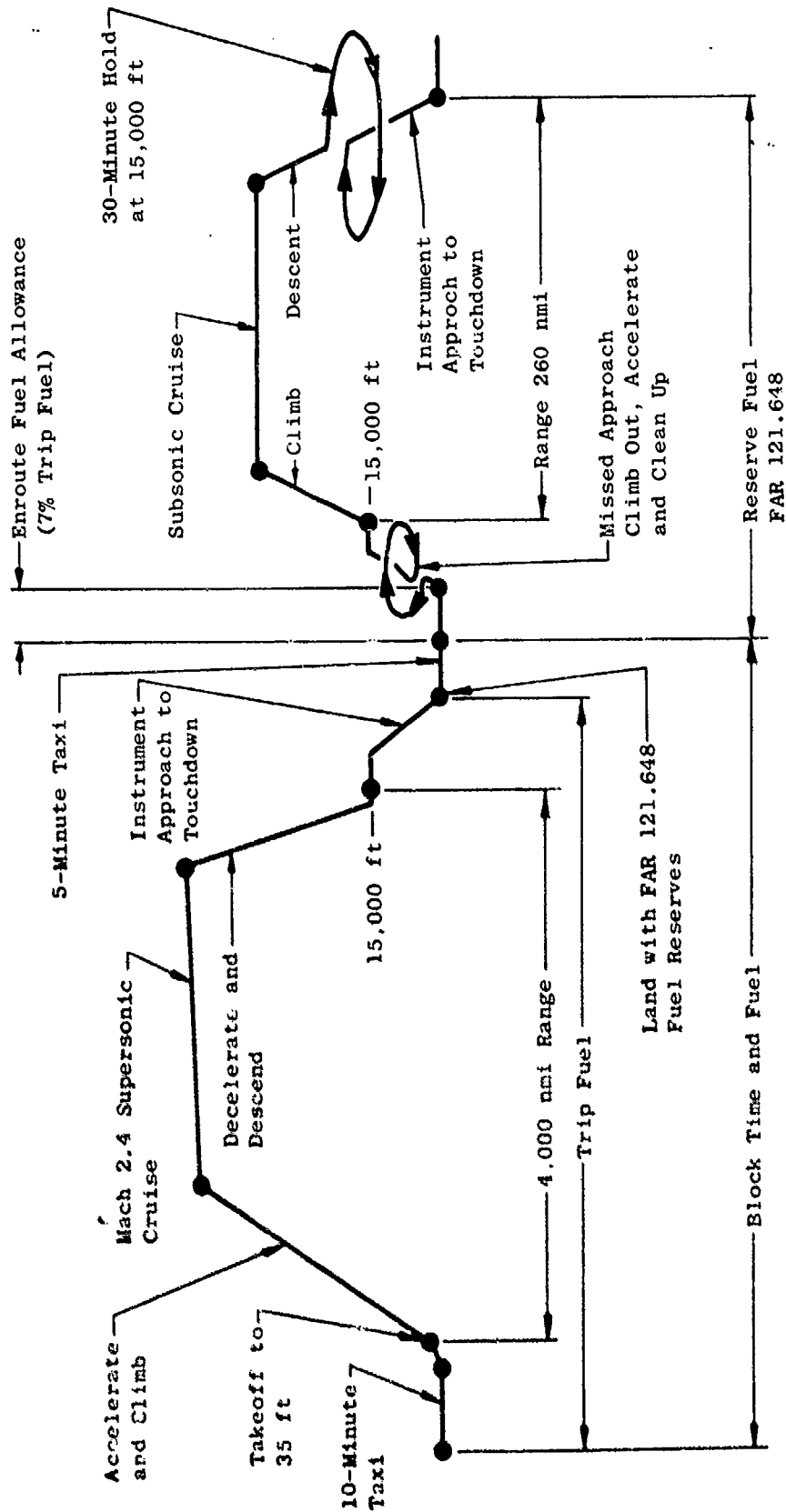
2

Table 4-1. Reference Configuration Geometric Characteristics.

Geometry	Wing	Horiz	Vert	Vert Fin on Wing
Area (Gross) S ft ²	10996.365	600.000	109.000	233.275 each
Mac (Gross) C in.	1343.0684	254.964	194.124	310.560
Area (Ref.) S ft ²	9963.000	---	---	---
Mac (Ref.) C in.	1154.8625	---	---	---
Area (Exposed) S ft ²	---	441.0	---	---
Span b ft	137.7778	32.0	7.6	10.75
Aspect Ratio (Gross)	1.72627	1.707	0.527	0.495
Aspect Ratio (Ref.)	1.90417	---	---	---
Sweep Ale deg	74.0; 70.84;	60.64	68.20	73.42
	60.0			
Root Chord in.	2196.935	367.200	278.400	458.400
Tip Chord in.	211.6667	82.80	66.00	62.40
Root T/C %		3.0	2.996	2.996
Tip T/C %		3.0	2.996	2.996
Taper Ratio	---	0.257	0.237	0.136
Incidence deg	---	---	---	---
Dihedral deg	---	-15.0	---	---
Vol Coeff (Gross) v	---	0.070	0.011	0.026
Vol Coeff (Ref.) v	---	0.090	0.012	0.029
Total Aircraft TOGW Moment of Inertia	Ix, Roll 105,115 x 10 ⁻⁶ lb-in. ²	Iy, Pitch 339,028 lb-in. ²	Iz, Yaw 471,667 lb-in. ²	

Table 4-2. Reference Configuration Weight Summary.

Item	Weight (lbs.)
Wing	83,347
Horizontal Tail	5,271
Vertical Tail	4,735
Canard	0
Fuselage	54,314
Landing Gear	28,965
Nacelle	19,015
Structure Total	(195,646)
Engines	59,832
Thrust Reversers	10,601
Miscellaneous Systems	1,780
Fuel System-Tanks and Plumbing	5,781
-Insulation	0
Propulsion Total	(77,994)
Surface Controls	9,981
Auxiliary Power	0
Instruments	3,400
Hydraulics	5,600
Electrical	5,050
Avionics	2,690
Furnishings and Equipment	25,111
Air Conditioning	8,200
Anti-icing	210
Systems and Equipment Total	(60,242)
Mfg and Certif Tolerance	0
Weight Empty	333,882
Crew and Baggage-Flight,	675
-Cabin,	1,640
Unusable Fuel	2,335
Engine Oil	795
Passenger Service	8,852
Cargo Containers	2,960
Adjustment for Computer Deviation	0
Operating Weight	351,139
Passengers	(292) 48,180
Passenger Baggage	12,848
Cargo	0
Zero Fuel Weight	412,167
Mission Fuel	349,833
Design Gross Weight	762,000



Note: Horizontal axis is not to scale

Figure 4-2. Definition of Supersonic Mission Profile.

- Engine Airflow 770 lbs/sec
- Fan Pressure Ratio 3.7
- Engine Overall Pressure Ratio 16.2
- Bypass Ratio 0.07
- High Pressure Turbine Rotor Inlet Temperature, Maximum 2500° F
- High Pressure Turbine Rotor Inlet Temperature, Cruise 2400° F
- Compressor Discharge Temperature, Maximum 1120° F
- Installed Engine Performance Includes Inlet and Afterbody Drags

A double bypass variable cycle engine (VCE) was defined for a supersonic cruise design Mach number of 2.4 with a fan which is high-flowed at takeoff. This engine concept provides the required takeoff thrust at lower jet velocity, plus cruise characteristics that better match the airplane performance requirements. Approximately 10 percent in engine weight is saved compared to a conventional cycle engine sized for the same takeoff noise level. The high flowing of the fan for takeoff is accomplished with a VCE by designing the fan for the high flow takeoff requirement and then by supplying the extra air through an auxiliary inlet feature which makes up part of the variable engine geometry.

The double bypass VCE can hold subsonic cruise airflow constant down to approximately 50 percent maximum dry thrust (which is the aircraft subsonic cruise requirement). Thus, the inlet spillage drag is zero, and the thrust loss due to afterbody drag is reduced by about one third. These reductions in installation drag improve the mission range capability substantially for the mission with the initial 600 nautical mile subsonic cruise leg; the all-supersonic mission range improves due to the good subsonic performance which reduces the fuel reserves that must be carried. The double bypass variable cycle engine defined for this study is described below.

- Engine Airflow 840 lbs/sec
- Fan Pressure Ratio 3.7
- Engine Overall Pressure Ratio 16.1
- Bypass Ratio 0.25
- High Pressure Turbine Rotor Inlet Temperature, Maximum 2800° F

- High Pressure Turbine Rotor Inlet Temperature, Cruise 2700° F
- Compressor Discharge Temperature, Maximum 1150° F
- Installed Engine Performance Includes Inlet and Afterbody Drags

The advanced turbojet and the double bypass variable cycle engine were operated to the inlet characteristics shown in Figure 4-3. These inlet characteristics were used to generate the installed performance of each engine.

Baseline engine performance was generated for mission and noise calculations. The data for noise calculations and thrust coefficients for the respective selected suppressors as discussed in Section 4.3 "Suppressor Selection" were measured. At rotation, the three thrust levels were selected to provide a takeoff thrust and noise range compatible with subsequent engine scaling to meet thrust requirements (61,400 lbs for 10,500 ft balanced field length and 53,500 lbs for a 12,500 ft field length). Each of the rotation data points dictated the suppressor design exhaust area, A_8 , for three advanced turbojet engine suppressors. With the respective suppressor designs, the engine was operated at the community point, 0.35M + 18° F and 1250 ft (12,500 ft BFL) and 1850 ft (18,500 ft BFL), respectively, at three thrust levels; the thrust levels were selected to accommodate scaling the engine size and to have performance data at the required thrust level of 34,000 lbs. The engine was operated at approach, 0.22M/370 ft/+ 18° F, with the exhaust suppressors retracted at three thrust levels selected to accommodate scaling the engine size and to have performance data at the required thrust level of 15,000 lbs.

Engine performance data were generated for mission analysis at supersonic cruise, subsonic cruise, hold, and climb/acceleration flight conditions.

A similar matrix of engine performance data was generated with the double bypass variable cycle engine with dual-flow suppressors.

The engine sizes were scaled to obtain the rotation required thrusts of 61,400 lbs and 53,500 lbs.

4.3 SUPPRESSOR SELECTION

The suppressors selected for evaluation in the aircraft integration study were chosen to illustrate the sensitivity of aircraft operating economics to various exhaust nozzle systems and were based on the acoustic and aerodynamic test data availability from previous studies. Four exhaust nozzle systems, including a baseline conical, were evaluated on the turbojet engine. The details of the suppressor configurations are summarized in Table 4-3. These were AR = 2.0 36-chute nozzle, AR = 2.5 36-chute nozzle, AR = 2.1 32-chute nozzle, and AR = 2.9 57-tube with a treated ejector nozzle.

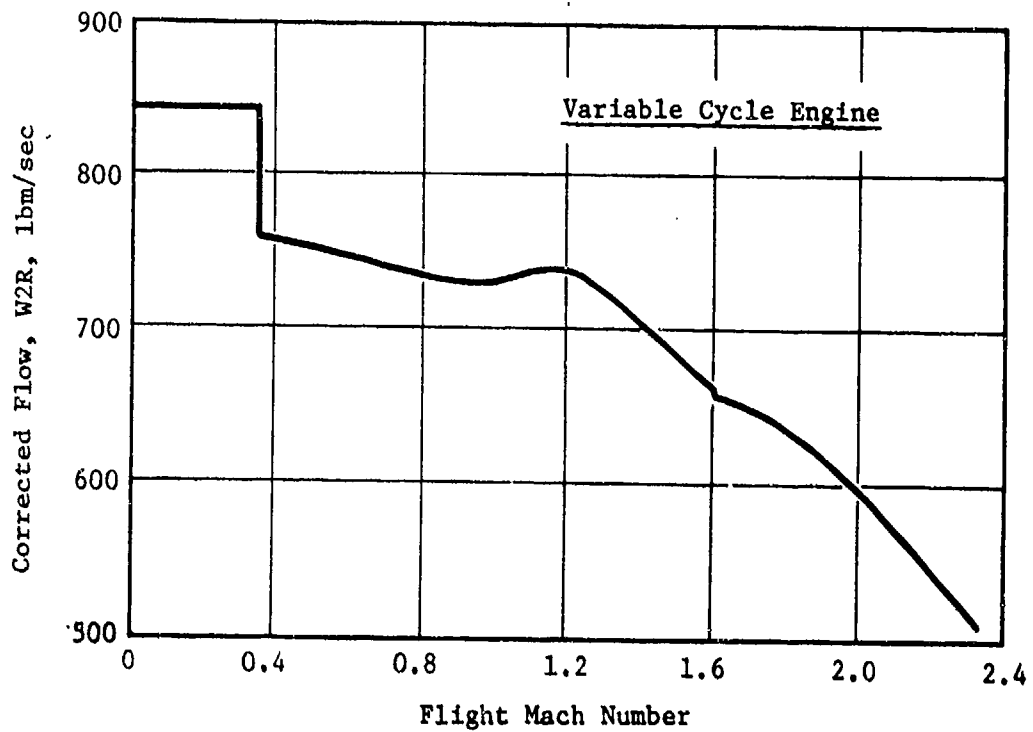
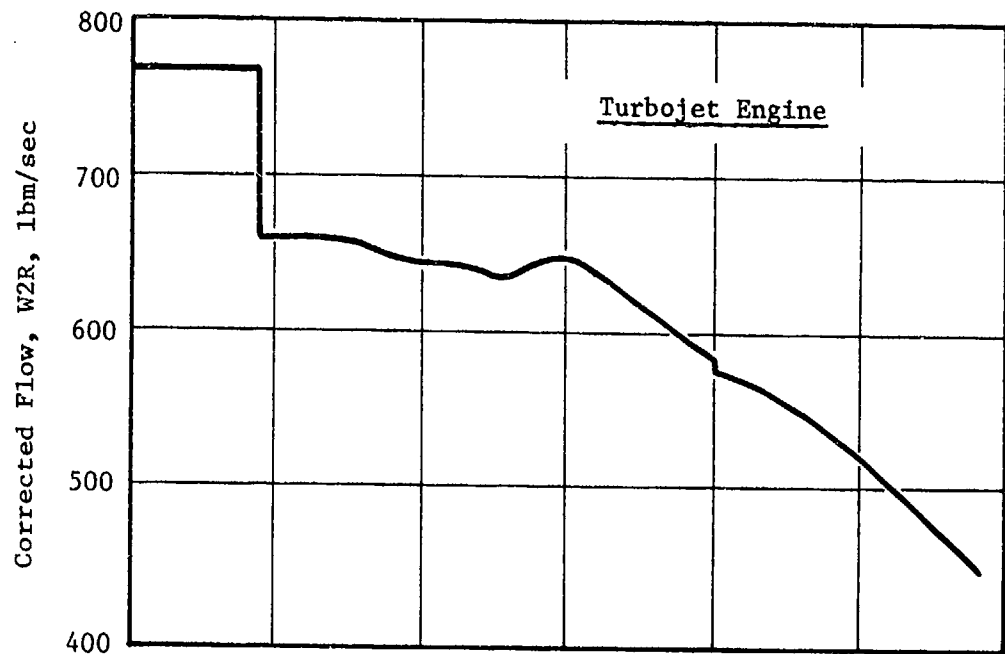


Figure 4-3. Inlet/Engine Airflow Match.

Table 4-3. Definition of Suppressors Used for the Aircraft Integration Study.

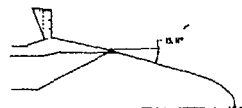
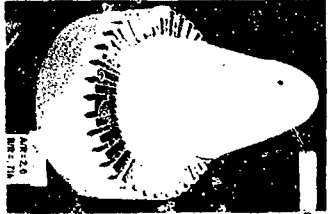
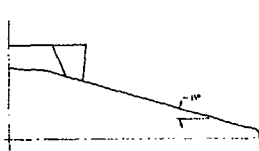
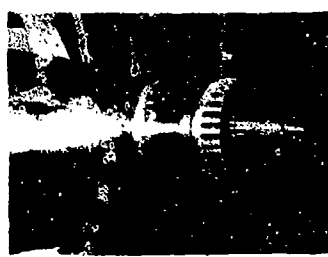
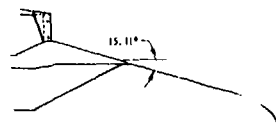

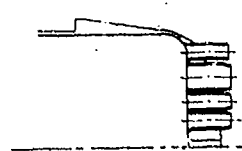
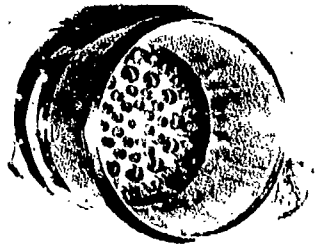
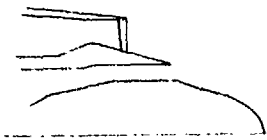
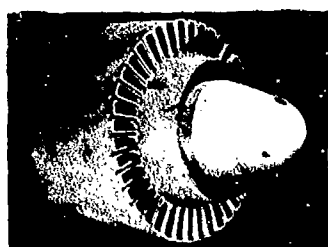
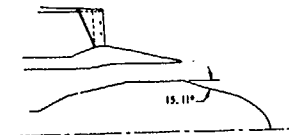
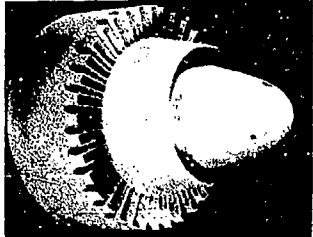
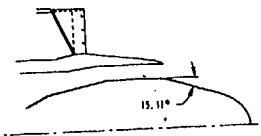

<u>Configuration</u>	<u>Engine Applicability</u>	<u>Schematic</u>	<u>Photograph</u>
AR = 2.0 36 Chute	Turbojet		
AR = 2.1 32 Chute	Turbojet		
AR = 2.5 36 Chute	Turbojet		
AR = 2.9 57 Tube Nozzle + AR = 3.0 Acoustically Treated Ejector	Turbojet		
AR = 1.75 40 Shallow Chute	Variable Cycle Engine		

Table 4-3. Definition of Suppressors Used for the Aircraft Integration Study (Concluded).

<u>Configuration</u>	<u>Engine Applicability</u>	<u>Schematic</u>	<u>Photograph</u>
AR = 2.0 36 Chute	Variable Cycle Engine		
AR = 2.5 36 Chute	Variable Cycle Engine		

The configurations selected all had high static peak PNL suppression levels in excess of 8 PNdB. Suppressor systems such as plug nozzles and low element number lobe nozzles were not considered because the suppression levels were not sufficient to have favorable range characteristics and still attain the required noise goals. Spoke nozzle configurations were also not considered because of their poor aerodynamic performance and limited increase in suppression relative to chute- and tube-type configurations (as discussed in Section 3.0).

The two 36-chute configurations (area ratios of 2.0 and 2.5) were chosen to illustrate the impact of suppressor area ratio, an important acoustic design parameter, on the aircraft mission. The two configurations also represent high radius ratio exhaust nozzle suppression systems which would adapt to the designs envisioned for advanced turbojet engines. The AR = 2.1 32-chute and AR = 2.9 57-tube with treated ejector nozzles were selected because of the high suppression and performance demonstrated relative to other types of single-flow suppressor nozzles (as discussed in Section 3.0). These configurations were the configurations defined as a result of studies described in References 4 and 5. The static scale-model suppression levels have also been verified by full-scale engine acoustic test programs.

Four configurations were chosen for evaluation on the variable cycle engine and are also summarized in Table 4-3. They are a baseline configuration which was a fully mixed conical nozzle, an AR = 1.75 40-shallow chute nozzle, an AR = 2.0 36-chute nozzle, and an AR = 2.5 36-chute nozzle. The suppressors chosen for the variable cycle engine differ from the turbojet suppressors. The VCE suppressors extend only across the outer stream of the dual-flow nozzle. The turbojet suppressors extend over the entire exhaust plane. These configurations were selected from the Task 3 program because of the availability of wind-on performance data. The selection of the area ratios of 2.0 and 2.5 was again to establish the impact of area ratio variation on aircraft mission, utilizing engines which have dual-flow exhaust systems. The AR = 1.75 40-shallow chute was chosen as a compromise between deep chute nozzles and spoke nozzles. Although spoke nozzles have significantly poorer performance than chute nozzles, they are much more adaptable to stowage, requiring a less complex and usually lighter and more reliable system. The shallow chute, basically, maintains the advantages of stowage but allows a significant performance improvement over spoke nozzle configurations.

The results of the mechanical design studies to evaluate the impact of each of these configurations on the aircraft system are discussed in Section 4.4.

4.4 MECHANICAL DESIGN STUDIES

The exhaust system configuration weight and size are affected considerably by the jet noise suppression arrangement used. Therefore, exhaust systems for each selected suppressor configuration and for the baseline conical and the baseline unsuppressed turbojet nozzles were studied from a mechanical designer's perspective to determine weight and maximum diameter variations.

A schematic of each exhaust system was made incorporating the scaled-up suppressor model based on the cycle data matched to each suppressor configuration. These schematics are typical of the type used to initiate layout drawings and to estimate weights during preliminary design. The outline drawings showed the maximum exhaust system radius (used to evaluate drag changes). The outline drawings were also the basis of estimating exhaust system weights using standard scaling techniques (which have been derived from past production and from similar current preliminary design exhaust systems). Figures 4-4 and 4-5 show typical suppressed single- and dual-exhaust stream nozzle flowpaths.

The suppressed exhaust systems are modifications to single-flow and conical-flow plug nozzles and include the following major features:

1. A plug nozzle to provide a high radius ratio exhaust discharge and storage space for suppressor devices during unsuppressed (stowed) operation. Plug nozzle performance is excellent over a wide range of exhaust pressure ratios.
2. A translating external cylindrical shroud positioned axially to obtain the optimum internal expansion area ratio for good performance throughout the wide range of pressure ratio in the mission.
3. Integration of thrust reverser cascades into the translating shroud to minimize actuation requirements.
4. A low temperature augmentor for thrust augmentation during climb.

The maximum diameter sizing requirement of the exhaust system has the largest effect on weight and exhaust nozzle drag. This maximum diameter is determined as the result of one of the following sizing checks:

1. A stackup is made through the turbine allowing for structure outside of the turbine tip, height of the bypass airflow duct, space for the translating shroud support structure, thickness of the translating shroud, and thickness of the outer cowl.
2. A stackup is made through the exhaust duct that provides for a plug support beam and sizes the duct for the augmented referenced Mach number.
3. The translating shroud exit is sized to closely maintain the full expansion area at supersonic cruise.
4. The requirements for jet noise suppressor implementation. The primary suppressor sizing parameters are exit radius ratio (R_1/R_0) and exit base area ratio ($A_{base}/A_{throat} = AR$).

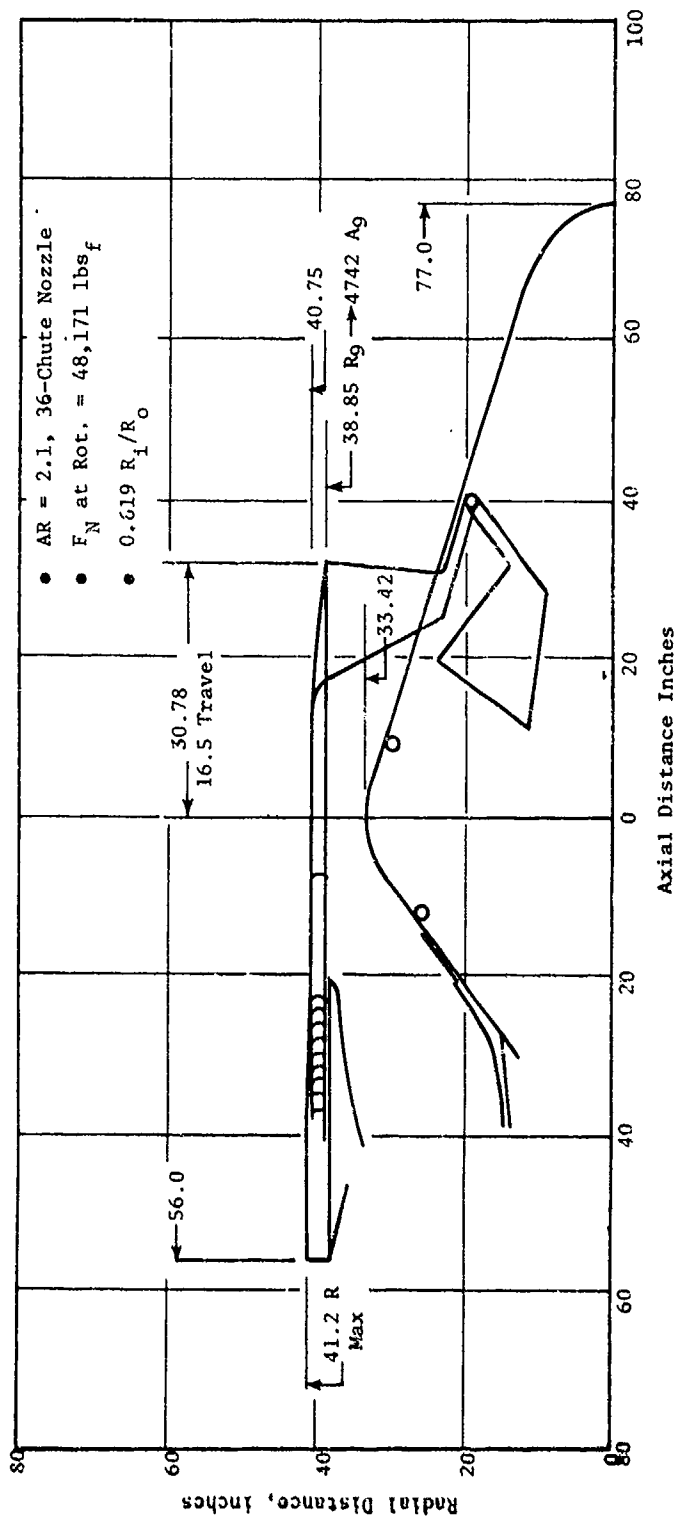


Figure 4-4. Typical Turbojet Exhaust System Schematic.

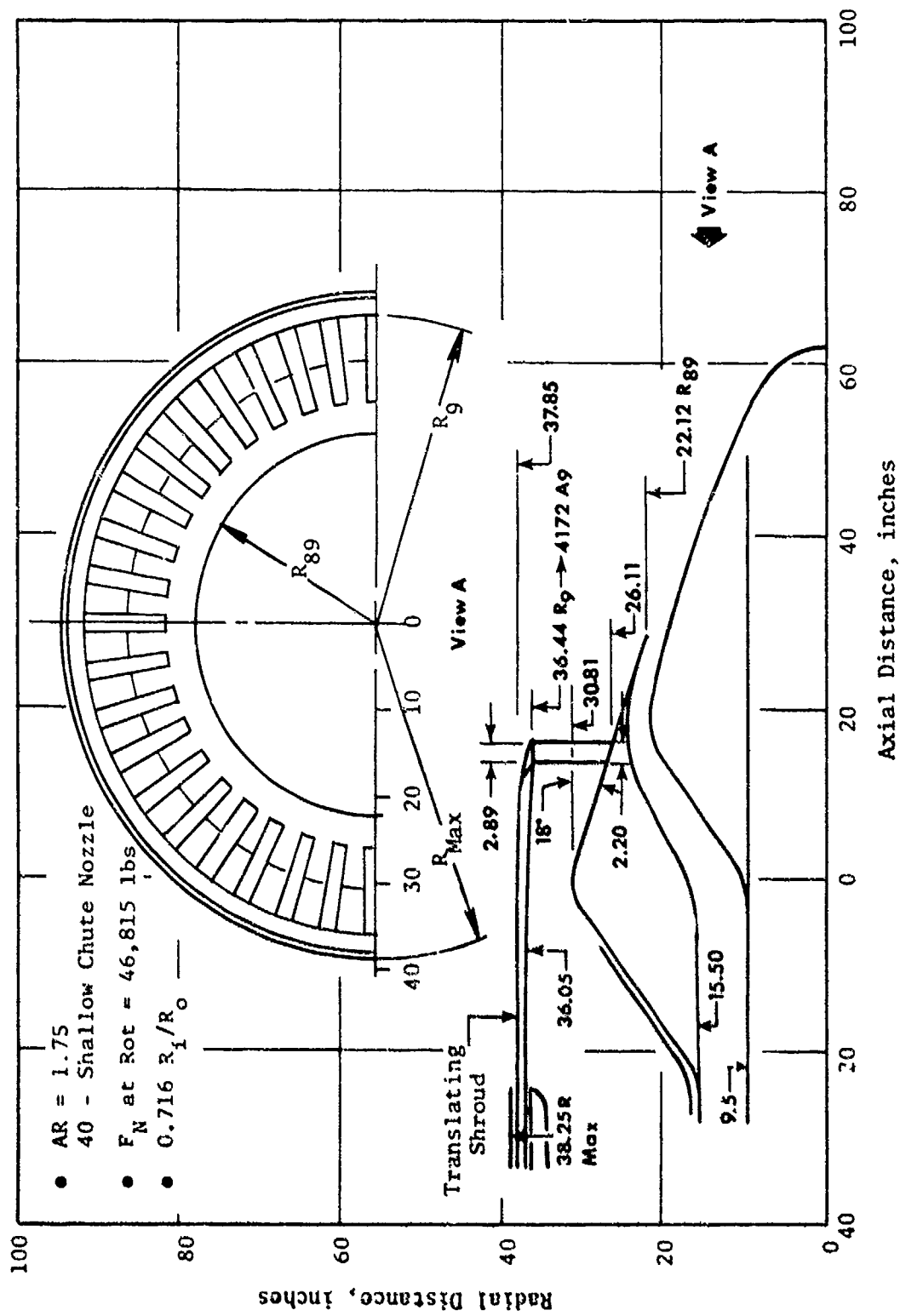


Figure 4-5. Typical VCE Exhaust System Schematic.

The stackups through the turbine frame and the exhaust duct generally do not determine the nozzle maximum diameter for AST engine cycles. Unsuppressed exhaust system maximum diameter is dictated by the full expansion area required at supersonic cruise. Suppressor area ratio and radius ratio requirements tend to make the nozzle larger than that required for full expansion. Therefore, a trade between suppressor requirements and increased exhaust system weight and drag must be made. The relationships between the nozzle exit radius (R_0), throat area (A_g), area ratio (AR), exit angle (α), and radius ratio (R_1/R_0) are shown in Figure 4-6. The discharge angle has a small effect on the nozzle radius. The graph on Figure 4-6 shows the increase in R_0 for any area ratio and radius ratios. An AR = 1 has no mechanical suppression device. Also shown on Figure 4-6 are the specific nozzles studied in this program and the full expansion size for the cycles used. A recommended maximum design limit of $R_0/\sqrt{A_g} \cos \alpha = 2.1$ is shown because values above 2.1 would result in excessively large and heavy exhaust systems. Figure 4-7 shows the weight trend with increasing radius ratio for an annular nozzle (AR = 1). Weight trends for mechanically suppressed nozzles (AR > 1) are the same, but the base weight at any R_1/R_0 would be higher because the nozzle diameter is larger when a mechanical suppression system is added.

The results of this study are summarized on Table 4-4. The dual-exhaust and single-exhaust stream nozzle diameters and weights relative to the unsuppressed dual- and single-stream plug nozzles for the selected suppressor models are presented. The nozzle diameter changes and weight changes correlate with the model positions shown in the graph of Figure 4-6. These exhaust system diameter and weight results were used in the studies to determine the impact on the performance, noise, and weight trade-offs. Exhaust system weight was scaled to the correct size necessary to meet the takeoff thrust requirements by using the following relationships:

$$\text{Exhaust system weight} = \left(\frac{\text{Takeoff Airflow}}{\text{Reference Airflow}} \right)^{1.2} \times \left(\frac{\text{Baseline Exhaust System Weight}}{\text{System Weight}} \right)$$

where reference airflow was 770 lbm/sec for the turbojet engine and 840 lbm/sec for the variable cycle engine.

4.5 NOISE PREDICTION METHODS

Jet noise estimates were required at the maximum sideline and community monitoring locations in order to size the propulsion suppressor systems to meet specified noise goals. These estimates were accomplished using the prediction procedure which was utilized in the NASA AST Studies conducted under Contract NASJ-19544. The procedure consists of the following steps:

1. The fully expanded isentropic velocity, weight flow, and total temperature are determined for each stream.

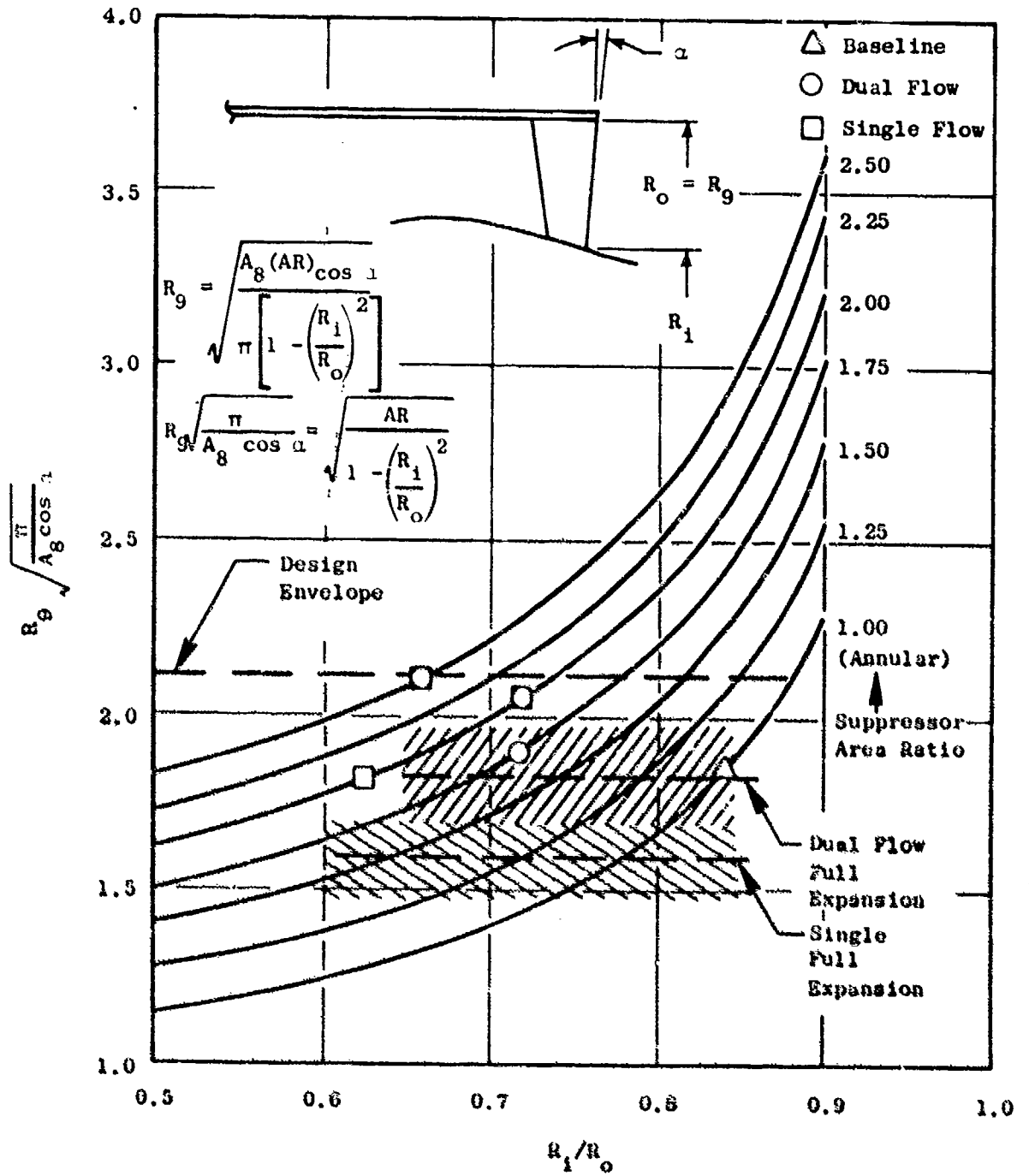


Figure 4-6. Relationship Between Nozzle Exit Radius, Throat Area, and Area Ratio.

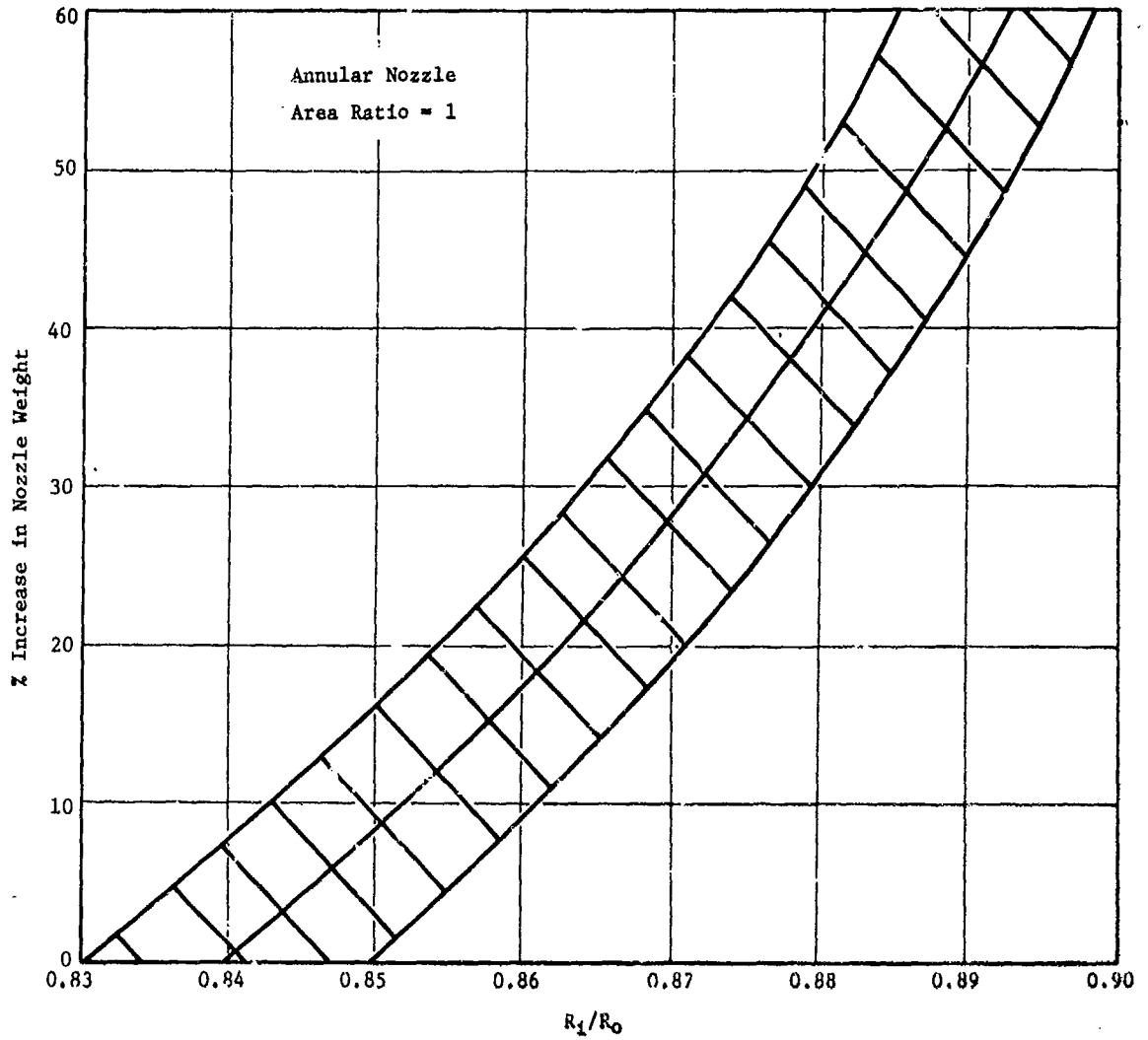


Figure 4-7. Weight Increase as a Function of Radius Ratio.

Table 4-4. Summary of Suppressor Weight Estimates.

a. Turbojet				
Configuration	AR=2.1 32-chute	AR=2.0 30-chute	AR=2.5 36-chute	AR=2.9 57-tube & Treated Ejector
Engine Airflow	770	770	770	770
Suppressor Area Ratio	2.1	2.0	2.5	2.8
Number of Elements	32	36	36	57
Element Type	Deep Chute	Deep Chute	Deep Chute	Tube
Suppressor Radius Ratio	0.619	0.716	0.652	N/A
Δ Diameter, in.	0.4	10.0	11.0	15.2
Δ Weight, lbs	1150	1800	2150	4050

b. Variable Cycle Engine			
Configuration	AR=2.0 36-chute	AR=1.75 Shallow Chute	AR=2.5 36-chute
Engine Airflow	840	840	840
Suppressor Area Ratio	2.0	1.75	2.5
Number of Elements	36	40	36
Element Type	Deep Chute	Shallow Chute	Deep Chute
Suppressor Radius Ratio	0.716	0.716	0.652
Δ Diameter, in.	9.4	1.5	10.3
Δ Weight, lbs	1300	550	1900

2. The ideal gross thrust, F_g , is computed for each stream using

$$F_g = V w/g, \text{ single flow; } F_g = \frac{v^i w^i + v^o w^o}{g}, \text{ dual flow}$$

3. The mass average velocity, V_{ma} , and total temperature, T_{ma} , are calculated using

$$V_{ma} = \frac{v^o w^o + v^i w^i}{w^o + w^i} \quad T_{ma} = \frac{T_T^o + w^o + T_T^i w^i}{w^o + w^i}$$

4. A modified density parameter $10 \log (\rho_{ma}/\rho_o)^{\omega-1}$ is calculated based on the mass averaged parameters. The exponent ω is defined in Figure 4-8 per Reference 15.
5. The normalized Peak PNL, PNL_N , at 2128 ft sideline is defined on Figure 4-9 for the conical reference nozzle. This curve was established based on data from References 8 and 9.
6. The normalized Peak PNL level, PNL_N , is extrapolated to the desired distance using

$$PNL_N \text{ at 2128 ft S.L.} - 25 \log \left(\frac{R}{2127} \right)$$

where R is the desired distance in feet.

7. The static peak PNL noise (PNL_S) level at the appropriate conditions is then calculated using

$$PNL_S = PNL_N + 10 \log (F_g) + 10 \log \left(\frac{\rho_{ma}}{\rho_o} \right)^{\omega-1}$$

8. The maximum angle flight effects are then determined

$$F.E. = 10 \log \left[\left(\frac{V_{ma}}{V_{ma} - V_a/c} \right)^5 \left(1 - \frac{V_a/c}{1135} \cos 140^\circ \right) \right]$$

The peak noise in flight, PNL_F , is then defined as

$$PNL_F = PNL_S + F.E.$$

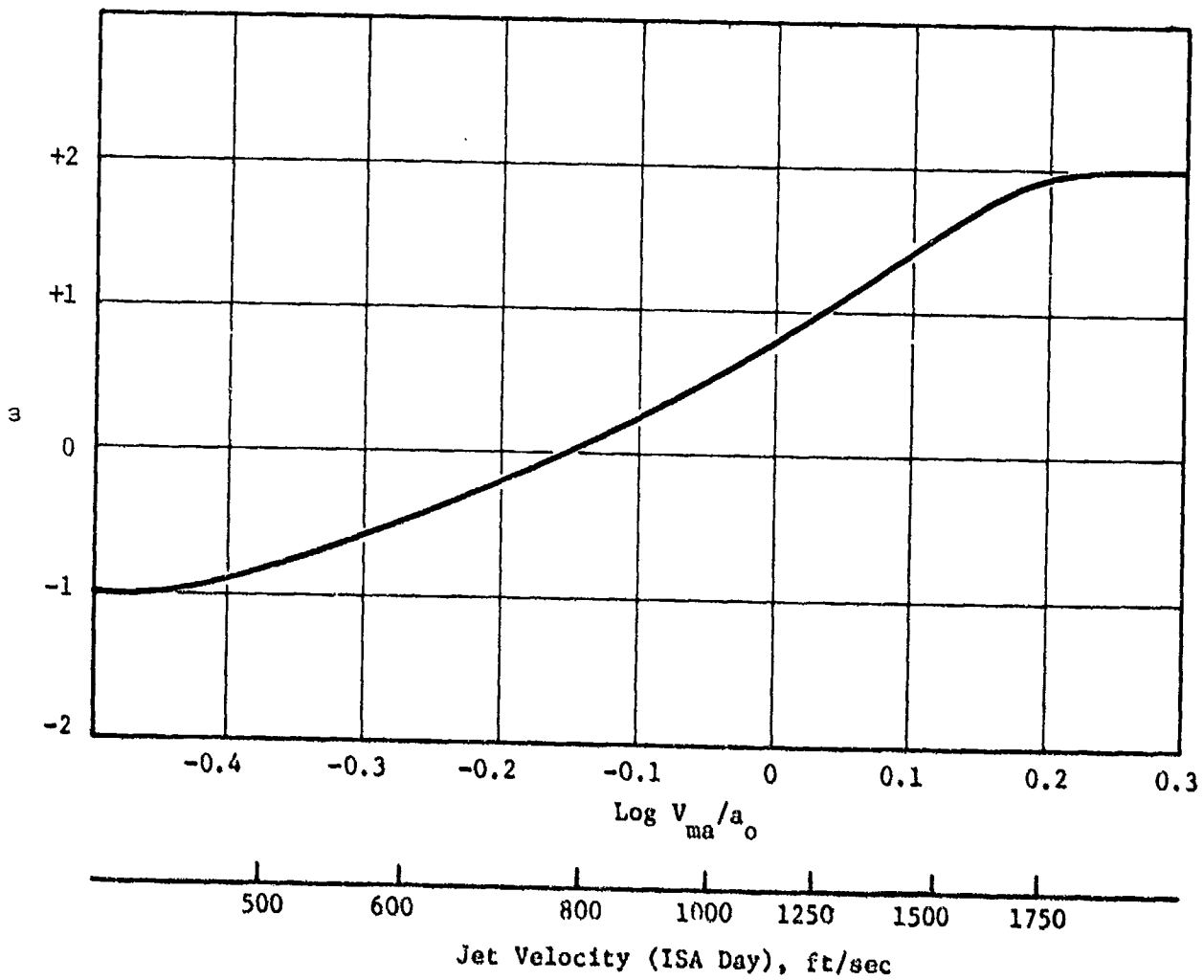


Figure 4-8. Definition of Jet Density Exponent (per Reference 15).

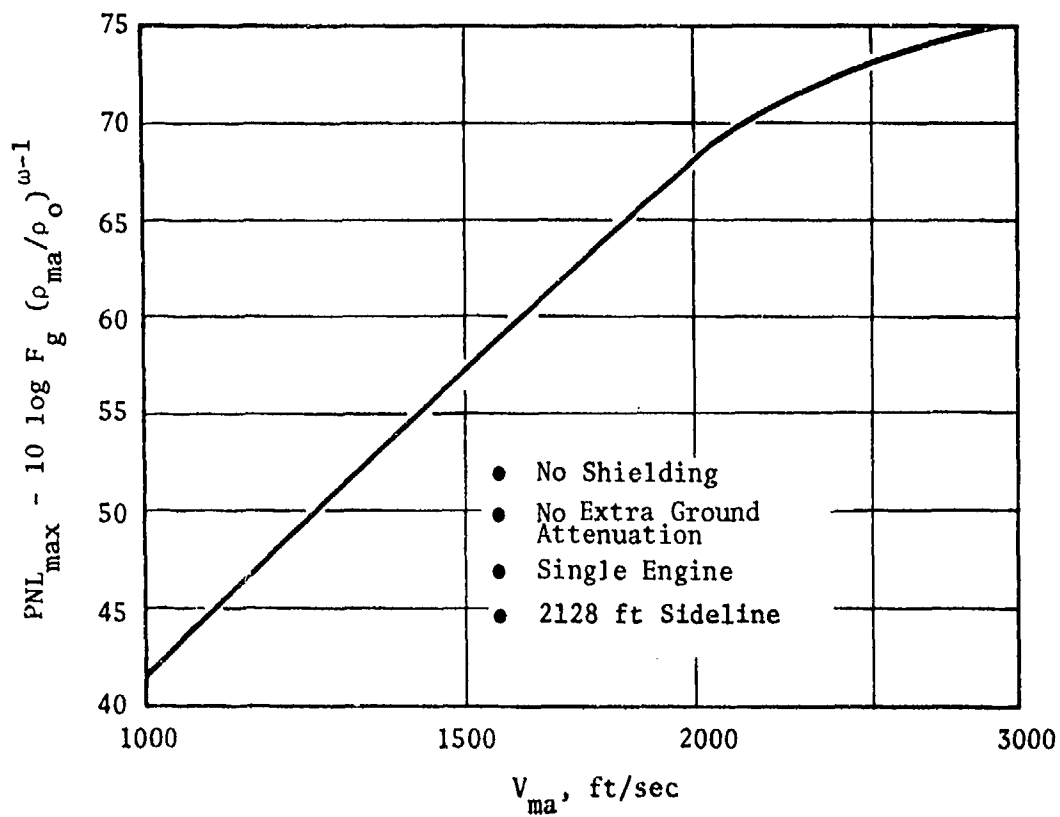
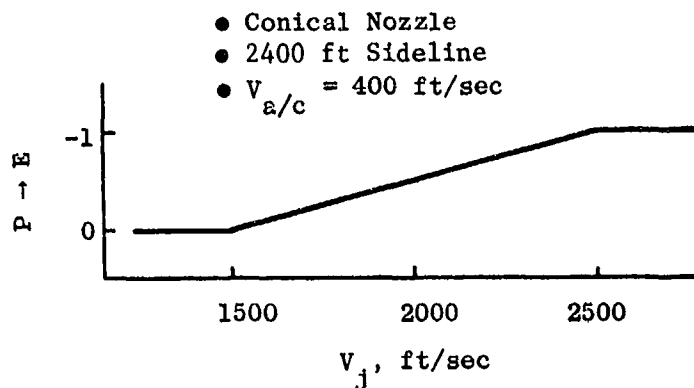


Figure 4-9. Definition of Conical Nozzle Normalized PNL.

Peak noise level of each baseline nozzle was established using this procedure. To predict the EPNL, however, the directivity or duration of noise must be considered. This is accomplished by applying a duration correction factor, designed P-E, to the peak PNL. This correction factor is defined for the conical nozzle as follows:



This curve was established by studies which calculated the duration correction using measured noise directivity patterns corrected for flight effects. The duration corrections for other distances and aircraft velocity may be established by utilizing the following corrections:

$$\text{Distance Correction: } 10 \log \frac{R}{2400}$$

$$\text{Aircraft Velocity Correction: } -10 \log \frac{V_a/c}{400}$$

Application of this duration correction to PNL_f allows the calculation of EPNL per the following:

$$EPNL = PNL_f + P-E$$

The EPNL is corrected for the number of engines, N , by adding $10 \log_{10} N$. This correction factor for all cases is 6.0 dB. This EPNL is then corrected for shielding and ground reflections. The shielding corrections were 2.0 dB at rotation and 0 dB at the community monitoring point. The ground reflection corrections were 1 dB at both monitoring points.

A modified procedure is employed for suppressor nozzle noise predictions. The noise reduction caused by each suppressor is established by scaling the scale-model data for each suppressor to be representative of a full-size engine. The normalized PNL levels are plotted as a function of jet velocity. Peak PNL suppression levels are then obtained by subtracting the normalized PNL level of the suppressor from the normalized PNL level of the fully mixed conical nozzle at the specified velocity conditions. The suppression levels for each of the seven configurations evaluated are summarized on Figures 4-10 and 4-11. The peak noise angle flight effects corrections are determined using the velocity index method presented in Reference 16. An additional correction is applied to the single-flow configurations because the peak noise of the suppressors does not occur at 140° . The correction was established noting that the suppressors normally peak at 120° . The flight effects were, therefore, applied to the peak PNL noise level assuming that the peak noise level occurred at 120° . The duration correction presented in Figure 4-12 was found to be generally applicable for suppressor nozzles.

This procedure allows the variation of Effective Perceived Noise Level, EPNL, at the sideline and community monitoring locations to be determined as a function of engine airflow size. This generalized procedure is illustrated on Figure 4-13 and also in Sketch 3 of Section 4.0. A specific example of how EPNL varies with engine airflow at the takeoff and community monitoring locations is presented on Figure 4-14 for the AR = 1.75 40-shallow chute nozzle.

The curves were established for each of the seven suppressor configurations and were used to determine the noise levels for any airflow size in the range investigated.

4.6 PROCEDURE FOR ECONOMIC EVALUATION

The measure of merit chosen as the basis of economic trade studies was aircraft range. Economic analysis estimates were conducted using methods similar to those used in AST studies for NASA. As stated previously, the general ground rules for this analysis are to hold aircraft takeoff gross weight, payload, and engine cycle constant (although an advanced turbojet and a variable cycle engine were each used). The engine size is then varied for each suppressor type studied in order to satisfy a noise goal. Each of two missions is analyzed and a range capability is calculated for each mission/suppressor/cycle evaluated.

The two missions used in the range performance evaluation include the supersonic mission (defined previously; see Figure 4-2) and the mission with a 600-mile subsonic cruise leg.

(1) Suppression Levels are Relative to a Conical Nozzle

- 2400 ft Sideline
- 590 F, 70% R.H.
- $A_{Total} = 1950 \text{ in.}^2$

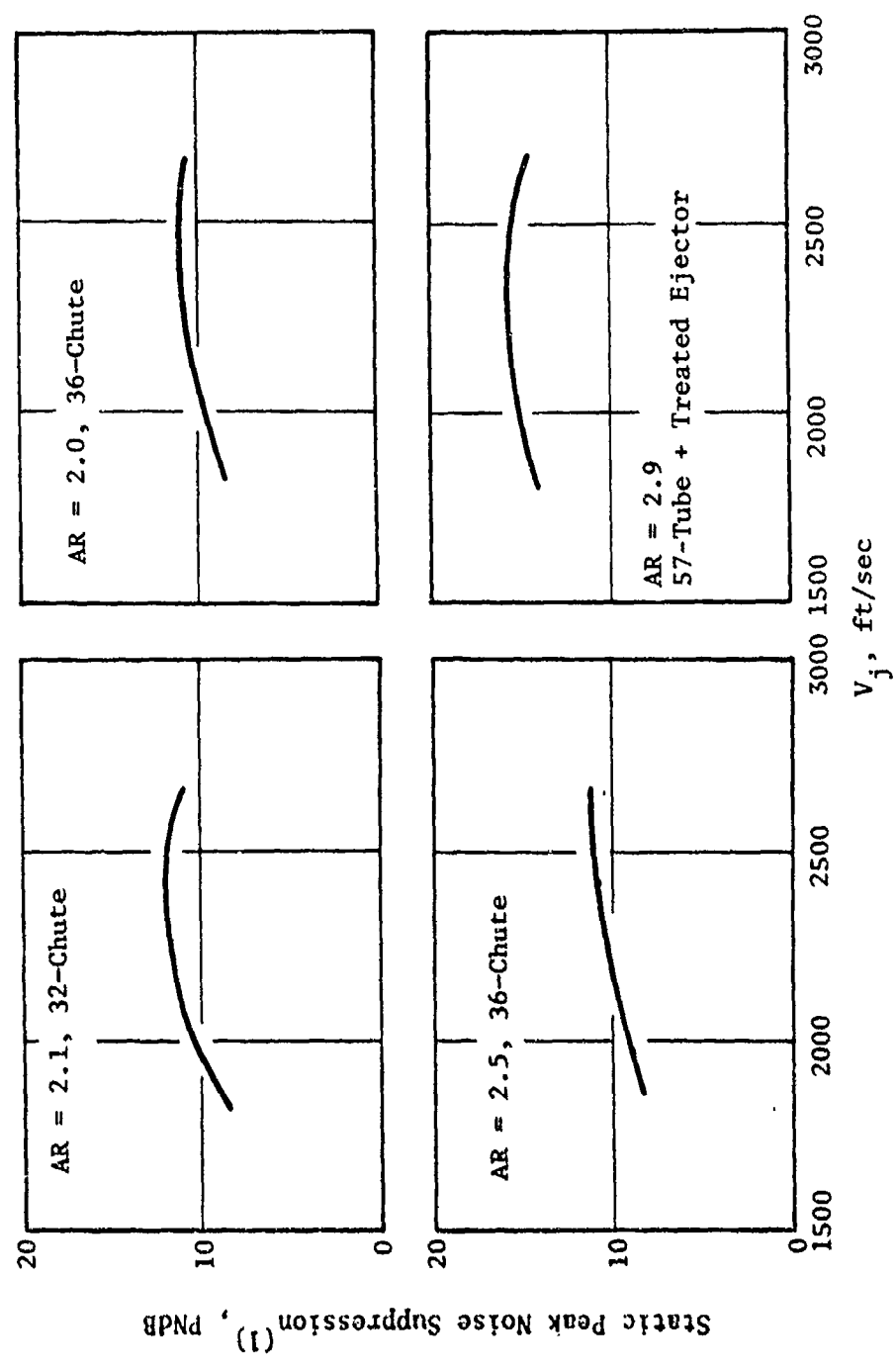
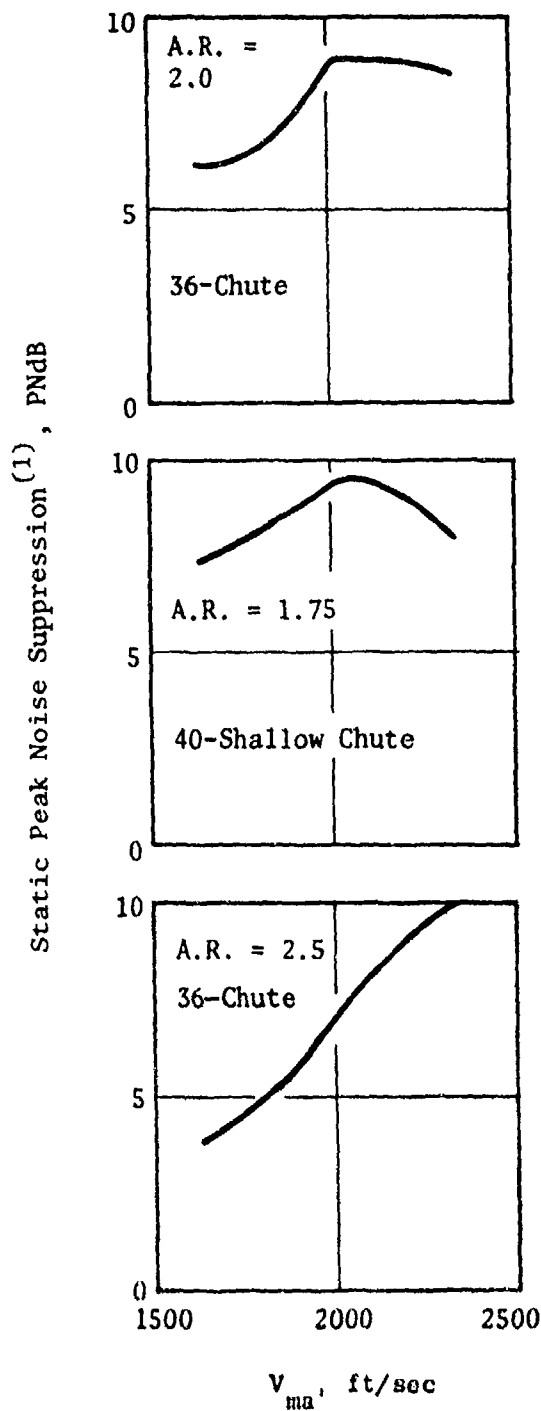


Figure 4-10. Summary of Single-Flow Nozzle Suppression Characteristics.



- 2400 ft Sideline
- 59° F, 70% R.H.
- $A_{Total} = 1950 \text{ in.}^2$

(1) Suppression Levels are Relative to a Conical Nozzle of the Same Specific Thrust.

Figure 4-11. Summary of Dual-Flow Nozzle Static Suppression Characteristics.

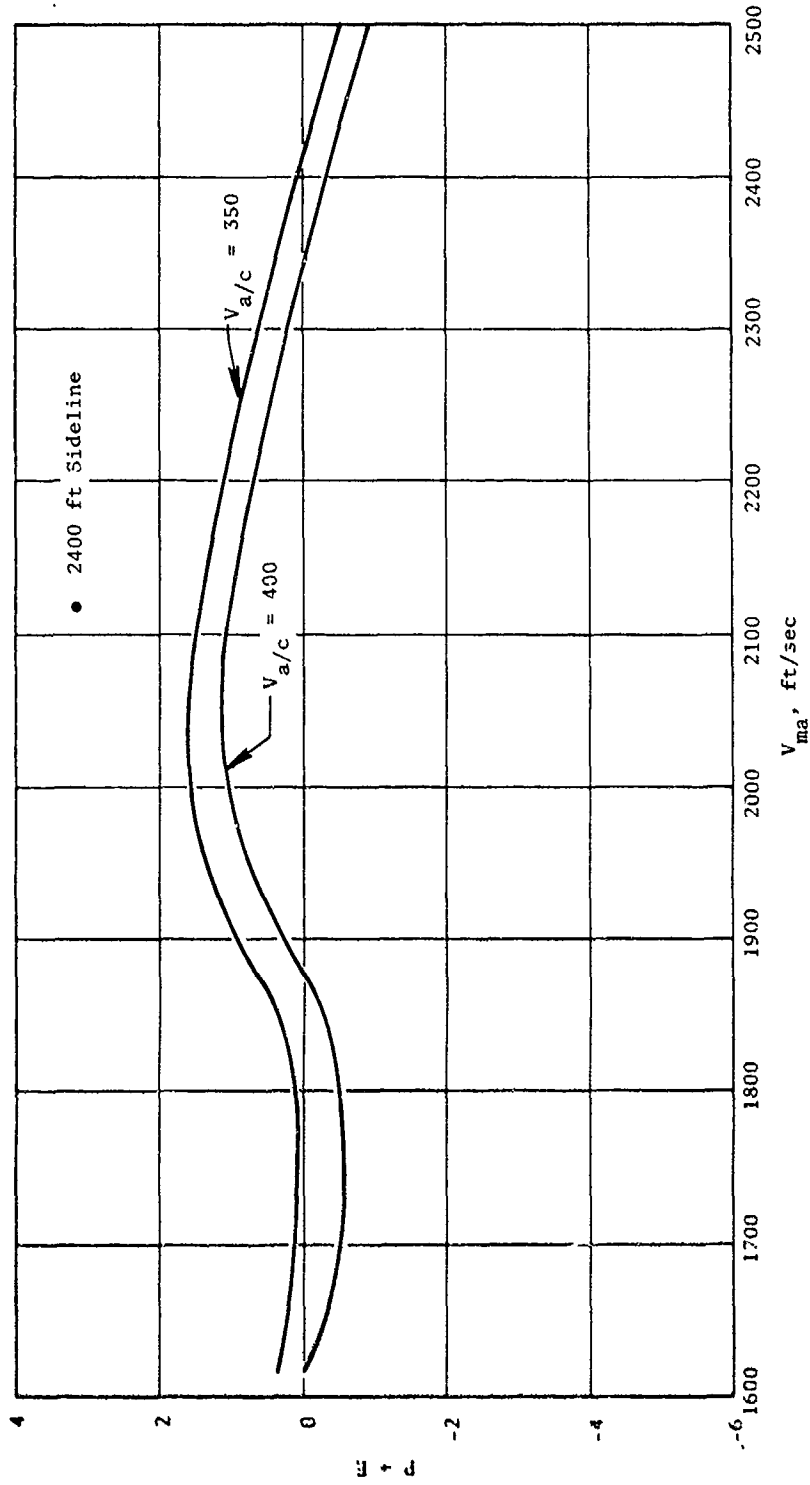


Figure 4-12. Definition of Duration Correction for Suppressor Nozzles.

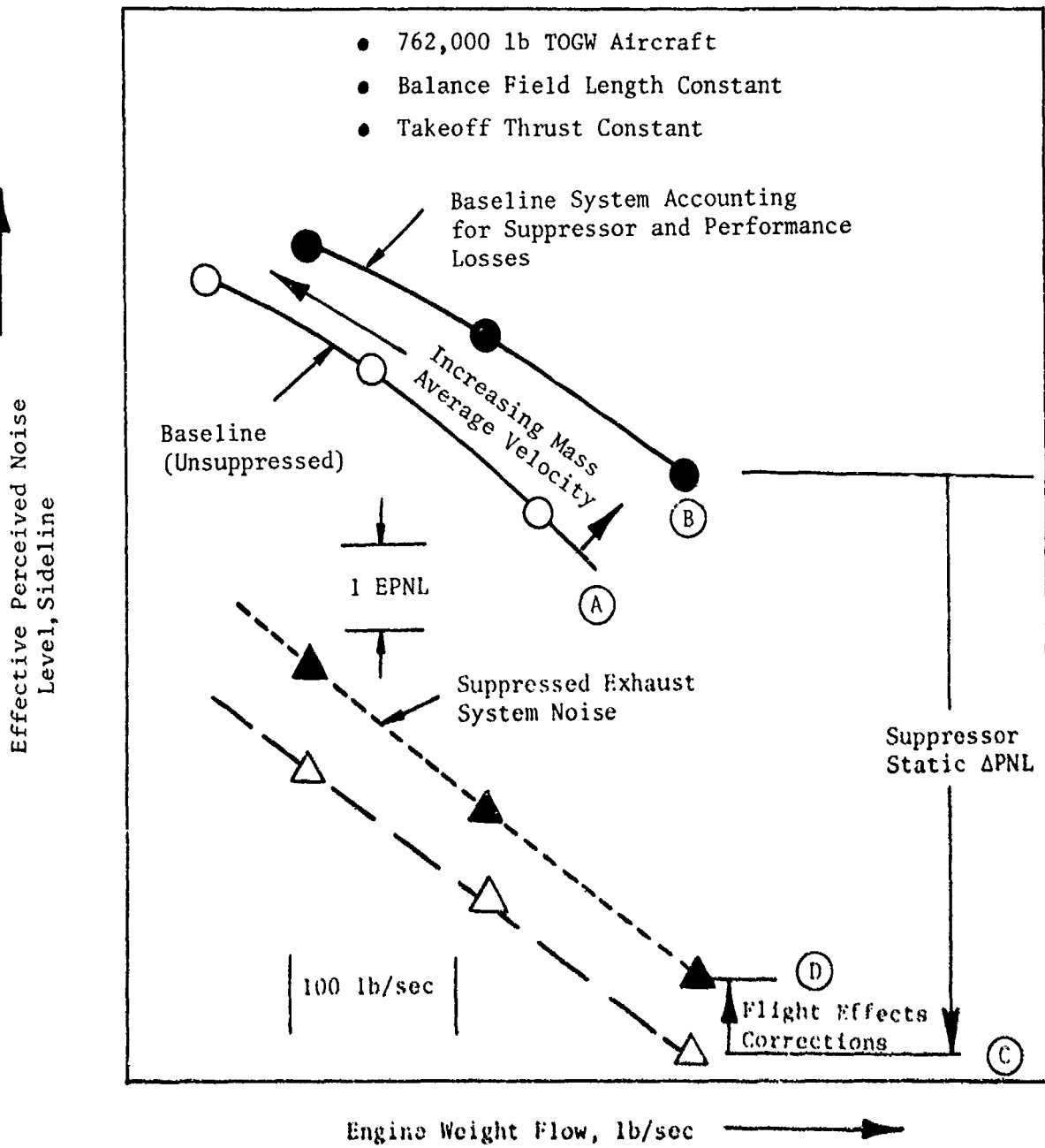


Figure 4-13. Determination of Sideline Effective Perceived Noise Levels for a Typical Suppressor.

- 4 Engines
- AR = 1.75, 40-Shallow Chute Suppressor (Inverted Velocity Profile)
- 12,500 ft Balance Field Length, 53,500 lb Thrust/Engine
- NASA Aircraft

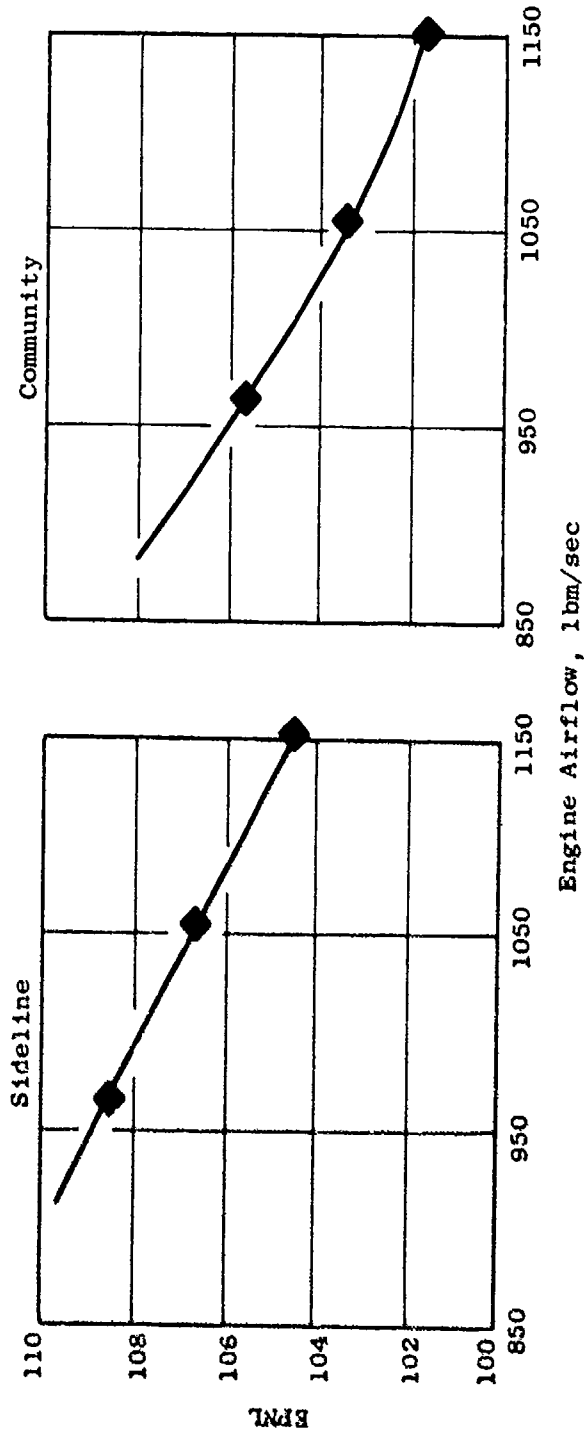


Figure 4-14. Summary of Typical Sideline and Community Jet Noise Levels - AR = 1.75 40-Shallow Chute Nozzle.

The engines are a turbojet and double bypass variable cycle engine. Engine size is varied, as mentioned, to satisfy predetermined noise level goals, and engine weight varied as a function of engine airflow size, and nozzle/suppressor type.

In order to hold takeoff gross weight and payload constant, fuel capacity is decreased as engine system weight increases. Trip block time and mission range are calculated using methods of previous NASA-sponsored SCAR studies and using appropriate sensitivities. Differences in internal nozzle performance and external drag characteristics were accounted for.

4.7 IMPACT OF SUPPRESSOR PERFORMANCE, NOISE REDUCTION, AND WEIGHT

The range versus noise characteristics for the baseline variable cycle and turbojet engine cycles are summarized on Figure 4-15. These curves are used to determine the benefit in range resulting from employing a mechanical suppressor and the corresponding smaller engine.

As an example, two dual-flow and two single-flow suppressor nozzles are evaluated for three noise goals (FAR36, FAR36 minus 2, and FAR36 minus 5 EPNdB). The dual-flow nozzles are an AR = 1.75 40-shallow chute nozzle and an AR = 2.5 36-deep chute nozzle. The single-flow nozzles are an AR = 2.1 32-chute nozzle and AR = 2.9 57-tube nozzle with a treated ejector.

The range versus noise characteristics of these four suppressor configurations were established using the procedure discussed in Section 4.5. A specific example to illustrate this procedure will now be discussed using the AR = 1.75 40-shallow chute nozzle. The range of this suppressor for a given noise goal is calculated using Equation 4-1:

$$\text{Total Range} = \text{range}_{\text{baseline}} + \Delta \text{range}_{\text{weight}} + \Delta \text{range}_{\text{diameter}} \quad (4-1)$$

where $\text{range}_{\text{baseline}}$ is determined using the appropriate mission curve defined in Figure 4-16.

$\Delta \text{range}_{\text{weight}}$ is the range loss, 85 miles per 1000 pounds of additional weight, caused by the suppressor.

$\Delta \text{range}_{\text{diameter}}$ is the range loss due to increasing the nacelle drag caused by the increase in nacelle diameter due to the addition of the suppressor.

Table 4-5 summarizes the results of applying Equation 4-1. The baseline range includes the effect of upsizing the engine to account for the thrust degradation caused by the suppressor.

- NASA Aircraft
- TOGW = 760,000 lbs
- 12,500 ft Balance Field Length
- Jet Noise Only

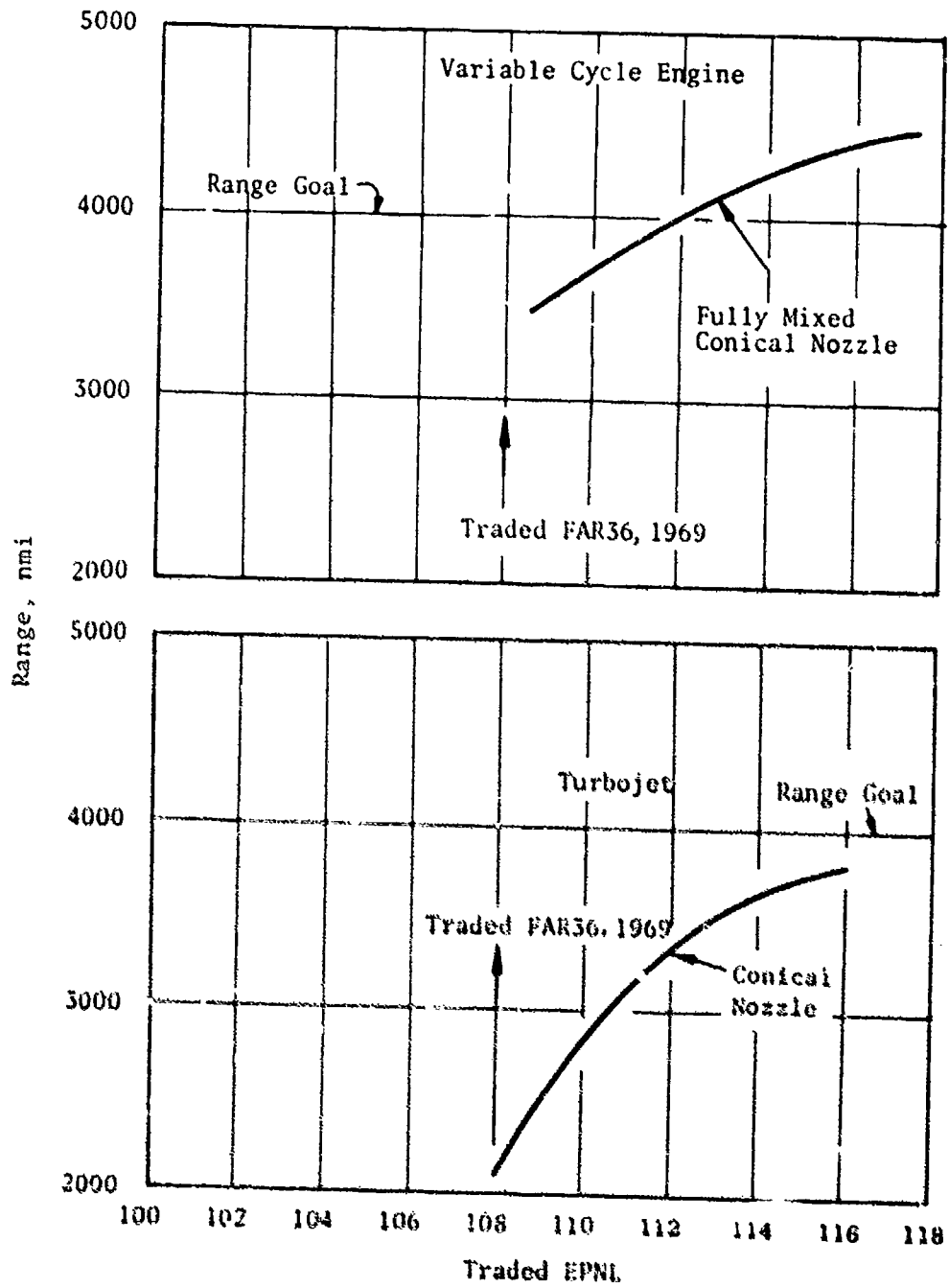


Figure 4-15. Baseline Nozzle Noise Characteristics.

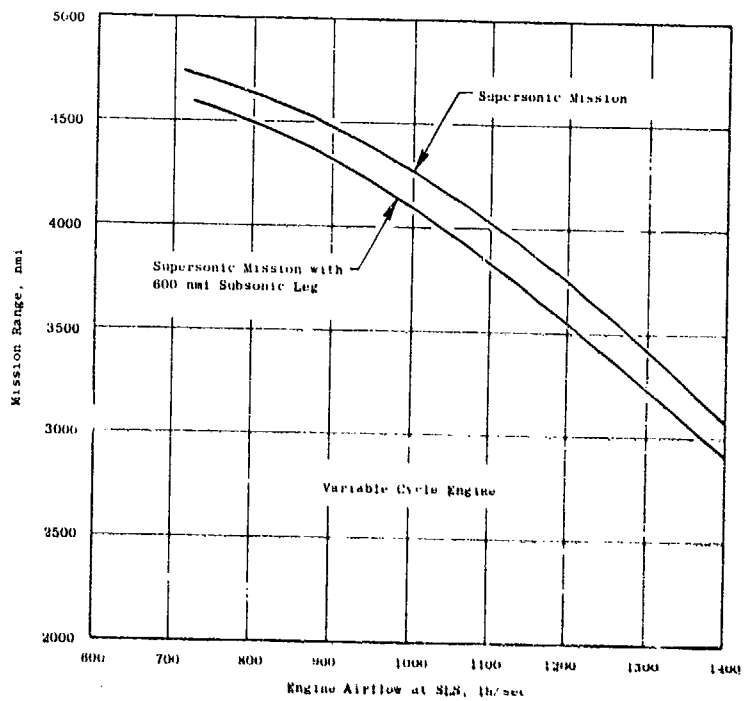
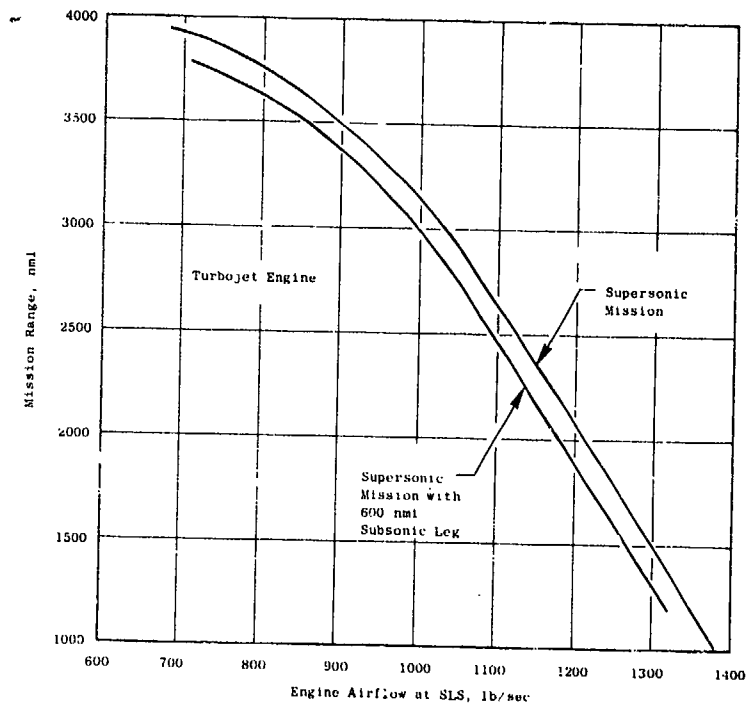


Figure 4-16. Aircraft Integration Study, Mission Characteristics.

Table 4-5. Dual-Flow System, 40 Shallow Chutes.

- 4 Engines
- 17,500 ft balance field length, 53,500 lbf thrust/engine
- Supersonic Mission

Engine Weight Flow, lbm/sec	Traded PAF to re: 108 EPAC	Sideforce	Community	Baseline (No suppressor) Range ⁽¹⁾ , nmi	Engine Weight Increase Caused by the Suppressor, lbm ⁽²⁾	Range Decrement ΔRange Weight	Nacelle Diameter Increase Caused by the Suppressor ⁽²⁾	Range Decrement ΔRange Diameter	Suppressed System Range, nmi
110	0	108.4	106.6	4420	621	-53	1.57 in.	-2.7	4364.3
1011	-2	107.6	104.4	4210	690	-55	1.65 in.	-2.8	4168.2
1166	-3	104.4	101.6	3560	810	-68.8	1.76 in.	-3.0	3788.2

(1) include the degradation of nozzle thrust coefficient caused by the addition of a suppressor.

(2) Weight and nacelle diameter estimates are based on Section 4.6.

The baseline range shown in Table 4-5 is established by determining the engine size required to meet a specified noise goal, utilizing Figure 4-14, determining the corresponding range utilizing Figure 4-16. Note that the range decrement due to diameter is less than 5 percent of the decrement due to suppressor weight.

A summary of the range versus noise characteristics for the configurations is presented in Figure 4-17. The addition of a properly designed mechanical suppressor causes a significant increase in aircraft range for a specified noise goal. For example, for a traded FAR36 noise goal of 108 EPNL, the addition of the 32-chute nozzle allows a range improvement of approximately 1700 miles. Note that this is a net improvement and that penalties for performance degradation and additional weight of the suppressors were included. A similar comparison for the variable cycle engine shows a range improvement of nearly 1000 miles for the 40-shallow chute nozzle at 108 EPNL. The range increase realized by adding a suppressor to the variable cycle engine is less than adding a suppressor to a turbojet engine, e.g., 1000 miles versus 1700 miles. In contrast, the AR = 2.5 36-chute nozzle is actually less effective than the 40-shallow chute nozzle if FAR36 levels of 110 or less are desired. The poorer showing is due primarily to the larger decrement in range due to weight (fuel off-load) plus the increase in nacelle diameter (drag). Also shown in Figure 4-17 are the range noise characteristics of an optimum nozzle described in Section 6.0. This projection is based on static measurements which have been completed under Task 5 of this program.

The results of the case studies were used to establish the relative importance of suppression level, performance, and weight for the range of variables evaluated. The 40-shallow chute nozzle is used to illustrate the importance of suppression level. Figure 4-18(a) shows the range improvement which is incurred due to an assumed suppression improvement of 2 dB. For this particular configuration, an improvement of 2 EPNL resulted in a range increase of 200 miles to 400 miles depending on the specified noise goal.

Trend curves to establish aircraft range penalties caused by the suppressor performance degradation may be established by holding net thrust constant and varying the thrust coefficient. Net thrust is defined as:

$$F_{net} = (F_G) (C_{fg}) - D_{ram}$$

where F_G is the ideal gross thrust

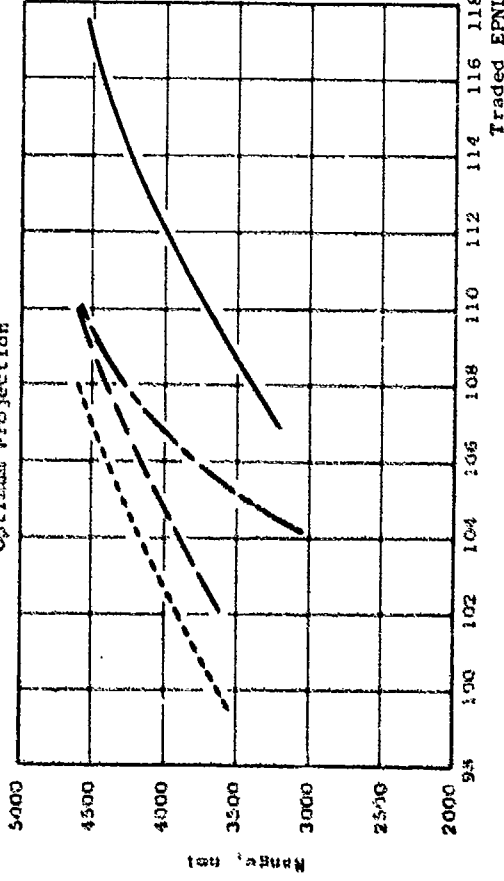
C_{fg} is the nozzle thrust coefficient at specified V_a/c

$$D_{ram} \text{ is the ram drag} = \frac{W_a V_a/c}{g}$$

- Four Engines
- 12,500-ft Balance Field Length; 53,500-lbf Thrust Engine
- NASA Aircraft

VARIABLE-CYCLE ENGINE

- Nozzle Type
- Fully Mixed, Conical
 - - - 36-Chute, AR = 2.5
 - 40-Shallow-Chute
 - - - Optimum Projection



TURBOJET ENGINE

- Nozzle Type
- Baseline, Conical
 - - - 32-Chute, AR = 2.1
 - - - 57-Tube + Ejector, AR = 2.9

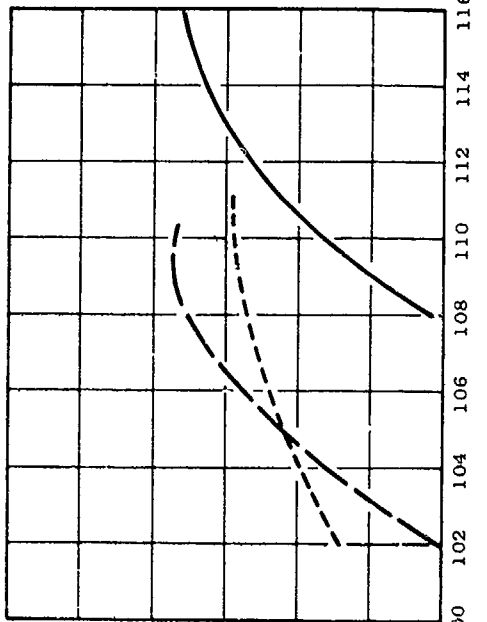


Figure 4-17. Summary of Range and Noise Characteristics for Several Baseline and Suppressor Nozzles.

- AR = 1.75, 40 Shallow Chutes
- 4 Engines
- 10,500 ft Balance Field Length, 61,400 lbs Thrust/Engine
- Aircraft TOGW = 762,000 lbs

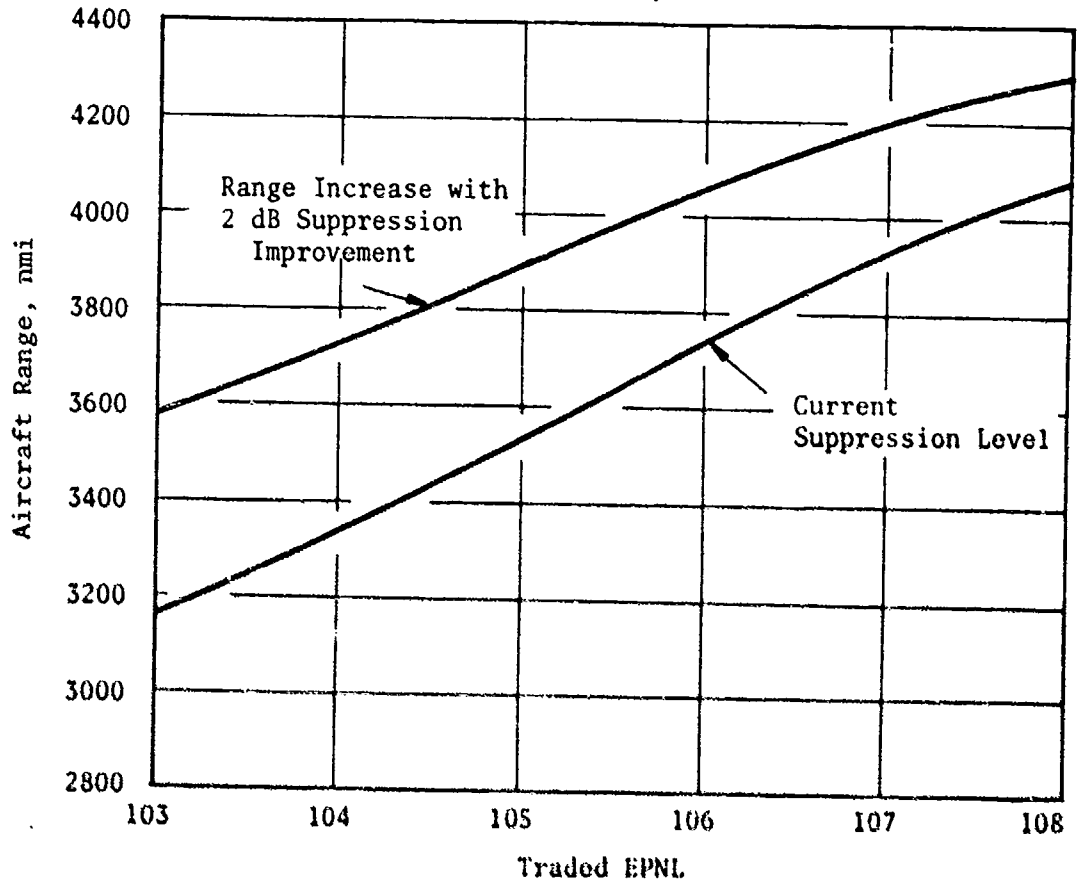


Figure 4-18(a). Impact of Suppression on Aircraft Range.

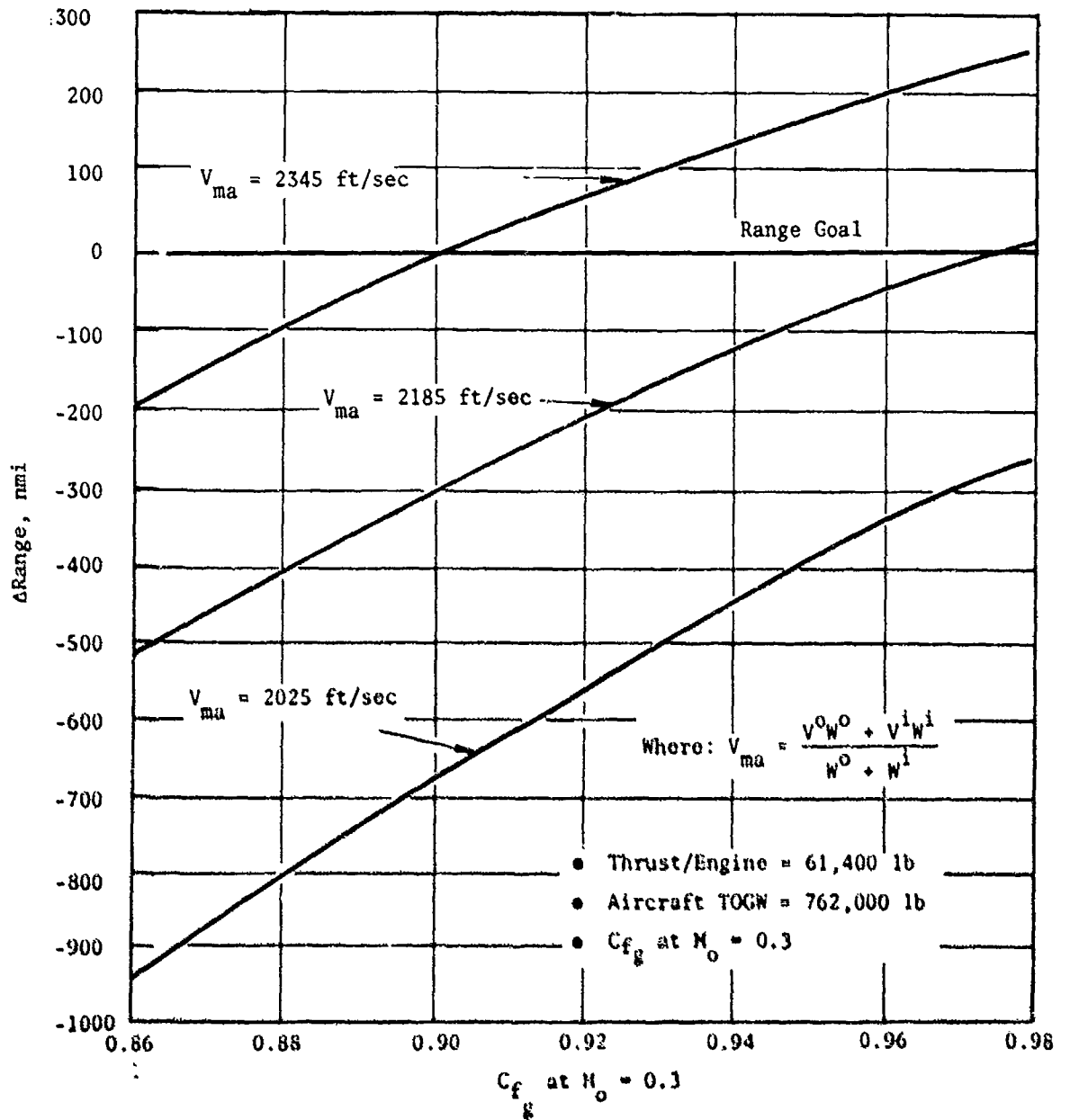


Figure 4-18(b). Impact of Aero Performance on Aircraft Range.

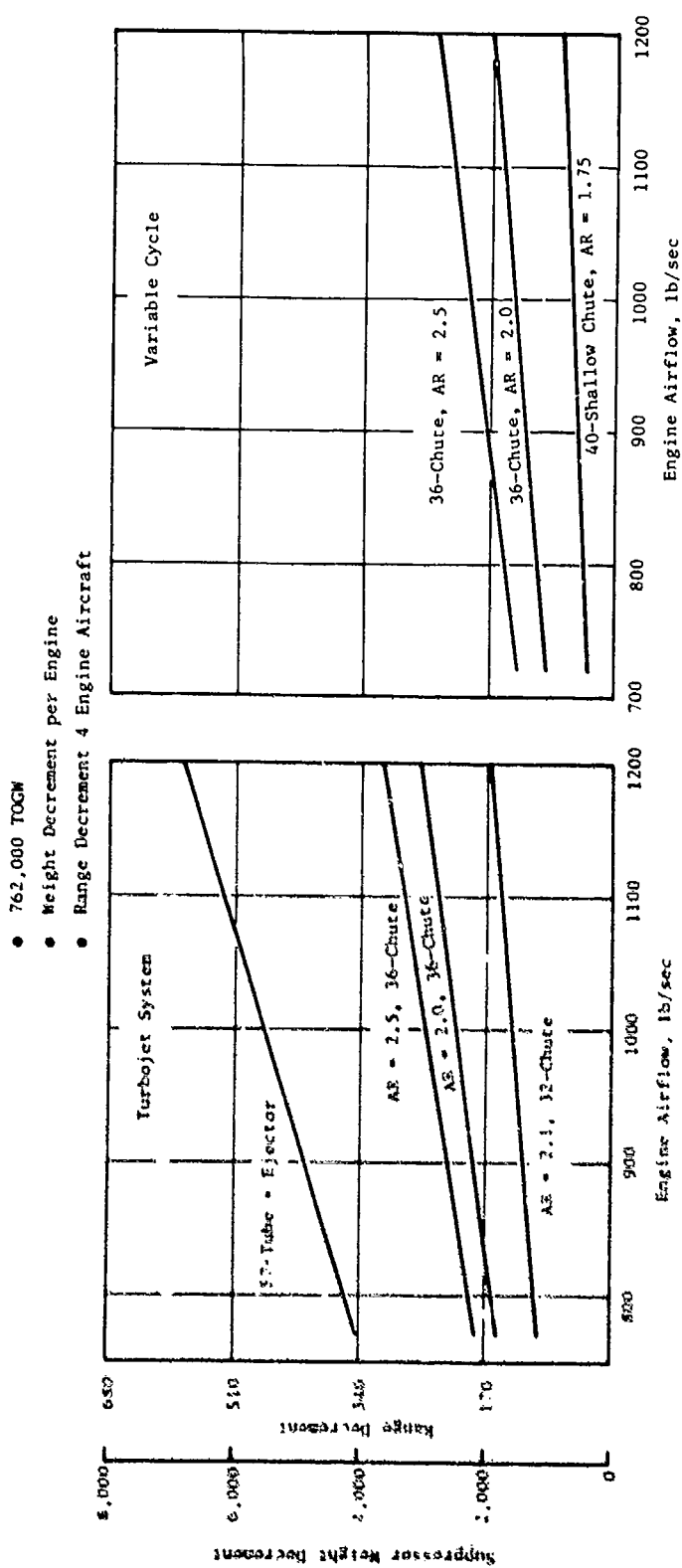


Figure 4-18(c). Typical Suppressor Weight Decrements.

If net thrust is held constant as thrust coefficient decreases, engine size must be increased. Increasing engine airflow results in a range penalty. The change in range due to thrust coefficient is summarized in Figure 4-18(b). If one assumes a suppressor performance loss of 6 percent, the corresponding range decrement is 175 miles at a velocity of 2345 ft/sec. Suppressor weight as a function of engine airflow is summarized in Figure 4-18(c), and the corresponding range decrement is identified. The curves illustrate the large difference in range decrement due to weight which occurs between a simple suppressor such as the 40-shallow chute nozzle and a complex suppressor such as the 57-tube nozzle with a treated ejector. For example, at engine airflow of 1000 lbm/sec, the range decrements are 60 miles and 470 miles, respectively.

Case studies were completed for the two baseline and seven suppressor configurations defined in Section 4.3. These studies were done at balance field lengths of 10,500 ft and 12,500 ft. Increasing balance field length lowers the takeoff thrust requirement and reduces engine size. However, the aircraft is at a lower altitude at the community monitoring point. Range versus noise characteristics for the two balance field lengths are summarized on Figure 4-19 for the single-flow baseline and suppressor configurations. Figure 4-19 illustrates that a significant improvement occurs due to an increase in balance field length for the baseline single-flow configuration. However, the improvement is less dramatic for the 32-chute suppressor nozzle. The suppressor is found to result in greater range advantage relative to the baseline configuration for 10,500 ft balance field length.

In general, increasing balance field length, which results in a lower thrust requirement, resulted in an improvement in mission range.

Noise footprint area has also been considered. The footprint areas are calculated using the procedure described in Reference 17.

The footprint areas for the suppressor configurations are summarized in Table 4-6 in terms of square nautical miles. Although the configurations are compared at the same traded EPNL noise level, there are significant differences in footprint area. This is due to throttle cutback at the community monitoring point. Therefore, although the traded EPNL level of the configurations are equivalent, the community levels are not necessarily the same. This point is illustrated by considering the following example. The 40-shallow chute nozzle has sideline and community noise levels of 110 EPNL and 101.6, respectively, for a traded noise goal of 108 EPNL. The 36-chute, AR = 2.0, configuration has levels of 110 and 104 for the same noise goal. There is a 2.4 PNdB difference between the community noise level of the two configurations, and the 40-shallow chute nozzle has a significantly smaller footprint.

Mission sensitivity was established by considering the second mission which has a 600 nautical mile subsonic leg. Case studies were done for several suppressor and baseline configurations. Results of these studies indicated that for all configurations a range decrement of 100 to 200 miles

- 4 Engines
- NASA Aircraft
- Supersonic Mission

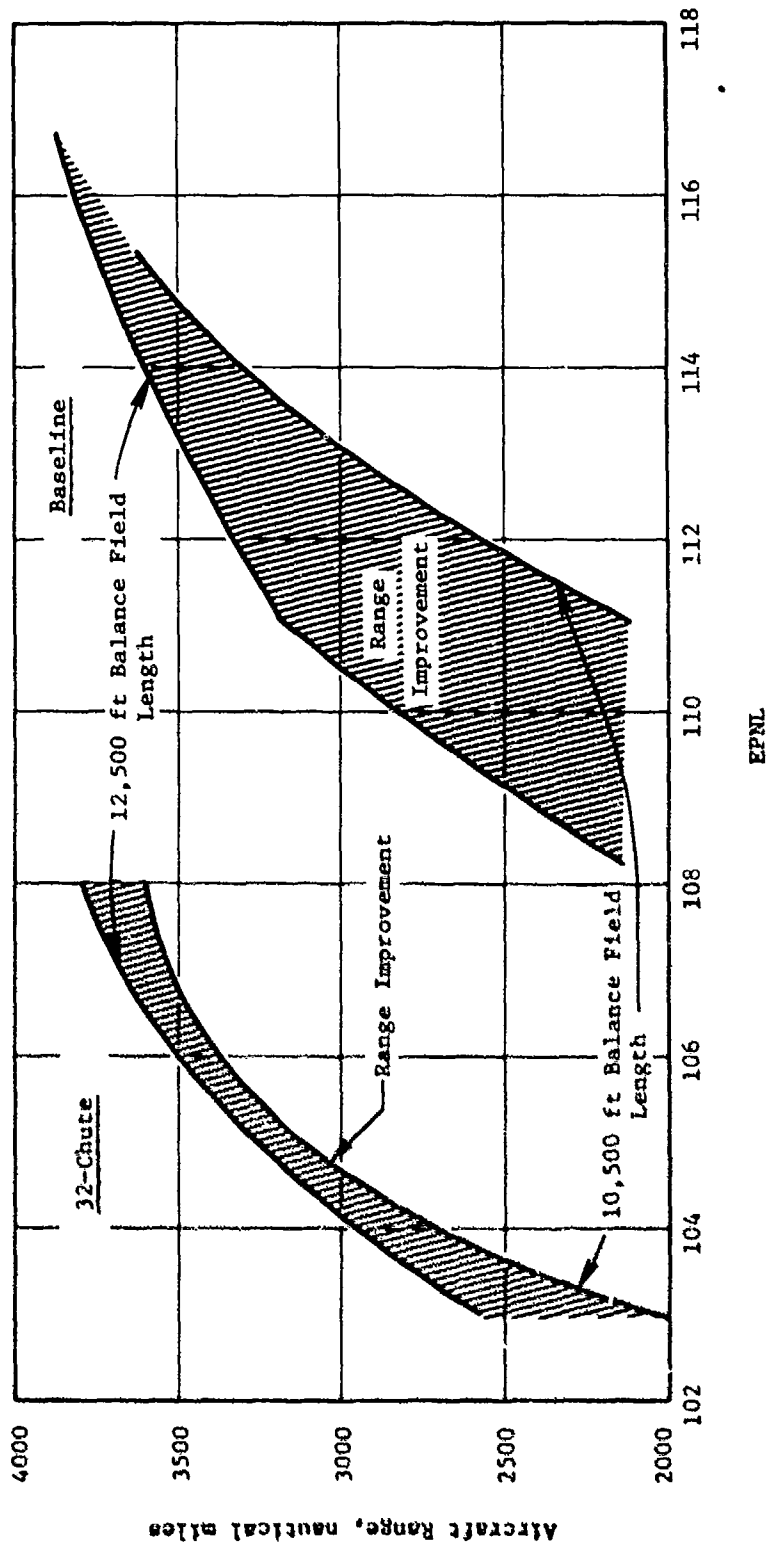


Figure 4-19. Influence of Balanced Field Length on Noise Characteristics of a Single Flow Baseline and Suppressor Nozzle.

Table 4-6. Summary of Suppressor Noise Footprint Characteristics.

Suppressor	Footprint, nmi ² 100 EPNL		Footprint, nmi ² 90 EPNL	
	Noise Goal*		Noise Goal*	
	0	-2	0	-2
32-chute, AR=2.1	8.2	6.5	55.1	48.5
36-chute, AR=2.0	10.9	6.6	70.6	49.2
36-chute, AR=2.5	11.8	6.5	76.1	48.5
40-shallow chute, AR=1.75	5.1	3.9	32.1	22.9
36-chute, AR=2.0	6.8	4.5	46.2	31.7
36-chute, AR=2.5	8.5	6.9	60.1	51.3

* Relative to FAR36 (1969)

was incurred due to the addition of a 600 nautical mile subsonic leg. The range decrements were not configuration-sensitive but varied as a function of the engine airflow size required to meet a specific noise goal. A lesser penalty was incurred for baseline and suppressor configurations utilized on engines having lowest takeoff airflow.

4.8 CONCLUSIONS

The objective of the aircraft integration study was to assess the influence of suppression level, aerodynamic performance, and suppressor weight on the aircraft mission. Suppression level was found to have a significant impact on aircraft range. Typical examples show a 1 dB improvement in suppression would result in a range increase of 100 to 200 miles. Aerodynamic performance losses and weight increase caused by the suppressor nozzle ranked second and third, respectively. The performance losses caused by the suppressors ranged from 5 to 9 percent relative to a plug nozzle. Engine weight increase caused by the addition of a mechanical suppressor ranged from 4 to 20 percent. Increasing balance field length from 10,500 ft to 12,500 ft caused a significant increase in aircraft range for a specified noise goal. The inclusion of a 600 nautical mile subsonic leg into the mission resulted in a range decrement of 100 to 200 miles. The noise footprint areas were found to be 2 to 7 times that of a typical wide body transport.

The relative ranking of each suppressor was found to be dependent on the measured noise goal. Generally speaking, although the addition of a mechanical suppressor increases weight and reduces performance, for a specified noise goal the suppressor allows the use of a smaller engine which results in a range advantage. Based on jet noise considerations only, Traded FAR36 levels of 105 without margin, and aircraft mission ranges of 4000 nautical miles are feasible, utilizing variable cycle engines with mechanical suppression devices of the type considered in this study.

5.0 FIGURE OF MERIT

Figure of merit (F.O.M.) is a term which may be defined as a procedure or method for determining the relative merit of competing systems on a quantitative basis. For example, specific fuel consumption (sfc) is a common figure of merit for aircraft engines. Any meaningful figure of merit for a mechanical suppressor must incorporate the effects of suppression level, performance level, and weight. The results of the aircraft integration study (Section 4.0) show that aircraft range includes these effects when a proper engine integration and mission analysis study is performed. The major drawback of using aircraft range as a noise abatement nozzle F.O.M. is that it requires the characteristics of the aircraft mission to be defined, and requires mechanical design and installation studies which in turn require information about the aircraft and the engine. Unfortunately, the aircraft integration studies demonstrate that this type of analysis is the valid way to fairly evaluate suppressor nozzles.

In general, a nozzle with the highest suppression level, least performance degradation, and the lightest weight will be superior. The aircraft engine integration studies discussed in Section 4.0 show that suppression is usually the most important design criterion with weight and takeoff performance ranked second and third, respectively. The trade studies of Section 3.0 demonstrate that the ratio of $\Delta\text{PNL}/\Delta\text{C}_{f_g}$ is inadequate because it ignores absolute suppression level limitations and penalties due to suppressor weight.

In the course of conducting any aircraft integration study, the preliminary designer, however, has to rely on several interim criteria to assist him in screening various suppressor configurations. A parameter such as $\Delta\text{PNL}/\Delta\text{C}_{f_g}$ versus ΔPNL is one typical example often used. This problem of how to screen the suppressor configurations without resorting to the lengthy mission approach might be resolved by considering several relatively simple ranking techniques.

The first screening technique, referred to as the Composite Score (C.S.), simply degrades a perfect score, 100, by the suppression relative to some current feasible value, say 15 ΔPNdB , the performance loss and the weight associated with the suppressor relative to the baseline, unsuppressed, engine weight. This is simply expressed as:

$$\text{C.S.} = 100 - [(15 - \Delta\text{PNL}) + \Delta\text{C}_{f_g} + \Delta\text{Wt}/\text{Wt}]$$

where ΔPNL = Static Suppression Re Conical at Same \bar{V}_{ma}

ΔC_{f_g} = Performance Loss Re Plug Nozzle at Rotation
Mach No. (-0.3 + 0.36) in Percent

$\Delta\text{Wt}/\text{Wt}$ = Suppressor/Baseline Engine Weight Ratio in
Percent

This very simple ranking procedure basically tells the preliminary designer the suppressor with highest noise reduction, lowest weight, and least performance degradation should be a candidate for the mission study. The second approach, the Overall Ranking Number (O.R.N.), attempts to provide a "weighting" factor or "modifier" to several of the suppressor parameters previously discussed. By "weighting" the key suppressor performance parameters, it may permit the designer to further discriminate among candidate systems that on a simple "nonweighting" basis appear at or below par. The suppression level (ΔPNL) could be modified to reflect how efficiently a given configuration achieves it (i.e., $\Delta PNL/\Delta C_{fg}$), while the percent suppressor weight ratio ($\Delta Wt/Wt$) could also be modified to recognize whether the mechanical suppressor is deployed in a full (turbojet) or half-spin (VCE) mode, as well as relating its simplicity of mechanical design (i.e., $\Delta Wt/Wt$) to the attendant performance loss (ΔC_{fg}). One way of expressing Overall Ranking Number is as follows:

$$O.R.N. = \frac{\Delta PNL}{\Delta C_{fg}} (1.66 \Delta PNL) + (33.3 - 1.66 \Delta C_{fg}) + \left[\frac{A_T}{A_S} \left(\frac{1}{\Delta Wt/Wt / \Delta C_{fg}} \right) (33.3 - 1.33 \Delta Wt/Wt) \right]$$

where ΔPNL , ΔC_{fg} , $\Delta Wt/Wt$ = Same as in C.S. method

A_T = Total engine flow area

A_S = Flow area in which suppressor is deployed

In general, the higher O.R.N. (no upper limit) the more likely that the suppressor selected for the mission study will be a competitive one.

Using the seven suppressor configurations evaluated in the aircraft integration (Section 4.0), their ranking or rating independent of mission restraints (i.e., noise level and thrust are variables), was determined using both C.S. and O.R.N. techniques. The results are tabulated in Table 5-1 and the bar chart of Figure 5-1. One of the more obvious differences between the C.S. and O.R.N. is illustrated when one compares the 32-chute/plug and the tube + ejector suppressor nozzles. Clearly the O.R.N. method permits the high $\Delta PNL/\Delta C_{fg}$ of tube + ejector suppressor to compensate for its extremely poor suppressor weight penalty, thus making it more or less equal to its 32-chute/plug counterpart. This is illustrated in Figure 5-2. Although the O.R.N. is essentially the same for both suppressor systems, the bar chart clearly delineates how the various "weighting" parameters affect the total ranking. On the other hand, both the C.S. and O.R.N. techniques suggest that the 40-shallow chute/AR = 1.75 suppressor from the VCE series is the best of the three candidates.

Table 5-1. Comparison of the "Composite Score" and "Overall Ranking Number" Techniques in Rating Suppressor/Engine Systems.

Aircraft Integration Configurations	"Interim Criteria"	
	Composite Score (C.S.)	Overall Ranking Number (O.R.N.)
<ul style="list-style-type: none"> • <u>Turbojet</u> (Single Flow) - 32-Chute/Plug/AR = 2.1 - 36-Chute Plug/AR = 2.0 - 36-Chute/Plug/AR = 2.5 - 57-Tube + Trested Ejector/AR = 2.95 	85.7	94.7
<ul style="list-style-type: none"> • <u>VCE</u> (Dual Flow) - Shallow Chute/AR = 1.75 - 36-Chute/AR = 2.0 - 36-Chute/AR = 2.5 	77.3 76.4 73.9	61.2 59.6 94.6
	80.9 + 82.9	111.5 + 118.7
	76.5 + 77.0	58.6 + 60.7
	72.2 + 74.1	48.1 + 57.0

- Static ΔPNL Re Conical at Same \bar{V}_{ma}
- ΔC_f Corresponding to Rotation Mach No. (Re-Plug Nozzle C_{fg})
- $\Delta Wt/Wt$ -Suppressor Weight Relative to Baseline Engine without Suppressor
- No Mission Restraints

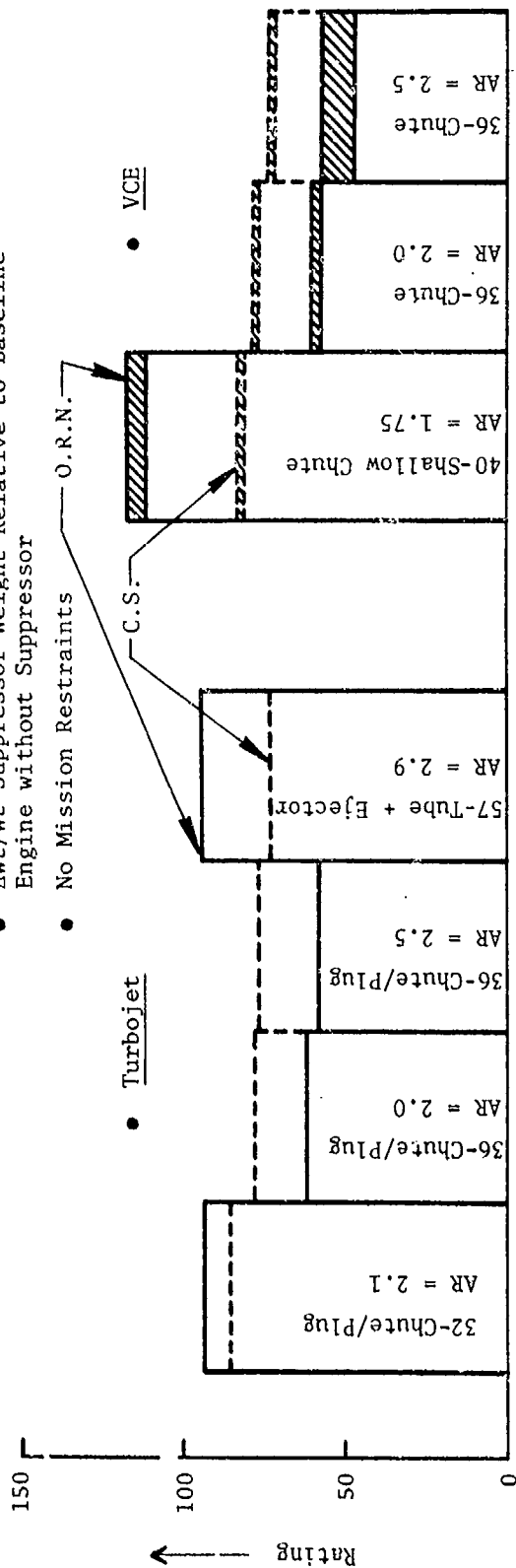


Figure 5-1. Rating of Mechanical Suppressors Utilizing the Composite Score (C.S.) and Overall Ranking Number (O.R.N.) Techniques.

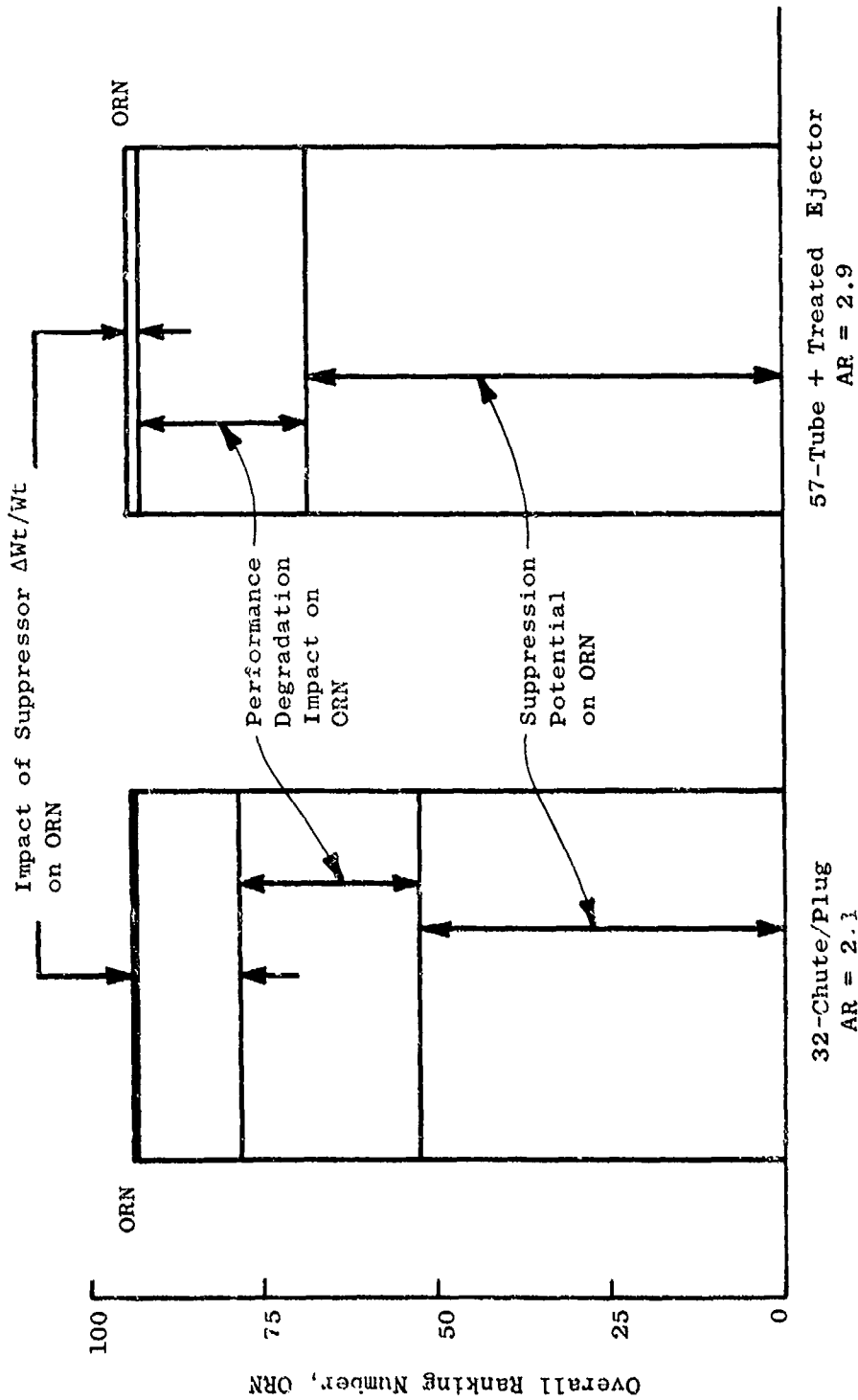


Figure 5-2. Impact of Mechanical Suppressor ΔPNL , ΔCfg , and $\Delta Wt/Wt$ on Overall Ranking Number.

The last few paragraphs have attempted to provide the preliminary designer some guidance as to which suppressor/engine system(s) may show enough promise to be subjected to a mission study by employing several elementary ranking tools. However, the designer must always keep in mind that whatever suppressor/systems are evolved from these "interim criteria," their benefit or viability to a given aircraft and its respective mission must wait for the results of the ultimate "Figure of Merit" - Range.

The following section will discuss how five configurations were selected, designed, and built for acoustic evaluation during Task 5 of the subject program utilizing the "Figure of Merit" discussed herein.

6.0 OPTIMUM SUPPRESSOR NOZZLES

The selection of five optimum suppressor nozzles was based on the results obtained from the following programs activities:

- FAA/DOT SST Phase I and II Studies presented in References 2, 3, 4, and 5.
- Engineering Correlation Studies presented in Volume I.
- Task 2 Aeroacoustic Modeling Activity (M*G*B) Jet Noise Predictions presented in Reference 7.
- Aero Performance and Acoustic Results - Subtask 2 presented in Sections 3.0 and 4.0 of Volume II.
- Trade Studies of performance versus suppression presented in Section 3.0 of this volume.
- Aircraft Integration Studies presented in Section 4.0 of this volume.


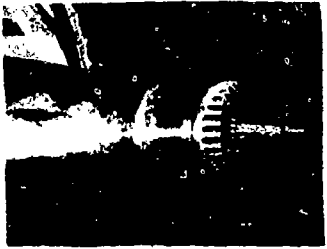

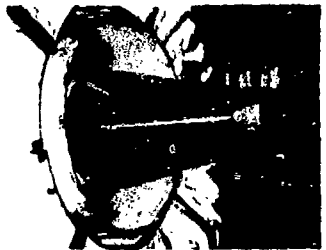
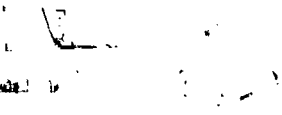
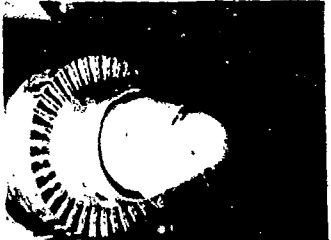
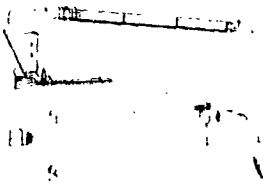


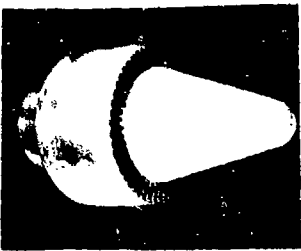
The Five Optimum Suppressor Nozzles

The five configurations selected for static and simulated flight acoustic testing based on the results of these studies are:

- 1 - 32-chute, AR = 2.1 - single flow
- 2 - 40-shallow chute, $(AR)_0 = 1.75$ - dual flow, Inverted Velocity Profile (IVP)
- 3 - 36-chute, $(AR)_0 = 2.0$ dual flow, IVP
- 4 - 3 with treated ejector - dual flow, IVP
- 5 - Coplanar mixer (54-element) - dual flow, Side-By-Side

These configurations are illustrated in Table 6-1 along with some of the key geometric parameters. Each of five optimum nozzle configurations was selected by evaluating the compromises among suppression level, performance loss, and mechanical complexity. However, consideration was also given to having a wide variety of configurations in order that the Task 5 testing could allow the projection of flight noise suppression levels for several suppressor families. This approach was considered appropriate because of the extremely limited data base available to optimize suppressor designs in flight, especially for dual-flow nozzle configurations as previously discussed in Section 3.0.

Table 6-1. Optimum Suppressor Nozzle Designs.

<u>Model No.</u>	<u>Configuration</u>	<u>Schematic</u>	<u>Photograph</u>
1	32 Chute AR = 2.1		
2	40 Shallow Chute AR = 1.75		
3	36 Chute AR = 2.0		
4	36 Chute with Treated Ejector AR = 2.0		
5	54 Element Coplanar Mixer		

Configuration 1, 32-chute AR = 2.1 nozzle, was selected to be representative of suppressor nozzles which were applicable to single-flow exhaust systems. This 32-chute nozzle was evaluated as a result of the parametric test series described in Reference 4. The selection of this configuration was also justified by the results of the aircraft integration studies described in Section 4.0. The mechanical design studies indicated that the area ratio of 2.1 does fall within the range of acceptability. The static and flight aerodynamic performance of this nozzle was documented based on wind tunnel testing data. The other three turbojet suppressors considered were those evaluated in the aircraft integration study described in Section 4.0. This may at first seem to be a limited group of nozzles but, in actuality, it represents a substantial portion of the suppressor nozzle work performed during the past 25 years. The 32-chute nozzle and 57-tube plus ejector nozzle are configurations which were evolved after extensive studies conducted by General Electric and the Boeing Company after cancellation of the SST. These nozzles were evolved based on limited analytical, and extensive experimental studies conducted by the respective companies and described in References 4 and 5. The 36-chute nozzle area ratios 2.0 and 2.5 were configurations evolved for parametric testing during this current program and are more representative of the type of mechanical suppressors which could be implemented on a high radius ratio plug nozzle. Selection of the optimum nozzle Number 1 was based on maximum range attainable in order to meet current FAR36 (i.e., EPNL = 108) noise levels. Table 6-2 summarizes how each of the nozzles compares. The 32-chute, AR = 2.1 was selected due to its weight advantage and high performance.

The remaining four optimum nozzles were selected from the dual-flow family. The second configuration was chosen to be AR = 1.75 40-shallow chute nozzle with a modified core-plug geometry. This configuration was evolved as a result of the experimental data presented in Volume II of this report and the mechanical design studies described in Section 4.4. The experimental results presented in Section 3.4.2.2 of Volume II show that a modification to the core-plug geometry of the 40-shallow chute nozzle would result in a 1.5 PNdB improvement in suppression with essentially no change in exhaust system performance or weight. This conclusion is supported by the static data presented in Figure 6-1.

The acoustic data base to project flight suppression levels for dual-flow configurations is very limited, as discussed in Section 3.0. This configuration, based on the experimental data discussed in Volume II, Section 3.4.2.3, has the potential for maintaining suppression in flight. This projection is made based on the experimental observation that in flight, a significant low frequency reduction occurs for the suppressor, whereas little or no change occurs in the high frequency portion of the spectra. The 40-shallow chute when compared to the other shallow chute configurations generally exhibits the lowest high frequency noise levels and should, therefore, perform best in the flight environment.

Configuration 3 was selected to be an AR = 2.0 36-chute nozzle which incorporated several unique design features. A nozzle area ratio of 2.0 was selected because it represents the best compromise from a suppression and

Table 6-2. Single Flow System Comparison.

- Size/range for traded FAR36=0 (108 EPNL)
- TOGW = 762,000 lbs
- 10,500 ft balance field length

Nozzle Configuration	Suppressed System Range (nautical mi)	Engine Weight Flow (lbm/sec) SLS	C_{fg} at $M_0 = 0.30$
● 32-Chute, AR = 2.1*	3531	880	~0.93
● 36-Chute, AR = 2.0	3228	935	~0.91
● 36-Chute, AR = 2.5	3163	940	~0.914
● 57-Tube, AR = 2.9 + Treated Ejector**	3183	835	~0.93

* - SST Phase II - Optimum Nozzle, GE/FAA Contract DOT-FA-72WA-2894

** - SST Phase II - Optimum Nozzle, Boeing/FAA Contract DOT-FA-72WA-2893

- Configuration No. 1 selected as optimum single flow system

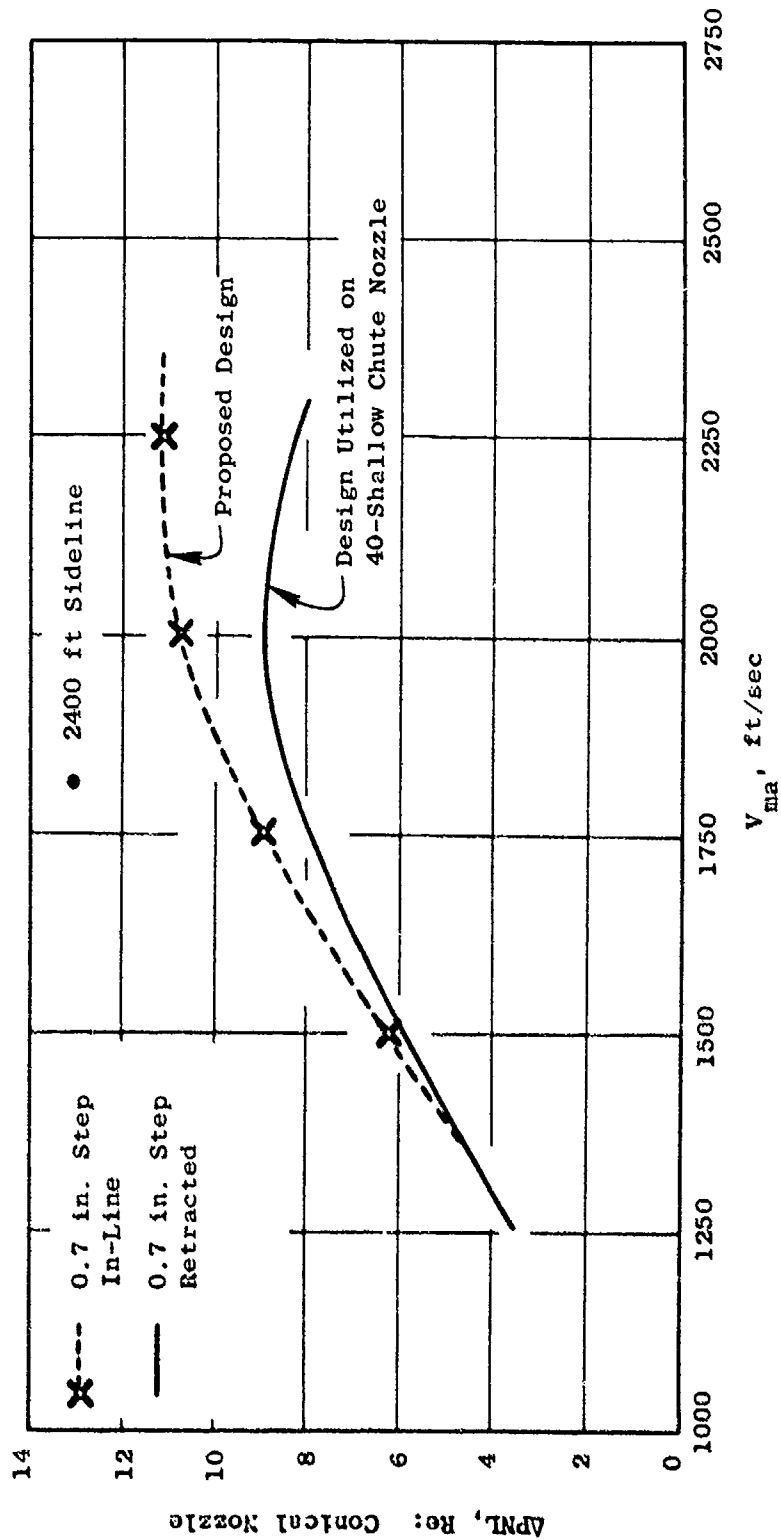


Figure 6-1. Impact of Auxiliary Injection Geometry on Peak PNL, $w_{core} = 30\% w_{duct}$.

weight point of view over a wide range of velocities. This trend is illustrated by the comparison of suppression characteristics with area ratio and the weight variation with area ratio presented in Figure 4-17. The core plug geometry of this configuration was designed based on the flow management studies described in Volume II. The small step height was selected to provide an outer-to-inner stream flow area ratio variation of 3.62. The element number was selected based on the engineering correlation studies which indicated very little improvement in suppression with increasing element number, and 36 was selected based on performance data availability and the adverse effect that increasing element number has on performance. The adverse effect on performance is discussed in detail in Section 4.0, Volume II.

The chute design itself was unique in that it incorporated a convergent-divergent flowpath to reduce the shock noise signature of the suppressor. The need for this design was predicted on test data presented in Volume II. The influence of shock noise on the directivity and spectra characteristics of a suppressor is illustrated by the following example. Consider an AR = 2.0 turbojet nozzle such as Configuration 16 in Volume II. Two test points were compared for this configuration to illustrate the importance of shock noise. The pressure ratio was held constant at approximately 3.3 and two temperature conditions were evaluated. These were 730° R and 1620° R, which result in velocities of 1600 and 2380 ft/sec, respectively. The PNL directivity characteristics of the two data points are presented in Figure 6-2. Previous results would indicate a significant decrease in PNL level as velocity is decreased. This trend is observed at acoustic angles of 90° and in the aft noise quadrant. In the forward quadrant, the PNL levels are equivalent even though there is a difference of 780 ft/sec in velocity. Spectra comparisons are presented in Figure 6-3 to provide further data. The high frequency portion of the spectra are equivalent in level whereas the low frequency levels are lower as expected. The insensitivity of high frequency noise is generally characteristic of shock noise. Therefore, if the shock noise could be reduced, a significant decrease in the PNL levels should occur. This is the reason for incorporation of the convergent-divergent chute design into this configuration. It is anticipated that this configuration should result in static suppression levels in excess of 10 PNdB and achieve a range goal of 4000 nautical miles with a traded FAR36 level of 103 based on jet noise consideration only.

This configuration with an ejector was selected as optimum nozzle No. 4. An ejector was chosen to be representative of a high suppression nozzle from a different family of exhaust nozzles. The ejector design incorporated a length-to-diameter ratio of 1 and utilized the design criterion that flow area be held constant throughout the annulus. These are the design criteria for good aerodynamic performance at takeoff conditions. The ejector treatment utilized was a broadband bulk absorber, Astroquartz.

The addition of a treated ejector to Configuration 3 is projected to increase PNdB suppression 2 to 4 PNdB. This configuration is projected to be a high suppression device, in excess of 12 PNdB. A typical example of the suppression improvement caused by the addition of a treated ejector is illustrated in Figure 6-4. The results are discussed in Section 3.4.2.5 of Volume II.

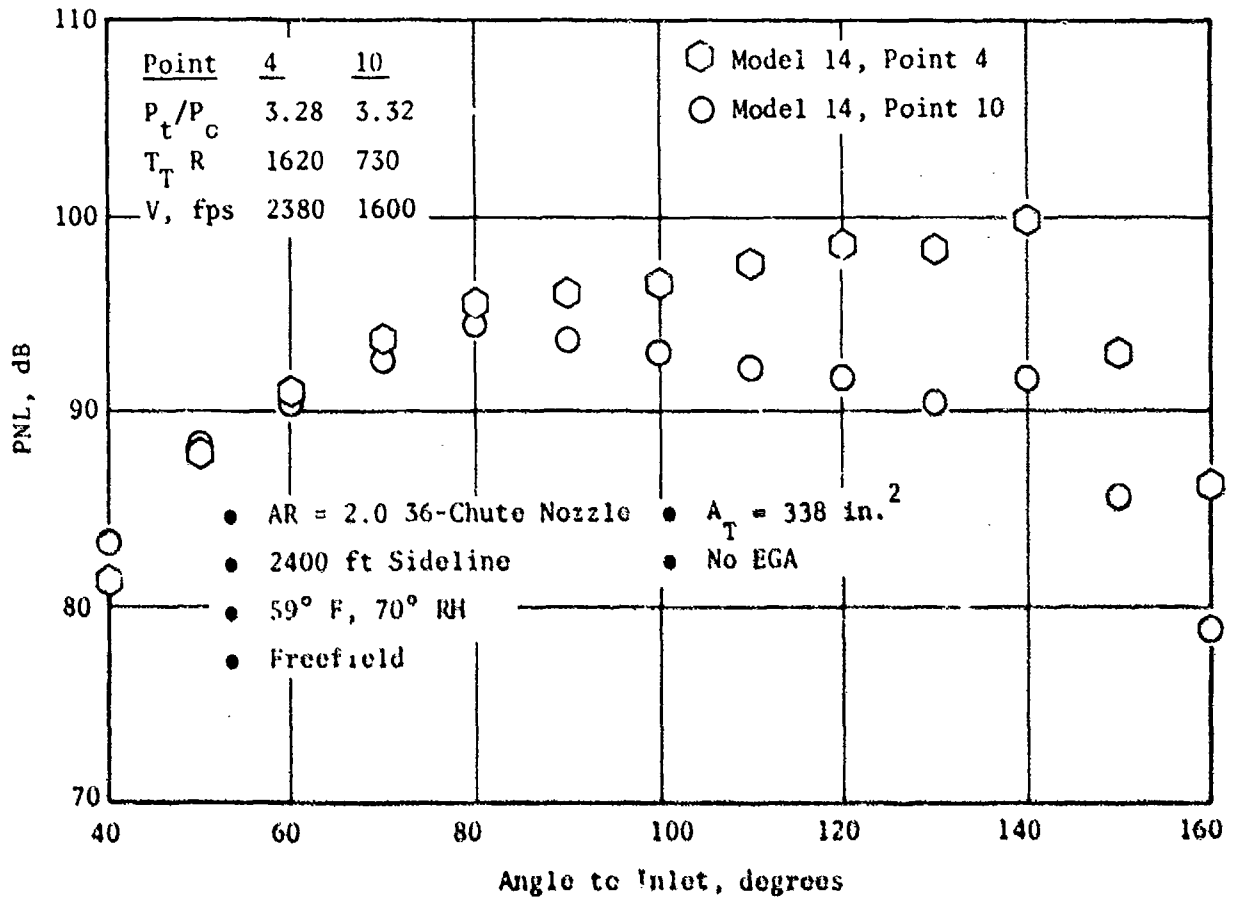


Figure 6-2. Typical Suppressor PNL Directivity Characteristics at Constant Pressure Ratio.

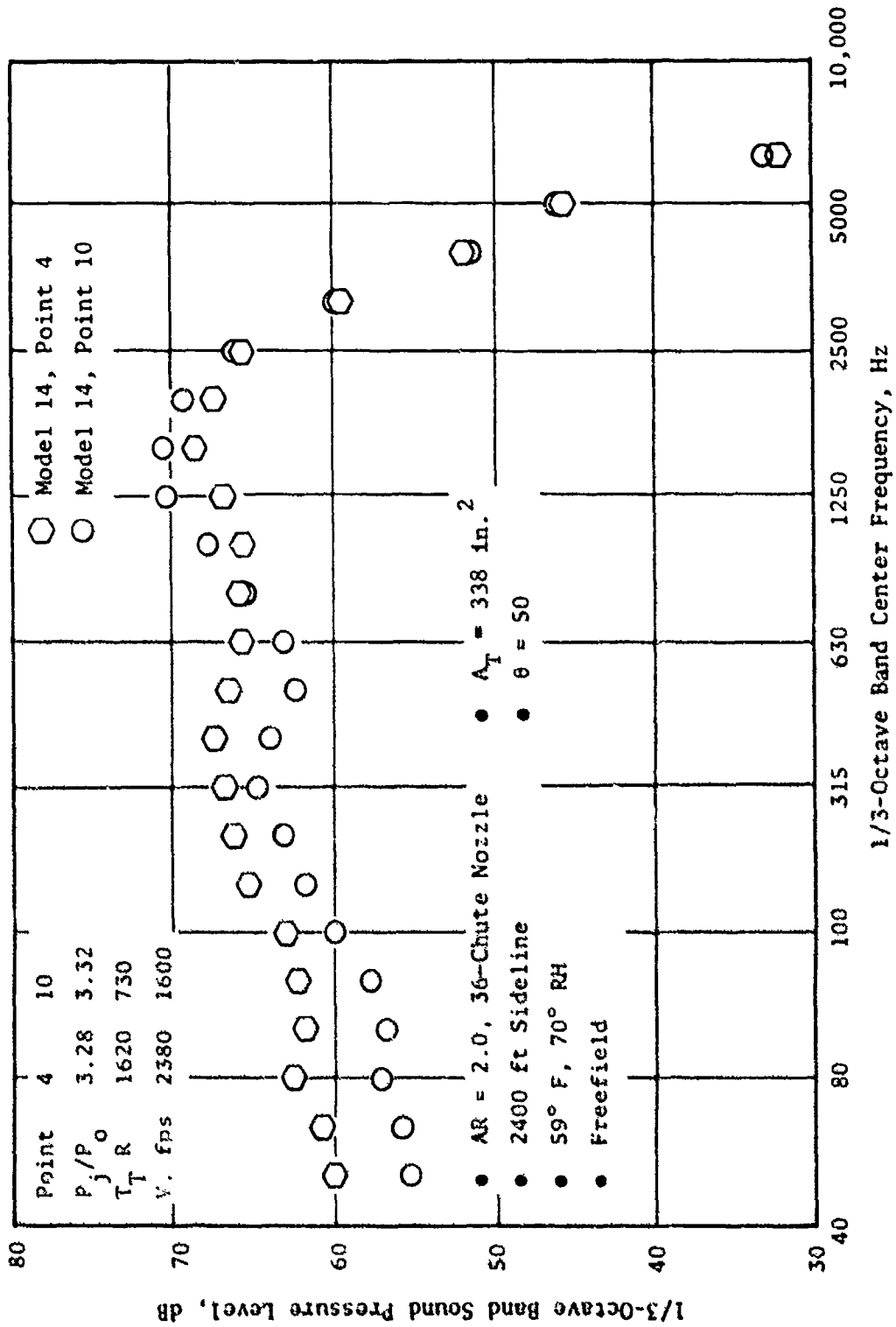


Figure 6-3. Typical Suppressor Spectra Characteristics at Constant Pressure Ratio.

- 0.7 in. Step Plug, Retracted
- $A_{Duct}/A_{Core} = 2.0$
- Radius Ratio = 0.716 (Duct)
- $A_T = 338 \text{ in.}^2$
- 2400 ft Sideline, No EGA
- 59° F, 70% R.H. Freefield

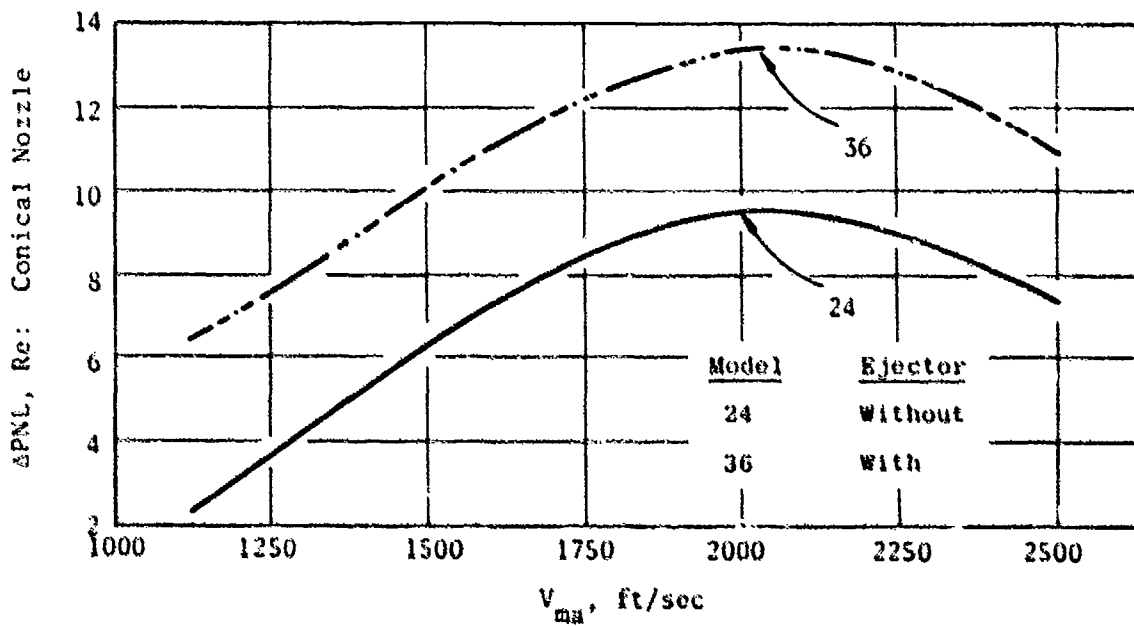


Figure 6-4. Impact of Acoustically Treated Ejector on Peak PNL of Dual Flow 36-Chute, Area Ratio = 2.0, With and Without Ejector.

System No. 5 is a coplanar mixer plug nozzle (alternate hot and cold flow elements), which was evolved because of its predicted aero performance and suppression considerations. This model configuration was selected from the application of the theoretical concepts developed in Task 2, Reference 7. Extensive diagnostic studies on multichute nozzles were carried out in Task 2, Reference 7. From these studies, a nozzle concept was developed which attempts to capitalize on the identified mechanisms of jet noise suppression. The first concept employed was that of injecting low velocity flow between the "chutes", which would provide several benefits: (1) reduce the shear, and hence the higher frequency noise, in the chute premerged zone, (2) eliminate the dependency of chute mixing on ambient air entrainment, and (3) improve the relative velocity effect in the flight condition. The low velocity flow between the chutes could be supplied by the bypass stream on an engine system application.

The second concept employed from Task 2 involved injecting low velocity flow between the chutes as a bypass stream, rather than through an inner core nozzle or base-bleed step. The plume should decay more rapidly with axial distance, because the bypass stream does not "fill up" the center of the plume. Instead, it is mixed with the ambient air along with the primary stream. This should produce lower convection Mach numbers and, hence, reduce the convective amplification effects at aft angles.

The employment of chutes for flow-splitting was deemed desirable from the standpoint of reducing shock-cell broadband noise. By using a 54-chute configuration, hydraulic diameter can be minimized, thus greatly shortening the shock structure and pushing the peak frequency of the shock noise component high enough to render it inaudible or highly vulnerable to air attenuation. The shock cell noise may also be controllable by properly matching primary and secondary stream pressure ratios. Finally, because the secondary (bypass) flow replaces the chute "base area", the aerodynamic performance of this concept over a conventional chute nozzle should be much improved ($C_{fg} = 0.96$, $M_0 = 0.30$).

In summary, these configurations are representative of systems that are applicable to single- and dual-flow advanced engine systems. The designs were based on experimental data and analytical methods from Government and industrial research programs. The designs, except for Configuration 5, were extracted from experimental data. Stronger emphasis was placed on the inverted flow profile dual-flow designs to establish a comprehensive free-jet data base on dual-flow nozzles to project full-scale flight noise levels. All configurations chosen are designed to yield high suppression levels in excess of 10 PNdB peak noise reduction. Based on jet noise considerations only, this suppression level will permit future commercial sustained supersonic cruise aircraft to meet subsonic aircraft noise regulations, FAR36, 1969.

These configurations were subjected to static and free-jet testing in the General Electric Anechoic free-jet facility. Flight suppression levels were established based on these test results and are reported in Task 5 of this contract.

7.0 CONCLUSIONS

The subject of this report has been suppressor concept optimization. Several procedures for rating suppressors have been discussed. Trade studies of performance versus suppression have indicated that static performance and suppression measurements are inadequate to define the characteristics of the suppressor exhaust system in flight. Flight performance and flight suppression must, as a minimum, be established based on wind tunnel aero performance testing and acoustic free-jet testing.

Aircraft integration studies have shown that to assess the impact of mechanical suppressors on the aircraft mission, acoustic suppression level, aero performance level, and suppressor weight must be considered simultaneously. The level of acoustic suppression was found to be the most important design variable, with performance degradation and engine weight increase ranking second and third, respectively. Generally speaking, although the addition of a mechanical suppressor increases weight and reduces performance, for a specified noise goal the suppressor allows the use of a smaller engine which results in a range advantage. Based on jet noise considerations only, it was found that ranges in excess of 4000 nautical miles could be achieved and still maintain a traded EPNL noise level of 108.

The figure of merit at the preliminary design level which incorporated suppression level, performance, and weight, was found to be aircraft range for a sustained supersonic cruise commercial aircraft. Several interim rating procedures were identified but were found to have a limited range of applicability. The optimum nozzle design studies, based on static experimental and analytical results, suggest that dual-flow suppressor nozzles may be designed with suppression levels ranging from 10 to 12 PNdB relative to a single-flow conical nozzle system of equivalent specific thrust.

Diameter scaling, based on Strouhal number, was found to provide adequate agreement between full-scale and scale-model data on the basis of peak noise and directivity characteristics within ± 2 PNdB. A standard conical nozzle should be used as the noise baseline by all industry and Government researchers.

APPENDIX A

ACOUSTIC SCALING DEMONSTRATION

1.0 INTRODUCTION

A program was conducted to further develop and confirm acoustic scaling procedures applicable to baseline and suppressor nozzles. The objective was achieved through a comparison of scale-model and full-scale acoustic test results. Current acoustic scaling methods for jet noise assume the agreement of normalized far-field acoustic data when nozzle size is scaled by a physical diameter change. Normalization is achieved through a linear expression with jet diameter and mean jet velocity by maintaining a constant Strouhal number, and by raising the density to various exponents. Previous experience has generally substantiated this scaling method, primarily on subjective parameters of peak PNL and PNL suppression. Spectral scaling has also been shown to be fairly consistent at the peak PNL angle for the same range of nozzle types. When scaling off-peak angles, however, particularly far from the peak jet noise, results have not been as consistent depending on the particular test vehicle and setup. Inaccuracies have been attributed to the mode of data acquisition, and to extraneous non-jet noise sources in most engine systems, which were not suppressed prior to test and which could not be confidently removed during data analysis. Influences such as these must be eliminated if real engines are to be used to provide a hot gas source for comparing large scale jet noise to model data over the entire spectrum of jet noise. Ground reflection must also be eliminated in the test setup (or confidently corrected for) through use of data reduction/analysis methods and appropriate measurement techniques.

2.0 METHOD OF APPROACH

The work scope encompassed the comparison of scale-model data with full size engine test data for the following configurations:

J79 Engine - Conical nozzle baseline, 32-element multichute suppressor with and without an acoustically treated ejector.

J85 Engine - Conical nozzle baseline, 8-lobe nozzle, and 104-tube suppressor.

Far-field acoustic data for the model and full-scale nozzles (same nozzle total pressures and temperatures, different only in size) were used to demonstrate agreement between model and full-scale results. Far-field acoustic scale-model data (SPL, PWL, PNL) corrected for air absorption and ground effects were compared with full-scale engine data after using conventional scaling factors, including Strouhal number, for the frequency-diameter relationship and nozzle throat area for the sound-power-level scale factor.

There is some possibility that the nozzle discharge airflow turbulence levels may be inherently different for model and engine operation such that the noise generation levels are affected. Model and full-scale J79, laser velocimeter surveys were therefore made of the exhaust plumes. This information was required to assess whether any differences between scale-model and full-scale noise comparisons should be expected. Ellipsoidal mirror measurements were also made at selected points for direct comparison of apparent noise source locations in the exhaust plume.

3.0 TEST FACILITIES AND HARDWARE DESCRIPTION

3.1 SCALE-MODEL ACOUSTIC TEST FACILITY

The Jet Engine Noise Outdoor Test Stand (JENOTS) is located at Evendale, Ohio. The sound field consists of 14 microphones arranged on 10° intervals around a 40-foot arc from 30° to 160°, centered at the nozzle discharge plane centerline which is 55 inches above the ground. The microphones are elevated 16 feet above the ground on specially designed "gooseneck" mounts to minimize the influence of reflections. This facility is described in detail in Reference 18.

Facility data consisting of airflow, total temperatures, total pressures, cooling water temperature and pressure, and meteorological data are recorded for each test run.

The facility also has a system which permits aerodynamic and acoustic in-jet instrumentation to traverse parallel to the jet exhaust plume axis. This system is normally used to accept either the ellipsoidal mirror (EM) (Figure A-1), for noise source location measurements, or the laser velocimeter (LV) (Figure A-2), for turbulent flow velocity measurements.

3.2 FULL-SCALE TEST FACILITY - J79 ENGINE

A J79-15 engine was installed at Edwards Flight Test Center, California, to obtain full-scale (effective nozzle diameter = 20.84 inches) jet noise data. The north site location was chosen due to the absence of surrounding buildings and obstructions.

The sound field used during the J79 exhaust nozzle tests consisted of 13 microphone stations distributed around a 160-foot arc extending from 40° to 160° (engine inlet plane referenced) in 10° increments. At each station, two microphones were erected to approximate heights of 2 feet and 12 feet above the ground. The ground surrounding the thrust pad was graded to obtain a smooth acoustic arena. The control room was 3/4 submerged underground to eliminate sound reflections. This facility is described in detail in Reference 18.

The engine was fitted with elaborate inlet and exhaust acoustically treated ducts, plus turbine treatment, to eliminate as best possible all rotating-parts noise contamination of jet noise. An acoustically treated half-box was also used to shield any casing-transmitted noise from the microphone field. The afterburner section and tailpipe assemblies, which are normally connected to the turbine frame, were replaced by an acoustically treated turbine exhaust suppressor to which the exhaust nozzles could be fastened using different adaptor spools. Eight wall static taps and two 4-element combination total pressure and total temperature rakes were

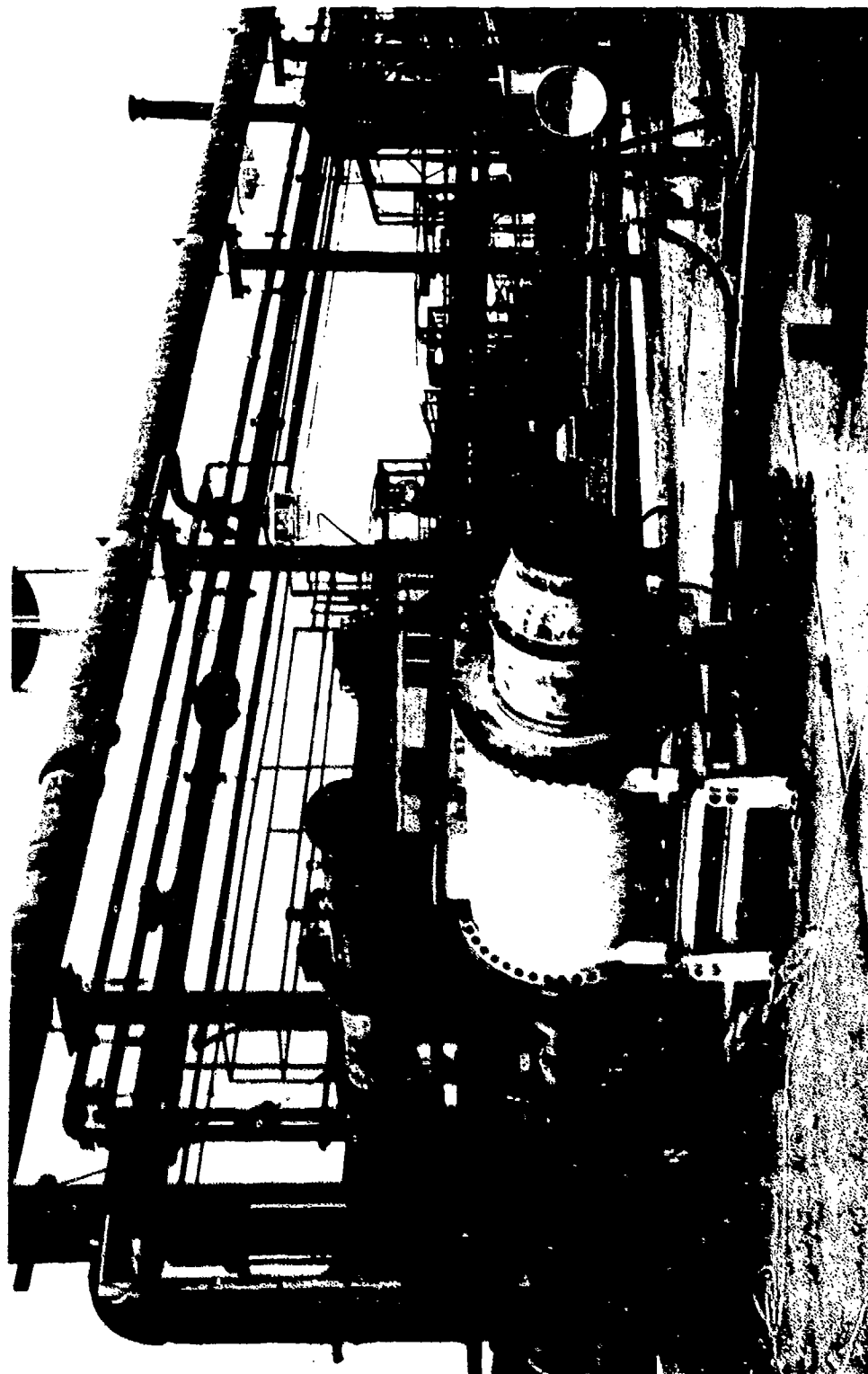


Figure A-1. Ellipsoidal Mirror Setup at JENOTS.

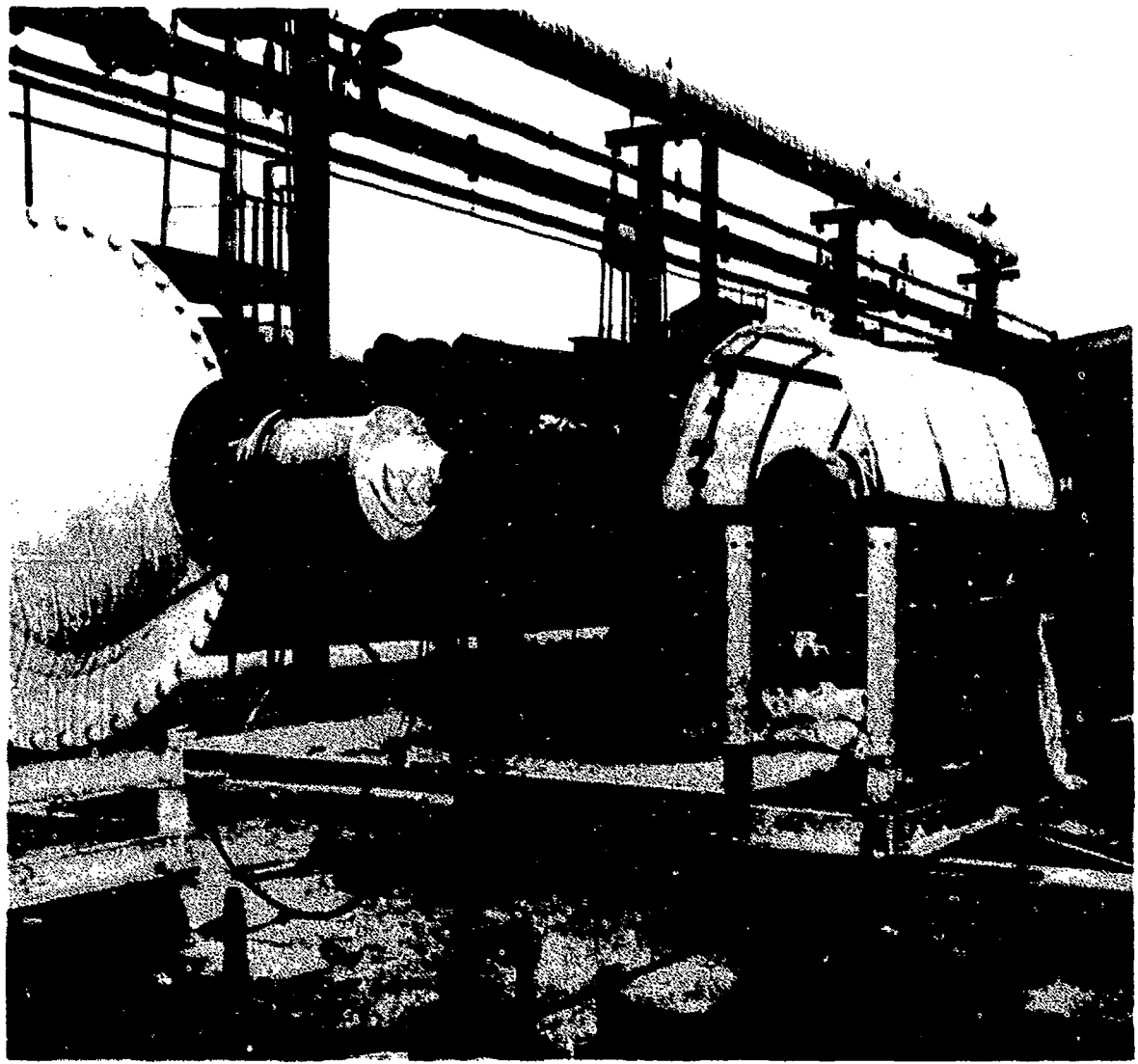


Figure A-2. Laser Velocimeter Setup at JENOTS.

installed in the adaptor spool. The engine was mounted on a stand secured to a thrust pad such that the engine centerline was 12 feet above the thrust pad. A schematic and a photograph of this installation are presented in Figures A-3 and A-4.

3.3 FULL-SCALE TEST FACILITY - AEROTRAIN WITH J85 ENGINE

The Aerotrain test facility is located at Gometz, France. The Aerotrain is operated on a 6-km track. It is propelled by a J85 turbojet engine (modified to have a 1.97-ft treated inlet and 3.28-ft treated exhaust duct) and is supported by an air cushion which is provided by a Palouste engine. The inlet and fan exhaust of the Palouste engine are also treated to minimize the contamination of the J85 jet noise signature. The vehicle is capable of static operation and of simulating flight speeds of up to 275 ft/sec.

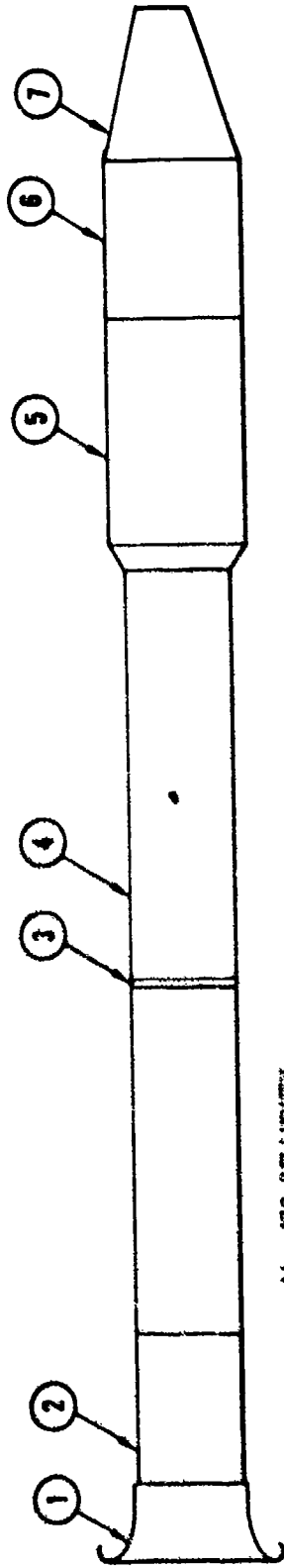
Far-field acoustic measurements were made during the Aerotrain test program. The measurements were made using four 1/4-inch B&K microphones placed at a sideline distance of 164 feet from the test track. Three of the microphones were at a height of 51 feet and spacing of 39.4 feet, while the fourth microphone was at a height of 24.6 feet on the center pole. The spacing between the three microphones was chosen to provide statistically independent data samples. The two microphone heights were chosen to provide information on the impact of ground reflections.

This facility is described in detail in Reference 10.

3.4 TEST CONFIGURATIONS

Test data from 14 conical and suppressor nozzle configurations were used for the scaling studies. Eight model size configurations were tested at the JENOTS facility, three engine size configurations were tested at the Edwards Center, and three engine size configurations were tested on the Aerotrain. Descriptions of all configurations along with schematics and photographs are given in Table A-1. A detailed description of each model can be found in the reference corresponding to each model.

The J79 suppressor configurations were duplicated and tested in an equivalent flow model size of 5.7-inch diameter, and the J85 suppressor configurations were duplicated and tested in a model size of 4.0-inch diameter. Four scale-model conical nozzles having diameters of 2.0 inches, 3.56 inches, 4.0 inches, and 5.7 inches were evaluated. (The 4.0-inch nozzle duplicated the internal and external flowpath of the Aerotrain conical nozzle; the three configurations were typical baseline configurations from this and the free-jet test program described in Reference 10.)



- 1) J79 BELLMOUTH
- 2) ACOUSTICALLY TREATED INLET SUPPRESSOR
- 3) SLIP JOINT
- 4) J79-15 ENGINE
- 5) ACOUSTICALLY TREATED EXHAUST SUPPRESSOR
- 6) NOZZLE ADAPTER SPOOL, INCLUDING TWO 4 ELEMENT Pt-Ti COMBINATION EXHAUST RAKES AND EIGHT WALL STATIC TAPS ON OUTER WALL
- 7) CERTIFICATION CONIC NOZZLE: 338 IN²

Figure A-3. J79 Engine Stackup.

110

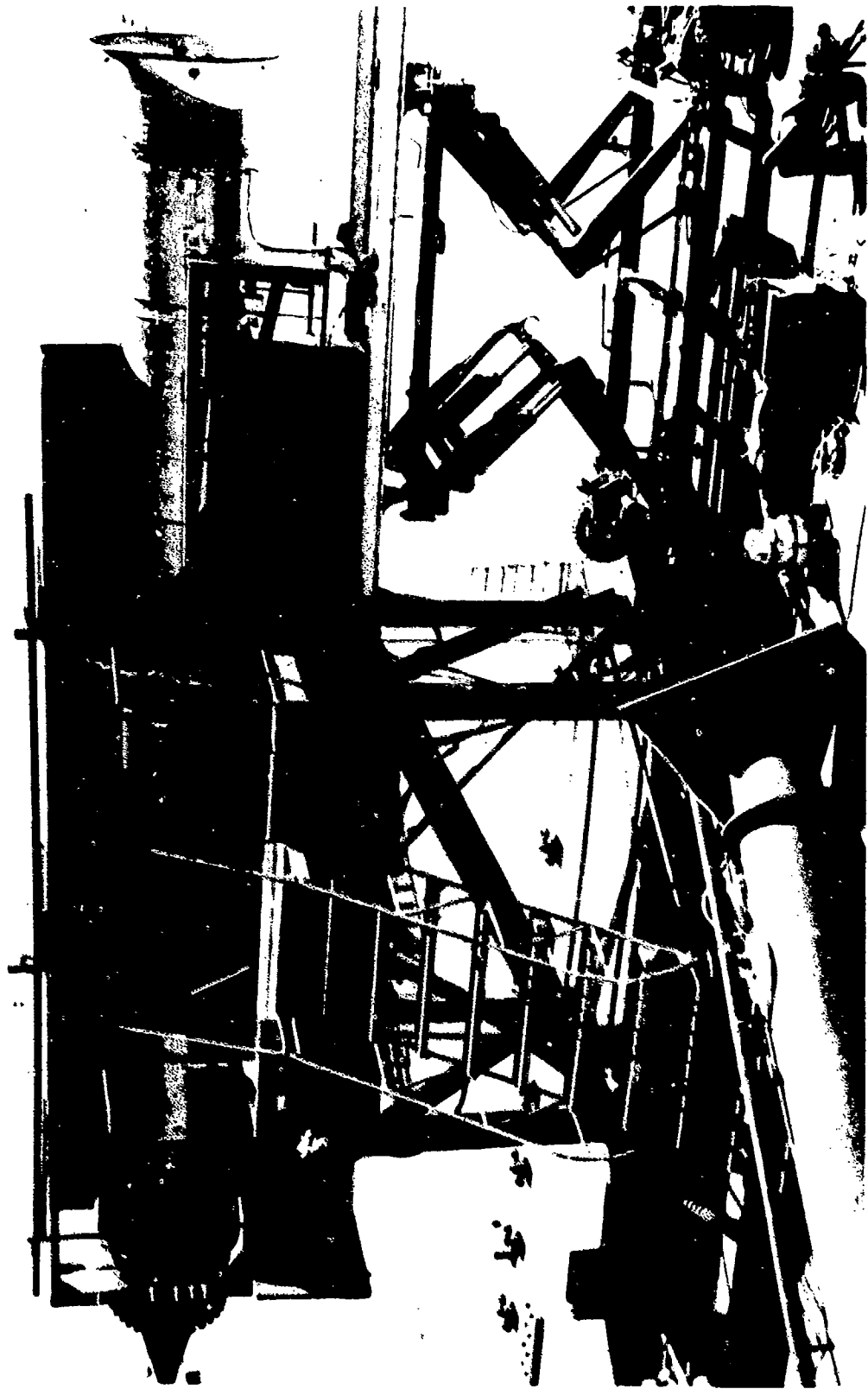
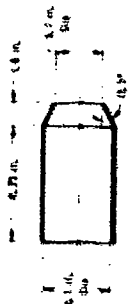



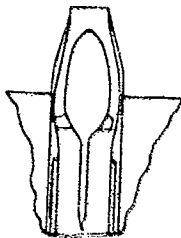






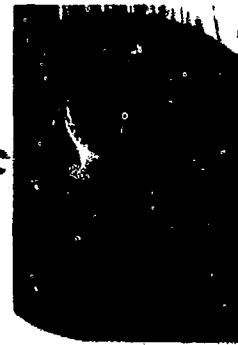
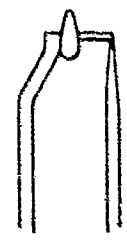

Figure A-4. Unshielded View of J79 Engine Installation at GE/EFTC.

Table A-1. Description of Test Configurations.

<u>Model No.</u>	<u>Title</u>	<u>Site</u>	<u>Test Location</u>	<u>Area in.²</u>	<u>Scale Factor</u>	<u>Details in Ref.</u>	<u>Schematic</u>	<u>Photograph</u>
1	5.7 inch Conical Nozzle	Model	JENOTS	23.63	3.64	3		
2	4.0 inch Conical Nozzle	Model	JENOTS	12.57	5.17	Values in		
3	3.56 inch Conical Nozzle	Model	JENOTS	9.95	3.71	10		

104

Table A-1. Description of Test Configurations (Continued).

Model No.	Title	Size	Test Location	Area in.²	Scale Factor DVS/ME	Deflection in Ref.	Schematic	Photograph
4	2.0 Inch STA Conical Nozzle	Model	JEMOPS	3.14	2.89	10		
5	104-Tube	Model	JEMOPS	12.03	2.88	10		
6	B-Lobe	Model	JEMOPS	12.56	2.94	10		

100

Table A-1. Description of Test Configurations (Continued).



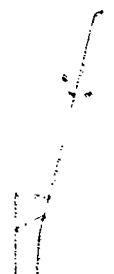




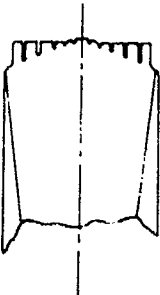


<u>Model No.</u>	<u>Title</u>	<u>Silo</u>	<u>Test Location</u>	<u>Area in. 2</u>	<u>Scale Factor DFT/BM</u>	<u>Details in Ref.</u>	<u>Schematic</u>	<u>Photograph</u>
7	32-Chart	Model	JENNINGS	26.15	3.59	4		
8	32-Chart * 1/2 Factor	Model	JENNINGS	26.15	3.59	4		
9	Conic	J79 Engine	Edwards AFB	215	1.0	4		

Table A-1. Description of Test Configurations (Continued).

<u>Model No.</u>	<u>Title</u>	<u>Size</u>	<u>Test Location</u>	<u>Area in.²</u>	<u>Scale Factor DFS/DM</u>	<u>Details in Ref.</u>	<u>Schematic</u>	<u>Photograph</u>
10	32-Chute	J79 Engine	Edwards AFB	338	1.0	4		
11	32-Chute + Ejector	J79 Engine	Edwards AFB	338	1.0	4		
12	Conic	J85 Engine	Aerotrain Gometz, FR	108.6	1.0	10		

Table A-1. Description of Test Configurations (Concluded).

<u>Model No.</u>	<u>Title</u>	<u>Size</u>	<u>Test Location</u>	<u>Area</u>	<u>Scale Factor</u>	<u>Details</u>	<u>Photograph</u>
				15.2	DPS/DM	in Ref.	
13	104-Tube	J85 Engine	Aerobatic Cometz, FR	108.6	1.0	10	
							
14	8-Tube	J85 Engine	Aerobatic Cometz, FR	108.6	1.0	10	
							

3.5 LV AND EM TEST HARDWARE

The LV system used at JENOTS and Edwards Center is a two-part system consisting of the laser velocimeter optics package and the laser velocimeter signal processing equipment. The laser velocimeter optics package was specifically designed for outdoor operation in the high noise, high vibration environment near the exhaust plume. The LV optics package was mounted on a remotely actuated platform on tracks parallel to the jet axis. The laser velocimeter signal processor was located in the control room along with recording and display equipment. Since the LV has a fixed working range of 85 inches, measurements at different points in the jet are accomplished by traversing the platform along three axes: horizontal, vertical, and axial (jet axis). The LV was operated in a traversing mode to obtain continuous profiles of mean axial velocity, and it was operated in a stationary mode to construct velocity histograms for determination of both mean and rms turbulent axial velocities at discrete points. The LV system is described in detail in Reference 18. A photograph of the test setup for the LV mounted on the traversing cart at the Edwards facility is shown on Figure A-5. This setup is described in Reference 4.

The 18-inch ellipsoidal mirror was installed on a traversing cart for detailed mapping of the noise sources in the jet plume of a conical nozzle. Measurements were taken by slowly moving the cart parallel to the jet axis. A 1/8-inch B&K 4138 microphone was installed in the mirror's elliptic focus with the second focus at the center of the jet. The EM system is described in detail in Reference 18.

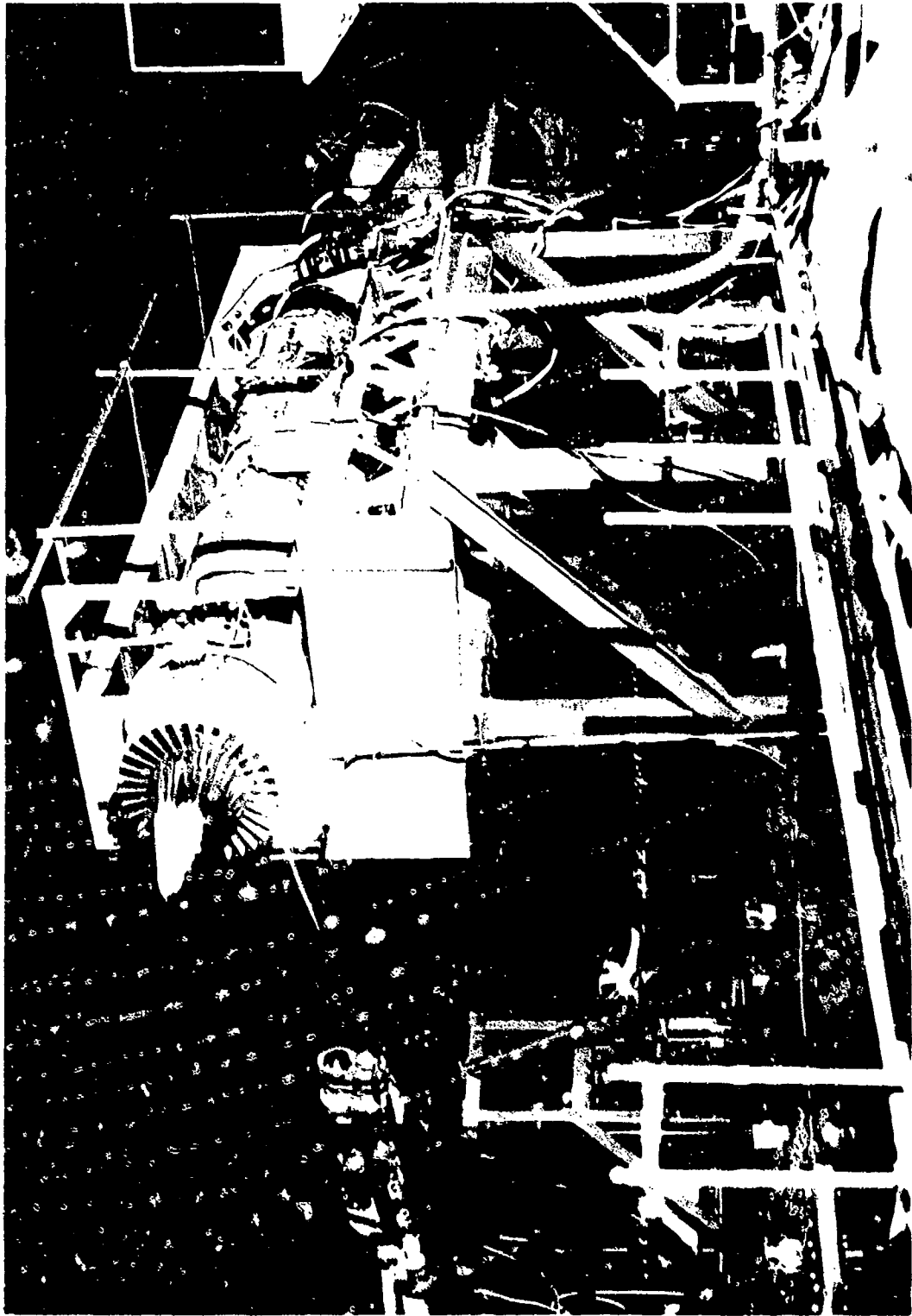


Figure A-5. Laser Velocimeter Measurements on the J79 Engine with 32-Chute Nozzle.

4.0 TEST MATRIX

The test matrix was designed to cover a range of conditions which would provide sufficient data for a meaningful scaling comparison. The range of conditions chosen is shown in Table A-2 for both model size and engine size tests. A wide range of conditions from the subsonic velocity regime through the supersonic velocity regime was covered, as shown on the table.

A detailed summary of all test points for all 14 configurations is presented in Tables A-3 through A-14.

Table A-2. Range of Test Conditions.

Size (Location)	P_{T8}/P_0	T_{T8} ($^{\circ}$ R)	V_8 (ft/sec)
Model (JENOTS)	1.08+3.85	506+1878	466+2899
J79 (Edwards)	1.07+2.59	1005+1652	496+2189
J85 (Aerotrain)	1.55+2.46	1367+1850	1400+2254

Table A-3. Test Matrix, 5.7-inch Model.

Data Point	P _t /P _o	T _t	V _j	M _j	50° OASPL	90° OASPL	Max OASPL	90° PNL	50° PNL	Max PNL	Normalized by 10 log [(ρ _j /ρ _{ISA}) ^m (A _j /R ²)]				10 log (ρ _j /ρ _{ISA}) ^{m-1}	10 log [(ρ _j /ρ _{ISA}) ^m (A _j /R ²)]	OAPWL-10 log (ρ _j /ρ _{ISA}) ^{m-1}			
											50° OASPL	90° OASPL	Max OASPL	90° PNL			50° PNL	Max PNL	90° OASPL	50° OASPL
1	1.089	1067	556	0.355	82.4	84.1	91.7	86.4	88.5	92.1	160	160	160	121.0	122.7	130.3	130.7	125.0	127.1	135.3
2	1.294	1089	967	0.625	92.5	95.5	102.4	100.4	104.0	109.3	160	160	160	134.1	137.1	150.0	150.9	142.0	145.6	152.3
5	1.901	1347	1598	1.015	106.2	108.7	125.1	114.4	118.9	130.4	150	150	150	151.9	154.4	170.8	176.1	160.1	164.6	172.5
7	2.848	1318	1728	1.083	108.3	110.7	126.9	116.9	121.1	133.5	150	150	150	154.8	157.2	173.4	180.0	163.4	167.6	175.2
10	2.285	1365	1890	1.172	112.2	113.7	128.7	121.2	124.6	136.4	140	140	140	159.2	160.7	175.7	183.4	168.2	171.6	177.9
11	2.453	1460	2015	1.231	110.9	115.8	130.9	121.7	127.1	138.6	140	140	140	158.2	163.1	178.2	185.9	169.0	174.4	180.2
12	2.515	1473	2049	1.251	115.7	116.8	130.9	125.5	128.2	139.0	140	140	140	163.0	164.1	178.2	186.3	172.8	175.5	180.8
15	2.586	1582	2155	1.275	116.8	118.3	132.3	126.6	129.8	140.6	130	130	130	164.6	166.1	180.1	188.4	174.4	177.6	182.6
17	2.947	1806	2834	1.372	121.3	123.0	138.0	130.3	133.9	146.9	130	130	130	170.1	171.8	186.8	195.7	179.1	182.7	188.1

Table A-4. Test Matrix, 4.0-inch Model.

Data Point	F _T /P ₀	T _T	V _j	K _j	50° OASPL	90° OASPL	Max OASPL	50° PNL	90° PNL	OAPFL	log(V _j /a ₀)	10 log(O _j /P _{ISA}) ⁻¹	10 log(O _j /P _{ISA}) ^w (A _j /R _j) ⁻¹	Normalized by 10 log [(O _j /P _{ISA}) ^w (A _j /R _j) ⁻¹]						OAPFL-10 log (O _j /P _{ISA}) ⁻¹	
														50° OASPL	90° OASPL	Max OASPL	50° PNL	90° PNL	Max PNL		
12	2.545	1693	2197	1.25	115.8	118.4	131.2	130	140.8	125.8	0.294	-4.1	-48.5	164.3	166.9	179.7	189.3	174.3	178.4	183.4	183.4
30	2.281	1693	2079	1.17	112.2	115.9	130.7	140	136.8	122.0	0.270	-4.2	-48.8	161.0	164.7	179.0	187.6	170.8	175.9	181.7	181.7
31	2.472	1003	1658	1.22	116.5	115.5	126.7	150	134.8	126.5	0.172	-1.4	-43.6	160.1	159.1	170.3	178.4	170.1	170.6	176.1	176.1
32	3.004	999	1800	1.36	120.7	120.3	130.6	140	139.0	130.7	0.208	-1.4	-43.3	164.0	163.6	173.9	182.3	174.0	175.1	179.9	179.9
33	3.506	1001	1804	1.47	123.5	123.2	133.2	140	141.8	133.5	0.232	-1.3	-43.0	166.5	166.2	176.2	184.8	176.5	177.3	182.3	182.3
34	2.697	1497	1981	1.23	115.5	117.0	130.5	140	139.1	125.9	0.249	-3.3	-46.9	162.4	163.9	177.4	186.0	172.8	175.6	181.0	181.0
35	2.994	1411	2145	1.36	120.6	121.0	133.1	140	141.7	130.8	0.284	-3.1	-46.5	167.1	167.5	179.6	188.2	177.3	179.0	185.9	185.9
36	3.489	1386	2245	1.47	123.0	123.7	133.9	130	143.7	133.2	0.304	-2.8	-45.9	168.9	169.6	179.8	189.6	179.1	180.8	185.4	185.4
37	2.389	1799	2192	1.21	113.6	117.2	130.6	130	140.5	123.5	0.294	-4.4	-49.2	162.8	166.4	179.8	189.7	172.7	177.7	183.1	183.1
38	3.135	1692	2396	1.40	121.0	122.6	133.9	130	143.7	131.3	0.332	-3.8	-48.0	169.0	170.6	181.9	191.7	179.3	182.1	186.0	186.0
39	3.432	1708	2486	1.47	122.6	123.8	135.0	130	144.4	133.0	0.348	-3.8	-47.9	170.5	171.7	182.9	192.3	180.9	183.3	187.0	187.0
12	2.545	1693	2197	1.25	115.1	117.7	130.4	130	141.5	126.9	0.294	-4.1	-49.4	164.5	167.1	179.8	190.9	176.3	180.2	178.9	178.9
30	2.281	1693	2079	1.17	111.5	115.2	129.4	140	139.8	123.4	0.270	-4.2	-49.7	161.2	164.9	179.1	189.5	173.1	177.7	177.1	177.1
31	2.472	1003	1658	1.22	115.7	114.8	125.9	150	135.9	127.5	0.172	-1.4	-44.4	160.1	159.2	170.3	180.3	171.9	172.2	171.6	171.6
32	3.004	999	1800	1.36	120.0	119.6	129.8	140	140.1	131.4	0.208	-1.4	-44.1	164.1	163.7	173.9	184.2	175.5	176.4	175.4	175.4
33	3.506	1001	1904	1.47	122.7	122.5	132.5	140	142.8	134.1	0.232	-1.3	-43.8	166.5	166.3	176.3	186.6	177.9	178.7	177.8	177.8
34	2.697	1407	1981	1.23	114.8	116.3	129.7	140	140.0	126.9	0.249	-3.3	-47.8	162.6	164.1	177.5	187.8	174.7	177.2	176.4	176.4
35	2.994	1411	2145	1.36	119.9	120.3	132.4	140	142.6	131.8	0.284	-3.1	-47.3	167.2	167.6	179.7	189.9	179.1	180.4	179.4	179.4
36	3.489	1386	2245	1.47	122.3	123.0	133.1	130	144.2	134.1	0.304	-2.8	-46.8	169.1	169.8	179.9	191.0	180.9	182.5	180.9	180.9
37	2.389	1799	2192	1.21	112.9	116.5	129.8	130	140.9	124.7	0.294	-4.4	-50.1	163.0	166.6	179.9	191.0	174.8	179.5	178.6	178.6
38	3.135	1692	2396	1.40	120.3	121.9	133.2	130	144.1	132.2	0.332	-3.8	-48.9	169.2	170.8	182.1	193.0	181.1	183.7	181.4	181.4
39	3.432	1708	2486	1.47	121.6	123.1	134.3	130	145.0	133.6	0.348	-3.8	-48.8	170.6	171.9	183.1	193.8	182.4	184.8	182.4	182.4

Table A-5. Test Matrix, 3.56-inch Model.

Data Point	P _r /P _o	T _r	V _r	M _r	50°		Max OASPL	Max PNL	50° PNL	OASPL	90° PNL	Normalized by 10 log [(ρ _r /ρ _{ISA}) ^m (A _r /R _r ²)]						10 log (ρ _r /ρ _{ISA}) ⁻¹	10 log [(ρ _r /ρ _{ISA}) ^m (A _r /R _r ²)]	10 log (ρ _r /ρ _{ISA}) ⁻¹			
					OASPL	Max PNL						90° OASPL	Max PNL	90° OASPL	Max PNL	90° OASPL	Max PNL				90° OASPL	Max PNL	
1	1.171	1204	799	0.486	83.2	87.7	93.6	140	160.2	92.7	97.7	137.7	-0.145	3.4	-41.3	124.5	129.0	134.9	141.5	134.0	139.0	134.3	134.3
2	1.352	1255	1118	0.679	91.3	96.3	104.7	150	111.9	101.7	107.3	148.2	0.001	0.7	-44.0	135.3	140.3	148.7	155.9	145.7	151.3	147.5	147.5
3	1.475	1262	1265	0.775	94.6	99.0	110.1	150	116.8	104.6	110.1	152.4	0.054	-0.4	-45.1	139.7	144.1	155.2	161.9	149.9	155.2	152.8	152.8
4	1.605	1435	1581	0.863	99.1	104.1	115.5	150	122.6	110.0	115.5	157.8	0.123	-2.2	-47.3	146.4	151.4	162.8	169.9	157.3	162.8	160.0	160.0
5	1.957	1464	1760	1.041	104.4	108.3	121.7	150	130.7	115.3	120.6	164.0	0.198	-3.5	-48.5	152.9	157.2	170.2	179.2	163.8	169.1	167.5	167.5
6	2.090	1582	1857	1.063	105.5	109.5	123.4	140	132.5	116.2	121.6	165.5	0.221	-4.0	-49.3	154.8	159.1	172.7	181.8	165.5	170.9	169.5	169.5
7	2.278	1697	2080	1.168	108.6	112.9	126.6	140	136.3	119.9	125.0	168.8	0.270	-4.2	-49.7	158.3	162.6	176.3	186.0	169.6	174.7	173.0	173.0
8	2.447	1844	2351	1.226	111.0	114.9	128.3	150	137.9	122.8	127.4	170.7	0.305	-4.5	-50.3	161.3	165.2	178.6	188.2	173.1	177.7	175.2	175.2
9	3.128	1687	3340	1.401	118.0	119.6	131.9	160	141.1	129.4	132.0	174.5	0.331	-3.8	-48.9	166.9	168.3	180.8	190.0	178.3	180.9	178.3	178.3
10	3.542	1704	2856	1.469	119.6	120.7	133.2	140	142.0	130.5	132.6	175.8	0.348	-3.8	-48.7	168.3	168.9	181.9	190.7	179.2	181.3	179.6	179.6
11	3.740	1799	2627	1.527	120.8	121.4	133.4	140	142.2	131.9	134.0	176.3	0.372	-3.9	-49.0	169.8	170.4	182.4	191.2	180.9	183.0	180.2	180.2
12	1.569	1435	1466	0.853	98.3	101.0	114.7	140	122.2	108.9	114.1	157.3	0.119	-2.1	-47.2	145.5	150.2	161.9	169.4	156.1	161.3	159.4	159.4
13	1.983	1561	1834	1.054	104.9	109.5	123.4	150	132.3	115.7	121.2	165.6	0.216	-3.9	-49.2	154.1	158.7	172.6	181.5	164.9	170.4	169.5	169.5
14	2.655	1877	2253	1.228	110.9	114.8	128.6	140	138.1	122.9	127.2	171.0	0.305	-4.5	-50.2	161.1	165.0	178.8	188.3	173.1	177.4	175.5	175.5
43	2.492	997	1660	1.222	112.8	111.5	124.3	150	131.9	124.7	124.6	166.0	0.172	-1.4	-44.3	157.1	155.8	168.6	177.2	169.0	168.9	167.4	167.4
44	2.987	997	1796	1.356	117.6	116.8	127.5	150	136.6	128.7	129.2	170.5	0.207	-1.4	-44.1	161.7	160.9	172.0	180.9	172.8	173.3	171.9	171.9
45	2.683	997	1856	1.464	120.4	119.2	130.8	150	140.0	130.9	131.8	173.3	0.230	-1.3	-43.8	164.2	163.5	174.6	183.8	174.7	175.6	174.6	174.6
46	2.892	1400	1974	1.231	111.8	112.8	127.2	140	136.6	123.6	125.6	168.9	0.248	-3.2	-47.7	159.5	160.5	174.9	184.3	171.3	173.3	172.1	172.1
47	2.995	1399	2134	1.366	117.3	116.8	130.2	140	139.5	128.6	129.5	172.3	0.282	-3.0	-47.2	164.5	164.0	177.4	186.7	175.8	176.7	175.3	175.3
48	3.491	1402	2256	1.472	119.6	119.6	132.8	140	141.4	130.9	132.3	175.3	0.306	-2.8	-46.9	166.7	166.7	179.7	188.3	177.8	179.2	178.1	178.1

Table A-6. Test Matrix, 2.0-inch Model.

Data Point	F _r /P _o	T _r	V _j	M _j	50° OASPL	90° OASPL	Max OASPL	θ _i	Max PNL	50° PNL	90° PNL	OASPL	OASPL	Max PNL	50° PNL	90° PNL	Normalized by 10 log [(ρ _j /ρ _{ISA}) ^w (A _j /R ²)]		10 log [(ρ _j /ρ _{ISA}) ^{w-1} (A _j /R ²)]	10 log [(ρ _j /ρ _{ISA}) ^{w-1} (A _j /R ²)]	10 log [(ρ _j /ρ _{ISA}) ^{w-1} (A _j /R ²)]		
																	50° OASPL	90° OASPL				Max PNL	50° PNL
202	1.155	1302	765	0.465	84.1	87.7	95.0	150	100.1	93.5	96.4	139.2	128.8	141.2	134.6	137.5	135.6						
203	1.146	1256	1110	0.674	93.1	97.3	107.9	150	113.3	103.2	107.0	150.7	141.2	151.8	147.1	150.9	149.9						
204	1.467	1274	1263	0.770	96.9	100.9	112.4	150	118.5	107.1	110.9	155.1	146.0	157.5	163.6	152.2	156.0	155.5					
205	1.575	1287	1375	0.847	99.4	103.1	115.8	150	122.4	109.4	113.3	158.1	149.0	161.7	168.3	155.3	159.3	159.3					
206	1.405	1418	1632	0.970	103.7	107.4	122.1	150	130.0	114.0	117.9	164.1	155.3	170.0	177.9	161.9	165.8	167.0					
207	1.968	1509	1794	1.047	106.5	110.0	124.0	150	133.9	116.8	120.9	167.0	158.8	173.4	182.7	165.6	169.7	170.7					
208	2.262	1700	2074	1.163	110.3	113.6	127.5	130	137.3	126.8	125.1	170.8	163.3	177.2	187.0	170.5	174.8	175.0					
209	2.516	1694	2194	1.750	113.8	116.1	129.5	130	139.7	125.7	128.0	172.6	164.2	178.9	189.1	175.1	177.4	176.7					
210	3.125	1691	2192	1.401	120.9	120.6	132.6	130	142.5	131.8	132.5	175.6	169.8	181.5	191.4	180.7	181.4	179.4					

Table A-7. Test Matrix, 32-Chute Model.

Data Point	Pr/Po	Tt	Vj	Mj	50° OASPL	90° OASPL	Max OASPL	61	Max PNL	50° PNL	90° PNL	OASPL	PNL	OASPL	PNL	Max OASPL	Max PNL	Normalized by 10 log [(ρj/ρISA) ^ω (A _j /R ²)]							
																		10 Log(pj/pISA) ^{ω-1}		10 Log(pj/pISA) ^ω (A _j /R ²)		50°		90°	
																		Log(Vj/ao)				OASPL	PNL	OASPL	PNL
1	1.082	1100	541	0.142	80.1	81.5	86.2	120	94.4	88.5	91.7	137.1	137.1	120.9	132.8	124.6	132.8	126.9	130.1	131.9					
2	1.215	1034	622	0.140	86.2	90.2	94.5	120	105.7	97.9	102.2	144.9	144.9	130.8	146.3	135.1	146.3	138.5	142.8	142.4					
3	1.670	1184	1401	0.950	98.6	103.1	107.5	120	120.0	112.5	116.4	157.6	157.6	147.7	152.1	152.1	164.6	157.1	161.0	158.8					
4	1.659	1166	1384	0.999	109.9	108.0	116.4	120	123.1	114.3	119.3	160.6	160.6	151.8	156.2	156.2	168.9	160.1	165.1	163.1					
5	1.786	1180	1403	0.965	101.1	106.3	110.9	120	121.6	114.6	119.5	161.0	161.0	153.0	157.6	157.6	170.3	161.3	166.2	163.7					
6	1.485	1259	2271	0.764	91.5	102.0	106.2	120	118.9	110.7	114.9	156.3	156.3	146.3	151.0	151.0	163.2	155.0	159.2	156.8					
9	2.035	1348	1740	1.078	102.7	107.1	112.9	150	125.4	115.9	120.8	162.8	162.8	154.1	159.6	159.6	172.1	162.6	167.5	165.8					
10	2.760	1446	1920	1.166	104.1	109.7	116.7	150	126.6	116.3	123.0	165.2	165.2	157.1	162.1	162.1	174.0	165.7	170.4	168.7					
11	2.181	1505	2014	1.207	106.1	111.2	118.9	150	128.8	120.5	124.8	166.7	166.7	158.8	166.5	166.5	176.4	168.1	172.4	170.3					
12	2.656	1597	2108	1.233	106.6	111.1	120.6	150	126.7	119.8	124.4	167.7	167.7	159.4	168.7	168.7	176.8	167.9	172.5	171.5					
13	2.652	1683	2246	1.292	108.8	113.1	123.5	150	130.4	122.0	126.5	169.8	169.8	161.5	171.9	171.9	178.8	170.4	174.9	173.8					
14	2.997	1870	2494	1.384	111.4	115.3	128.0	150	134.0	124.9	128.1	173.3	173.3	164.3	177.0	177.0	183.0	173.9	177.1	177.6					
15	3.221	1825	2574	1.437	113.0	116.1	129.7	150	135.5	126.4	128.8	174.9	174.9	165.2	178.6	178.6	184.4	175.3	177.7	179.2					
16	3.515	1998	2735	1.500	114.6	117.6	131.4	150	137.2	128.3	129.9	177.0	177.0	166.9	180.7	180.7	186.5	177.6	179.2	181.4					
17	3.848	2116	2899	1.563	116.1	119.2	133.1	150	140.0	130.0	131.3	179.1	179.1	168.8	182.7	182.7	189.6	179.6	180.9	183.7					
18	3.228	1941	2515	1.439	113.0	116.5	129.7	150	135.7	126.2	129.1	175.1	175.1	165.7	178.9	178.9	184.9	175.4	178.3	179.5					
19	2.997	1860	2463	1.384	111.4	115.4	128.2	150	134.3	124.7	128.3	173.7	173.7	164.4	177.4	177.4	183.3	173.7	177.3	178.0					
20	2.490	1987	2116	1.243	106.6	111.7	121.7	150	129.3	119.7	124.6	168.2	168.2	159.7	169.7	169.7	177.3	167.7	172.6	172.0					
21	2.291	1465	1945	1.177	103.2	110.1	117.8	150	127.7	118.5	123.3	165.9	165.9	157.6	165.3	165.3	175.2	166.0	170.8	169.4					
22	1.692	1270	1607	1.014	106.8	105.9	110.9	150	123.6	114.1	119.2	161.0	161.0	151.8	156.8	156.8	164.5	160.0	165.1	163.4					
24	1.219	1017	630	0.544	83.1	89.1	93.4	120	104.9	97.1	101.5	143.8	143.8	129.9	134.0	134.0	145.5	137.7	142.1	141.4					
25	1.692	1190	1426	0.916	95.1	101.1	107.8	120	120.7	111.7	116.1	157.8	157.8	147.8	152.5	152.5	164.4	156.4	161.0	159.2					
27	2.109	1392	1742	1.107	102.2	107.8	113.3	150	125.6	115.4	121.1	163.0	163.0	154.1	159.6	159.6	171.9	161.7	167.4	165.8					
32	3.036	1877	2511	1.394	111.9	116.2	128.9	150	135.0	125.5	129.1	174.5	174.5	165.2	177.9	177.9	184.0	174.5	178.1	178.6					

Table A-8. Test Matrix, 32-Chute + Ejector Nozzle.

Data Point	P _i /P ₀	T _i	V _i	N _i	30° OASPL	90° OASPL	Max OASPL	θ _i	Max PNL	50° PNL	90° PNL	OAPNL	Log(V _i /a ₀)	10 log(ρ _j /ρ _{ISA}) ^{w-1}	10 log((ρ _j /ρ _{ISA}) ^w (A _j /R ²))	Normalized by 10 log ((ρ _j /ρ _{ISA}) ^w (A _j /R ²))								OAPNL-10 log (ρ _j /ρ _{ISA}) ^{w-1}
																50° OASPL	90° OASPL	Max OASPL	Max PHL	50° PNL	90° PNL	50° OASPL	90° OASPL	
1	1.077	1070	504	0.331	77.7	80.9	85.3	120	91.0	87.1	86.8	135.5	-0.345	4.8	-38.3	116.0	119.2	123.6	129.3	125.4	125.1	130.7		
2	1.224	2025	835	0.550	55.9	55.6	94.0	120	103.1	98.0	97.7	143.9	-0.126	2.4	-40.7	126.6	129.3	134.7	144.0	138.7	138.4	143.5		
4	1.405	1537	1625	1.020	98.5	103.6	106.0	120	119.8	111.1	115.5	158.2	0.163	-2.5	-46.1	144.6	148.7	154.1	165.9	157.2	161.6	160.7		
5	2.104	1355	1782	1.106	99.9	104.7	110.0	120	121.2	112.2	117.6	161.0	0.203	-3.1	-46.8	146.7	151.5	156.8	168.0	159.0	164.4	164.1		
6	2.319	1442	1945	1.187	101.7	106.9	113.9	130	122.1	113.9	119.3	164.1	0.241	-3.5	-47.3	149.0	154.2	161.2	169.4	161.2	166.6	167.6		
7	2.410	1490	2017	1.217	102.6	107.9	115.5	130	123.4	114.6	120.4	165.6	0.257	-3.6	-47.5	150.1	155.4	163.0	170.9	162.1	167.9	169.1		
8	2.487	1528	2109	1.243	103.7	109.1	117.4	130	125.2	115.5	121.4	167.3	0.276	-3.8	-47.9	151.6	157.0	165.3	173.1	163.4	169.3	171.1		
12	2.950	1820	2444	1.373	109.3	114.5	127.8	150	132.4	120.3	126.5	173.2	0.340	-4.2	-48.8	158.1	163.3	176.6	181.2	169.1	175.3	177.4		
16	2.969	1878	2490	1.378	109.8	114.7	129.3	140	135.3	120.6	126.6	174.6	0.349	-4.4	-49.1	158.9	163.8	178.5	184.4	169.7	175.9	179.0		
17	2.511	1545	2124	1.250	104.6	110.0	121.7	150	125.4	116.3	122.4	167.6	0.280	-3.8	-47.9	152.5	157.9	169.6	173.3	164.2	170.3	171.4		
18	2.311	1458	1960	1.190	102.6	107.8	113.9	130	122.4	114.9	120.3	164.7	0.245	-3.5	-47.4	150.0	155.2	161.3	169.8	162.3	167.7	168.2		
19	1.902	1290	1626	1.020	99.0	103.2	107.3	110	120.3	111.9	116.6	158.5	0.164	-2.5	-46.1	145.1	149.3	153.4	166.4	158.0	162.7	161.0		
20	1.698	1210	1439	0.917	97.4	100.2	105.1	120	117.1	110.8	113.3	161.0	0.110	-1.5	-44.9	142.3	145.1	150.0	162.0	155.7	158.2	142.5		
21	2.440	1496	2034	1.227	103.6	109.1	116.0	130	124.1	115.7	121.6	166.7	0.261	-3.6	-47.5	151.1	156.6	163.5	171.6	163.2	169.1	170.3		

Table A-9. Test Matrix, 8-Lobe Model.

Data Point	P ₁ /P ₀	T ₁	V ₁	W ₁	50° OASPL	90° OASPL	Max OASPL	50° PNL	90° PNL	OASPL	Normalized by 10 log [(p _j /p _{ISA}) ^w (A _j /R ²)]						10 log [(p _j /p _{ISA}) ^w (A _j /R ²)]	10 log [(p _j /p _{ISA}) ^{w-1}	Log(V ₁ /e ₀)	OASPL	50° OASPL	90° OASPL	Max OASPL	Max PNL	50° PNL	90° PNL	OAPWL	10 log [(p _j /p _{ISA}) ^{w-1}	OAPWL-10 log (p _j /p _{ISA}) ^{w-1}
											50° OASPL	90° OASPL	Max OASPL	Max PNL	50° PNL	90° PNL													
65	1.159	1199	835	0.510	87.7	92.9	95.4	120	107.1	99.3	105.1	142.5	0.126	3.0	-41.6	128.8	134.5	137.4	148.7	140.9	146.7	139.5							
69	1.183	1246	1151	0.395	95.5	100.6	104.0	116	117.2	108.5	113.6	151.2	0.014	0.5	-44.2	139.7	144.8	150.2	161.4	152.7	157.8	130.7							
70	1.501	1263	1292	0.792	97.7	103.5	109.2	130	120.6	110.9	116.8	154.4	0.064	-0.6	-45.2	142.9	148.7	154.4	166.0	156.1	162.0	155.0							
71	1.611	1294	1412	0.834	102.4	108.5	112.1	130	124.4	115.6	121.3	158.2	0.102	-1.5	-46.1	146.5	154.4	158.2	170.5	161.7	167.4	159.7							
72	1.818	1403	1638	0.976	102.7	108.5	115.4	130	128.1	115.9	121.9	160.8	0.165	-2.9	-47.8	150.5	156.3	163.6	175.9	163.7	169.7	163.7							
73	1.990	1497	1800	1.056	104.5	110.4	117.4	150	130.9	117.6	123.7	162.9	0.208	-3.7	-48.7	153.2	159.1	166.1	179.6	166.3	172.4	166.6							
74	2.285	1686	2037	1.150	106.3	113.1	120.5	130	131.1	121.0	126.5	165.7	0.270	-4.2	-49.6	157.9	162.7	170.1	182.7	171.6	176.1	169.9							
75	2.559	1689	2300	1.596	110.9	114.1	127.1	130	134.9	124.8	127.5	167.3	0.295	-4.1	-49.4	160.3	163.5	171.5	184.3	174.2	179.2	175.2							
76	3.151	1689	2498	1.406	114.4	116.8	128.4	140	138.1	128.6	130.0	173.3	0.332	-3.8	-48.9	163.7	165.7	177.7	187.0	177.7	179.2	175.2							
77	3.465	1699	2487	1.873	112.3	118.1	131.0	140	139.6	130.0	131.8	173.3	0.248	-3.7	-48.9	165.0	166.8	179.7	188.5	178.7	180.5	177.0							
78	3.746	1791	2621	1.827	117.7	119.5	131.6	130	141.6	130.9	133.3	175.0	0.371	-3.9	-49.0	166.7	168.9	180.8	190.6	179.9	182.3	178.9							
79	1.575	1240	1372	0.842	100.6	106.7	110.7	130	128.0	113.7	121.9	157.8	0.091	-1.2	-45.9	146.5	154.5	156.6	169.9	159.6	167.8	159.0							
80	1.971	1490	1796	0.956	105.1	110.6	117.7	150	131.2	118.4	124.2	163.1	0.207	-3.7	-48.7	153.8	159.5	166.4	179.9	167.1	172.9	166.8							
81	2.528	1482	2156	1.287	111.4	114.6	123.1	150	134.8	125.6	128.1	167.2	0.292	-4.1	-49.4	160.8	164.0	171.5	184.2	175.0	177.5	171.3							
110	2.501	991	1636	1.224	110.0	110.8	118.0	150	131.4	124.3	124.4	163.0	0.172	-1.4	-44.3	154.3	155.1	162.3	175.7	168.6	168.7	164.4							
111	2.974	991	1728	1.318	114.2	113.6	122.5	150	134.3	128.2	127.8	166.3	0.205	-1.4	-44.0	158.2	157.6	166.5	178.3	172.2	171.8	167.7							
112	3.479	991	1800	1.464	116.1	116.1	126.2	150	136.7	129.4	130.3	169.4	0.229	-1.3	-43.8	159.8	159.8	169.9	180.4	173.1	174.0	170.7							
113	2.503	1394	1976	1.234	110.9	113.3	121.0	150	134.7	125.2	126.7	165.9	0.248	-3.2	-47.7	158.6	161.0	168.7	181.9	172.9	174.4	169.1							
114	2.972	1486	2125	1.366	114.3	115.0	125.8	140	136.1	128.4	128.7	168.9	0.280	-3.0	-47.2	161.5	162.2	173.0	183.3	175.6	175.9	171.9							
115	3.483	1398	2254	1.472	116.9	117.4	129.4	140	138.8	130.5	131.3	172.1	0.305	-2.8	-46.9	163.8	164.3	176.7	189.7	177.4	178.2	174.9							
200	1.598	1393	1454	0.878	101.0	108.0	110.9	210	123.6	113.9	120.9	156.3	0.115	-1.9	-46.9	147.9	154.9	157.8	170.5	160.8	167.8	160.2							
201	1.932	1584	1828	1.041	104.0	109.7	116.3	240	128.8	117.1	123.1	162.8	0.214	-4.0	-49.3	153.3	159.0	165.5	178.1	166.4	172.4	166.8							
202	2.333	1721	2160	1.188	108.1	113.2	120.3	240	131.9	121.6	126.4	166.5	0.287	-4.4	-50.1	158.2	163.7	170.4	183.0	171.9	176.5	170.9							
206	2.564	1691	2304	1.258	108.9	113.3	127.1	240	134.0	122.6	126.7	167.5	0.296	-4.1	-49.4	158.3	162.7	171.5	183.4	172.0	176.1	171.6							

113

Table A-12. Test Matrix, J79 32-Chute Model.

Data Point	F _z /P ₀	r _z	V _z	M _z	50° OASPL	90° OASPL	Max OASPL	θ _z	Max PNL	50° PNL	90° PNL	OAPWL	Log(V _z /a ₀)	10 Log(p _z /p _{ISA}) ^{w-1}	10 Log[(p _z /p _{ISA}) ^w (V _z ² /R ²)]	Normalized by 10 Log [(p _z /p _{ISA}) ^w (A _z /A ₀ ²)]						OAPWL-10 Log(p _z /p _{ISA}) ^{w-1}
																50° OASPL	90° OASPL	Max OASPL	Max PNL	50° PNL	90° PNL	
1	1.082	1055	530	0.340	77.1	81.6	86.2	130	94.4	85.3	90.5	135.7	-0.323	5.0	-38.4	124.6	132.8	123.7	128.9	130.7		
2	1.219	1018	871	0.543	82.3	88.5	93.8	130	105.1	94.0	101.0	143.2	-0.133	2.5	-40.6	129.1	134.4	145.7	134.6	141.6	140.7	
3	1.081	1045	525	0.338	77.0	81.3	86.2	130	94.4	83.2	90.5	135.6	-0.328	5.0	-38.4	119.7	124.6	132.8	123.6	128.9	130.6	
4	1.219	1014	816	0.542	82.3	88.3	93.7	130	105.2	94.3	100.9	143.1	-0.135	2.5	-40.6	122.9	128.9	134.3	145.8	134.9	141.5	
5	1.685	1176	1431	0.904	95.3	101.5	107.0	150	119.8	108.9	114.9	157.3	0.099	-1.2	-44.5	139.8	146.0	151.5	164.4	153.4	159.4	
6	1.885	1267	1593	1.006	98.1	104.3	110.6	150	133.7	111.5	117.7	160.5	0.154	-2.3	-45.8	143.9	150.1	156.6	169.5	167.3	168.8	
7	2.079	1345	1754	1.090	100.7	108.7	115.7	160	127.3	113.5	122.2	163.3	0.196	-3.1	-46.7	147.0	155.4	162.4	174.0	168.9	166.4	
8	2.311	1455	1940	1.176	104.0	109.8	117.9	160	129.8	117.5	123.4	166.0	0.262	-3.5	-47.4	151.4	157.2	165.3	177.2	164.9	171.3	
9	2.430	1523	2029	1.217	105.2	110.1	119.4	160	130.0	118.7	123.4	167.0	0.280	-3.8	-48.0	154.0	158.8	168.6	177.5	167.5	172.3	
10	2.520	1596	2126	1.246	106.8	110.6	120.4	160	130.5	119.5	124.3	168.0	0.329	-5.0	-48.3	153.3	159.8	172.6	183.3	172.3	171.8	
11	1.950	1047	573	0.336	77.6	81.5	86.2	130	94.3	85.0	90.5	135.6	-0.133	2.4	-40.6	132.2	129.3	134.6	146.2	135.2	142.8	
12	1.222	1005	821	0.547	82.6	86.7	94.0	130	105.6	94.6	101.2	143.4	-0.133	2.4	-40.6	140.8	146.3	152.0	164.8	154.4	159.6	
13	1.691	1171	1404	0.907	96.3	101.8	107.5	150	128.3	109.9	113.1	157.8	0.100	-1.2	-44.5	144.1	150.5	156.9	169.6	157.4	163.8	
14	1.859	1263	1493	1.007	98.4	104.7	111.1	150	123.8	111.6	118.0	160.8	0.154	-2.3	-45.8	148.1	154.0	161.9	173.5	161.3	167.4	
15	2.195	1354	1775	1.169	101.7	107.2	115.1	160	126.7	114.5	120.6	163.6	0.202	-3.1	-46.8	148.1	154.0	161.9	173.5	161.3	167.4	
16	2.312	1456	1946	1.189	104.3	110.2	118.3	160	130.2	117.9	124.4	166.4	0.242	-3.5	-47.4	151.7	157.6	165.7	177.6	165.3	171.8	
17	2.419	1515	2024	1.214	104.7	109.9	119.7	160	129.5	118.0	123.4	166.9	0.260	-3.6	-47.6	152.3	157.5	166.9	177.4	165.6	171.0	
18	2.515	1595	2122	1.244	108.5	110.7	120.8	160	130.7	120.1	124.0	168.0	0.279	-3.8	-48.0	154.5	158.7	168.8	178.7	168.1	172.0	

Table A-13. Test Matrix, J79 32-Chute + Ejector Model.

Data Point	P ₁ /P ₀	V ₁	V ₂	V ₃	50° OASPL	90° OASPL	Max OASPL	50° FNL	90° FNL	Max FNL	10 Log(V ₁ /a ₀)	10 Log(O ₁ /I ₁ SA) ^{w=1}	10 Log(O ₁ /I ₁ SA) ^{w(A₁/R₁²)}	Normalized by 10 Log [(ρ ₁ /ρ ₀ ISA) ^{w(A₁/R₁²)}]						OAPWL-10 Log (O ₁ /I ₁ SA) ^{w=1}		
														50° OASPL	90° OASPL	Max OASPL	50° FNL	90° FNL	Max FNL			
1	1.075	1053	508	0.126	79.5	82.1	84.9	130	93.2	86.6	89.9	135.4	-0.342	5.2	-38.2	117.5	120.3	123.1	131.4	127.0	128.1	130.2
2	1.224	1023	831	0.149	86.5	87.4	91.0	140	104.6	100.3	105.6	142.6	-0.128	2.4	-40.7	127.2	128.1	132.7	145.3	141.0	141.3	140.2
3	1.224	1207	1432	0.185	91.3	99.3	104.3	150	116.4	111.8	112.3	155.5	0.114	-1.5	-44.9	142.2	144.2	149.2	161.3	156.7	157.0	157.0
4	1.425	1294	1831	0.222	98.4	101.7	106.6	160	128.1	121.4	115.0	158.5	0.164	-2.6	-46.1	144.5	147.8	152.7	164.2	158.5	161.1	161.1
5	1.425	1366	1808	0.211	100.5	104.3	112.8	160	121.3	114.4	117.4	161.5	0.210	-3.3	-47.0	147.5	151.3	159.8	168.3	161.4	164.4	164.8
6	1.425	1450	1868	0.218	102.4	106.7	115.1	160	121.3	113.9	118.9	163.9	0.246	-3.6	-47.5	148.9	153.7	162.6	170.0	161.4	166.4	167.5
7	1.425	1543	1951	0.218	102.4	107.7	117.2	160	124.2	114.8	120.8	165.4	0.264	-3.7	-47.8	150.2	155.5	165.0	172.0	162.6	168.6	169.1
8	1.425	1631	2051	0.220	103.2	108.4	119.4	160	126.0	115.0	121.4	166.9	0.285	-3.9	-48.2	151.4	156.6	167.8	174.2	163.2	169.6	170.8
9	1.425	1704	2096	0.218	104.2	111.8	121.7	160	126.0	115.0	121.4	166.9	0.352	-3.9	-48.2	151.4	156.6	167.8	174.2	163.2	169.6	170.8
10	1.706	1191	1426	0.149	86.6	87.7	91.0	150	105.1	100.5	105.6	142.6	-0.131	2.4	-40.6	127.2	128.3	132.1	145.7	141.1	141.5	140.2
11	1.912	1297	1641	0.185	91.3	99.3	104.3	150	118.6	112.5	113.6	155.4	0.107	-1.4	-44.7	142.0	144.2	149.5	163.5	157.2	158.3	156.8
12	1.912	1360	1683	0.185	93.4	103.2	109.4	150	119.0	112.9	117.3	158.8	0.167	-2.6	-46.2	145.1	149.4	155.6	165.2	159.1	163.5	161.4
13	1.912	1450	1750	0.185	95.4	104.6	112.1	150	120.7	114.9	118.0	161.7	0.208	-3.3	-47.0	147.8	151.6	159.1	167.7	161.9	165.0	165.0
14	1.912	1543	1812	0.185	97.4	106.7	115.1	150	122.5	114.7	118.9	163.8	0.247	-3.6	-47.5	149.2	153.8	162.6	170.0	161.7	166.4	167.4
15	1.912	1631	1872	0.185	99.4	107.4	115.1	150	124.1	115.1	120.2	165.2	0.266	-3.7	-47.8	150.5	155.2	162.6	172.1	162.9	168.0	168.9
16	1.912	1624	1848	0.227	103.6	108.9	119.0	150	125.1	116.1	121.9	166.5	0.284	-3.9	-48.2	151.8	157.1	167.2	173.3	164.3	170.1	170.4

5.0 DATA ACQUISITION AND REDUCTION

The output from the JENOTS model scale acoustic data acquisition system (14 microphones around a 40-foot arc) was taped and later reduced by a 1/3-octave analyzer. Printouts of the analyzed and system-corrected data were obtained by computerized techniques. This procedure is discussed in detail in Reference 18.

The output from Edwards full-scale acoustic data acquisition system (13 microphones around a 160-foot arc) was taped and then reduced as explained above. (Details can also be found in Reference 18.)

Nozzle aerodynamic data were obtained on three J79 engine nozzle configurations. For all test points, sufficient aerodynamic data were collected to determine inlet airflow, ideal fully expanded isentropic jet velocity, nozzle pressure ratio, exit gas temperature, and thrust.

The Aerotrain acoustic data were taped from four microphones using one-track Nagra-III tape recorders. The data were reduced to provide 1/3-octave spectra which was corrected to free-field. These spectra for each microphone and repeat passes were averaged before comparison with scale-model data. (See Reference 10 for more details.)

6.0 DATA ANALYSIS PROCEDURES

This section describes the scaling factors, normalization methods, and data comparisons used in the analysis of the data.

The acoustic model data were first scaled up to engine size and then compared with the respective engine data. Conventional scaling factors, including Strouhal number for the frequency-diameter relationship and nozzle throat area for the sound-level scale factor, were utilized. The engine-to-scaled-model comparisons were conducted on the basis of velocity, directivity, and spectra. Parameters evaluated included OASPL_{max}, OASPL directivity, PNL directivity, PWL spectra, and 1/3-octave band SPL spectra. All data were corrected for air absorption and ground effects. The acoustic data were normalized with a density, area, and distance factor; i.e., $10 \log [(\rho_j/\rho_{ISA})^w (A_j/R^2)]$.

Laser velocimeter measurements of engine and model data were evaluated for plume aerodynamic flow-field mean and turbulent velocity distributions. Both radial and axial data traverses throughout the jet plume were evaluated. A single velocity (approximately 2100 ft/sec) was chosen to allow direct comparison of engine and model data. Both conical and 32-chute nozzle data were obtained. The details of the LV measurements are described in Reference 4.

The ellipsoidal mirror microphone was used to give the acoustic radiation per slice of jet for both engine and scale-model jets. EM data for the J79 engine and 3.56-inch and 2.0-inch-diameter conical nozzles are presented in Section 7. A single velocity (i.e., approximately 2200 ft/sec) was chosen to allow direct comparison of engine and model data. The EM data were processed by integrating the SPL's over the length of the jet for each 1/3-octave band, with inverse square law and air attenuation adjustments.

7.0 SCALING RESULTS

To determine if diameter scaling holds for values of peak overall sound pressure level ($OASPL_{max}$), a comparison of normalized conical nozzle data from engine and model static tests was made and is shown in Figure A-6. Values of $OASPL_{max}$ normalized for density, area, and distance are shown for a range of normalized velocities. The diameters of the conical nozzles ranged from 2.00 to 20.84 inches. The data correlate reasonably well over the entire velocity range evaluated. Fitting of the data utilizing a stepwise linear regression program resulted in a standard error estimate of 1.64 dB. The 1975 SAE prediction curve, Reference 20, is shown to establish data validity.

The normalized velocity values of $\log(V_j/a_0) = 0.29$ and 0.2 were selected to illustrate directivity scaling. The directivity plots for these conditions are shown in Figure A-7. The normalized OASPL shows a ± 2 dB variation about a mean line through the data at the $\log(V_j/a_0) = 0.29$ setting. At the lower velocity, e.g., $\log(V_j/a_0) \approx 0.20$, forward quadrant variance is increased at the lower velocity due to higher shock noise of the 4.0-inch-diameter conical nozzle. The other five nozzles were operated at a nominal pressure ratio of 2.2, whereas the 4.0-inch-diameter nozzle pressure ratio was operated at 2.5.

A separate comparison of only the J85 conical and the 4-inch conical data is presented in Figure A-8 and shows improved agreement. This is expected, since the 4-inch nozzle was the only conical nozzle designed to be a scaled replica of the J85 model. The OASPL values for the 3.56-inch-diameter conical model are lower than the other configurations in the forward quadrant at the high velocity condition. The difference between the 3.56-inch-diameter model and J85 engine conical nozzle occurs over the majority of angles in the lower velocity case (Figure A-7). The plug in the 3.56-inch-diameter model is located approximately $1/2$ nozzle diameters upstream of the nozzle exit while the J85 plug is approximately $6-1/2$ nozzle diameters upstream. Thus, the exit flow profiles will differ and different noise levels are expected.

The comparisons for the J79 engine and model ($D = 5.7$ inches) are shown in Figures A-9 and A-10. Individual curves for the conical, 32-chute, and 32-chute with ejector are presented. The agreement between engine and model is quite good for normalized values of both PNL_{max} and $OASPL_{max}$ (Figures A-9 and A-10, respectively). The standard error estimate between the J79 engine and model suppressor noise data is 0.9 dB for the 32-chute nozzle and 1.7 dB for the 32-chute with ejector.

The comparison for the J85 engine and respective models is shown in Figures A-6, A-11, and A-12. Individual curves for the conical 8-lobe, and 104-tube configurations are presented. The agreement between engine and model sizes is also quite good for normalized values of both PNL_{max} and $OASPL_{max}$ (Figures A-11 and A-12, respectively). The 4-inch-diameter

Sym	Scale	Location	Area (in. 2)	Dia (in.)	DFS/DM
○	J85	Aerotraine	108.6	11.76	1.0
□	J79	Edwards	338	20.84	1.0
◇	Model	JENOTS	9.95	3.56	3.31
△			25.63	5.71	3.64
▽			3.14	2.00	5.89
◁			12.57	4.00	5.17

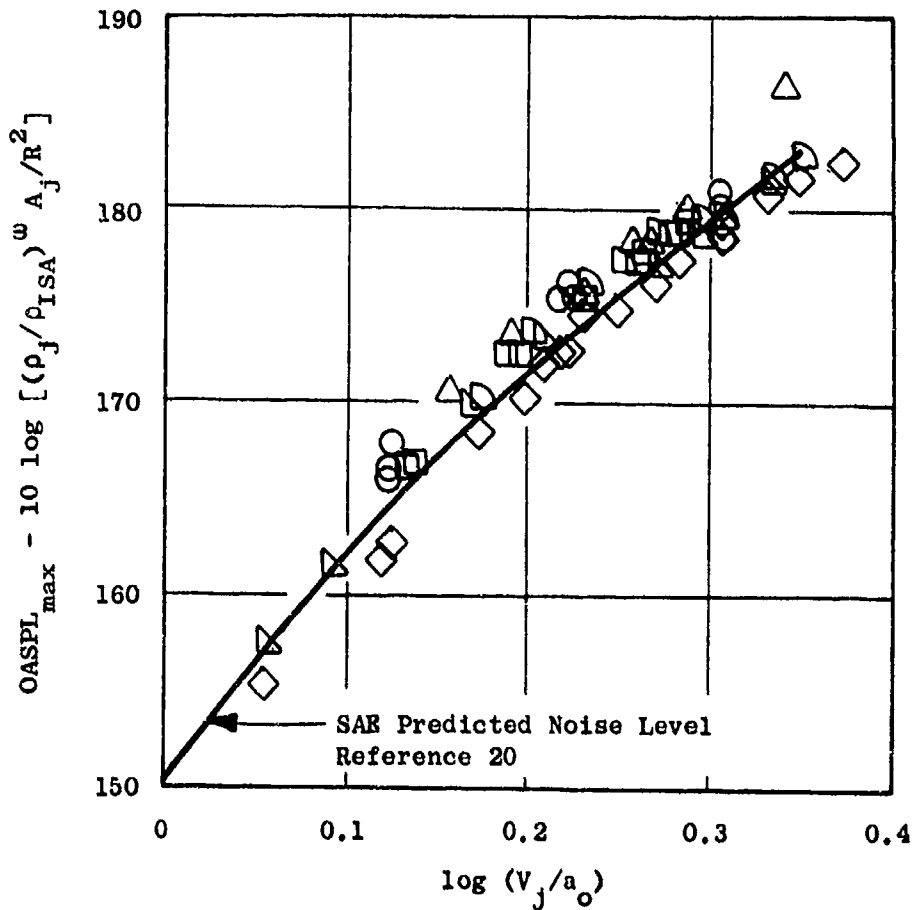


Figure A-6. Comparison of Conical Nozzle Data from Engine and Model Static Tests.

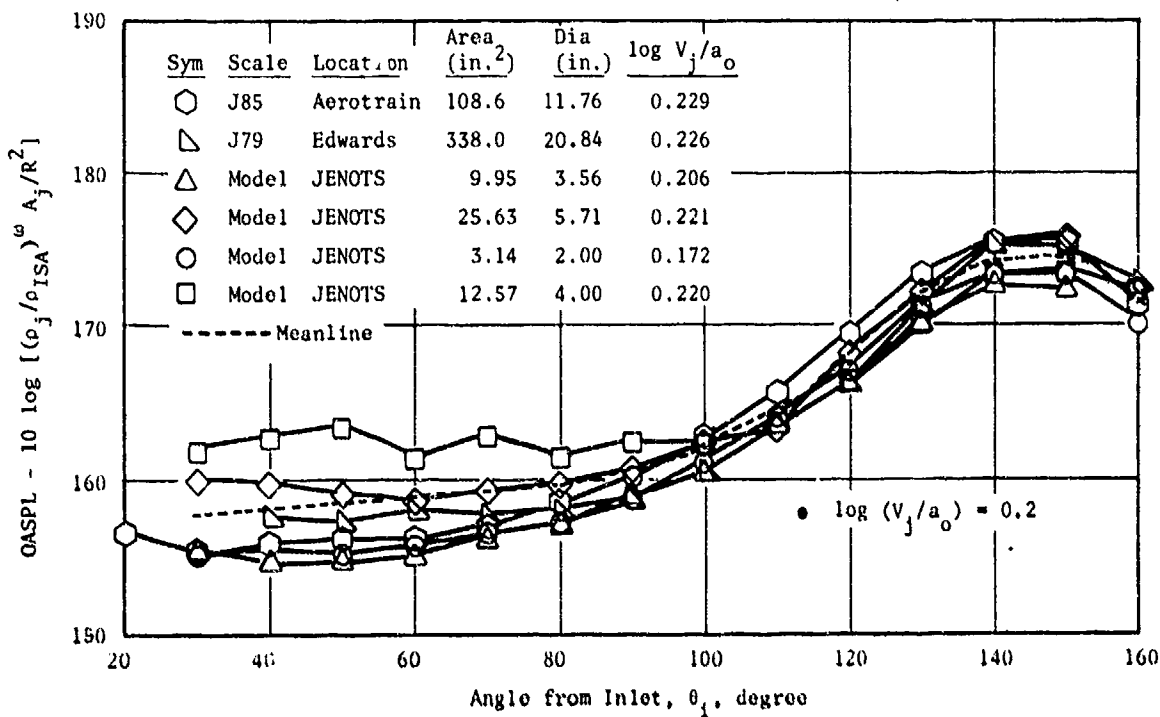
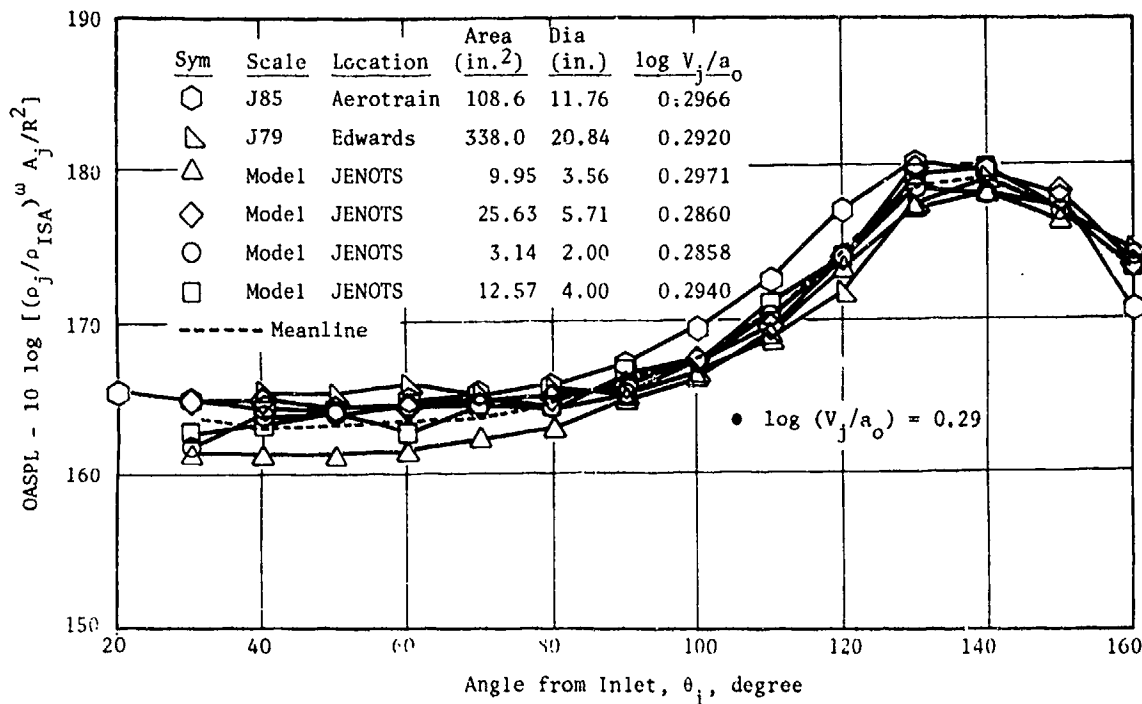


Figure A-7. Directivity Comparison of Conical Nozzle Data from Engine and Model Static Tests.

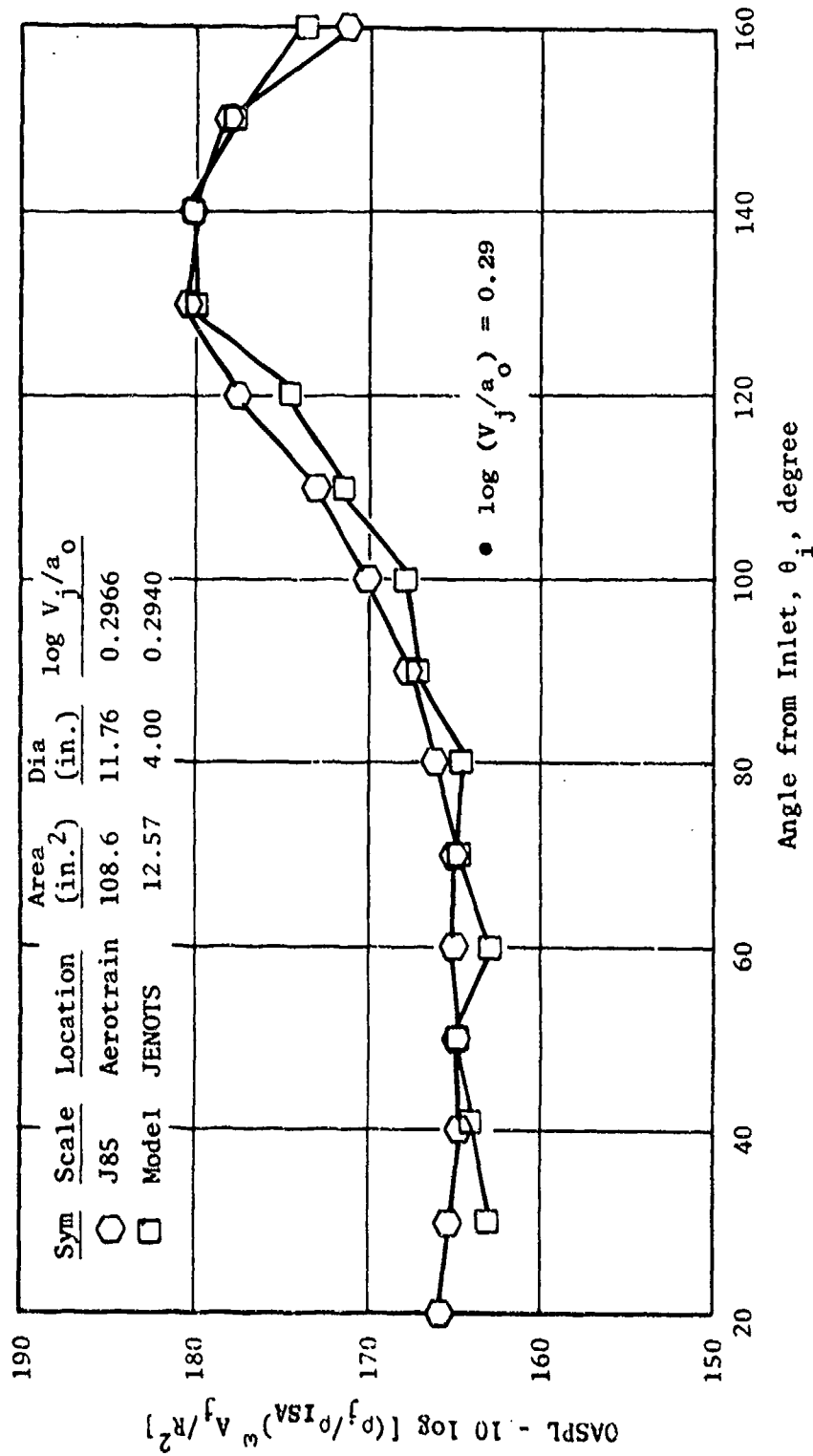


Figure A-8. Directivity Comparison of Conical Nozzle Data from Engine and Model Static Tests.

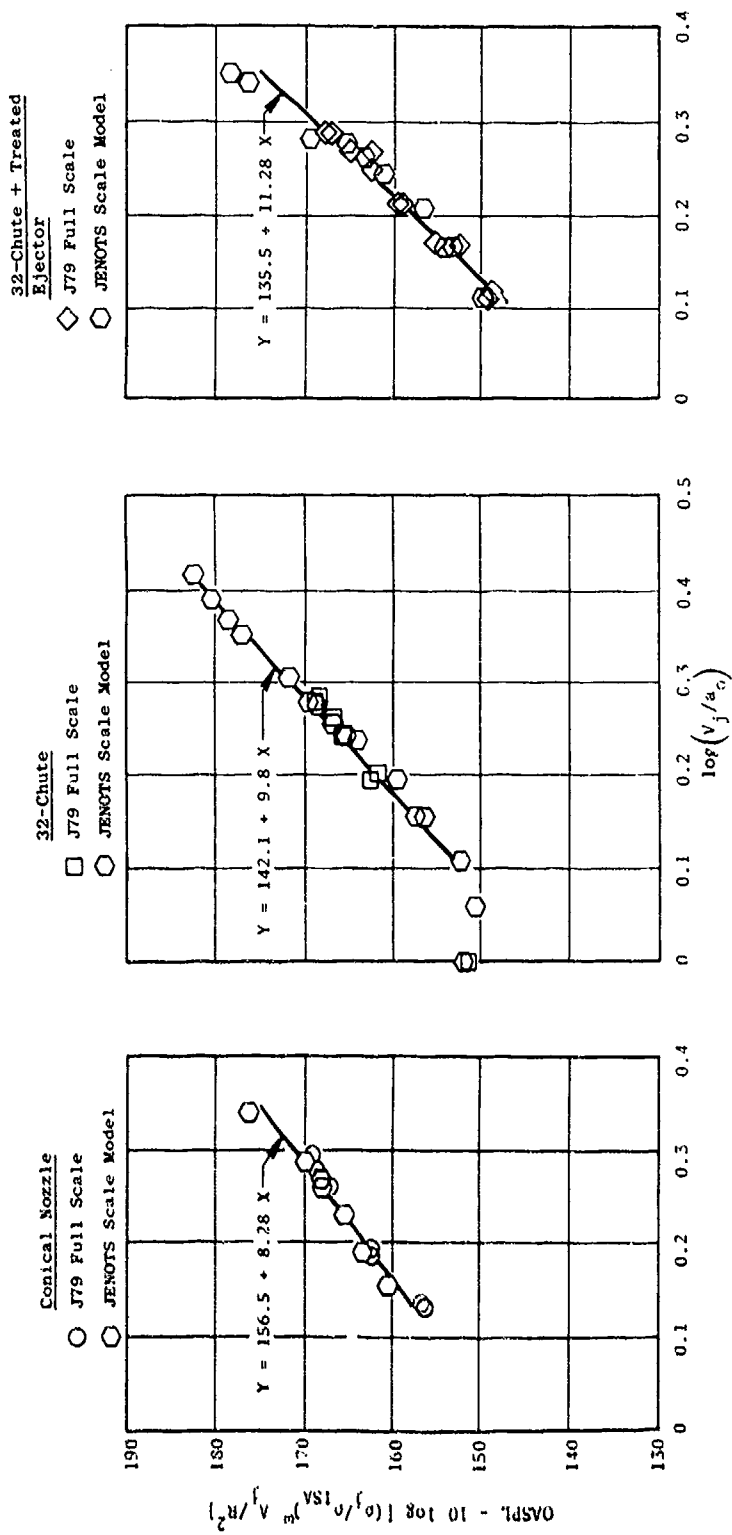


Figure A-9. Comparison of Scale Model and J79 Maximum OASPL Characteristics.

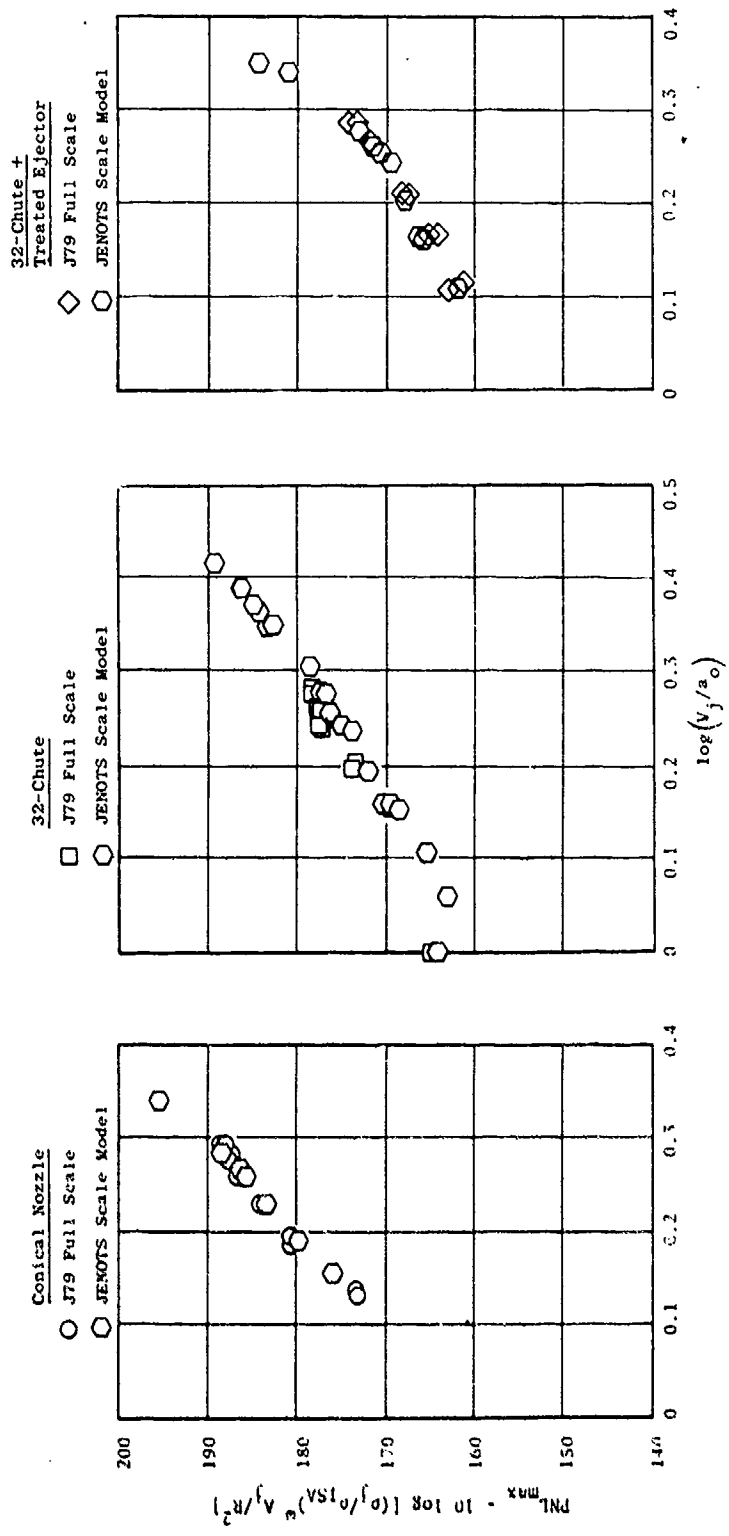


Figure A-10. Comparison of Scale Model and J79 Maximum PNL Characteristics.

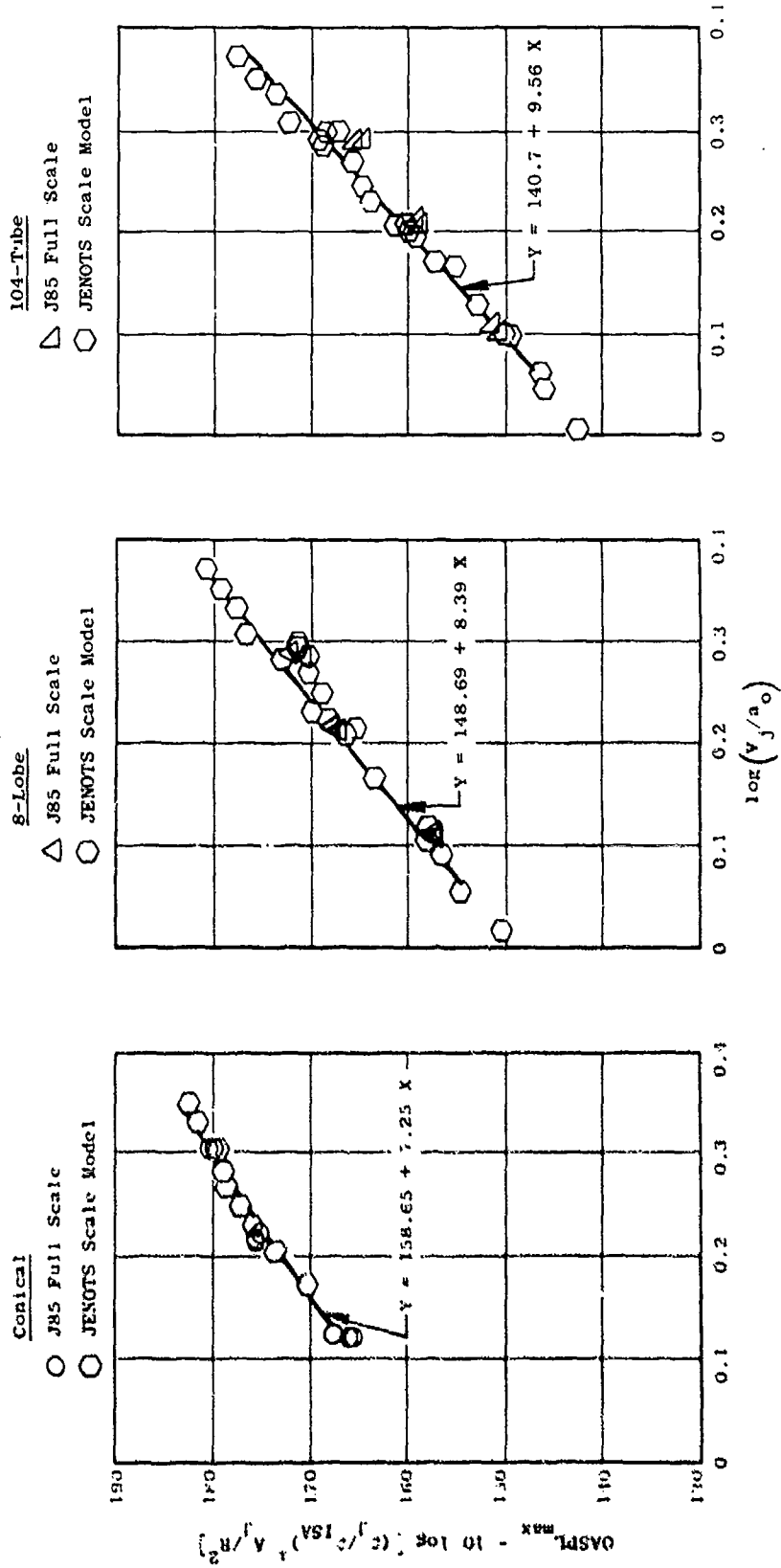


Figure A-11. Comparison of Scale Model and J85 Maximum OASPL Characteristics.

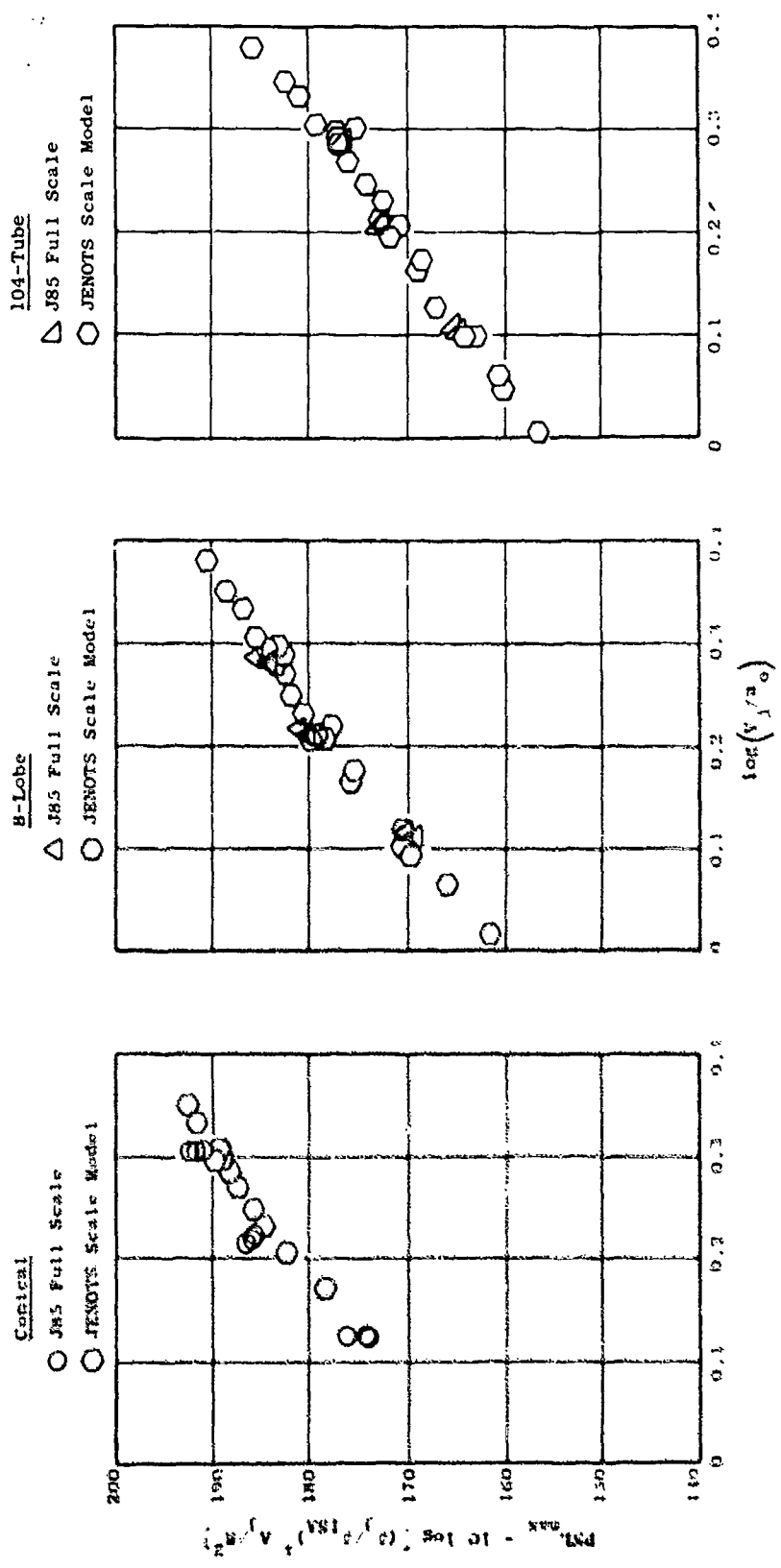


Figure A-12. Comparison of Scale Model and J85 Maximum PNL Characteristics.

conical model data were used to provide an accurate comparison with the engine. The standard errors of estimates were 0.9 dB for the conical nozzle, 1.3 dB for the 8-lobe nozzle, and 1.3 dB for the 104-tube nozzle.

In summary, the scaling method used provides good agreement between engine and model tests for normalized PNL_{max} and $OASPL_{max}$ data. The biggest difference in level occurs when comparing the six conical nozzles. This illustrates the importance of using an exact replica of the engine nozzle when making acoustic comparisons as was done in the 4-inch-diameter model/J85 engine conical comparison. The 4-inch-diameter conical model will be used on all of the following J85 engine comparisons and the 5.7-inch-diameter conical nozzle will be used for acoustic comparisons with the J79 engine data.

Acoustic Velocity Scaling

Acoustic velocity scaling comparisons (PNL_{max} and $OASPL_{max}$ versus velocity) have been made by others. This study, however, evaluates the agreement between the model and engine sizes at two angles other than the maximum noise angle (namely 90° and 50°). This helps to ensure that the agreement observed at the peak angle is representative of that at other angles.

The normalized $OASPL$ comparisons at 90° and 50° of the J79 engine and model data are shown in Figure A-13. Individual curves for the conical, 32-chute, and 32-chute with ejector are presented. The good agreement found at the maximum noise angle is shown to continue at both 90° and 50° . The maximum deviation between the J79 engine and model curves is shown to be less than 2 dB.

The normalized $OASPL$ comparisons at 90° and 50° of the J85 engine and model data are shown in Figure A-14. Individual curves for the conical, 8-lobe, and 104-tube configurations are presented. The good agreement found at the maximum angle is shown to continue at both 90° and 50° . The maximum deviation at 90° between the J85 engine and model curves is shown to be less than 2 dB for the 8-lobe and 104-tube nozzle. The conical nozzle deviation from the engine data is due to shock noise. Several conical nozzle data points were at nozzle pressure ratio greater than 3.0, thus providing an increase in shock noise relative to the J85 conical nozzle, which was evaluated at a maximum pressure ratio of 2.5. This was also the reason for increased deviation between model and full-scale data at the 50° angle.

Acoustic Directivity Scaling

Directivity comparisons of the J79 engine and model are shown in Figures A-15 and A-16. Individual curves for the conical, 32-chute, and 32-chute with ejector are presented. Good agreement is shown at all angles for both PNL and $OASPL$ (Figures A-15 and A-16, respectively). The average deviation between the J79 engine and model curves is shown to be less than 2 dB.

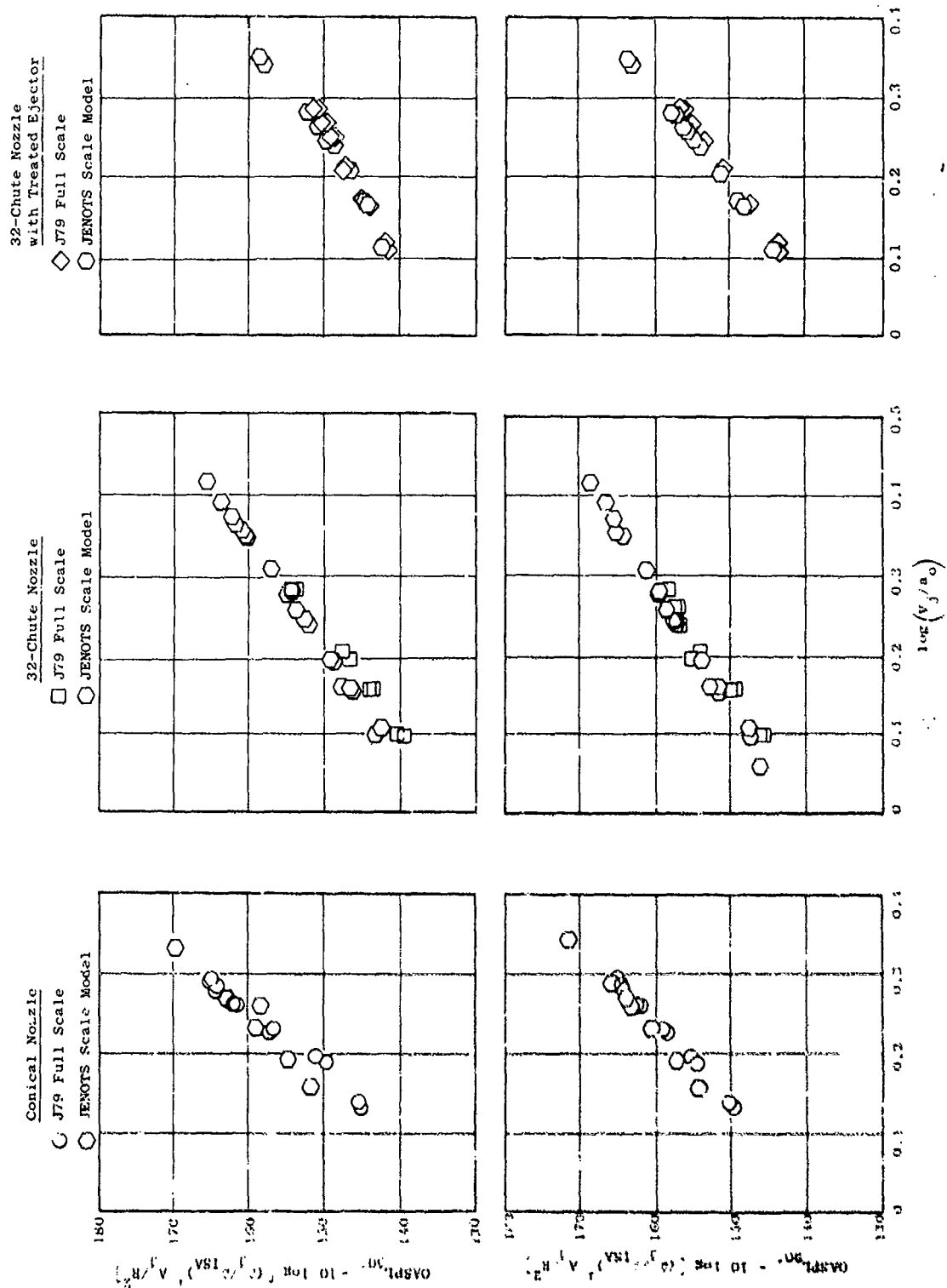


Figure A-13. Comparison of Scale Model and J79 90° and 50° OASPL Trends.

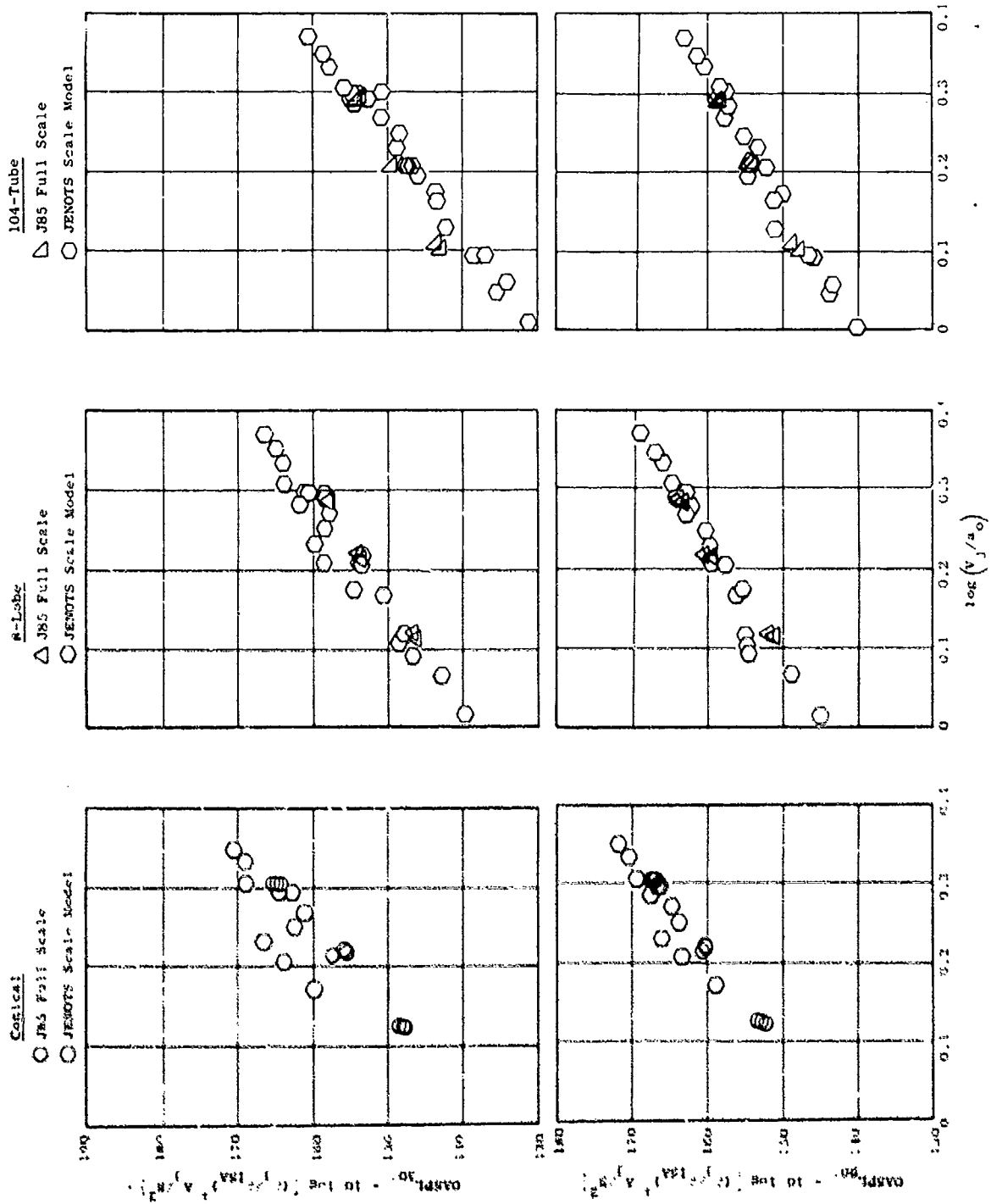


Figure A-14. Comparison of Scale Model a.r.d J85 90° and 50° OASPL Trends.

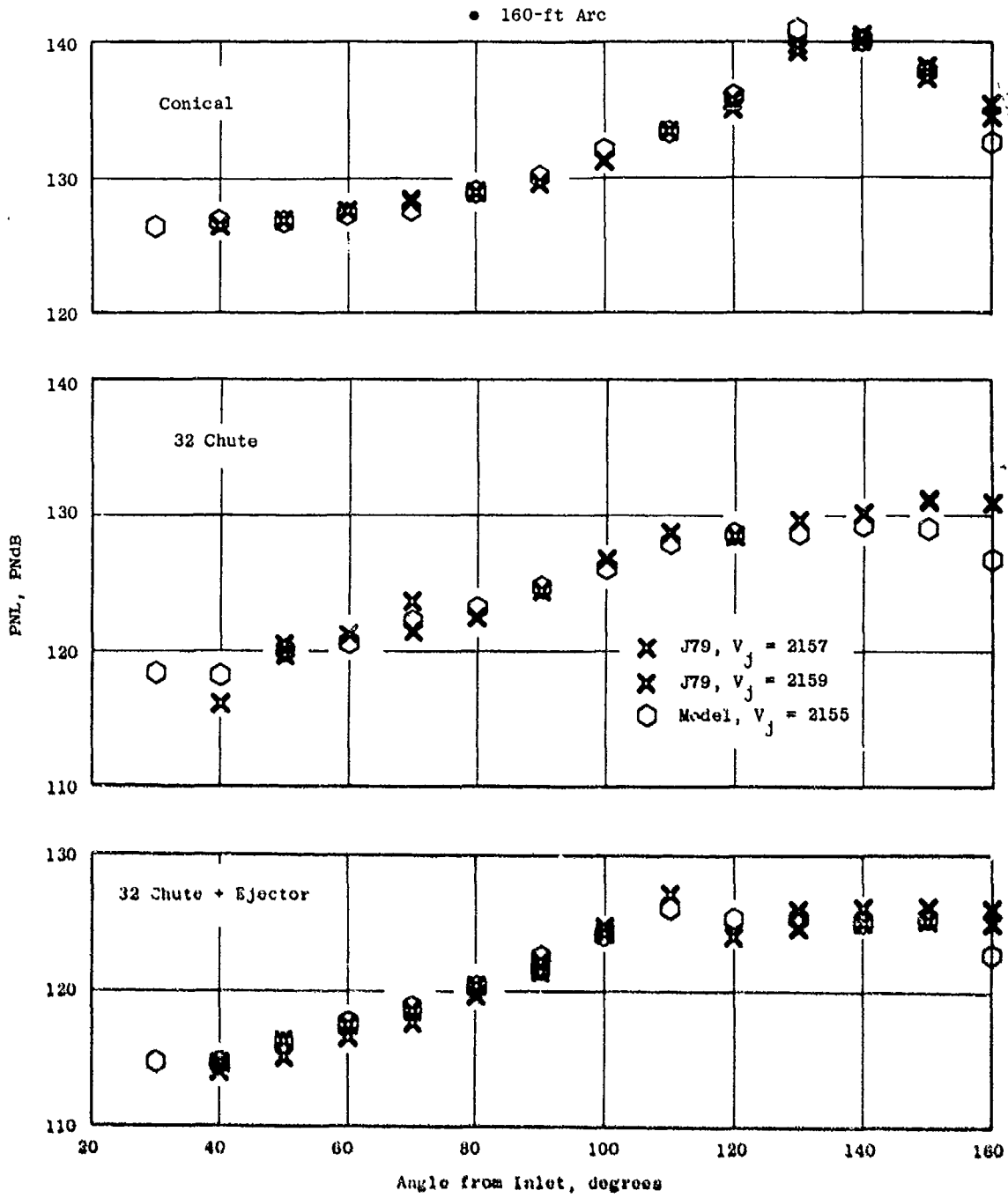


Figure A-15. Comparison of Model and J79 PNL Directivity Patterns.

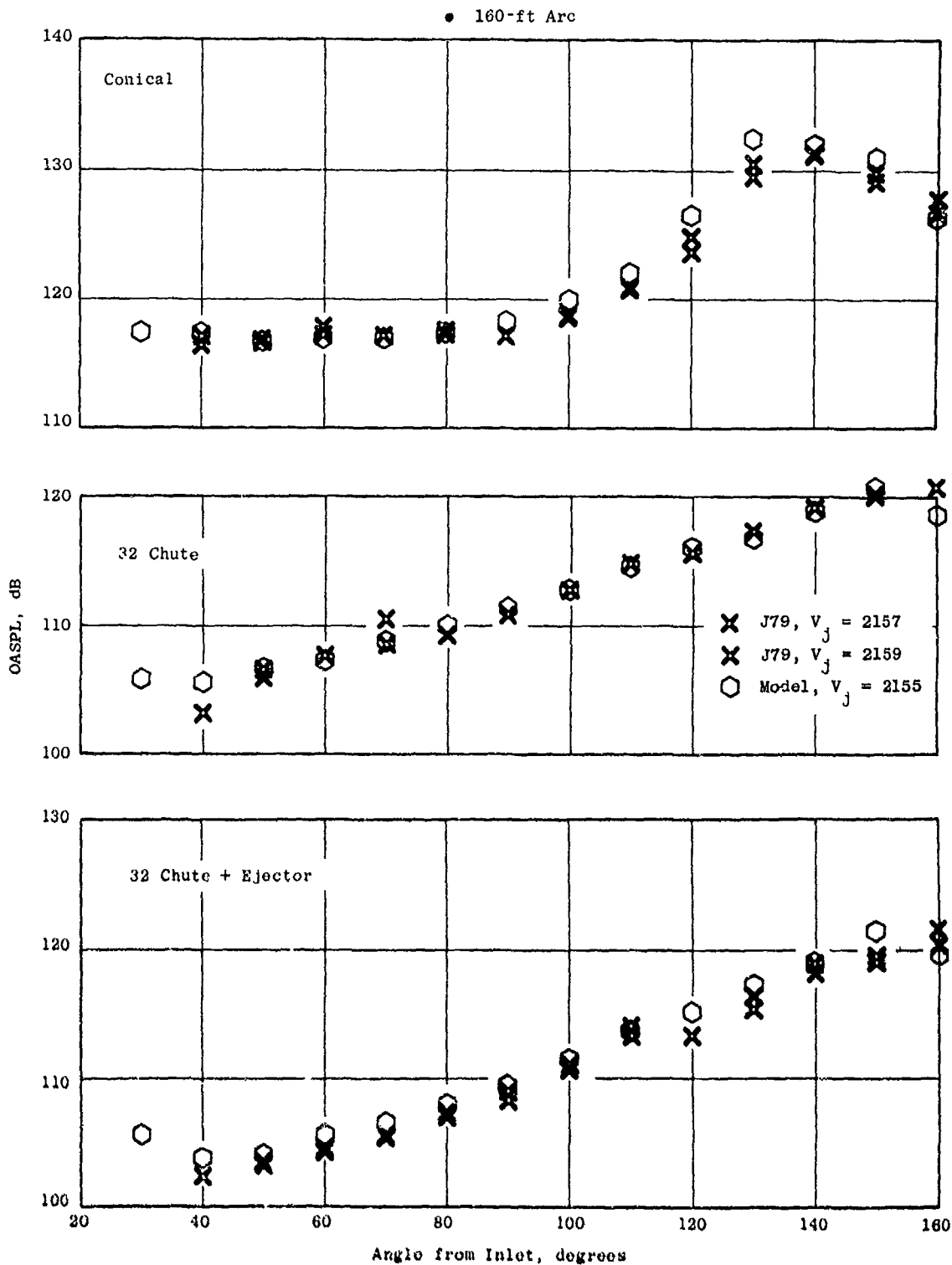


Figure A-16. Comparison of Model and J79 OASPL Directivity Patterns.

The directivity comparisons of the J85 engine and respective model data are shown in Figures A-17 and A-18. Individual data curves for the conical, 8-lobe, and 104-tube configuration are presented. The average deviation between the J85 engine and model curves is shown to be less than 2 dB.

Acoustic Spectra Scaling

The scale-model and full-scale power level spectra (PWL) comparisons at a velocity of 2150 ft/sec are presented in Figures A-19 and A-20. The maximum deviation between the engine and model data is shown to be less than 2 dB for the J79 comparisons except for the low frequency region of the conical nozzle spectra where 6 dB is observed. For the J85 comparison, deviations up to 5 dB occur in select frequency bands but the average deviation is less than 2 dB.

A range of angles (50°, 90°, and maximum noise) was examined to assess the accuracy of diameter scaling for 1/3-octave spectrum levels. The 50° angle was specifically chosen to illustrate agreement at an angle dominated by shock noise. Spectra comparisons, for the conical nozzle between the J79 engine and scale-model data at a nominal jet velocity of 2150 ft/sec, are presented in Figure A-21. At 50°, the region of the engine and scale-model spectra dominated by shock noise agree well. The Harper-Bourne, Fisher predicted peak frequency, calculated as described in Reference 19, is in good agreement with the data. At low frequencies, however, the J79 engine and scale-model show poor agreement. The same is true at 90° except that the difference between J79 engine and scale-model at low frequencies is decreased. At maximum angle (140°), the agreement over the complete spectra is good.

The J85 engine and scale-model comparisons at angles of 50°, 90°, and 130° for the conical nozzle are shown in Figure A-22. These comparisons illustrate improved agreement between the engine data and scale-model data. This point is emphasized because this conical nozzle was the only one which duplicates exactly one of the conical nozzles that was tested on an engine. The 50° spectra agree within ± 2 dB at the location of peak noise. The levels between 160 Hz and 500 Hz differ by 5 dB. Spectra comparisons at 90° and 130° indicate excellent agreement both in shape and level with a maximum deviation of 5 dB with an average deviation of less than 2 dB.

The 32-chute and 32-chute with ejector J79 engine and scale-model comparisons are shown in Figures A-23 and A-24 for a nominal velocity of 2130 ft/sec. Good agreement is shown for the 32-chute (Figure A-23) at 50° except for the low frequency region. Much better agreement is shown at 90° and at maximum angle (130°). The same is true for the 32-chute with ejector shown in Figure A-24. The low frequency difference is reduced at aft angles with good agreement on an overall basis at all angles.

• 100-ft Arc

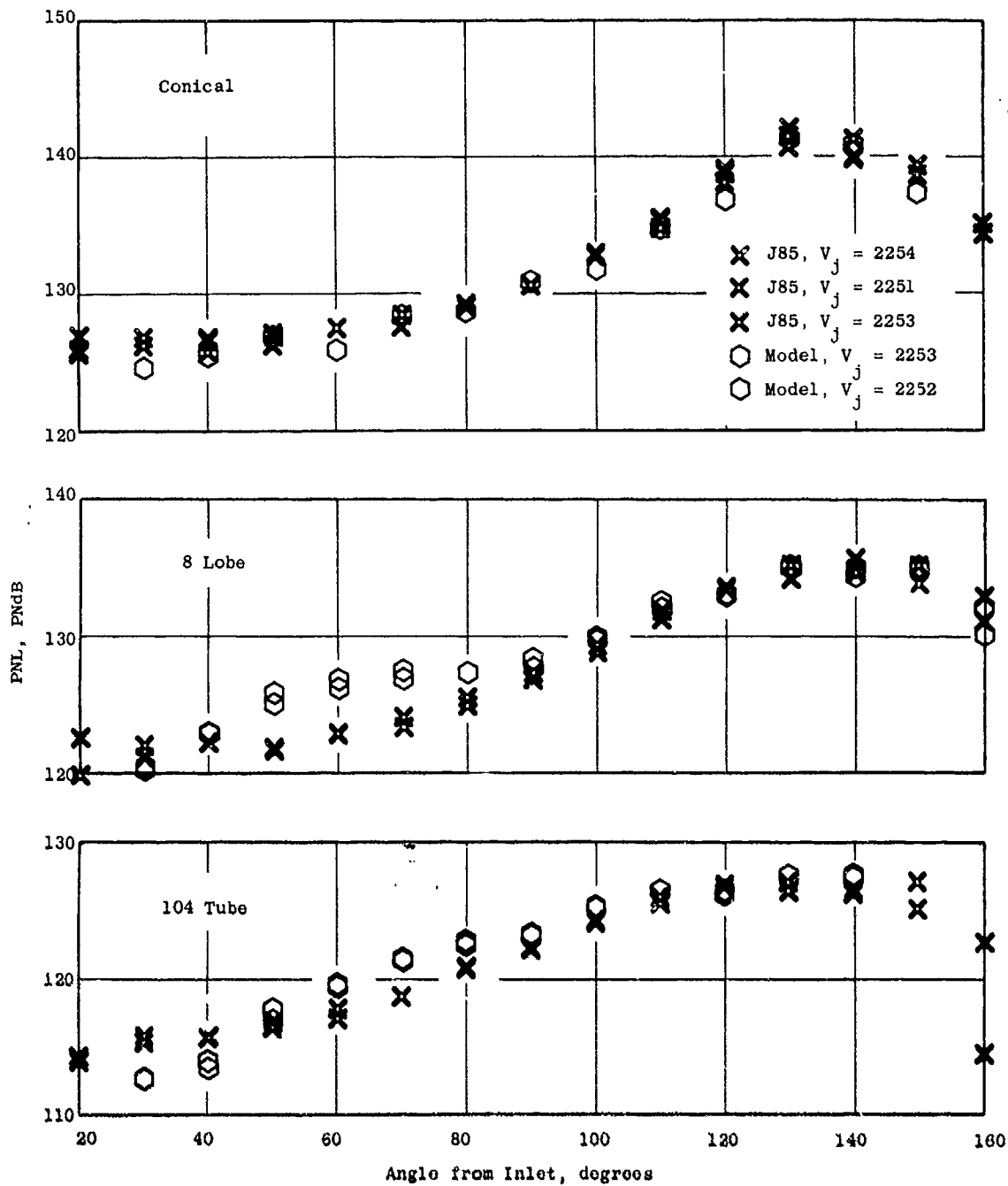


Figure A-17. Comparison of Model and J85 PNL Directivity Patterns.

• 100-ft Arc

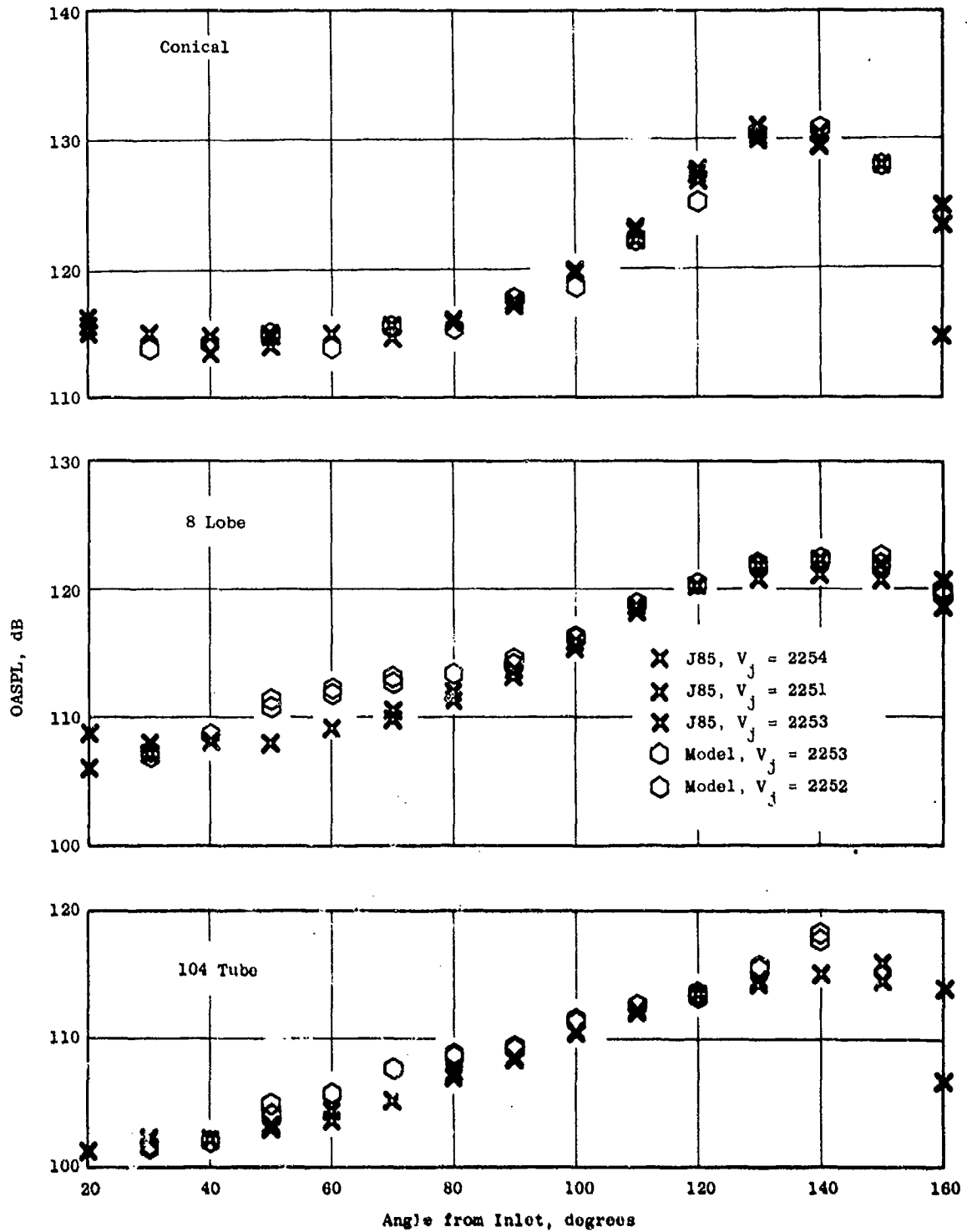


Figure A-18. Comparison of Model and J85 OASPL Directivity Patterns.

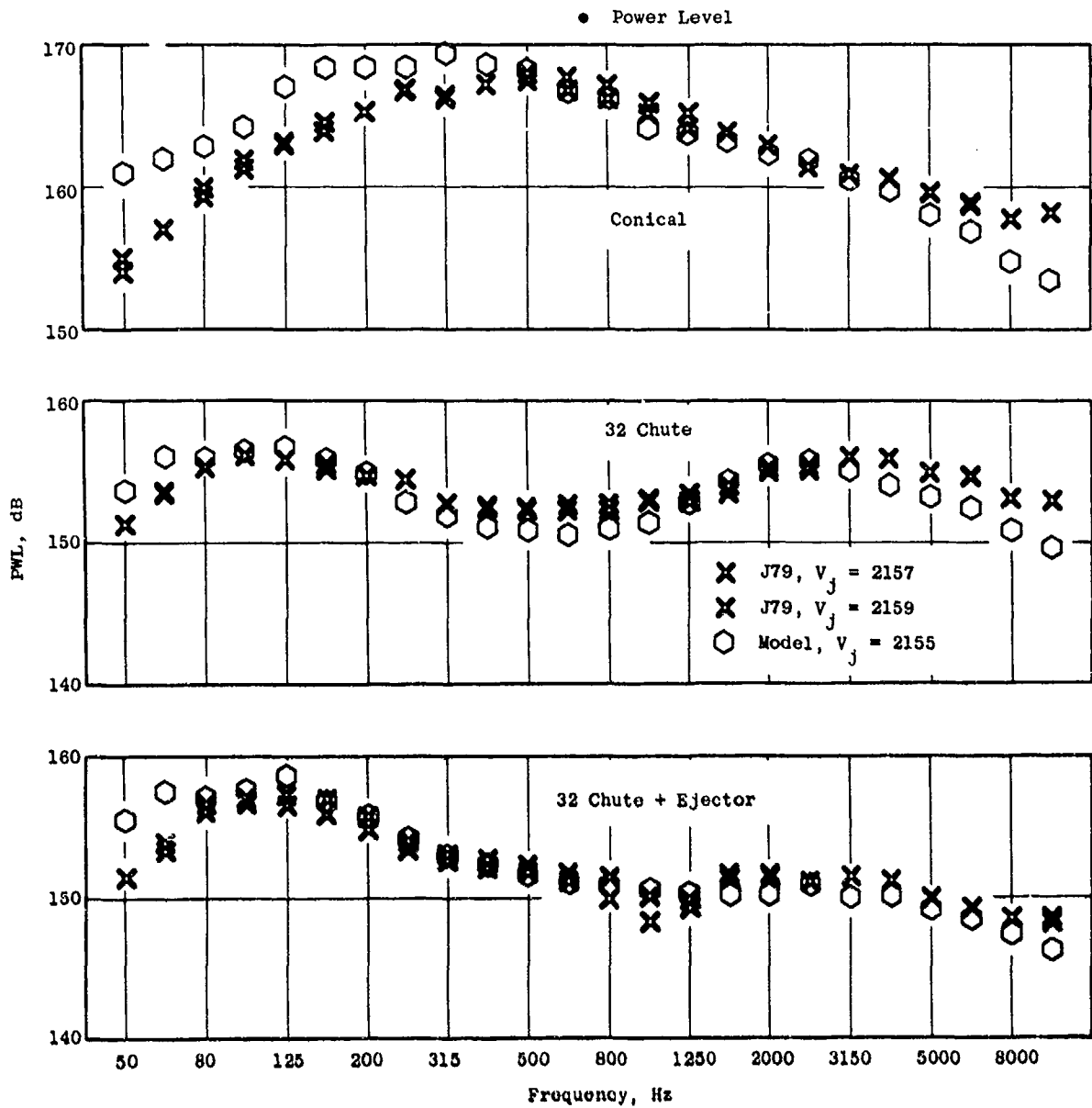


Figure A-19. Model and J79 Power Spectra Comparisons.

• Power Level

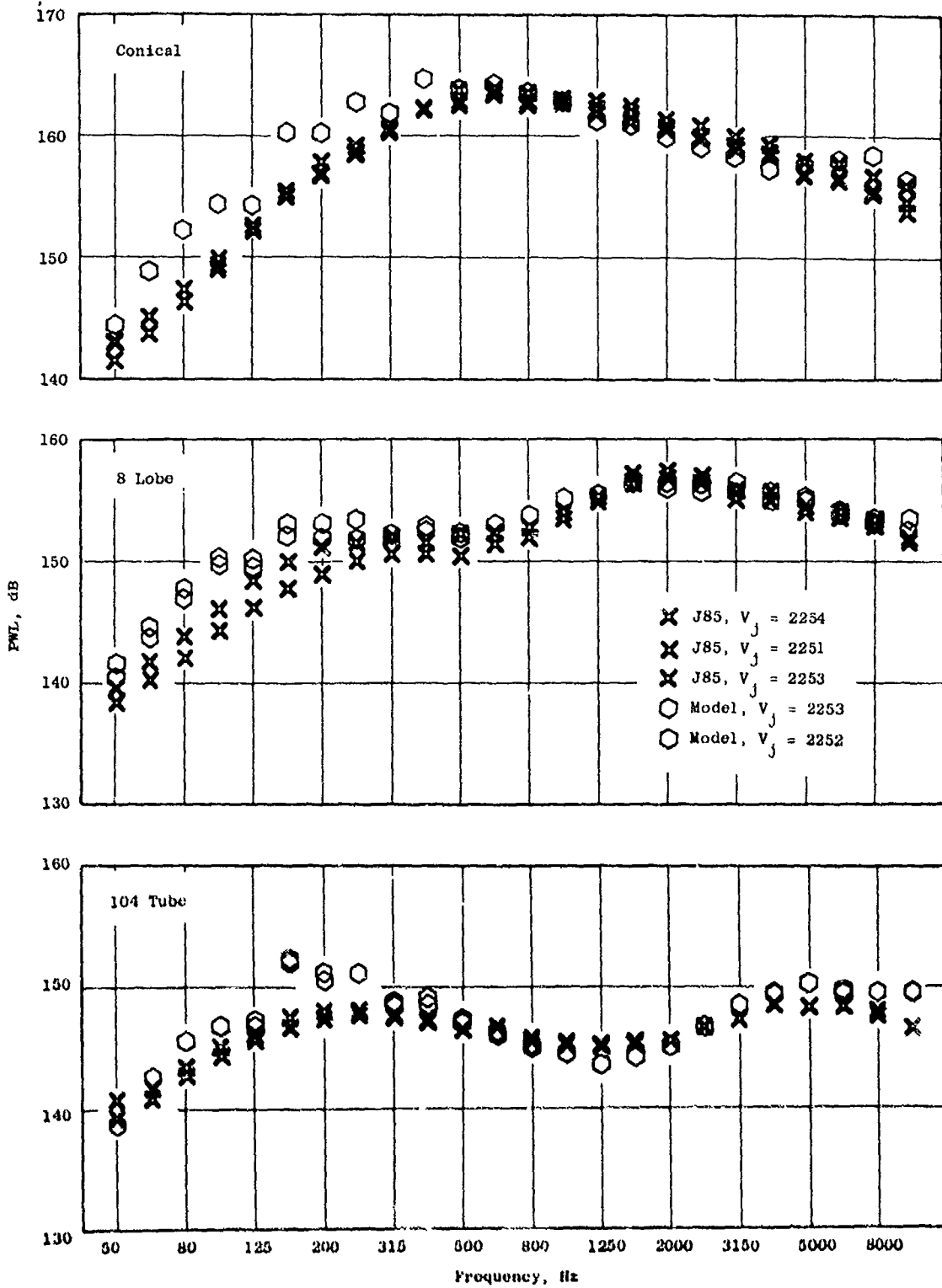


Figure A-20. Model and J85 Power Spectra Comparisons.

• 160-ft Arc

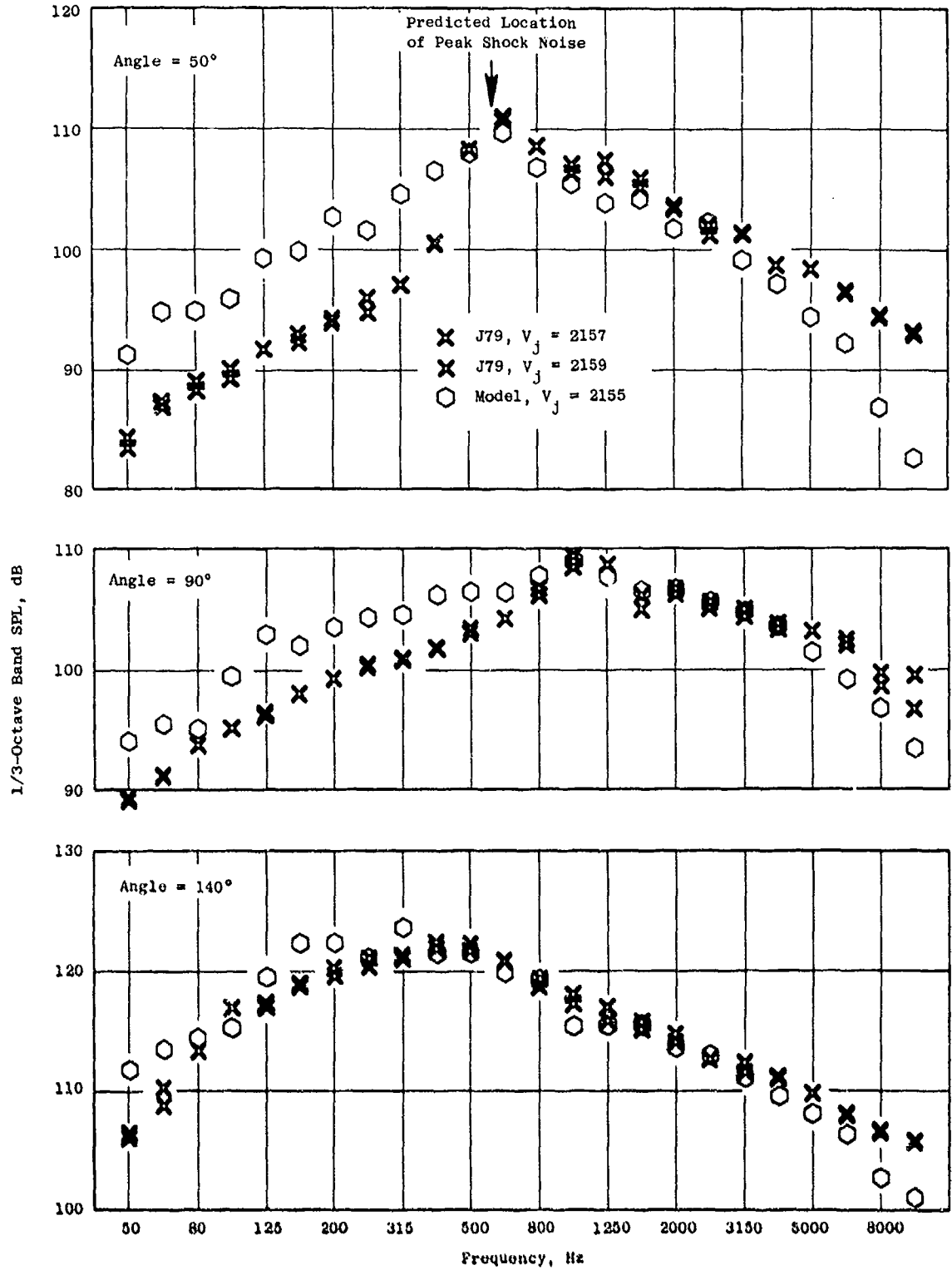


Figure A-21. Model and J79 Conical Nozzle Spectra Comparisons.

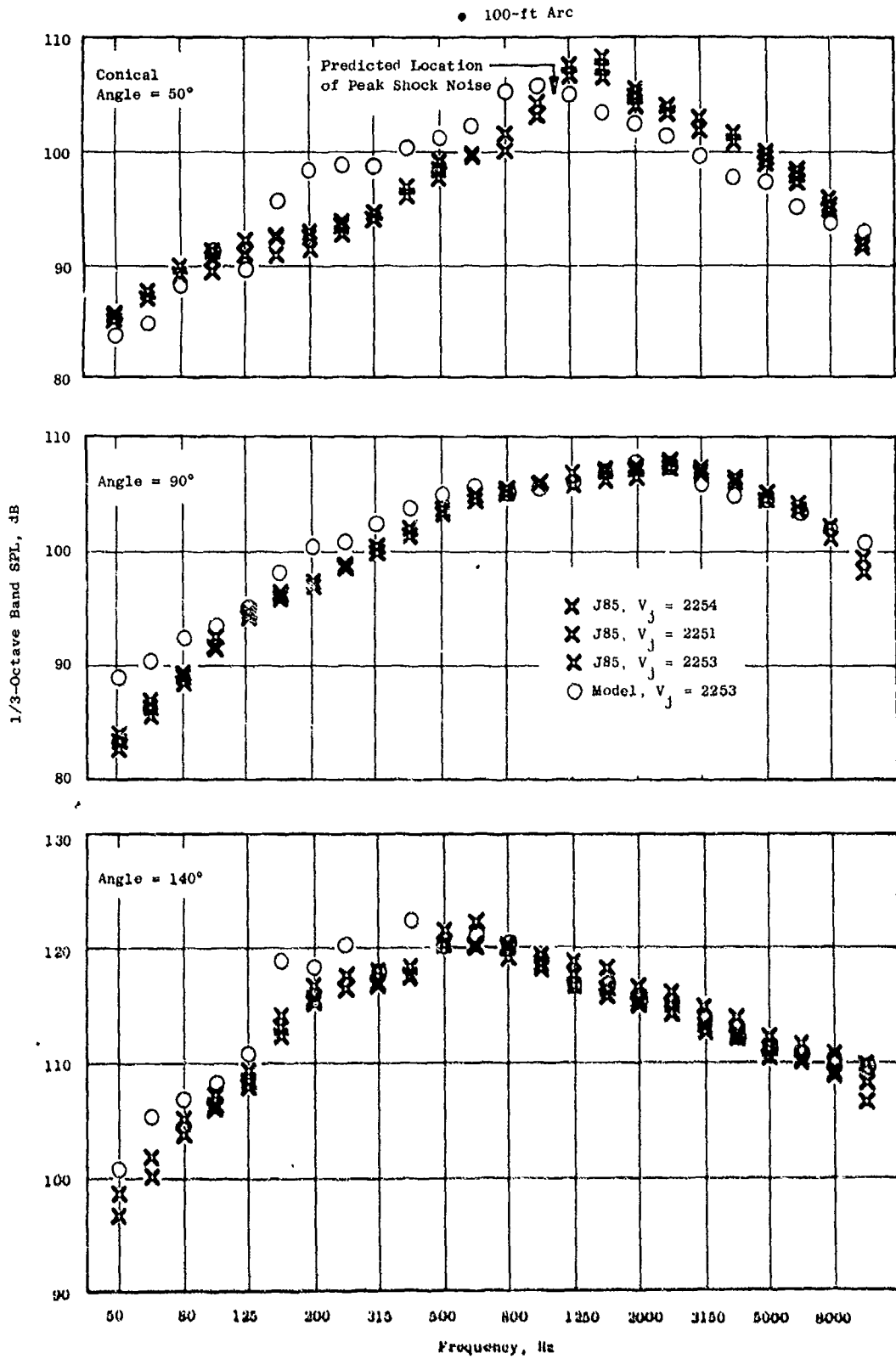


Figure A-22. Model and J85 Conical Nozzle Spectra Comparisons.

• 160-ft Arc

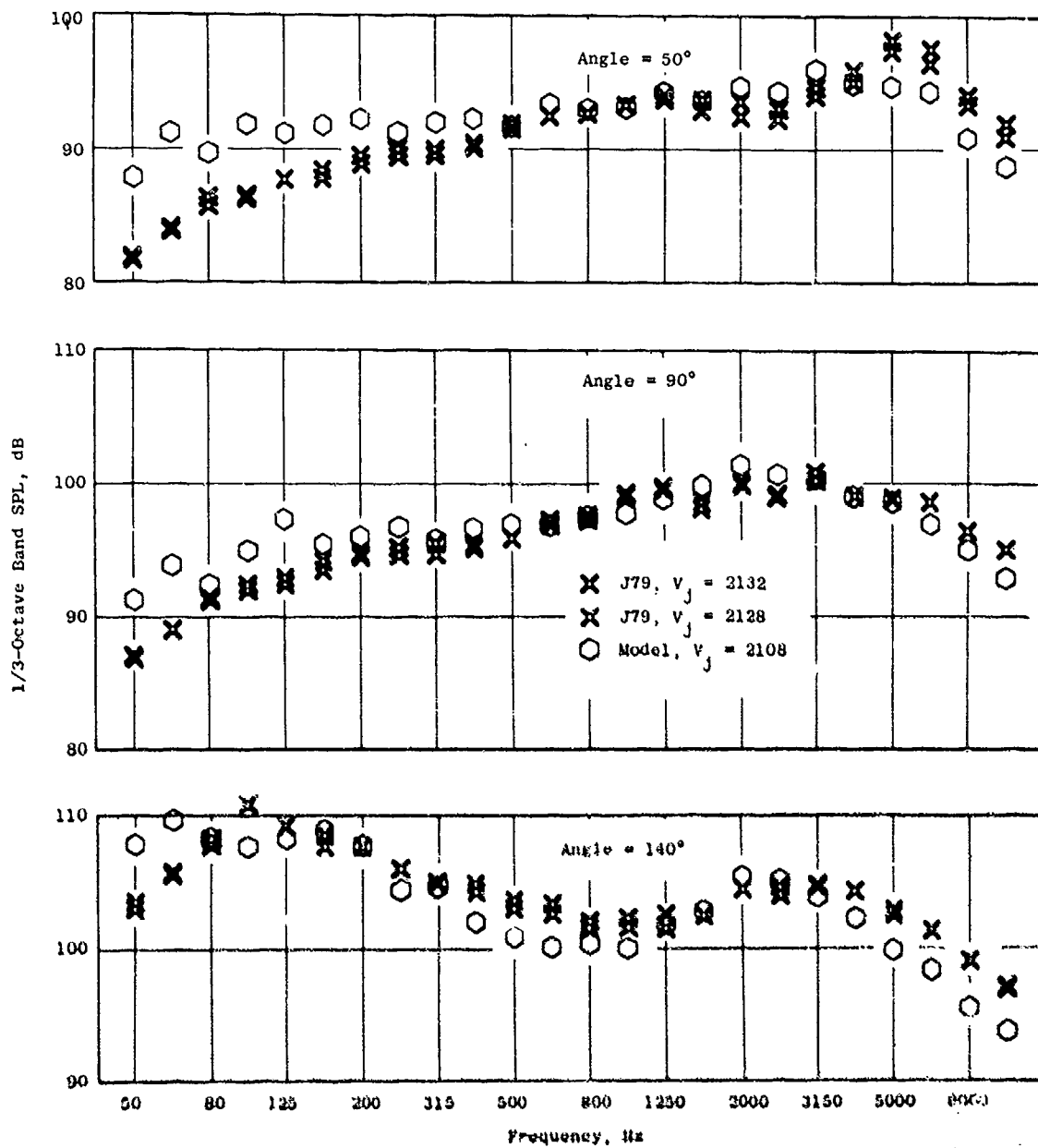


Figure A-23. Model and J79 32-Chute Nozzle Spectra Comparisons.

• 160-ft Arc

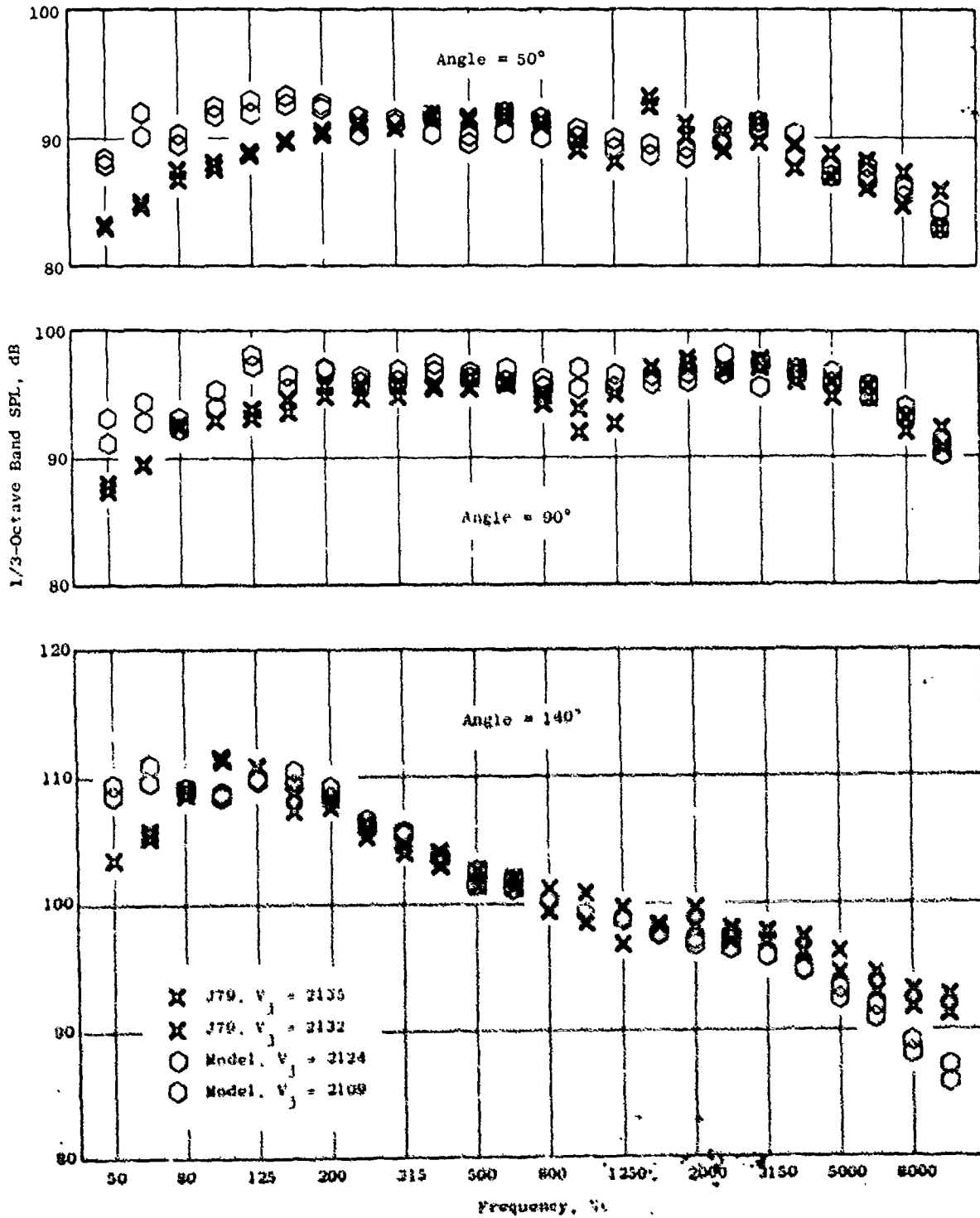


Figure A-24. Model and J79 32-Chute + Ejector Spectra Comparisons.

The 8-lobe and 104-tube nozzle J85 engine and scale-model comparisons are shown in Figures A-25 and A-26 for an approximate velocity of 2160 ft/sec. The agreement for the 8-lobe nozzle (Figure A-25) at 50° is somewhat erratic. However, very good agreement is found at 90°, differing only at the lowest frequencies. Agreement at maximum angle (140°) is quite good down to 250 Hz while lower frequencies exhibit differences as high as 5 dB between model and full scale. The agreement for the 104-tube (Figure A-26) at 50° is good except for a portion of the low frequency region and at the highest frequency. The agreement at 90° is again very good. The agreement at 140° was very good except for the 175 to 250 Hz region, where a deviation up to 7 dB is observed.

In summary, the peak shock noise regions scale well. However, values at other frequencies (especially the low) are not duplicated using the conventional scaling method. The scaling agreement is improved at 90° and aft.

Velocity Distributions (Laser Velocimeter Measurements)

This section will present comparisons between laser velocimeter measurements made on scale-model nozzles tested on the JENOTS facility with configurations tested on the J79 engine at the Edwards test facility. Only select comparisons are presented because the engine measurements were not as extensive as those made on the scale model.

Velocity characteristics for conical and 32-chute nozzles were obtained with a laser velocimeter. Axial and radial distributions are shown for both mean velocity and turbulence levels. Comparisons are made for the 3.56-inch-diameter conical model and the J79 engine, except for one case which includes the 2.0-inch-diameter conical nozzle. These configurations had LV data with comparable velocities of 2100 ft/sec.

The axial mean velocity distribution along the centerline, $r/r_0 = 0$, of two conical nozzles is shown in Figure A-27. The 3.56-inch-diameter conical model has an internal plug, previously noted, while the 2.0-inch-diameter conical model has no internal obstruction. The J79 engine, with an internal plug (~2 nozzle diameters upstream), compares well with the 3.56-inch-diameter nozzle, with an internal plug (~1/2 nozzle diameter upstream). The first six diameters downstream are dominated by shock patterns as shown. J79 engine data were not available for comparison upstream of the six diameters. The 2.0-inch-diameter conical nozzle, without internal obstruction, retains a higher velocity than the 3.56-inch-diameter nozzle in the downstream directions.

The axial mean velocity distribution along the outer lip, $r/r_0 = 1$, is also shown in Figure A-27 for both the J79 engine and 3.56-inch-diameter conical configurations. The model mean velocity is somewhat greater than that for the J79 engine, especially near the nozzle exit plane.

• 100-ft Arc

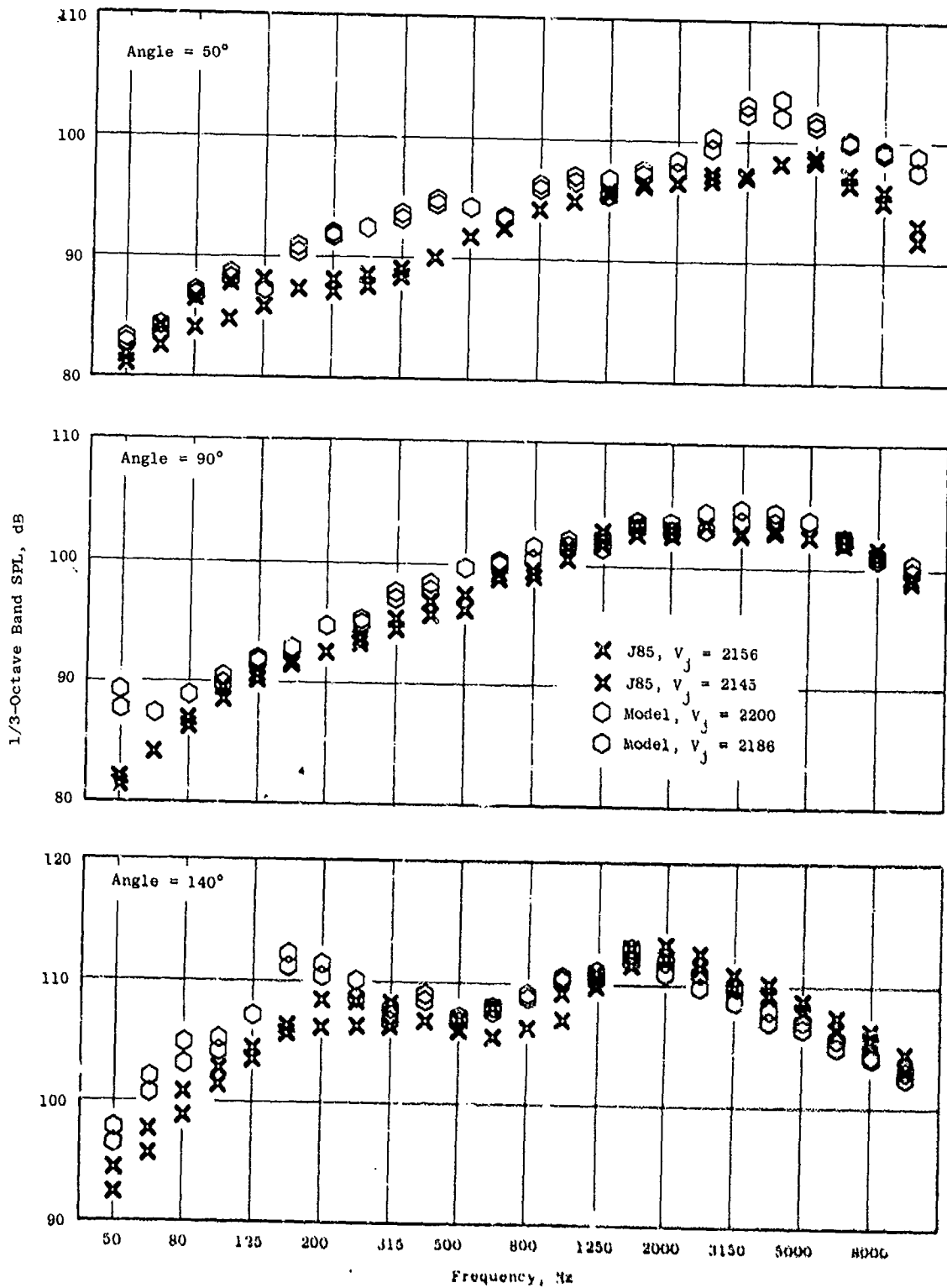


Figure A-25. Model and J85 8-Lobe Nozzle Spectra Comparisons.

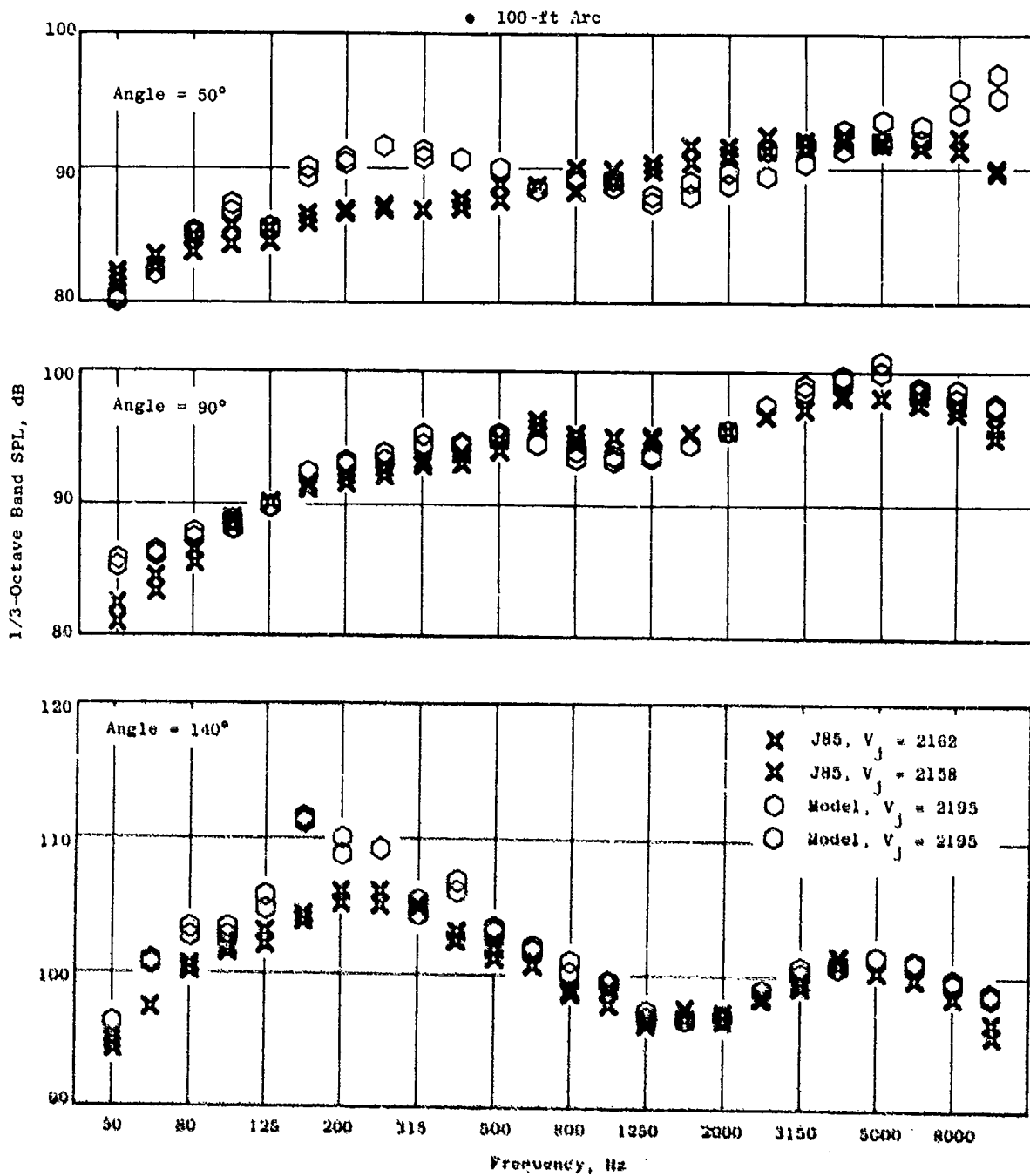


Figure A-26. Model and J85 104-Tube Nozzle Spectra Comparisons.

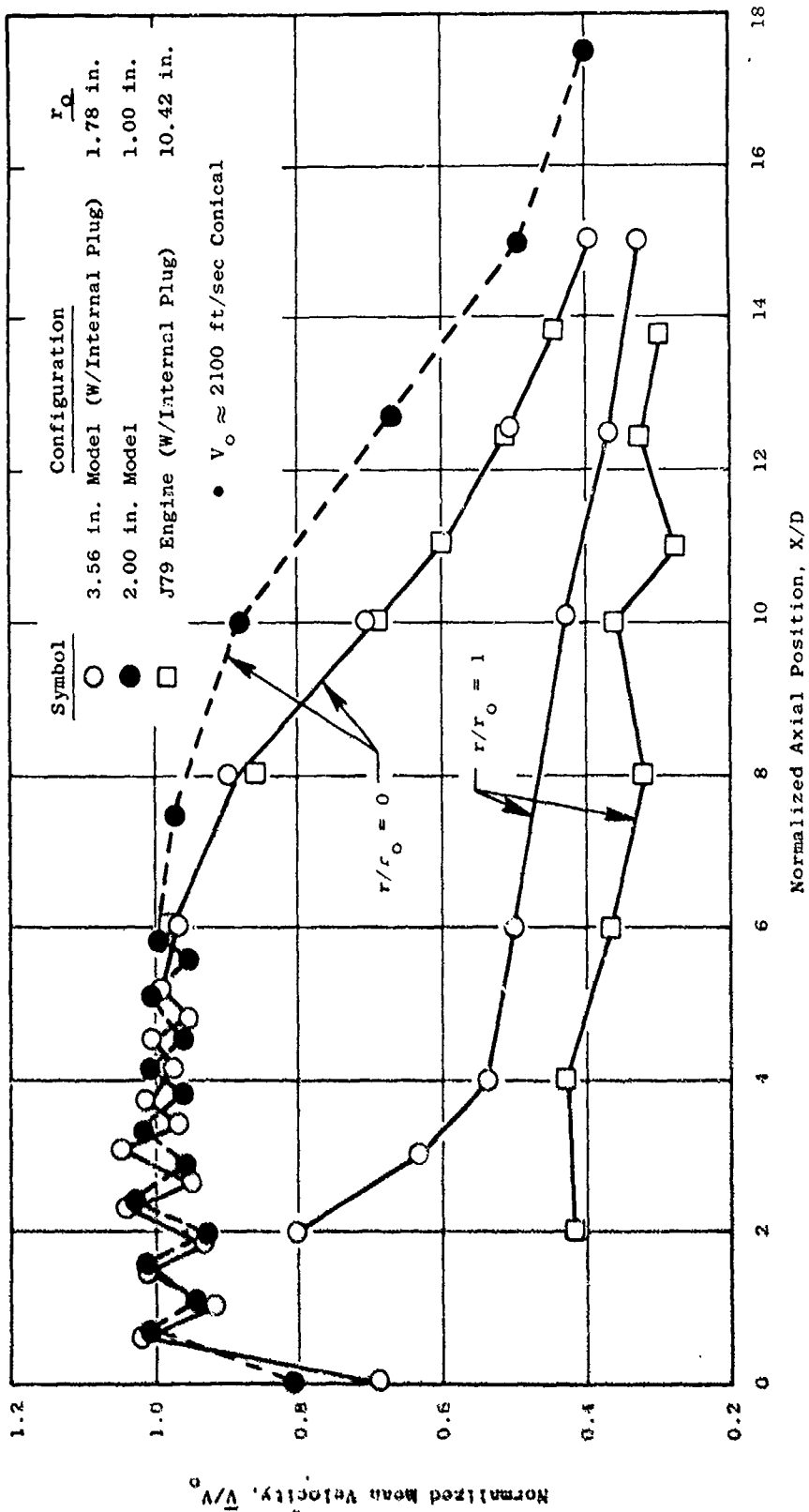


Figure A-27. Comparison of Conical Nozzle Axial Mean Velocity Distribution, Laser Velocimeter Data.

The comparison of radial mean velocity distribution at two diameters downstream ($x/D = 2$) is shown in Figure A-28 for the J79 engine and 3.56-inch-diameter conical configurations. Good agreement is shown out to approximately $r/r_0 = 0.8$. The model shows a greater mean velocity in the shear layer region than does the J79 engine.

The comparison of radial mean velocity distribution at six diameters downstream ($x/D = 6$) is shown in Figure A-28. The conical nozzle still shows a somewhat greater mean velocity in the shear layer region. The centerline and outermost velocities are the same for both engine and model.

The comparison of axial mean velocity distribution along the centerline of the J79 engine and scale-model, 32-chute configurations is shown in Figure A-29. Good agreement is shown except near the nozzle exit where the model's velocity is somewhat greater than the engine's.

The comparison of axial mean velocity distribution along the outer lip for the engine and model 32-chute configuration is shown in Figure A-29. Very good agreement is observed. No data beyond $x/D > 7$ was available.

The comparison of radial mean velocity distribution at two diameters and six diameters downstream for the engine and model 32-chute configurations is shown in Figure A-30. Very good agreement is observed over the complete radial traverse. The engine's centerline velocity is slightly lower than the model's.

The comparison of radial mean velocity distribution at six diameters downstream for the engine and model 32-chute configurations is shown in Figure A-30. Again, very good agreement is observed over the complete radial traverse.

The comparison of radial distribution of axial turbulence (u'/V_0) is shown in Figure A-31 for the conical configurations at two diameters downstream. The J79 engine and 3.56-inch-diameter model have the same turbulence level in the potential core region. Data for the engine at r/r_0 less than 0.5 are not available. The model has a somewhat lower turbulence level in the shear layer region, except at $r/r_0 = 1$ where the model is greater. The comparison for radial distribution of turbulence for the 32-chute configurations at two diameters downstream is also shown in Figure A-31. Very good agreement over the complete radial traverse is shown.

The axial distribution of turbulence along the centerline is shown in Figure A-32 to be the same for both the J79 engine and 3.56-inch-diameter model conical configurations. However, the same comparison at the outer lip ($r/r_0 = 1$, Figure A-29) shows poor agreement until well downstream. Here the model turbulence is nearly twice that of the engine.

The axial distribution turbulence on the centerline shows good agreement between the engine and model 32-chute nozzles (Figure A-33). The same comparison at $r/r_0 = 1$ also shows good agreement.

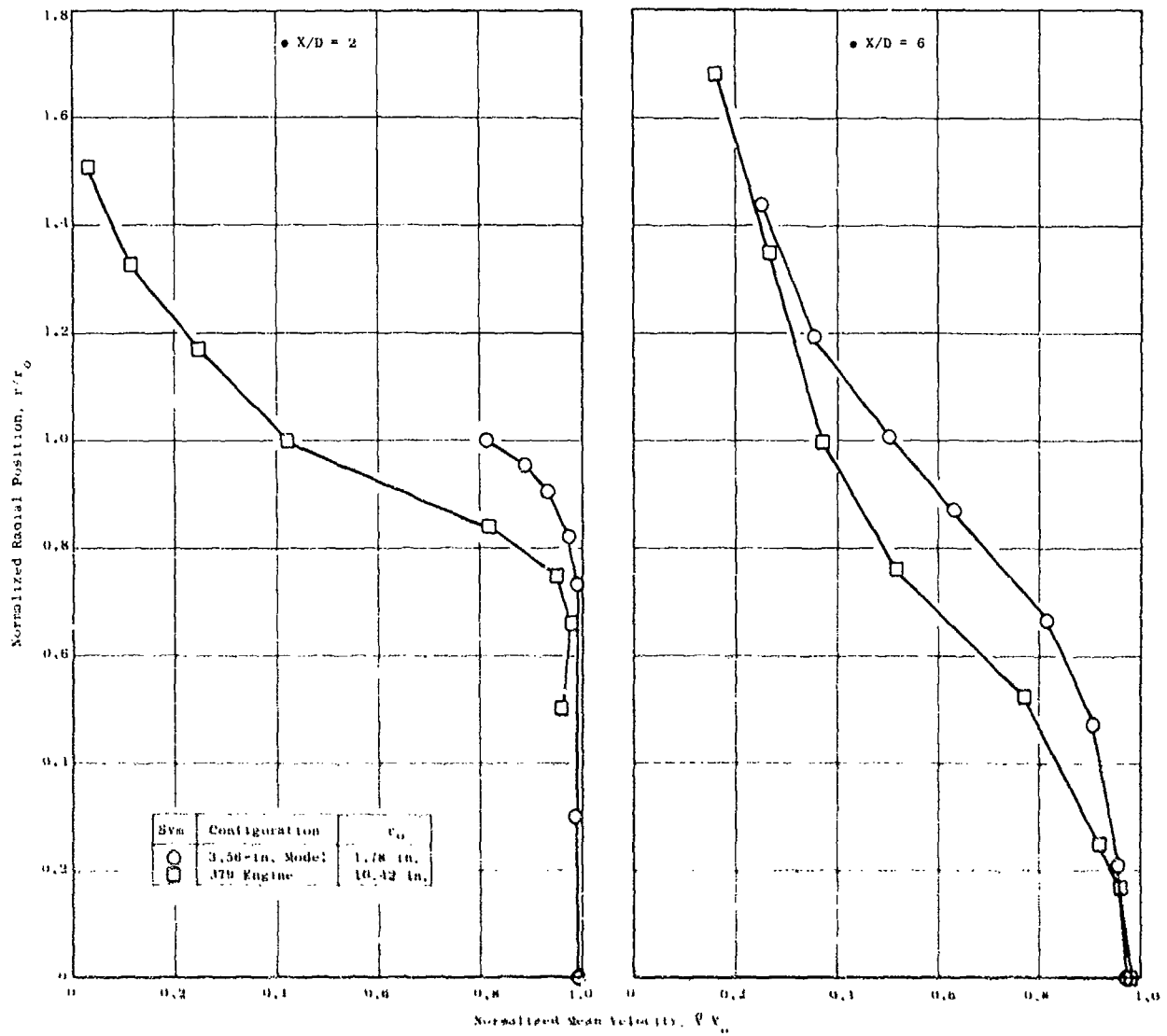


Figure A-28. Comparison of Conical Nozzle Radial Mean Velocity Distribution, Laser Velocimeter Data, $V_0 = 2100$ ft/sec.

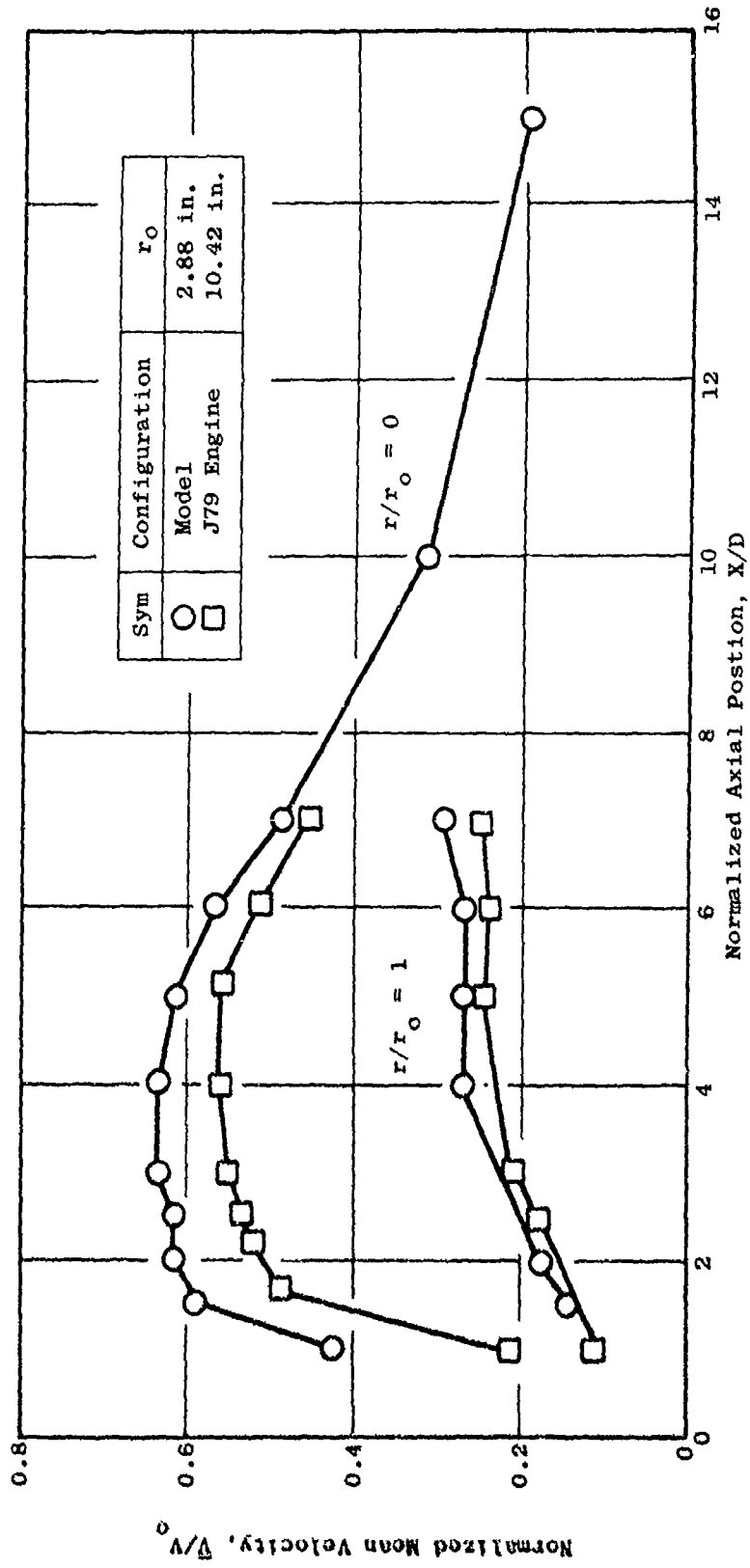


Figure A-29. Comparison of 32-Chute Nozzle Axial Mean Velocity Distribution, Laser Velocimeter Data, $V_0 = 2100$ ft/sec.

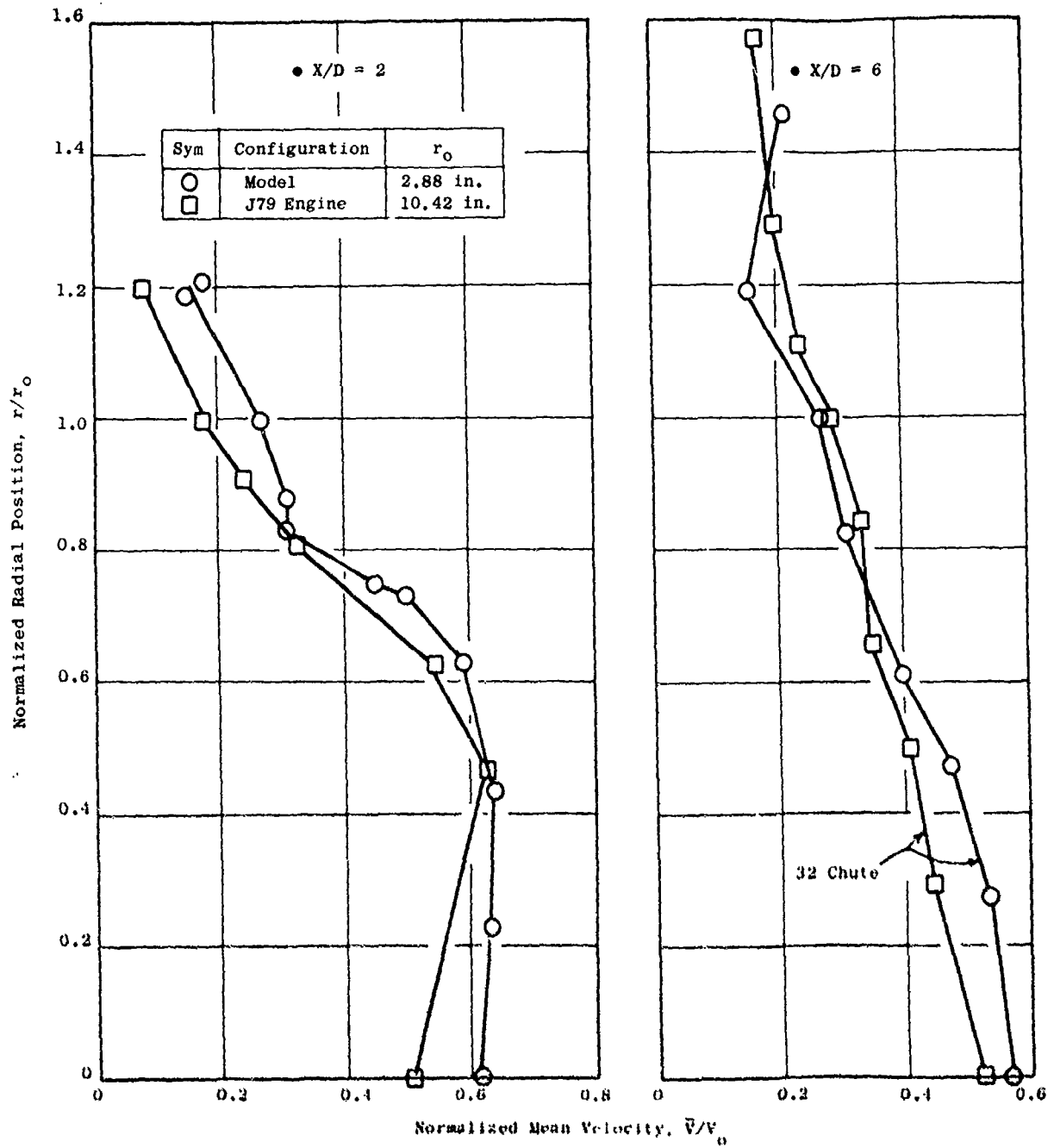


Figure A-30. Comparison of 32-Chute Nozzle Radial Mean Velocity Distribution, Laser Velocimeter Data, $V_0 = 2100$ ft/sec.

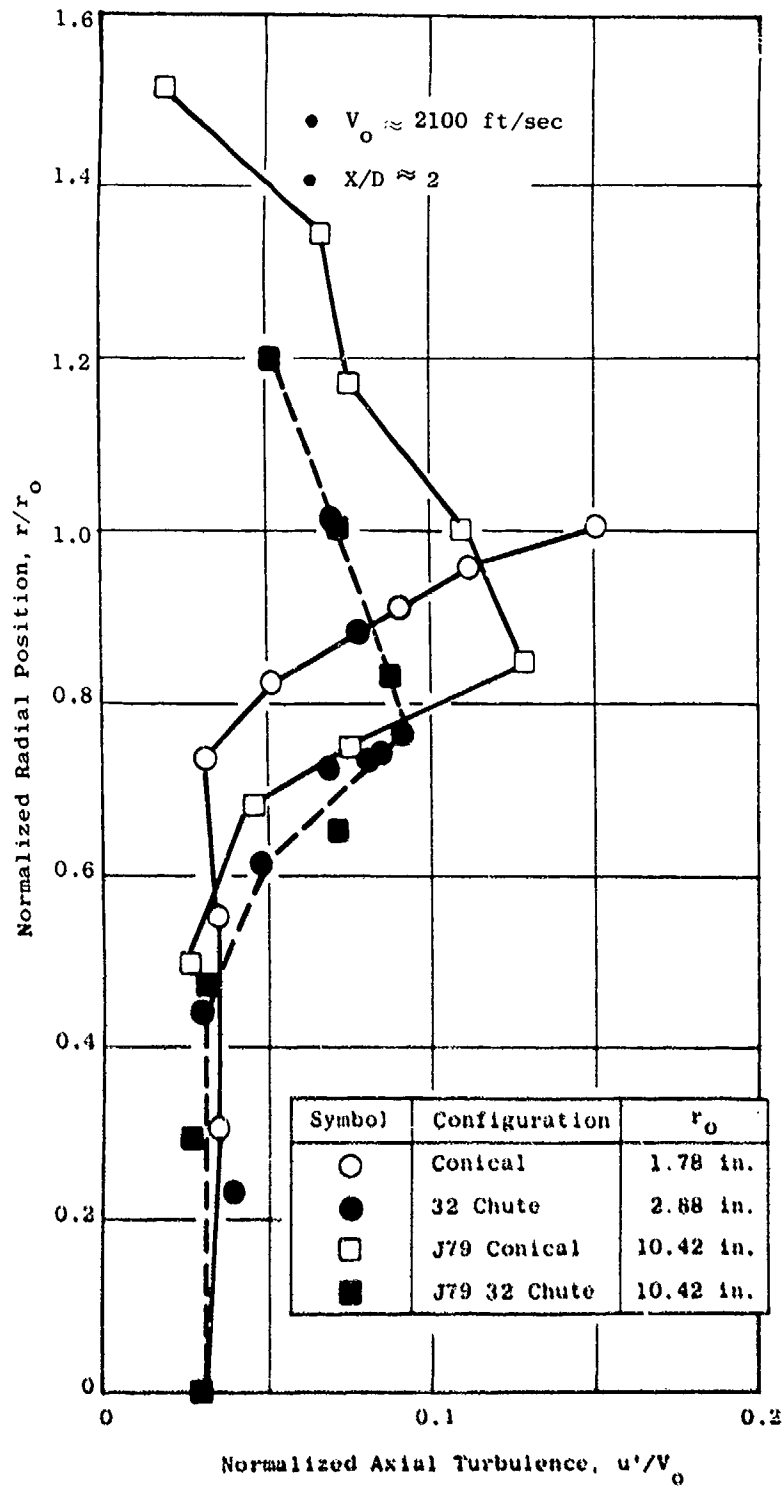


Figure A-31. Comparison of Radial Distribution of Axial Turbulence, Laser Velocimeter Data.

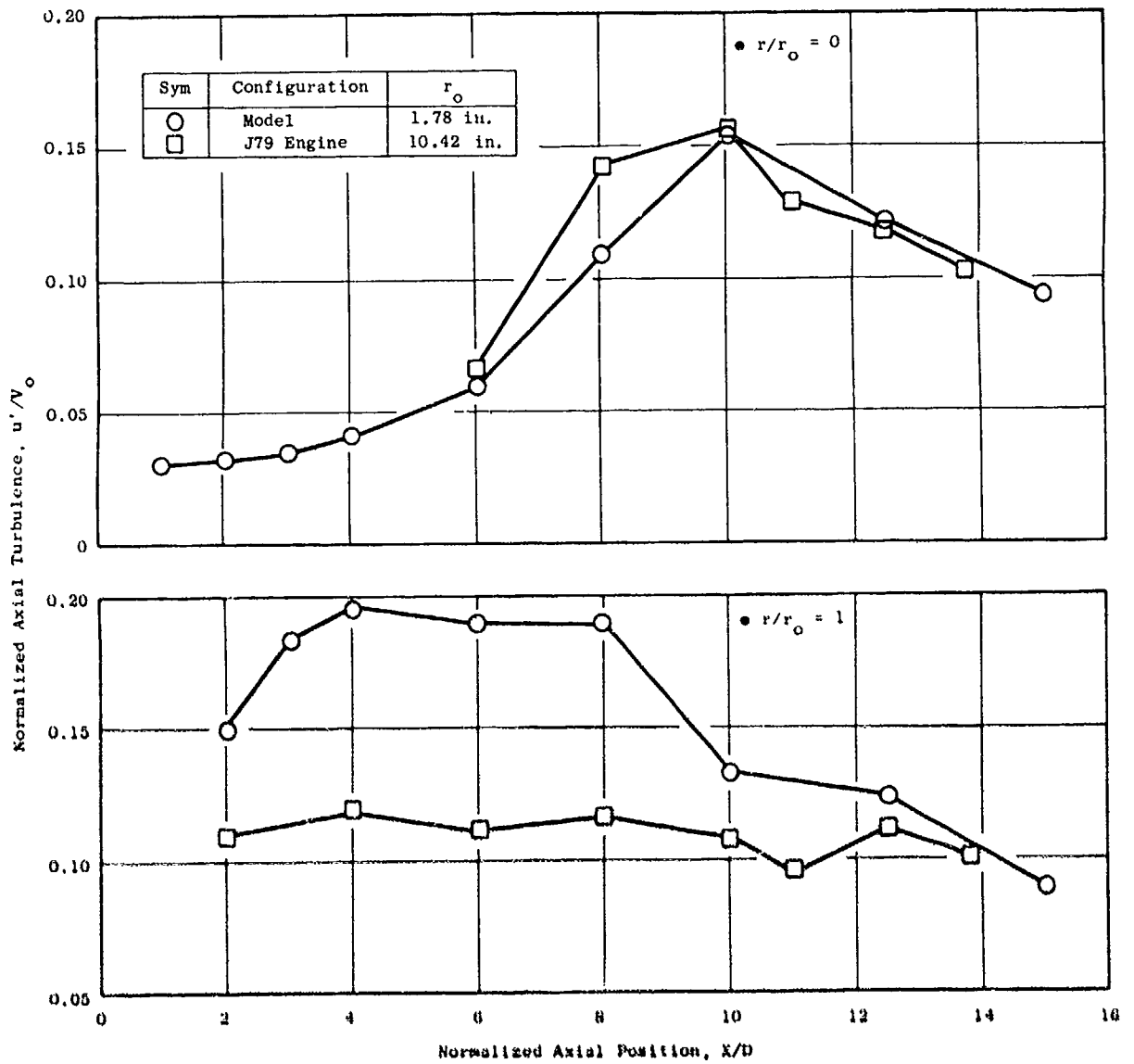


Figure A-32. Comparison of Conical Nozzle Turbulence Characteristics, Laser Velocimeter Data, $V_0 = 2100$ ft/sec.

Sym	Configuration	r_o
○	Model	2.88 in.
□	J79 Engine	10.42 in.

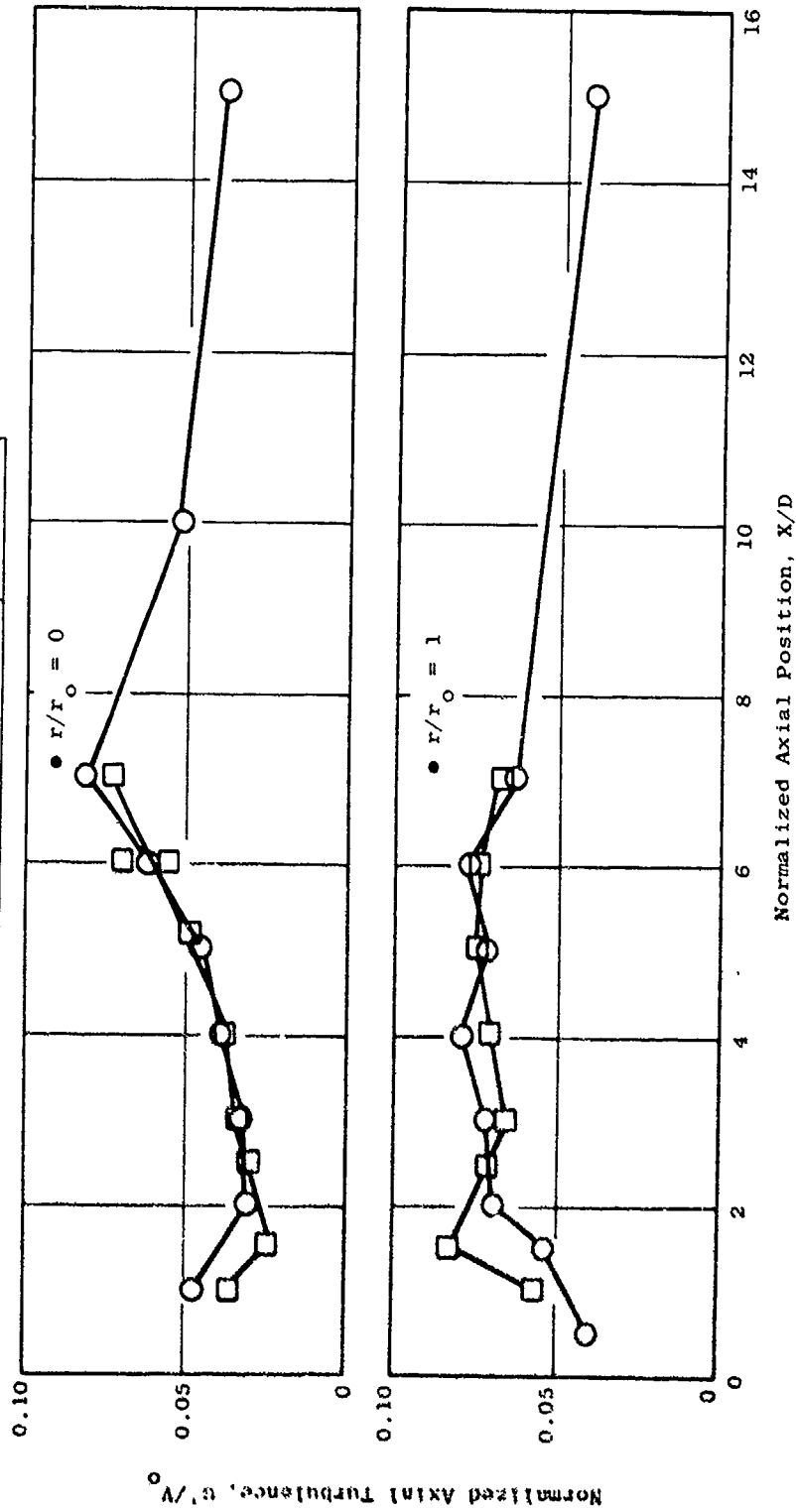


Figure A-33. Comparison of 32-Chute Nozzle for Axial Distribution of Axial Turbulence, Laser Velocimeter Data, $V_o = 2100$ ft/sec.

In summary, the J79 engine and 3.56-inch-diameter model velocity and turbulence levels differ mainly in the shear layer region. A reduction in axial mean velocity was observed for a conical nozzle with an internal plug compared to a conical nozzle without internal disturbance. The agreement of 32-chute nozzle velocity and turbulence levels is good in all cases. It should be noted that the 32-chute, scale-model and full-scale nozzle were duplicates, whereas the conical nozzles were not.

Noise Source Location (Ellipsoidal Mirror)

The Strouhal variation with axial location is shown in Figure A-34 for both J79 engine and scale-model conical nozzles. The agreement is very good over the range covered. The larger diameter J79 engine extends to higher Strouhal values than the model, while the model extends to lower levels than the engine. Both 3.56-inch- and 2.00-inch-diameter conical nozzles show good agreement.

The 90° spectral comparison of engine and scale-model ellipsoidal mirror data is shown in Figure A-35. The agreement is fairly good (within ± 2 dB) from 1000 Hz to 20,000 Hz. The 18-inch-diameter mirror is not designed to accurately measure data below 1000 Hz, due to diffraction effects. (See Reference 18 for details.)

In summary, the limited comparison of ellipsoidal mirror data for J79 engine and scale-model conical nozzles generally shows good agreement on a Strouhal basis and fair agreement on a spectral basis.

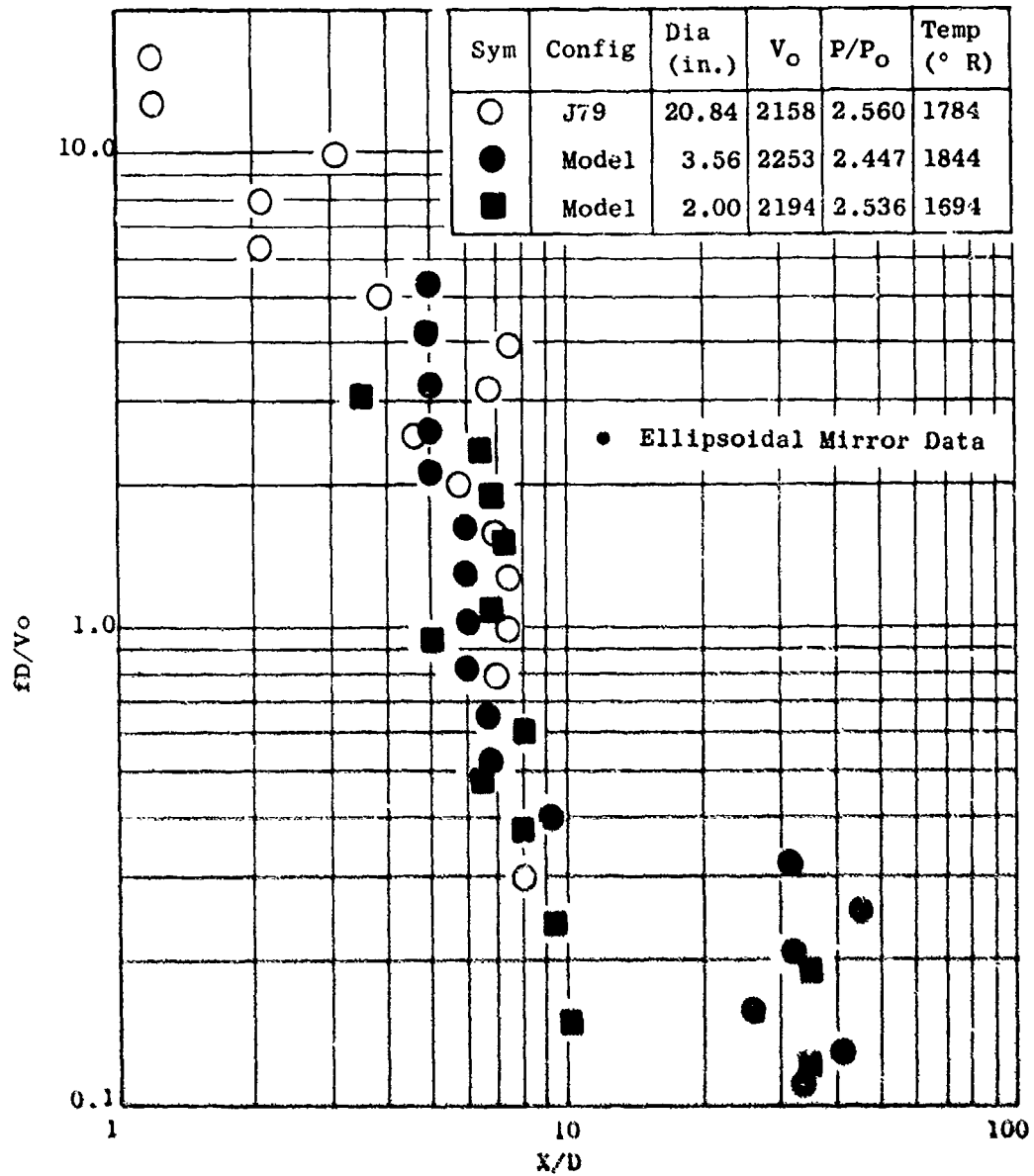


Figure A-34. Comparison of Model and Full-Scale Apparent Noise Source Location.

Sym	Scale	Dia, in.	Measurement	V, ft/sec	T _T , ° R
○	J79	20.84	EM	2158	1784
●	Model	3.56	EM	2253	1844

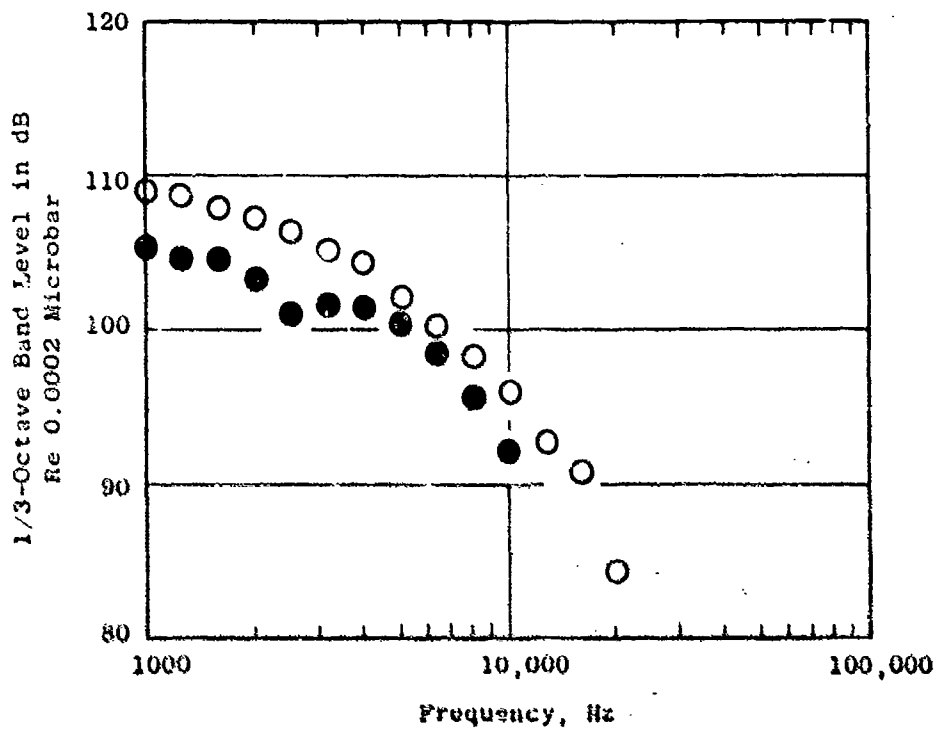


Figure A-35. Comparison of Conical Nozzle 90° Ellipsoidal Mirror Spectra from Engine and Model Static Tests.

8.0 CONCLUSIONS AND RECOMMENDATIONS

1. Diameter scaling holds well for $OASPL_{max}$ and PNL_{max} over the velocity range covered ($0 < \log V_j/a_0 < 0.4$), for both unsuppressed and suppressed nozzles.
2. Diameter scaling holds reasonably well for OASPL and PNL over the directivity range covered ($20^\circ < \theta_i < 160^\circ$), for both suppressed and unsuppressed nozzles.
3. Diameter scaling holds fairly well for PWL and 1/3-octave band SPL over the frequency range covered ($50 < f < 10K$ Hz F.S.) for both suppressed and unsuppressed nozzles. Differences occurring at high and low frequencies are most pronounced in the forward quadrant.
4. Diameter scaling holds well for the shock noise dominated region of the spectrum, with the peak frequency correctly predicted by the Harper-Bourne, Fisher equation. Poor scaling agreement is found at low frequencies.
5. The LV values of normalized mean velocity and turbulence along the centerline agree for both engine and model conical (unsuppressed) nozzles. However, the model has higher values than the engine in the shear layer region.
6. Good agreement for both engine and model 32-chute (suppressed) nozzle LV data is found throughout the flow for both mean velocity and turbulence intensity.
7. The EM comparison shows good agreement between engine and scaled conical model data on an axial Strouhal basis and fair agreement on a spectral basis.
8. An exact replica model of the engine must be used when making acoustic comparisons.
9. A standard conical nozzle should be used as the baseline by all industry and Government (analogous to the ASME standard bellmouth, orifice designs, etc.).

APPENDIX B

TABULATION OF ACOUSTIC AND AERODYNAMIC
PERFORMANCE DATA

A summary of the data used for performing the trade studies of aerodynamic performance versus acoustic suppression is presented on Table B-1. Acoustic suppression and aerodynamic performance levels are relative to a round convergent nozzle. The appropriate reference is also defined if more information about a specific configuration is desired.

Table B-1. Summary of Suppression and Performance Characteristics.

Configuration	Source	Suppression Level Static	Suppression Level Flight	Static Performance Loss, % Relative to Round Convergent Nozzle (1)	Flight Performance Loss, % Relative to Round Convergent Nozzle (1)	$\frac{\Delta PNL}{\Delta C_p}$ Static	$\frac{\Delta PNL}{\Delta C_p}$ Flight	$\frac{\Delta PNL}{\Delta C_p}$ Flight
Unsuppressed plug	4	7.5	2.5	1.4	0.5	1.8	5.0	0.5
40 Chutes	4	8.1	---	15.7	14.7	0.5	0.6	---
40 Chutes	4	14.0	---	15.3	15.7	0.9	0.9	---
16 Chutes	4	8.5	---	2.0	4.5	4.3	1.9	---
16 Chutes + 1 Hardwall Ejector	4	9.5	---	-0.8	4.0	-11.9	2.4	---
16 Chutes + 2 Hardwall Ejectors	4	9.5	---	2.4	5.9	4.0	1.6	---
16 Chutes + 1 Treated Ejector	4	10.5	---	-0.8	4.0	-13.1	2.6	---
16 Chutes + 2 Treated Ejectors	4	10.5	---	2.4	5.9	4.4	1.8	---
72 Tube	4	13.0	---	9.4	---	---	---	---
Unsuppressed 1-D + Hardwall Ejector	4	3.0	---	1.8	2.3	1.7	1.3	---
Suppressed 1-D + Hardwall Ejector + Wing	4	9.0	---	1.5	2.8	6.0	3.2	---
12 Deep Chutes	4	12.0	9.0	2.9	6.1	4.1	2.0	1.5
12 Deep Chutes + Hardwall Ejector	4	12.0	---	0.0	5.4	---	2.2	---
AE = 1.5 16 Chutes Dual Flow	8	10.2	---	3.5	---	2.9	---	---
AE = 1.5 16 Chutes Dual Flow Sharp Inlet	8	13.7	---	0.9	---	14.7	---	---
Multi-tube Suppressor	5	10.7	---	3.9	---	2.7	---	---
Unsuppressed Conventional Nozzle With Plug	5	13.2	---	2.8	---	4.7	---	---
Unsuppressed Conventional Nozzle Without Plug	9	---	---	0.6	6.5	---	---	---
AE = 1.31, EE = 0.907 Coarse Lar Nozzle	9	5.2	---	2.0	3.6	2.6	1.4	---
AE = 1.0, EE = 0.902	9	4.8	---	0.6	2.6	7.7	1.8	---
AE = 0.91, EE = 0.91	9	5.6	---	1.8	2.4	3.1	2.3	---
AE = 1.0, EE = 0.902	9	5.2	---	3.2	4.1	1.4	1.3	---
AE = 0.61, EE = 0.811	9	3.6	---	1.0	1.1	3.8	3.5	---
AE = 1.4, EE = 0.916	9	5.0	---	2.7	2.5	1.9	2.0	---
AE = 0.91, EE = 0.811	9	4.3	---	2.0	1.5	2.15	2.9	---
AE = 2.0, 21 Spokes	3	11.2	---	4.1	9.7	2.7	1.2	---
AE = 2.0, 12 Spokes	3	11.6	---	9.7	13.2	1.2	0.9	---
AE = 2.0, 48 Spokes	3	16.0	---	19.9	21.4	0.8	0.7	---
AE = 2.0, 12 Parallel Spokes	3	13.7	---	20.0	21.4	0.7	0.6	---
AE = 1.7, 12 Tapered Spokes	3	8.4	---	8.4	9.1	1.0	0.9	---
AE = 1.7, 12 Tapered Spokes	3	11.5	---	9.2	16.4	1.3	0.7	---
AE = 2.0, 12 Tapered Spokes at 10° Fwd	3	11.5	---	7.0	11.3	1.6	1.0	---
AE = 2.0, 12 Tapered Spokes at 10° Aft	3	14.5	---	11.6	15.8	1.3	0.9	---
AE = 2.0, 12 Tapered Chutes	3	13.5	---	4.7	7.6	2.9	1.8	---
AE = 2.5, 16 Chutes, Retracted Plug	Vol. 11	7.4	---	3.0	7.0	3.1	1.3	---
AE = 2.0, 16 Chutes, In-Line	Vol. 11	10.7	---	5.2	7.4	2.1	1.4	---
AE = 2.0, 16 Chutes, Retracted Plug	Vol. 11	9.7	---	5.2	7.5	1.9	1.3	---
AE = 2.0, 16 Chutes, In-Line	Vol. 11	11.9	---	5.2	7.8	2.3	1.5	---
AE = 2.0, 16 Chutes, Retracted	Vol. 11	11.5	---	5.2	7.8	2.2	1.5	---
AE = 6.582								
AE = 2.0, 16 Chutes, Retracted								
AE = 6.582								

(1) Plus sign signifies increase in performance vs. Convergent Nozzle

Table B-1. Summary of Suppression and Performance Characteristics (Continued).

Configuration	Source	Suppression Level Static	Suppression Level Flight	Static Performance Loss, % Relative to Round Convergent Nozzle (1)	Flight Performance Loss, % Relative to Round Convergent Nozzle (1)	APNL Static acFg Flight	APNL Static acFg Flight
AR - 1.5, 16 Chutes Retracted	Vol. II	11.2	---	3.0	7.0	---	---
AR - 2.0, 16 Spokes Retracted	Vol. II	10.4	---	13.3	14.9	1.6	---
AR - 1.75, 20 Shallow Chutes Retracted	Vol. II	9.2	---	3.3	5.5	0.7	---
AR - 1.75, 40 Shallow Chutes Retracted	Vol. II	8.2	---	5.3	7.59	2.8	---
AR - 2.0, 16 Spokes In-Line	Vol. II	10.8	---	13.3	14.9	1.1	---
AR - 1.5, 16 Chutes Turbojet	Vol. III	7.9	---	6.3	7.3	1.1	---
AR - 2.0, 16 Chutes Turbojet	Vol. III	11.6	8.3	5.6	9.1	1.4	0.9
AR - 1.3, 1 Tubas Close-Packed Array, Elliptical Tubas with Round Converg. Ends	Vol. II	12.3	9.3	3.4	8.3	1.5	1.1
AR - 3.3, 197-CPA-EV/RC	Vol. II	6.8	---	0.3	---	---	---
AR - 3.3, 377-CPA-EV/RC	5	-11.2	---	1.2	---	22.7	---
AR - 3.3, 615-CPA-EV/RC	5	12.5	---	1.9	---	9.3	---
AR - 2.75, 377-CPA-EV/RC	5	13.6	---	3.4	---	1.3	---
AR - 4.5, 377-CPA-EV/RC	5	10.7	---	1.9	---	4.0	---
AR - 6.0, 377-CPA-EV/RC	5	13.8	---	1.9	---	5.6	---
AR - 3.3, 377-RA-EV/RC	5	12.0	---	2.5	---	7.3	---
AR - 4.5, 377-RA-EV/RC	5	11.5	---	2.0	---	4.8	---
AR - 3.75, 317-RA-EV/RC	5	12.3	---	0.7	---	5.8	---
AR - 2.6 Ejector	5	16.0	---	-1.6	---	17.6	---
AR - 3.1 Ejector	5	13.8	---	-5.2	---	-10.0	---
AR - 3.7 Ejector	5	13.5	---	-4.5	---	-2.7	---
LSEP-3, 65 Tube Nozzle	5	16.4	---	9.2	---	-3.0	---
LSEP-4, 31 Tube Nozzle	5	11.6	---	3.8	---	1.8	---
LSEP-2, 57 Tube Nozzle	5	14.7	---	4.8	---	3.1	---
LSEP-2 (17-in. Lined Ejector)	5	16.6	11-12	3.5	6.2	3.1	---
LSEP-3 (17-in. Lined Ejector)	5	19.0	---	8.5	---	4.7	1.8-1.9
LSEP-4 (17-in. Lined Ejector)	5	21.5	---	8.2	---	2.2	---
LSEP-4 (12-in. Lined Ejector)	5	15.2	---	1.1	---	2.6	---
8 Lobe Nozzle	10	6.0	5.5	2.2	3.6	2.7	1.5
104 Tube Nozzle	10	13.5	11.5	10.2	12.2	1.3	0.9
12 Chutes	11	8.0	5.0	5.0	5.5	1.5	0.9
45 Tubas	11	---	5.5	7.0	11.0	---	0.5
32 Spokes	11	11.6	8.0	9.0	14.0	1.3	0.6
104 Tubas	11	---	12.5	10.0	15.0	---	0.8

(1) Minus Sign Signifies Increase in Performance Re: Convergent Nozzle

Table B-1. Summary of Suppression and Performance Characteristics (Concluded).

Configuration	Source	Suppression Level Static	Suppression Level Flight	Static Performance Loss, % Relative to Round Con- Nozzle	Flight Performance Loss, % Relative to Round Con- Nozzle	APNL ΔC _{Fg} Static	APNL Static ΔC _{Fg} Flight	APNL ΔC _{Fg} Flight
194 Tubes • Acoustic Straws	11	---	14.5	8.0	15.0	---	---	1.0
17 Chords • Acoustic Straws	11	---	10.5	---	20.5	---	---	0.5
48 Tubes • Acoustic Straws	11	---	14.0	17.5	24.5	---	---	0.6
64 Spokes	11	13.4	8.0	24.5	22.5	0.5	0.6	0.4
80-AP-44 17 Tubes, Hex Array, AE = 5.1	2	9.0	---	1.0	---	9.0	---	---
80-AP-53C 17 Tubes, AE = 1.1	2	14.0	---	1.0	---	14.0	---	---
80-AP-51 17 Spokes, AE = 2.1	7	6.5	---	1.2	---	5.4	---	---
80-AP-50A 17 Tubes, AE = 4.1	2	14.5	---	6.0	---	2.4	---	---
80-AP-50 24 Spokes, AE = 2.0	2	8.0	---	5.9	---	1.3	---	---
80-AP-41A 17 Tubes, 24 Spokes, AE = 1.2	2	12.5	---	6.2	---	2.0	---	---
80-AP-40A 17 Tubes, 24 Spokes, AE = 4.4	2	10.7	---	8.0	---	1.3	---	---
80-AP-40 17 Tubes, 24 Spokes, AE = 4.4	2	3.9	---	2.5	---	1.6	---	---
80-AP-41 17 Tubes, AE = 1.1	2	13.5	---	4.7	---	2.9	---	---
80-AP-42 17 Tubes, AE = 5.2	2	11.8	---	3.8	---	3.1	---	---
80-AP-43 17 Tubes, AE = 2.8	2	13.0	---	5.9	---	2.2	---	---
80-AP-44 17 Tubes, AE = 4.0	2	14.7	---	11.0	---	1.3	---	---
80-AP-45 16 Spokes, AE = 2.1	2	8.5	---	8.0	---	1.1	---	---
80-AP-46 16 Spokes, AE = 4.1	2	12.0	---	20.5	---	0.6	---	---
80-AP-47 16 Spokes, AE = 1.8	2	10.3	---	15.0	---	0.7	---	---
80-AP-17 Annuli, AE = 1.0	2	6.0	---	7.2	---	0.8	---	---
80-AP-18 17 Tubes, 17 Spokes Ends, AE = 4.65	2	10.0	---	1.2	---	8.3	---	---
80-AP-18A 17 Tubes, 17 Spokes Ends, AE = 4.0	2	15.3	---	5.5	---	2.8	---	---
80-AP-20 Annular Slot/Creams Ring, AE = 6.5	2	13.2	---	7.2	---	1.8	---	---
80-AP-21 15 Spokes, AE = 1.4	2	9.0	---	4.0	---	2.2	---	---
80-AP-22 15 Spokes, AE = 1.4	2	5.2	---	3.9	---	1.3	---	---
80-AP-23 15 Spokes, AE = 1.4	2	6.0	---	1.0	---	6.0	---	---
80-AP-24 15 Parallel Slots, AE = 1.0	2	9.0	---	3.0	---	3.0	---	---
80-AP-25 5 Parallel Slots, AE = 1.0	2	9.0	---	3.0	---	2.7	---	---
80-AP-26 24 Spokes, AE = 5.0	2	8.0	---	8.0	---	1.0	---	---
80-AP-27 24 Spokes, AE = 6.0	2	8.0	---	8.5	---	0.9	---	---
80-AP-35 170 Tube Annuli, AE = 1.0	2	16.5	---	10.8	---	1.5	---	---
80-AP-36 60 Tube Annuli, AE = 1.0	2	12.2	---	8.2	---	1.6	---	---
80-AP-37 17 Tubes, AE = 1.9	2	6.5	---	1.5	---	5.7	---	---
80-AP-38 17 Tubes, Hex Array, AE = 4.0	2	7.5	---	1.5	---	5.0	---	---
80-AP-39 17 Tubes, Hex Array, AE = 4.0	2	9.8	---	2.0	---	4.9	---	---
80-AP-40 17 Tubes, 17 Spokes Ends, AE = 1.1	2	16.0	---	10.0	---	1.6	---	---
80-AP-41 17 Tubes, 17 Spokes Ends, AE = 4.0	2	17.5	---	7.8	---	2.2	---	---
80-AP-42 17 Tubes, 17 Spokes Ends, AE = 1.1	2	15.0	---	6.5	---	2.3	---	---
80-AP-43 17 Tubes, 17 Spokes Ends, AE = 1.1	2	9.0	---	1.8	---	5.0	---	---

LIST OF SYMBOLS

Symbol

a_0	Ambient Speed of Sound, ft/sec
A	Nozzle exhaust area, ft ²
AR, A.R.	Suppressor area ratio; determined by the total nozzle area, excluding any plug, divided by the flow area of the nozzle
C_{fg} , C_{f_g}	Thrust coefficient
D, d	Diameter, ft or in.
DFS	Diameter - full size, ft or in.
DM	Diameter - model, ft or in.
f	1/3-octave band frequency, Hz
F_g	Ideal gross thrust, lbf
M	Jet Mach number
P	Pressure, lbf/in. ²
PNL	Perceived noise level, PNdB
EPNL	Effective perceived noise level, EPNdB
PWL	Sound power level, dB re: 10 ⁻¹³ watts
OAPWL	Overall sound power level
SPL	Sound pressure level, dB
OASPL	Overall sound pressure level, dB
T	Temperature, ° R
u'	Axial turbulent velocity, ft/sec
U, V	Jet velocity, isentropic, fully expanded, ft/sec
W, w	Weight flow rate, lbm/sec
X	Axial distance, ft
α	Nozzle exit angle, degrees
ρ	Density, lbm/ft ³
w	Density ratio exponent

REFERENCES

1. Lee, R., Kendall, R.M., et al., "Research Investigation of the Generation and Suppression of Jet Noise," General Electric Company, NOAS 59-6160-C, January 1961.
2. Simcox, C.D. et al., "SST Technology Follow-On Program - Phase I - A Summary of the SST Jet Noise Suppression Test Program," Boeing Company, FAA-SS-72-41, February 1972.
3. Brausch, J.F. and Doyle, V.L., "Summary of GE4/SST Acoustic Suppression Research, Supersonic Transport Noise Reduction Technology Program, Phase I," General Electric Company, FAA-SS-72-42, December 1972.
4. Stringas, E.J. and Kazin, S.B., "Supersonic Transport Noise Reduction Technology Program - Phase II," General Electric Company, FAA-SS-73-29-1, September 1975.
5. Atvars, J. et al., "SST Technology Follow-On Program - Phase II," Boeing Company, FAA-SS-73-11, March 1975.
6. Hawkins, R.C. and Hoch, R., "Studies into Concorde's Engine Noise Reduction," NATO, AGARD-PPP-131.
7. Mani, R. and Stringas, E.J., "High Velocity Jet Noise Source Location and Reduction - Task 2 - Theoretical Developments and Basic Experiments," General Electric Company, FAA-RD-76-79, II, May 1978.
8. Knott, P.R. et al., "Acoustics Tests of Duct-Burning Turbofan Jet Noise Simulation," General Electric Company, NASA Contractor Report 2966, July 1978.
9. Knott, P.R. et al., "Acoustic and Performance Investigation of Coannular Plug Nozzles," General Electric Company, NASA Contract NAS3-19777 (to be published).
10. Clapper, W.S. et al., "High Velocity Jet Noise Source Location and Reduction: Task 4 - Development/Evaluation of Techniques for In-Flight Investigation," General Electric Company, FAA-RD-76-79, IV, February 22, 1977.
11. Wilcox, F.A., "Comparison of Ground and Flight Test Results Using a Modified F-106B Aircraft," NASA TMX-71439, November 5, 1973.
12. Jaeck, C.L., "Static and Wind Tunnel Near-Field/Far-Field Jet Noise Measurements from Scale Model Single Flow Baseline and Suppressor Nozzles," Vol. 2 - Forward Speed Effects, Boeing Company, NASA CR-137914, November 1976.